(200)
R290
no.84-203

USGS LIBRARY-RESTON
3 1818 00064092 8

DEPARTMENT OF THE INTERIOR
U.S. GEOLOGICAL SURVEY

Open-file report (U.S. Geological Survey)

Geology of the Arabian Peninsula western shield area

by

G. F. Brown[1/], D. L. Schmidt[2/], and A. C. Huffman, Jr.[2/]

U.S. GEOLOGICAL SURVEY
RESTON, VA.
SEP 14 1984
LIBRARY

Open-File Report 84-203

In cooperation with the Ministry of Petroleum and Mineral Resources, Deputy Ministry for Mineral Resources, Jiddah, Kingdom of Saudi Arabia

tw anal

This report is preliminary and has not been reviewed for conformity with U.S. Geological Survey editorial standards and stratigraphic nomenclature.

1/ U.S. Geological Survey
Reston, VA 22092

2/ U.S. Geological Survey
Denver, CO 80225

1984

356749



Frontispiece

As seen from space the Arabian Shield appears as a red crescent on the west side of the Arabian Peninsula and as a continuation of the Sahara Desert extending across north Africa. Photograph from Apollo II Spacecraft at about 98,000 nautical miles from Earth.

Binder by RHG / USDS Library

FOREWORD

This volume, *"The Geology of the Arabian Peninsula,"* is a logical consequence of the geographic and geologic mapping project of the Arabian Peninsula, a cooperative venture between the Kingdom of Saudi Arabia and the Government of the United States. The Arabian-American Oil Co. and the U.S. Geological Survey did the fieldwork within the Kingdom of Saudi Arabia, and, with the approval of the governments of neighboring countries, a number of other oil companies contributed additional mapping to complete the coverage of the whole of the Arabian Peninsula. So far as we are aware, this is a unique experiment in geological cooperation among several governments, petroleum companies, and individuals.

The plan for a cooperative mapping project was originally conceived in July 1953 by the late William E. Wrather, then Director of the U.S. Geological Survey, the late James Terry Duce, then Vice President of Aramco, and the late E. L. deGolyer. George Wadsworth, then U.S. Ambassador to Saudi Arabia, and Sheikh Abdullah Sulaiman, then Minister of Finance of the Government of Saudi Arabia, lent their support to the plan. In November of the following year, 1954, Director Wrather approved the U.S. Geological Survey's participation and designated G. F. Brown responsible for the western Arabian shield region in which he had previously worked under U.S. foreign-aid programs. In January 1955 F. A. Davies, Chairman, Board of Directors, Arabian-American Oil Co., approved Aramco's participation and appointed the late R. A. Bramkamp, chief geologist, responsible for compilation of the area within the Kingdom where the sediments crop out. This responsibility fell to L. F. Ramirez following the death of R. A. Bramkamp in September 1958.

R. A. Bramkamp and G. F. Brown met in New York in February 1955 and planned the program, including scales of maps, areas of responsibility, types of terrain representation, and bilingual names. Thus there was established a cooperative agreement between the Kingdom of Saudi Arabia, the U.S. Department of State, and the Arabian-American Oil Co. to make available the basic areal geology as mapped by Aramco and the U.S. Geological Survey.

The agreement specified publication of a series of 21 maps on a scale of 1:500,000, each map covering an area 3° of longitude and 4° of latitude. Separate geologic and geographic versions were to be printed for each of the quadrangles; both versions were to be bilingual—in Arabic and English. A peninsular geologic map on a scale of 1:2,000,000 was to conclude the project.

High-altitude photography, on a scale of 1:60,000, of the Kingdom of Saudi Arabia was initiated during 1949 by the Aero Service Corp. and completed in 1959. Both third-order vertical and horizontal control and shoran were utilized in compiling the photography. This controlled photography resulted in highly accurate geographic maps at the publication scale which then served as a base for the geologic overlay. The topography of the sedimentary areas was depicted by hachuring and that of the shield region by shaded relief utilizing the airbrush technique.

The first geographic quadrangle was published in July 1956 and the last in September 1962. While preparation of the geographic sheets was in progress, a need arose for early publication of a 1:2,000,000-scale peninsular geographic map. Consequently, a preliminary edition was compiled and published in both English and Arabic in 1958. The second edition, containing additional photography and considerable new topographic and cultural data, was published in 1963. The first of the geologic map series was published in July 1956 and the final sheet in early 1964. The cooperative map project was completed in October 1963 with

As work on the quadrangles progressed, geologists, companies, and governments working in areas adjacent to the Kingdom of Saudi Arabia were consulted by Aramco and invited to participate in the mapping project. The number of cooperating participants was expanded to 11, which included the operating oil companies in the peninsula and which are identified elsewhere in this text; the Overseas Geological Surveys, London; the Government of Jordan; F. Geukens, who had worked in Yemen; and Z. R. Beydoun, who had studied the Eastern Aden Protectorate. With the close cooperation of the authors, the new data were added to data already plotted on the base map of the Arabian Peninsula.

As the geological coverage of the peninsular map grew, the need for a text to accompany the map became apparent to both the U.S. Geological Survey and the Aramco geologists. Exploratory conversations were begun by Aramco with companies working in the other countries of the Arabian Peninsula for their participation in the preparation of a monograph on the geology of the Arabian Peninsula. Each author prepared a description of the geology of the area for which he was responsible, as shown in the sources of geologic compilation diagram on the peninsular map. The U.S. Geological Survey undertook the publishing of the volume as a professional paper, and the Government of Saudi Arabia was to finance its printing. It was early agreed that there would be no effort to confine the contributions to a standard format and that no attempt would be made to work out an overall correlation chart other than shown on the "Geologic Map of the Arabian Peninsula." Thus, the individual style of authors of several nationalities is preserved.

Cooperation and relations have been of the highest order in all phases of the work. The project would not have been possible without the full support of the U.S. Department of State, the Kingdom of Saudi Arabia, and all contributors. In fact, the funds which made publication of this volume possible were contributed by the Saudi Arabian Government.

The data provided by the maps and in the professional paper provide information for an orderly scientific and economic development of a subcontinent.

O. A. Seager

O. A. SEAGER,
Arabian-American Oil Co. (Retired).

W. D. Johnston Jr.

W. D. JOHNSTON, JR.,
Former Chief, Foreign Geology Branch,
U.S. Geological Survey.

CONTENTS

	Page
ABSTRACT	1
INTRODUCTION	5
Previous geologic work	6
Nature and scope of recent work	7
Acknowledgments	8
GEOGRAPHY	
Physical geography	10
Climate	10
Human geography	13
Flora	14
Relation of flora to rainfall by J. D. Tothill	16
The seven zones	17
Ar Rub al Khali zone	18
The sallam desert zone	18
The Asak-Commiphora-desert zone	18
The samr desert zone	18
The Kleinia - Pastoral zone	19
The Euryops-Barley zone	20
The rose-juniper-agricultural zone	20
PRECAMBRIAN LAYERED ROCKS OF THE ARABIAN SHIELD	25
Historic geologic divisions	25
Current geologic divisions	26
Ultramafic and ophiolitic rocks	26
Baish-Bahah groups	28
Jiddah group	29
Ablah group	31
Fatimah	32
Silasia formation	33
Halaban group	33
Murdama group	37
Shammar group	38
Jubalah group	39
PRECAMBRIAN PLUTONIC ROCKS OF THE SHIELD	42
Distribution and classification	42
Dioritic suite	43
Granitic suite	44
CHEMISTRY OF THE PRECAMBRIAN VOLCANIC AND PLUTONIC ROCKS	45
Introduction	45
Chemical variation of volcanic and plutonic rocks	79
Volcanic rocks	79
Plutonic rocks	80
Tholeiitic, calc-alkalic, and alkalic compositions	83
General statement	83
Volcanic rocks	83
Plutonic rocks	85
Discussion of chemistry	86

Page

GEOCHRONOLOGIC DATA FOR THE ARABIAN SHIELD 90
First radiometric age determinations 90
Early tabulation of Rb-Sr and K-Ar ages by G. F. Brown, Carl Hedge and Richard Marvin 95

CRUSTAL HISTORY OF THE PRECAMBRIAN SHIELD 104
General statement 104
Early crustal history 106
Early collisional orogeny 107
Late crustal history 109
Culminant orogeny and post-tectonic granites. . . 109
Najd faulting event 112
PALEOZOIC SEDIMENTARY COVER ROCKS AT EDGE OF SHIELD 116
Cambro-Ordovician sandstones 116
Siq Sandstone 116
Saq Sandstone and Ram Umm Sahm Sandstones 117
Wajid Sandstone 117
Khuff Sandstone 119
MESOZOIC SEDIMENTARY ROCKS 119
Khums Formation 119
Definition. 119
Occurrence and thickness. 119
Lithologic character. 120
Paleontology and age. 121
Amran Formation. 122
Definition. 122
Occurrence and thickness. 122
Lithologic character. 123
Nature of contact 124
Paleontology and age. 124
Khurma Formation 126
MESOZOIC-CENOZOIC SEDIMENTARY ROCKS 127
Usfan Formation. 127
Definition 127
Distribution and Thickness. 127
Lithologic character. 127
Nature of contact 128
Paleontology and age. 128
CENOZOIC ROCKS. 131
Umm Himar Formation-Paleocene. 131
Occurrence and thickness. 131
Lithologic character 131
Nature of contacts 131
Laterite and saprolite 131
Shumaysi Formation 132
Definition 132
Distribution and thickness. 132
Lithologic character. 140
Nature of contacts 140
Paleontology and age. 140
Baid Formation 141
Definition. 141
Distribution, thickness, and lithology. 141
Paleontology and age. 142

Page

Bathan Formation-Miocene 143
Definition 143
Lithology and thickness 143
Occurrence and nature of contents 143
Paleontology and age 143
Raghama Formation - Miocene. 144
Definition. 144
Distribution, thickness, and lithology. 145
Nature of contacts. 145
Paleontology and age 145
Cenozoic igneous rocks 147
Hypabyssal Tertiary igneous rocks 147
Basaltic lava flows 149
The harras 157
GEOMORPHOLOGY 169
Cycles of erosion 2/ 169
The arid cycle. 169
The common desert erosion cycle 170
The Tihamat 172
The Scarp Mountains 174
The Hijaz and Hisma Plateaus 176
The Najd Pediplain 177
BIBLIOGRAPHY. 179

TABLES

		Page
Table 1.	Temperatures and relative humidity at selected sties in Western Saudi Arabia	12
2.	Summary of rainfall estimates (in inches)	23
3.	Description and classification of crystalline rocks of the Saudi Arabian Shield for which chemical analyses are given in table 4	47
4.	Chemical analysis of shield rocks and C.I.P.W. normative molecules	59
5.	Isotopic chemistry of samples - Aldrich	91
6.	Rock type, sample location, and ages of minerals by T. Aldrich	92
7.	Rubidium-strontium ages - Hedge, et al	93
8.	$K^{40}Ar$ ages - Marvin, et al	96
9.	Chemical analyses of Tertiary igneous rocks, and C.I.P.W. normative molecules	133
10.	Isotopic ages igneous rocks - Marvin, et al	150

ILLUSTRATIONS

			Page
Frontispiece			
Figure	1.	Index map showing location of the Arabian Shield, Arabian Peninsula.	6a
	2.	Geologic map of the Arabian Shield.	In Pocket
	3.	Estimated rainfall distribution.	11a
	4.	Examples of a few phreatophytes, indicating permanent ground water.	15a
	5.	Amygdaloidal metabasalt at the Jabal Ess ophiolite complex.	27a
	6.	Baish-Bahah Group.	28a
	7.	Hornblendite interbedded with pink marble of the Jiddah (Samran) Group in Wadi Fatimah, and pillow lava in basalt of Baish Group, Hilwa area.	30a
	8.	Oblique aerial views to northwest across the Ablah and Jiddah groups.	31a
	9.	Views of the Ablah group.	32a
	10.	Fatimah Group, North Wadi Fatimah.	32c
	11.	Silasia formation showing siliceous hematite outcrops.	33a
	12.	View north of Wassat stratabound gossan in Halaban Group.	34a
	13a.	Type locality of Murdamah Group.	37a
	13b.	Slate and shale of the Hadiyah group beneath the Siq Sandstone.	37b
	14.	Shammar and Jubaylah groups.	38a
	15a.	Jubaylah Group at outcrop at the north edge of the Sahl Matran quadrangle.	39a
	15b.	Aerial view to the southeast of Jabal Hassan at the edge of the shield.	39a
	16.	Incremental $^{39}Ar_K$ of Jubaylah andesite.	40a

ILLUSTRATIONS - cont'd

		Page
Figure 17.	Tectonic regions used to show regional variations and trends in the chemical data.	58a
18.	N_2O-CaO-K_2O diagram showing the chemical distribution (molar data) of control samples of metavolcanic rocks.	79a
19.	Na_2O-CaO-K_2O diagram showing chemical distribution (molar data) of metavolcanic rocks and a few dike rocks reported in tables 1 and 2.	79b
20.	Na_2O-CaO-K_2O diagram showing plutonic rock chemistry (molar data) of control samples classified by age.	80a
21.	Na_2O-CaO-K_2O diagram showing plutonic rock chemistry (molar data) of samples reported in tables 1 and 2 and classified by age.	80b
22.	Na_2O-CaO-K_2O diagram summarizing all the plutonic rock chemistry (molar data) examined in this report (combination of figures 4 and 5).	82a
23.	AFM diagram showing metavolcanic rock chemistry (weight percent data) or control samples classified by age.	83a
24.	AFM diagram showing chemical (weight percent data) distribution of metavolcanic rocks and a few dike rocks reported in tables 1 and 2.	83b
25.	AFM diagram showing chemical (weight percent data) distribution of rocks of the diorite suite from the Saudi Arabian Shield.	83c
26.	AFM diagram showing chemical (weight percent data) distribution of rocks of the granite suite from the Saudi Arabian Shield.	83d
27.	Alkali-silica diagram showing metavolcanic rock chemistry (weight percent) for control samples of the Baish-Bahah and Jiddah basalt.	83e
28.	Alkali-silica diagram showing metavolcanic rock chemistry (weight percent) for control samples of the Murdama, Shammar, and Jubaylah groups.	83f

		Page
Figure 29.	Alkali-silica diagram showing plutonic rock chemistry (weight of rocks of the Fatimah group and the Jubaylah group.	83g
30.	Alkali-silica diagram showing plutonic rock chemistry (weight percent data) of granitic suite.	83h
30a.	Histogram showing distribution of K-Ar and Rb-Sr ages.	89
31.	Vertical aerial photograph of the northern portion of the An Nimas batholith.	106a
32.	Aerial oblique view to the northwest of orthogneiss dome enfolded into amydaloidal metabasalt flows of the Baish Group.	108a
33.	Schistose gneiss at Wadi Dhuqiyah 65km southeast of Ta'if.	109a
34.	Aerial view south of the eastern edge of the Khamis mushayt gneiss dome.	109b
35.	Geochronologic analyses of Paleozoic and Precambrian rocks.	109c
36.	Oblique aerial photo viewed to southeast from 45°05' E. long., 23°05' N. lat., near the east edge of the shield.	111a
37.	View to northwest of Najd fault zone.	112a
38.	Jabal Adhqan al Hajun at 22°41' N. lat. 44°06' E. long.	112b
39.	Diagrams showing variations in initial $^{87}Sr/^{86}Sr$ (upper diagram) and Rb/Sr (lower diagram) ratios with age.	114
40.	The Siq Sandstone.	116a
41.	The Triassic Khums sandstone.	119a
42.	Toe of Asir mountains east of Gizan with Amran (Hanifa) limestone dipping west.	122a
43.	Type section of the Amran (Hanifa) formation.	122b
44.	Type section of the Usfan Formation at Usfan Pass.	127a
45.	Composite columnar section of the Umm Himar Formation	131a

		Page
Figure 46.	Laterite under Sirrat lava.	131b
47.	Type locality of the measured Shumaysi Formation.	132a
48.	Stratotype section of Baid Formation.	141a
49.	Diabase sill (d) cutting Baid Formation.	141b
49b.	The Ragahama Formation	141b
50.	Map showing Cenozoic igneous rocks.	In Pocket
51.	Modal analyses of Tertiary continental dikes.	148a
52.	Histogram of selected Tertiary igneous rocks from around the Red Sea.	157a
53.	Alkalies plotted against silica for Tertiary igneous rocks.	158a
54.	Crest of Harrat ar Raha.	159a
55.	Eolian undercutting of Ram Um Sahm sandstone at Nabatean tomb at Medain Salah.	160a
56.	Basalt front above sandstone bench.	160b
57.	Bathan Formation.	161a
58.	Ternary diagrams of Tertiary igneous rocks.	161b
59.	White rhyolite crater, Jabal al Abayad.	161c
60.	Jabal Ithnayn, Harrat Ithnayn.	162a
61.	Jabal Hibran, Harrat Hutaym.	162b
62.	Cinder-ash cone, Jabal al Qishr.	163a
63.	Wabar phreatic crater. Holocene eruption.	165a
64.	Oblique aerial view of Harrat al Kishb showing linearity of Holocene craters.	167a
65.	The arid cycle.	169a
66.	Landsat image showing effects of wind erosion.	171a
67.	Physiographic map of Arabian Peninsula.	In Pocket

		Page
Figure 68.	Sharms along the Red Sea.	In Pocket
69.	Terrace benches above the Red Sea and Landsat image of the erosional scarp of Asir.	173a
70.	Loessal silt in Tathlith valley above Hamdh.	176a
71.	Bornhardt at Jabal Kursh.	177a
72.	Spines of Jabal Shar and conical inselberg of Jabal al Gharamul.	177b
73.	Wadi Schism yardang valley.	178a
74.	Yardang troughs following one set of joints parallel to the wind direction.	178b

GEOLOGY OF THE ARABIAN PENINSULA SHIELD AREA OF WESTERN SAUDI ARABIA

by

Glen F. Brown, Dwight L. Schmidt, and A. Curtis Huffman, Jr.

ABSTRACT

Western Arabia lies within the low latitude desert of north Africa and the Middle East, the core being the Arabian segment of the African shield, a complex of basement rocks comprising about 670,000 km^2 or one-third of the Arabian peninsula. Reconnaissance mapping of these crystalline rocks, together with bordering sedimentary rocks and volcanic flows, begun in 1950, resulted during the next 13 years in a series of geologic and geographic maps without extensive texts. The maps served as general guides for natural resources development including water supplies, ore deposits, and building materials. An intensive exploration program that began in 1963 has vastly increased geologic information resulting from the efforts of numerous geologists.

Rainfall in Arabia is meagre and episodic, and vegetation is sparse except in isolated copses on the crest of the Hejaz range. Comparison of flora with similar species in the Sudan, where records have long been kept, allows evaluation of mean annual precipitation. Wandering Beduin following fodder created a delicate balance between population and water supply--now disturbed by wells drilled in alluvium and lava fields.

A trapezoidal region of Precambrian crystalline rocks lies along the northeast flank of the Red Sea with two long prongs extending northwest and southeast for a total of 1,800 km. These basement rocks of the Arabian Shield are well exposed on the uplands, scarp mountains, and coastal pediments where the Phanerozoic cover rocks have been stripped as a result of Paleozoic epeirogeny and Tertiary ramping. The shield outcrops are divided into three tectonic provinces by N45°W-trending shear zones of the Najd fault system of latest Proterozoic and possibly earliest Paleozoic time. The southwestern province, the Asir upland, was sharply uplifted and tilted to the northeast during the Neogene. The northwestern province, consisting of the Al Jisr-Al Hisma upland as well as Jabal Shammar farther east, similarly was uplifted and tilted. These two provinces are separated by the flat-lying median Najd province chiefly bounded by the principal Najd faults.

The outcrops of the shield rocks are of the late Proterozoic Eon--upper Riphean to Vendian or Infracambrian epochs, including the Ediacarian System. The most reliable isotopic ages range from about 900 to 560 Ma, but some Middle Proterozoic rocks may occur in the easternmost Shield. The rocks are divided into six lithostratigraphic sequences, two platonic suites, and an ophiolitic suite. The mafic and ultramafic, volcanic and plutonic rocks of the ophiolite suite everywhere were emplaced tectonically and are probably of different ages in different places. Some ophiolite occurs as obducted blocks, but most is highly deformed and altered to serpentinite in fault zones that mostly define sutures between different tectonic blocks or terranes within the shield.

Three of the lithostratigraphic sequences consist of mafic to silicic volcanic rocks and volcanic-derived clastic rocks that with their subvolcanic, plutonic rocks of a dioritic suite probably formed in oceanic island arcs during convergent plate tectonism. These rocks make up the primary or first formed crust of the shield. Chemical analyses of the primary shield rocks regardless of age are principally calc-alkalic with some associated tholeiitic varieties. Most of the layered rocks are andesitic but range from basalt to dacite and in places contain intercalated pillow basalt, marble, chert, and carbonaceous or graphitic schist. Most of the plutonic rocks of the dioritic suite are dioritic but range from gabbro to trondhjemite and rarely contain potassium feldspar. The sequences and an associated dioritic suite become younger toward the eastern shield, that is, the primary crust of the shield youngs toward the east.

Two western sequences consist of the Jiddah (Samran) and Baish-Bahah group and range in radiometric age from about 900 to 800 Ma; the eastern sequence consists of the Halaban (Hulayfah) group and ranges from 800 to about 700 Ma. During subsequent orogeny, most of the rocks were intensely deformed and mostly metamorphosed to high-rank greenschist facies, but rising in places to the almandine-amphibolite facies.

Two other lithostratigraphic sequences with an associated plutonic granite suite are the products of two mountain-building episodes during which the primary crust was greatly thickened and converted into craton. The two sequences, comprising largely the Ablah (Al Ays) and Murdama (Shammar) groups, consist of abundant sedimentary rocks commonly arkosic, that are the erosional products of the orogenic mountains. They are several thousand meters thick. Less abundant calc-alkalic to alkalic volcanic rocks, commonly dacitic and rhyolitic, are intercalated with the sedimentary rocks. The plutonic rocks of the granitic suite in association with both sequences have syntectonic and posttectonic phases, are products of the orogenies, and are the principal new ingredients making the craton.

Gneiss domes were a significant part of these cratonization orogenies. In association with orogenic crustal heating, some of the low-density, more silicic tonalitic and trondhjemitic rocks of the primary crust rose as gneiss domes. Partial melting in the middle or lower crust below the gneiss domes produced large volumes of granitic magma that intruded the gneiss domes as granodioritic batholiths.

The Ablah group and older part of the granitic suite are about 775 to 740 Ma and are associated with the Ablah orogeny and cratonization in the western and earlier-formed half of the shield. The Murdama group and younger part of the granitic suite are about 660 to 580 Ma and are associated with the culminant orogeny and late cratonization that was shield wide. The granitic suite during both orogenies consists of early, syntectonic granodiorite batholiths associated with the gneiss domes and late, posttectonic monzogranite plutons. Only during the culminant orogeny, late magmatic evolution produced syenogranite and alkali-feldspar granite commonly in circular and ring-structured plutons and with associated explosive volcanic deposits (Shammar group); final products were peralkalic and peraluminous, some of which have economic potential. The late plutonism of the culminant orogeny was distinctly bimodal in that subordinate gabbroic rocks are associated with the granites.

Various building blocks or terranes of the andesitic and dioritic primary crust were collisionally agglomerated during the Ablah orogeny, early cratonization, whereas the entire shield as presently exposed was further collisionally accreted and compressioally consolidated during the culminant orogeny, final cratonization. Thousands of kilometers of oceanic crust had to be suducted in about 300 million years to form the large primary crust of the Arabian Shield. The inevitable collisional events during consumption of such a large volume of oceanic crust invariably led to numerous collisional orogenies that collectively encompass the widely known Pan African tectonic episode.

The youngest lithostratigraphic sequence, the Jubalah group, is essentially postcratonic, although it is the end product of the collisional culminant orogeny. Final east-west compression of the entire shield from about 580 to 560 Ma caused the craton to fracture along the large northwest-trending, left-lateral faults and elsewhere along lesser, northeast-trending, right-lateral, conjugate fault, of the Najd fault system. Erosional products of this more localized deformation were the sedimentary rocks of the Jubalah group which also includes intercalated andesitic to basaltic volcanic rocks of a mafic alkalic compositional trend.

The collisional edge of an old continental plate (or tectonic fragments thereof), suspected on the eastern edge of the Arabian Shield, has not been shown with certainty to be exposed as yet. Presumably, widespread contamination from such an old continental crust effects U-Pb, Sm-Nd, Rb-Sr, and common lead ratios in the young plutonic rocks of the easternmost shield. One mass of anorthosite near Jabal Kidah on the central eastern edge of the shield may be a fragment of this old continental plate in that associated granodiorite may be as old as 1600 to 1800 Ma.

Epeirogenic uplift, erosion, and cooling of the uppermost shield during Early and Middle Cambrian time is indicated by an average fission track age of 510 + 52 Ma ,on sphene from diorite (hornblende K-Ar age of 615 + 12 Ma) in the southwestern part of the shield. The hiatus was followed by extensive deposition of the Cambro-Ordovician Saq Sandstone in the north and northeast and Wajid Sandstone in the southeast and south of the shield. The Cambrian Siq Sandstone had already been deposited in the northern part. During the middle and late Paleozoic, broad epeirogeny caused further erosion of the shield until marine transgression deposited the Upper Permian Khuff Formation at least in the eastern part of the shield. In the southwestern shield, the nonmarine, Upper Triassic Khums Sandstone was deposited variably on Wajid or Precambrian rocks and is overlain by the middle Upper Jurassic Amran Formation.

Except for shallow marine sandstone of problematic Cretaceous age deposited on the Amran in the southwestern shield and on Precambrian in the northwestern shield, the younger beds on the shield are Paleocene and younger with the possibility that the lowermost are upper Maestrichtian. The early Tertiary beds contain vertebrate fossils of coastal marine or estuarine environment 250 km east of the Red Sea in the central shield. Marginal marine sediments were deposited in a western tongue of the latest Tethys Sea as late as Eocene on the western shield at least as far south as Jiddah.

The great harras of flood basalt erupted on the western shield during late Oligocene and early Miocene at the same time as a 2000-km-long continental rift developed along the future Red Sea axis. Within this rift, Baid freshwater tuffaceous lake beds were deposited between mafic and silicic volcanos. During the late early Miocene time, the Red Sea opened at a rate of 4.4 cm/yr in a first-stage movement while continental dikes and swarms of oceanic tholeiitic dikes, gabbro, and granophyre plutonic rocks were intruded into the rift sedimentary and volcanic rocks at the newly formed continental margin. The continental margin was deformed and greatly extended at this time. About 14 or 15 Ma ago, as the first-stage spreading stopped, the Red Sea Escarpment rose; its erosion caused deposition of coarse conglomerate of the Bathan Formation. About 3000 m of evaporite were deposited on the young Red Sea oceanic crust during the late Miocene dessication crisis.

A second stage of sea-floor spreading from about 4-5 Ma ago produced the Red Sea axial trough consisting of oceanic crust as well as renewed uplift and tilting of the three tectonic provinces in response to compression from counterclockwise rotation against the Dead Sea rift. This late movement caused widespread major stream capture especially along the wadis that formerly drained southwesterly or northwesterly, the channels turning westward through narrow gorges to the coastal plain and the Red Sea.

GEOLOGY OF THE ARABIAN PENINSULA SHIELD AREA OF WESTERN SAUDI ARABIA

By

Glen F. Brown, Dwight L. Schmidt, and A. Curtis Huffman, Jr.

"Nay, the very slate beds of Snowdonia have not forced their way up from under the mountain without long and fearful struggles. They are set in places upright on end, then horizontal again, then sunk in an opposite direction, then curled like sea-waves, then set nearly upright once more, and faulted through and through...."

Charles Kingsley in Town Geology

INTRODUCTION

The geology of the Arabian Shield of Saudi Arabia as shown on Map I-270 by the U.S. Geological Survey (USGS)/Arabian-American Oil Company (1963) during the period 1950 to 1958, was part of a larger program undertaken by the Kingdom of Saudi Arabia and the Government of the United States (see Foreward for details). The geology shown on the geologic map of this report (fig. 2) is a revision of Map I-270, and presents a compilation of geologic mapping done as part of the USGS-Saudi Arabian program from 1963 to the present. As Chapter A of Professional Paper 560, this report synthesizes and brings up-to-date a large amount of geologic data gathered by many individuals.

Prior to the inception of U.S. Geological Survey (USGS) field work in 1950, almost no geologic studies of the western part of the Arabian Shield (fig. 1, 2) had been made. This lack contrasted sharply with the wealth of data available for central and eastern Arabia where the petroleum companies have been actively exploring for nearly 50 years. Field work from 1950 to 1958 contributed information for the western part of the geologic map of the Arabian Peninsula (U.S. Geological Survey-Arabian American Oil Co., USGS-ARAMCO, 1963) and for a series of 20 quadrangle maps. As a base for geologic mapping, the USGS field party used aerial photography and necessarily described petrologic units in field terms because it was soon recognized that the crystalline rocks that could be classified into lithostratigraphic groups ranged from nonmetamorphosed through greenschist and amphibolite metamorphic facies. These Precambrian rocks are intricately folded and faulted, in addition to being intruded by numerous hypabyssal and plutonic igneous rocks. Nonetheless, from 1950 to 1963 the USGS laid the groundwork for economic development of the Arabian Peninsula other than hydrocarbons by completing and publishing reconnaissance maps of 670,000 km^2 of complex basement rocks--and also accomplishing its primary purpose of evaluating the economic, primarily hydrologic, possibilities of the region. The resulting maps were published as a series of quadrangle maps at 1:500,000 scale (geologic I-200 to 220 A, geographic I-200-220 B), and a geologic map of the entire Peninsula published at 1:2,000,000 scale (I-270 A).

The economic boom of the past 15 years (1965-1980) in Saudi Arabia has since led to more detailed mapping by many geologists from several nations, besides a growing number of Saudi Arabian geologists, with the result that the quality of geologic knowledge and interpretation of the western part of the shield now approaches that obtained by the earlier petroleum exploration in the area of sedimentary cover of the shield. This report describes the layered and massive igneous rocks of the Arabian Shield area in western Saudi Arabia, and traces the evolution of the geologic nomenclature in 1950 to the geologic names as they are currently being used (1980). Data from geophysical and geochemical field studies have aided these intensified surveys, as have results of chemical and petrographic analyses prepared in laboratories in Jiddah and abroad. Diamond drilling at encouraging prospects has added some third dimension. Perhaps the most important studies have been isotope measurements for determining radiometric ages (Aldrich and others, 1978; Fleck and others, 1976, 1980; Baubron and other, 1976; Cooper and others, 1979) which supply the "pegs" on which the Precambrian geologic history hangs, because fossils in the Arabian Shield are limited to stromatolitic and related forms of debatable value as time markers. Fortunately, the Arabia segment of the African megacraton is well exposed, and ideas can and have been challenged on the outcrop. The diversity of geologic concepts from various disciplines and many cultural backgrounds has done much to elucidate the geology of the segment.

Like Chapter D of Professional Paper 560 (Powers, and others, 1966), this report is essentially a compilation which, without the chronological data and the large volume of work done by many geologists since the preliminary map was published, would be less useful. This report discusses the stratigraphic and tectonic history of the shield area, and relates the stratigraphic terminology of the 1963 map to present concepts.

Previous geologic work

The first areal geologic descriptions of western Arabia (fig. 1) in modern times are those of Charles Doughty (1888), who prepared a general geologic map colored in along the routes of his trips in 1875 to 1878 and described in "Travels in Arabia Deserta." He separated the granites and traps most of which crop out in what he called the central plutonic country extending from Jabal Shammar (Ha'il) to Makkah from the overlying sandstone and limestone of the Great Nefud and the Qasim, and the still younger volcanic eruptions, the extensive basaltic lava fields (harras) of Tertiary and Quaternary age.

Concurrently with Doughty's travels and 4 years later, though their trails never crossed, Charles Huber travelled in central and northern Arabia as far as Jabal Shammar and Al Qasim (Huber, 1891). His map, published posthumously, carries scarce geologic information, but he collected rock specimens which were later studied by S. Meunier (1891) and P. Lamare (1923). The distribution of alkalic granite plutons and peralkalic rhyolite in the Shammar region was noted by Lamare (1923, 1930 a and b).

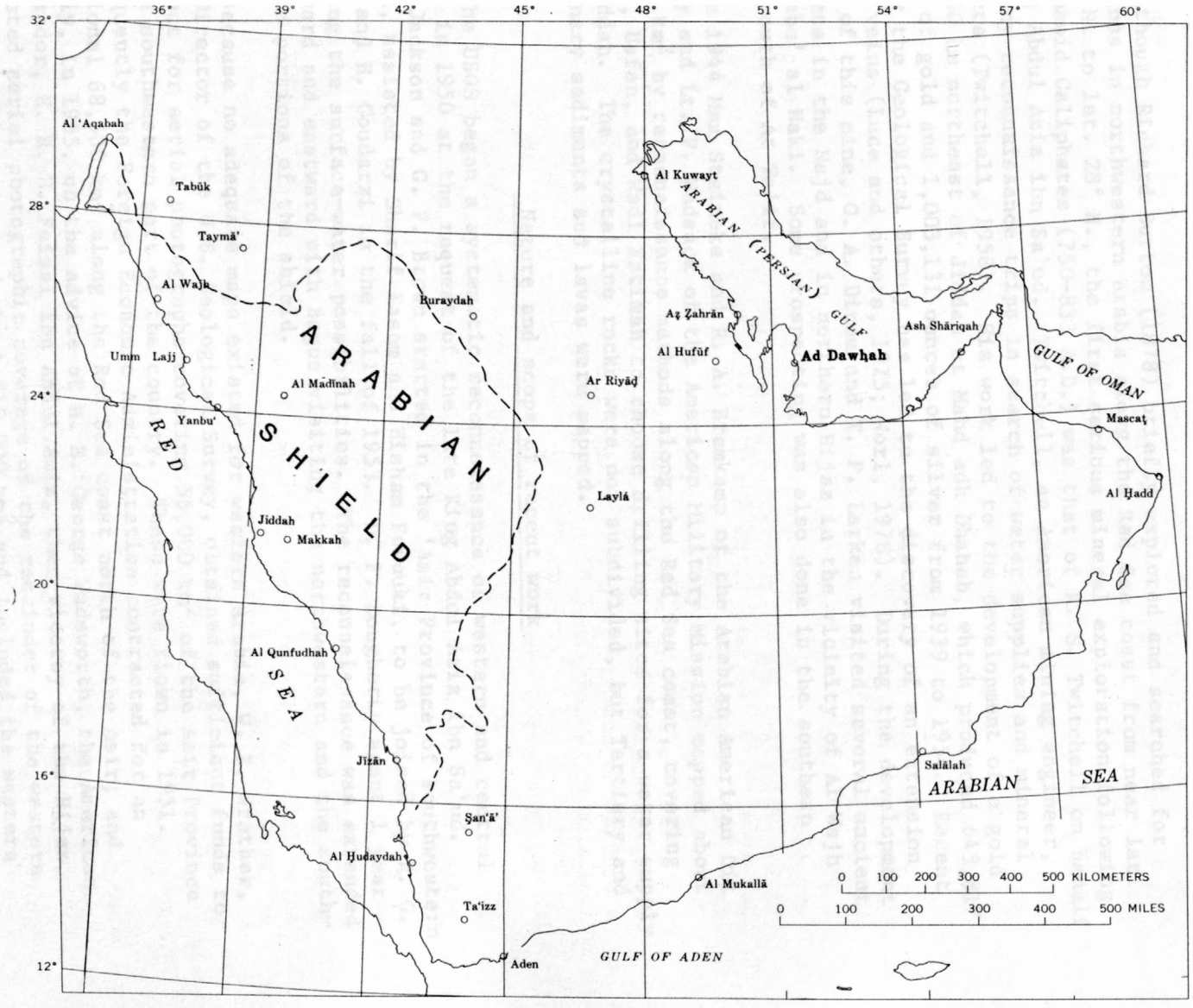

Figure 1. Index map showing location of the Arabian Shield, Arabian Peninsula.

In 1908-1915 Alois Musil explored and mapped much of northwestern Arabia. L. Kober (1911) accompanied him in 1910 to make geologic observations that gave the first general sequence, mostly of the Phanerozoic, of that part of Arabia.

Although Richard Burton (1878) briefly explored and searched for gold mines in northwestern Arabia along the Red Sea coast from near lat. 27°30' N. to lat. 28° N., the first serious mineral exploration following the Abbasid Caliphates (750-833 A.D.) was that of K. S. Twitchell on behalf of King Abdul Aziz ibn Sa'ud. Twitchell, an American mining engineer, made many reconnaissance trips in search of water supplies and mineral prospects (Twitchell, 1958). His work led to the development of a gold mine 400 km northeast of Jiddah at Mahd adh Dhahab, which produced 643,817 ounces of gold and 1,003,131 ounces of silver from 1939 to 1954. Recent work by the Geological Survey has led to the discovery of an extension of the veins (Luce and others, 1975; Worl, 1978). During the development period of this mine, G. A. Dirom and T. P. Larken visited several ancient prospects in the Najd and in northern Hijaz in the vicinity of Al Wajh and Yanbu' al Nakl. Some prospecting was also done in the southern Hijaz south of At Ta'if.

In 1944 Max Steineke and R. A. Bramkamp of the Arabian American Oil Company and Lt. F. Wadsack of the American Military Mission mapped about 10,000 km^2 by reconnaissance methods along the Red Sea coast, covering Jiddah, Usfan, and Wadi Fatimah to choose drilling sites for a water supply for Jiddah. The crystalline rocks were not subdivided, but Tertiary and Quaternary sediments and lavas were mapped.

Nature and scope of recent work

The USGS began a systematic reconnaissance of western and central Arabia in 1950 at the request of the late King Abdul Aziz ibn Sa'ud. R. O. Jackson and G. F. Brown started in the 'Asir Province of southwestern Arabia, assisted by Sharif Kasem and Hisham Farouki, to be joined by R. G. Bogue and H. Goudarzi in the fall of 1953. D. F. Dougherty spent 1 year studying the surface-water possibilities. The reconnaissance was extended northward and eastward with Bogue visiting the northwestern and the southeastern portions of the shield.

Because no adequate maps existed for western Arabia, W. E. Wrather, then Director of the U.S. Geological Survey, obtained sufficient funds to contract for aerial photographs covering 55,000 km^2 of the Asir Province in the southwestern part of the country. These were flown in 1951. Subsequently the Foreign Economic Administration contracted for an additional 68,500 km^2 along the Red Sea coast north of the Asir; and finally, in 1955, on the advice of H. E. George Wadsworth, the American Ambassador, H. R. H. Faisal ibn Abdul Aziz, then viceroy of the Hijaz, requested aerial photographic coverage of the remainder of the western provinces. This comprised about 810,000 km^2 and included the western part of a belt of trimetrogon photography taken earlier that extended from Jiddah to Dhahran on the east coast. The aerial photographs served as a base for compilation of the series of geographic and geologic maps, at scales of 1:500,000 and 1:2,000,000, published between 1956 and 1963.

In 1954, under the direction of Dr. F. K. Kabbani, the Directorate General of Petroleum and Mineral Affairs began geologic work, much of which was done by D. F. Schaffner, and W. H. McLean, assisted by Hashim Shigdar and Ahmed Al-Shanti; G. F. Brown assisted this work in 1957-58. In 1954, the Bundesanstalt fur Bodenforschung sent four geologists, G. Richter-Bernburg, H. R. von Gaertner, W. Schott, and H. Schurenburg, who made a rapid reconnaissance along the major roads and trails. In 1955, Roman Karpoff of the Societe Lyonnaise des Eaux et de l'Eclairage, Paris, made two trips across the shield and travelled to the vicinity of Al Madinah and Al Lith. In 1956-58, G. F. Brown made a reconnaissance of the northeastern part of the shield, and, in December 1962, travelled from Tabuk westward to Wadi 'Ifal and south to Al Wajh in the company of Dr. F. K. Kabbani.

Following this early geological reconnaissance, more intensive geological surveying was began in 1963 under the direction of G. F. Brown, USGS, for Sheikh Ahmed Zaki Yamani, Minister of Petroleum and Mineral Resources. The aerial work was extended in 1962, 1965-67 and to the present (1984) to include airborne magnetic and total-gamma radiation measurements. In 1963, the U. S. Geological Survey sent W. C. Overstreet, Richard Goldsmith, R. F. Johnston, J. W. Mytton, J. W. Whitlow, C. L. Hummel, and V. A. Trent to carry out reconnaissance and geochemical sampling under the direction of G. F. Brown; G. H. Sultan, Abdullah Ankary, Hashim Hakim, and Jamil Kouther, all of the Saudi Arabian Directorate General of Mineral Resources, assisted and mapped areas on their own responsibility. The early field work was supported by limited geochronological laboratory work by the Carnegie Institution, Washington.

Early in 1964 the Japanese Geological Survey sent a team of seven geoscientists to Arabia under the direction of Dr. Shizuka Okumi, and then, in 1966, under Dr. Ken Kirayama. These scientists concentrated their activities on specific mineral occurrences with emphasis on geochemistry and detailed mapping.

In 1965 the French Bureau de Recherches Geologique et Minieres (BRGM) began work for the Ministry, consisting mostly of areal mapping and prospecting, when they were given responsibility for a 140,000 km^2 region that was subdivided into three areas of the Arabian Shield. Begun under the direction of Jacques Reneaux, later under J. J. Altmann, much of the mapping has been directed by G. Eikelboom, J. Delfour, M. Bertucat, and currently C. Pellaton, as Chief Geologists. Under their direction and with their participation, quadrangle mapping has been accomplished by 25 geologists, supported by K-Ar and Rb-Sr isotopic dating in France (Baudron and others, 1976).

Acknowledgments

Thanks are due many members of the Government of Saudi Arabia who helped in the field, financed the work, and made the surveys possible. Of these, the work was started under the guidance of the late Sheikh Abdullah Sulaiman, former Minister of Finance, continued under Sheikh Abdullah Tariki, former Minister of Petroleum and Mineral Resources, and completed under Sheikh Ahmed Zaki Yamani, present Minister of Petroleum and Mineral Resources. Dr. Fadil Kabbani, former Deputy Assistant Minister of Petroleum and Mineral Affairs,

directed much of the later phases and accompanied G. F. Brown in the field in northwestern Arabia and east of Jiddah. Sheikh Ghazi H. Sultan followed Dr. Kabbani as Deputy Minister and both he and Sheikh Mohammed Qusai Assad provided assistance vital to the completion of this report. G. H. Sultan, Abdullah Ankary, A.Y. Bagdady, Haskim Hakim, A.M. Helaby, F. M. Kana'an, Ziad-al Koulak, M. M. Mawad, Mohammad Naqui, J. H. Kouther, Ghanum Jeri, Misfir bin Yam, A. O. Ankary, R. G. Bogue, Gus Goudarzi, and Wallace McLain spent many arduous months in the desert. K. S. Twitchell kindly made his field notes available, and Daniel Schaffner supplied his mine examination reports and the geologic reports written by members of the Saudi Arabian Mining Syndicate. Dr. Kabbani supplied the reconnaissance reports of the Bundesanstalt fur Bondenforschung, the notes of Sheikh Ahmad Fakhry who had earlier searched extensively for lost mines with Twitchell, and various unpublished reports prepared by the Directorate of Mineral Affairs.

Viktor Kahr, working for the Ministry of Petroleum and Mineral Affairs, mapped 7650 km^2 in northwestern Arabian and 1500 km^2 along the eastern edge of the shield. In addition A. Al-Shanti mapped 2,000 km^2 of the eastern shield and areas near Jiddah; W. K. Liddicoat mapped 10,000 km^2 north of Jiddah; and F. M. Kana'an mapped 2,850 km adjacent to Liddicoat's map, as did J. Kouther. Karl Nebert mapped 2,400 km^2 also north of Jiddah and 1,500 km^2 at the eastern edge of the shield, as well as directed work by students of the Research Center for Applied Geology along the northern flank of Wadi Fatimah between Jiddah and Makkah. These areas have been incorporated into our compilation together with later work where available from BRGM, Ministry geologists, Japanese Geologic Survey, and members of the geological department of King Abdulaziz University.

The French Oil Company Auxerap studied the coastal strip under the direction of Dr. Michel Gillmam in 1966 and 1967. They made their report available and gave permission for incorporation of the measured stratigraphic section of the Khums and Amran Formations.

P. K. Theobold, Jr., and Charles Thompson, USGS, gave support in geochemical prospecting and chemistry. Concurrently, W. J. Dempsey initiated a geophysical and diamond-drilling program, and the Topographic Division, USGS, sent G. W. Harbert, J. S. Crabtree, and T. E. Taylor to prepare the base maps and supervise aerial photography. Later this work was continued by F. G. Lavery, K. S. McLean, R. C. Nixon, G. C. Myers, C. M. Robins, and R. H. Tucker. A special team composed of R. E. Kenfield, G. E. Morrison, Jr., R. C. Nixon, A. A. Shands, W. E. Smith, and D. J. Winstead came to prepare topographic maps of the phosphate-bearing area in Wadi Sirhan near the Jordan frontier. More recent topographic map control has been continued by F.J. Fuller and D.J. Faulkender.

Under a 3-year extension, 1966-1969, of the 1963 agreement, which ended essentially in 1966, and subsequent to the earlier reconnaissance photogeologic mapping and search for mineral deposits, the work became more intensive in areas considered of greatest economic potential. It consisted of geological mapping, mostly at a scale of 1:100,000 (some more recently has been compiled at a scale of 1:250,000), utilizing helicopters and support by geophysical, geochemical, and drilling activities as well as petrographic, chemical, and geochronological support in the laboratory. A second 3-year extension of the working agreement began in 1969, continuing the work initiated in

1966 under the direction of G. F. Brown. This new extension was directed first by J. J. Norton, later by T. H. Kiilsgaard, followed by Frank Simons, and Donald Hadley, all assisted by R. O. Jackson. Currently, R. O. Jackson is continuing the direction of the field party. The program has continued to the present (1984); the last 9 years of work has been a part of the Saudi Arabian first and second Five Year Development Plans as directed by Sheikhs Ahmed Zaki Yamani and Ghazi Sultan. USGS geologists who contributed to the geologic and economic knowledge during the extended time include D. L. Schmidt and D.B. Stoeser as Chief Geologists, G. H. Allcott, R. E. Anderson, W. R. Brock, D. A. Brobst, R. W. Bailey (deceased), F. W. Cater, J. C. Cole, R. G. Coleman, H. R. Cornwall, F. G. W. Dodge, J. L. Doehrich, E. A. DuBray, R. L. Earhart, J. E. Elliot, G. M. Fairer, D. L. Gaskil, D. J. Faulkender, W. D. Fenton, R. C. Greene, Louis Gonzalez, W. R. Greenwood, D. G. Hadley, F. Hershey, K. S. Kellogg, R. W. Luce, Conrad Martin, C. R. Meissner, J. S. Pallister, W. C. Prinz, J. S. Ratte, R. J. Roberts, L. F. Rooney, D. L. Rossman, E. G. Sable, R. P. Sheldon, C. W. Smith, P. K. Theobald, F. V. Tompkins, A. E. Weissenborn, J. W. Whitney, K. L. Wier, and R. G. Worl. R. V. Allen, G. E. Andreasen, R. H. Blank, W. F. Davis, V. J. Flanigan, M. E. Gettings, Andrew Griscom, S. A. Hall, D. L. Hase, D. R. Mabey, and J. A. Pitkins gave geophysical support. R. W. Girdler served as consultant. After L. T. Aldrich's and T. W. Stern's pioneer work in geochronology, C. E. Hedge, R. F. Marvin, H. H. Mehnert, V. Merritt, B. R. Doe, and R. J. Fleck analyzed shield rocks for isotopic ratios and estimates of age. J. A. Cooper and J. S. Stacy analysed zircon by the U, Th-Pb method for dating (Cooper and others, 1979). J. F. Sutter measured $^{40}Ar/^{39}Ar$ of a sample from the youngest flows in the craton. Chemical analyses were made under the direction of M. Gonshor, and later of W. L. Campbell and K. J. Curry. Petrographic work was first directed by D. H. Johnson, followed by R. W. Luce, F. C. W. Dodge, and J. J. Matzko. Audrey Schmidt prepared many of the illustrations.

For this report Salman Bloch assisted with petrographic work and geologic compilation from March 1975 until April 1977. Subsequently, Richard Hoeksema recalculated the geochronological data to new constants published by the International Subcommission on Geochronology (Steiger and Jager, 1977) and plotted the histograms.

And finally it is impossible to give sufficient credit to Wenonah Bergquist who edited the report and supervised preparation of illustrations. Her sustained counsel and encouragement made completion possible.

GEOGRAPHY

Physical geography

Climate

Arabia lies in the center of the great trade-wind desert which extends across northern Africa into Asia. In Arabia, important modifications of its hot dry desert climate are due to the effect of the Red Sea and the flanking mountain ranges of Ash Shifa', Hijaz, and 'Asir.

Rainfall is meager and episodic, ranging from a minimum mean annual of less than 2 cm in the north to a maximum of about 30 cm along the southern crest of the 'Asir range in the southwest. Most of the region probably has an average annual rainfall of 10 cm (see fig. 3), but systematic records have been kept only for recent years. At Mahd adh Dhahab, in west-central Arabia, a 14-year record shows a range from a minimum of 1.2 cm to a maximum of 13.1 cm, with an average of 6.2 cm. At Jiddah, on the Red Sea coast, where the average is about 8 cm, infrequent rains during the last 15 years have been as much as 15 cm, falling within a few hours, although there are some years when no rain falls. Indeed, parts of the vast interior region, particularly north of Al Madinah and east of the 'Asir, have had no rain for periods of several years, according to Bedouin accounts and as attested by the sparseness of the vegetation. The northern regions, within the belt of westerly planetary winds, have winter precipitation. In the southern region, the monsoon season of late summer is marked by moisture-laden winds which, blowing from the southwest against the western rim of the high plateau of Yemen and Hijaz ('Asir), are forced upward to furnish the greatest precipitation along the crest. Records kept at San'a' in the Yemen, east of the crest, show an average of 30.2 cm (minimum 15.4 cm, maximum 49.5 cm), with the heaviest precipitation in July and August and a secondary peak in April. At Ar Riyad, in central Arabia, a 7-year record shows an average of 10 cm (minimum 2.8 cm, maximum 23.8 cm), almost all precipitation falling in the winter and spring months.

Even if rainfall could be recorded for many years, the episodic and local nature of most precipitation makes averages of doubtful value. A better guide has been provided by the late Dr. John Tothill's study of the vegetation along the Red Sea coast and in the 'Asir. He drew on his knowledge of the vegetation in the Sudan where rainfall records have been kept, and which allowed him to correlate precipitation with various index genera and floral groups common to the Sudan and western Arabia. Figure 3 is mainly based on his work, and is compared to a record compiled by Ali H. Al-Shalash, University of Riyadh, from 60 stations for a period of 3 to 14 years (Ministry of Agriculture and Water, written commun., 1974).

Temperatures range from below freezing during the winter months in the mountains and high plateaus to summer maxima of about 120° F (44.5°C). Temperatures have large diurnal ranges (table 1)--sometimes as much as 60° F (16° C)--caused by the rapid transmittal of heat from the bare rock surfaces as the desert passes from night to day and day to night.

Relative humidity (table 2) during the day is low away from the sea coast--in the summer about 10 percent, in the winter 45 percent, according to the fragmentary records that have been kept. The large diurnal range of temperature often produces an early morning dew when the rock surfaces and nearby air have cooled below the dew point; however, the low humidity and the first rays of the morning sun quickly evaporate it. The high humidity and heat along the Red Sea cause much discomfort and lethargy, especially as the dampening effect of the sea often holds the air temperature at a high level throughout the night.

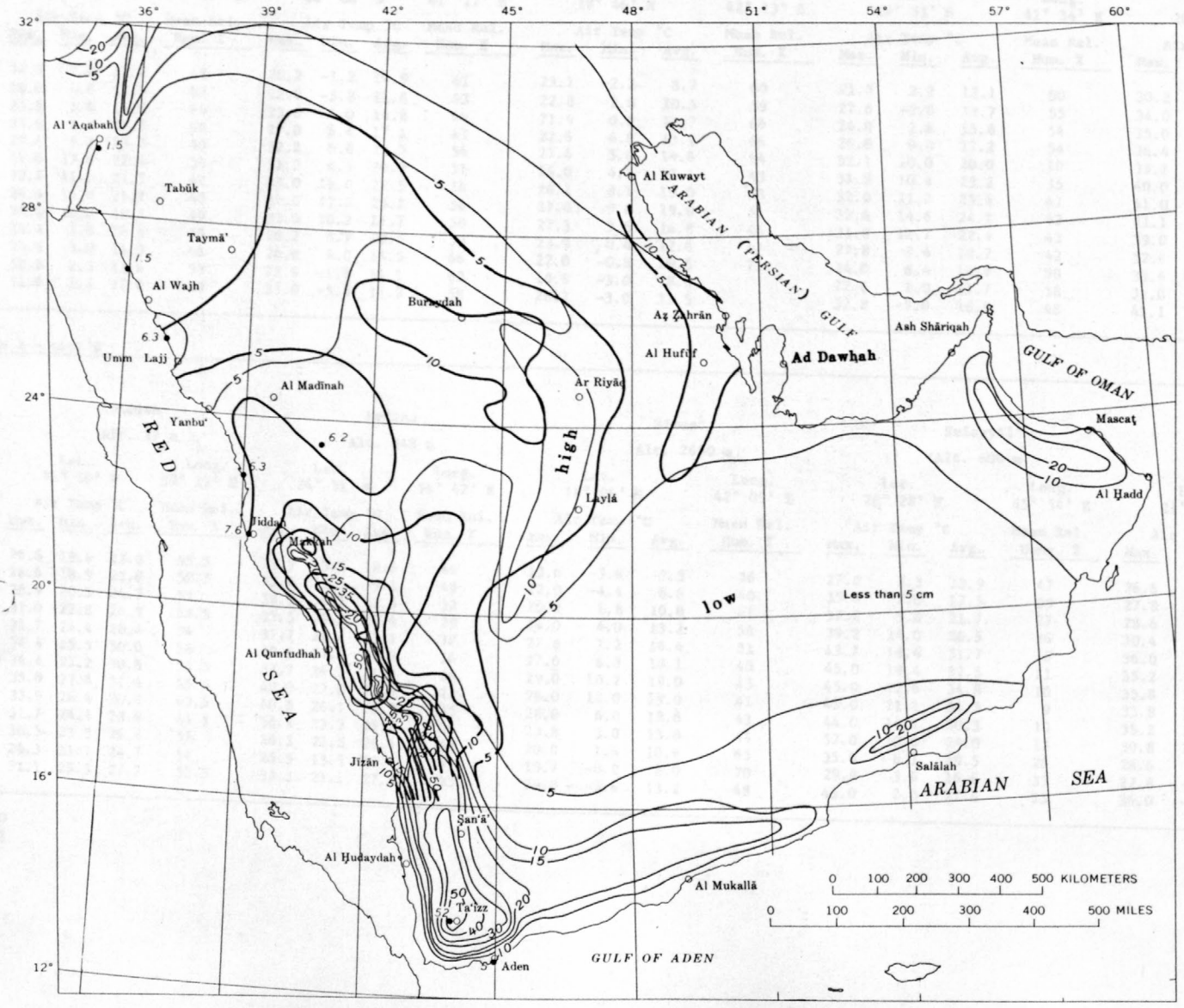

EXPLANATION

10

Rainfall contour

Contour interval 5 centimeters. Dashed where queried. Based on vegetation studies of J. D. Tothill plus records of precipitation.

50

Contour showing mean annual rainfall based on record for 3 to 14 years (average 5 years) at 60 stations. Contour interval variable in centimeters. Based on records compiled by Ali H. Al-Shalash, University of Riyadh, from weather stations of the Ministry of Agriculture and Water.

7.2

Point recordings of precipitation or estimate from vegetation.

Figure 3. Estimated rainfall distribution in the Arabian Peninsula.

Table 1. Temperatures (degrees centigrade) and relative humidity (%) at selected sites in Western Saudi Arabia
After Ministry of Agriculture and Water

Table 1

	Abha*				Al Mindak[1]				Belesmer[1]				Biljurshi[1]				Bishah[1]				Ha'il[1]			
	Alt. 2200 m				Alt. 1920 m				Alt. 2250 m				Alt. 2040 m				Alt. 1040 m				Alt. 1010 m			
	Lat. 18° 13' N			Long. 42° 29' E	Lat. 20° 06' N			Long. 41° 17' E	Lat. 18° 46' N			Long. 42° 13' E	Lat. 19° 51' N			Long. 41° 34' E	Lat. 20° 00' N			Long. 42° 36' E	Lat. 27° 28' N			Long. 41° 38' E
	Air Temp °C			Mean Rel.	Air Temp °C			Mean Rel.	Air Temp °C			Mean Rel.	Air Temp °C			Mean Rel.	Air Temp °C			Mean Rel.	Air Temp °C			Mean Rel.
	Max.	Min.	Avg.	Hum. %	Max.	Min.	Avg.	Hum. %	Max.	Min.	Avg.	Hum. %	Max.	Min.	Avg.	Hum. %	Max.	Min.	Avg.	Hum. %	Max.	Min.	Avg.	Hum. %
Jan	22.2	1.2	11.2	68	20.2	-1.2	10.9	61	23.1	-2.2	8.7	60	21.8	2.2	12.1	50	30.2	3.8	16.9	45	23.6	-3.0	10.1	54
Feb	20.0	4.8	13.3	67	22.0	-5.8	11.6	63	22.8	-2.0	10.5	59	22.6	-2.0	12.7	55	34.0	5.0	19.9	43	27.0	-4.4	12.0	45
Mar	23.0	2.8	14.8	64	23.6	4.0	14.8	64	21.4	0.5	11.7	66	24.0	3.8	15.8	54	35.0	9.0	22.4	36	30.4	1.6	17.2	31
Apr	25.8	9.2	17.8	56	27.0	6.4	17.1	63	22.6	4.8	13.1	66	26.0	9.0	17.2	54	36.4	13.0	24.8	41	33.1	7.0	19.3	30
May	29.6	8.8	20.3	40	32.2	6.8	19.5	54	27.6	5.0	14.6	64	32.1	10.0	20.0	40	39.1	16.8	27.9	40	38.8	12.4	25.2	23
Jun	31.0	13.6	22.4	34	31.2	6.5	20.9	51	26.0	4.2	17.1	43	31.2	10.4	23.2	35	40.0	14.8	28.0	27	38.0	15.0	26.6	15
Jul	29.4	11.6	21.3	42	33.0	11.0	22.5	54	28.2	8.1	19.0	43	32.8	11.2	23.6	41	41.0	18.0	30.3	26	41.0	18.0	30.1	13
Aug	29.4	14.0	21.7	40	32.2	11.2	23.2	56	27.8	9.8	19.0	51	32.6	14.6	24.1	43	41.1	19.4	30.8	30	41.0	19.0	30.1	15
Sep	29.0	10.0	19.4	40	32.0	10.2	21.7	50	27.3	3.6	16.8	46	31.9	11.7	22.4	43	39.0	10.0	26.4	28	40.2	13.2	27.7	13
Oct	25.4	7.0	16.6	39	28.2	5.7	18.5	50	23.0	0.4	12.6	47	27.8	8.4	18.7	42	32.6	6.6	20.0	23	34.2	8.0	21.6	16
Nov	23.0	5.0	14.0	46	26.6	4.0	14.5	66	22.0	-0.8	10.5	71	24.0	6.4	14.7	58	33.6	5.1	20.9	37	31.0	2.2	16.4	32
Dec	18.8	2.3	11.6	53	22.8	-1.8	11.1	62	19.8	-3.0	8.0		22.6	1.0	11.7	58	31.0	2.0	16.7	44	27.2	-5.0	9.8	45
Ann	31.0	1.2	17.0	49	33.0	-5.8	17.2	58	28.2	-3.0	13.5		32.8	-2.0	18.0	48	41.1	2.0	23.8	35	41.0	-5.0	20.5	28

Table 1 - cont'd

	Jiddah				Medina				Nimas[1]				Sulayyil[1]				Taif (Howiyah)[1]				Turayf			
	Alt. 17 m				Alt. 648 m				Alt. 2600 m				Alt. 600 m				Alt. 1530 m				Alt. 850 m			
	Lat. 21° 30' N			Long. 39° 12' E	Lat. 24° 31' N			Long. 39° 42' E	Lat. 19° 06' N			Long. 42° 09' E	Lat. 20° 28' N			Long. 45° 34' E	Lat. 21° 24' N			Long. 40° 27' E	Lat. 31° 41' N			Long. 38° 40'
	Air Temp °C			Mean Rel.	Air Temp °C			Mean Rel.	Air Temp °C			Mean Rel.	Air Temp °C			Mean Rel.	Air Temp °C			Mean Rel.	Air Temp °C			Mean Rel.
	Max.	Min.	Avg.	Hum. %	Max.	Min.	Avg.	Hum. %	Max.	Min.	Avg.	Hum. %	Max.	Min.	Avg.	Humg. %	Max.	Min.	Avg.	Hum. %	Max.	Min.	Avg.	Hum. %
Jan	26.6	19.4	23.0	55.5	23.9	13.3	18.6	46	12.6	-5.6	3.3	36	27.6	2.3	13.9	47	26.6	3.2	14.2	36	17.2	4.4	10.8	56
Feb	26.6	18.9	22.8	52.5	25.0	13.3	19.1	42	17.0	-4.4	8.6	40	35.6	2.0	17.5	39	27.8	1.8	16.6	37	15.5	3.3	9.4	49
Mar	28.9	20.5	24.7	52	28.9	16.1	22.5	32	20.2	1.8	10.8	41	37.2	5.8	21.7	27	28.6	9.8	19.5	42	20.0	6.7	13.4	48
Apr	31.0	22.8	26.9	54.5	35.5	23.3	29.4	29	24.0	4.0	13.2	58	39.2	14.0	26.5	26	30.4	10.0	20.2	34	26.6	19.4	23.0	26
May	32.7	24.4	28.6	54	37.7	24.4	31.1	37	27.8	7.2	16.4	51	43.7	18.4	31.7	18	36.0	8.0	22.9	29	32.7	15.4	24.1	17
Jun	34.4	25.5	30.0	56	40.5	27.8	34.2	16	27.0	6.8	18.1	40	45.0	18.4	32.5	11	35.2	14.8	26.1	15	37.7	20.0	28.9	21
Jul	34.4	27.2	30.8	53.5	37.7	26.1	31.9	26	29.0	10.2	19.0	43	45.0	22.6	34.8	10	35.8	16.8	27.2	18	35.5	20.0	27.8	19
Aug	35.0	27.8	31.4	55.5	40.0	27.8	33.9	22	28.0	12.0	19.0	41	45.0	21.1	34.5	9	35.8	18.8	27.3	20	37.7	20.5	29.1	18
Sep	33.9	26.6	30.3	63.5	40.5	26.1	33.3	25	28.0	6.0	18.0	43	44.0	14.1	30.3	10	35.2	13.0	25.0	18	32.7	16.7	24.7	16
Oct	32.7	24.4	28.6	61.5	36.1	23.3	29.7	26	23.8	3.0	13.8	44	37.0	10.0	24.0	13	30.8	10.2	20.8	24	28.9	14.4	21.7	26
Nov	30.5	23.3	26.9	57	28.3	27.8	28.1	43	20.0	1.4	10.6	65	35.0	6.1	19.5	26	28.6	8.2	18.0	36	18.9	9.4	14.2	41
Dec	28.3	21.1	24.7	54	25.5	13.3	19.4	47	19.7	-0.2	8.0	70	29.9	3.6	16.6	35	27.8	-1.4	13.6	36	17.2	4.4	10.8	53
Ann	31.1	23.3	27.2	55.5	33.3	21.1	27.2	33	29.0	-5.6	13.2	48	45.0	2.0	27.6	25	36.0	-1.4	21.0	29	26.6	12.2	19.4	33

*1970
[1]1971

Winds range widely in direction and velocity. A prominent northwesterly, the 'shimal,' blows strongly in spring and early summer in the central and eastern parts of the country. A southwestern wind direction in northwestern Arabia has produced prominent yardang troughs north of lat 24° N. Sand and dust storms are common, and eolian landforms and deposits are conspicious in the younger terranes (see fig 66a).

Human geography

Long the home of wandering Bedouin who traditionally follow the rains for forage, Saudi Arabia is changing rapidly as the few larger populated places grow at the expense of the nomadic groups and the smaller agricultural communities. Makkah, the religious center of the Moslem world, now has a permanent population of at least 200,000 (1980) which increases manyfold during the annual pilgrimage, as does that of Jiddah, the port for Makkah, which has a population of more than 1,300,000 (1980). Al Madinah, the second holy city, had a permanent population of perhaps 40,000 which has increased substantially in recent years, besides a very large influx during the annual pilgrimage season. At Ta'if, the summer capital near the crest of the Hijaz range east of Makkah, is comparable in size to Al Madinah and likely to grow at an increasing rate, provided there is sufficent water. The only large inland city is Ar Riyāḍ, the political capital, which has a population of about 1,000,000 (1980). Recently an important industrial complex is being built near Yanbu' Al Baḥr at the terminus of the east-west pipeline from Al Hasa.

A series of small agricultural communities extends southward from At Ta'if along the mountain crest through the southern Hijaz and the 'Asir into Yemen. They comprise the districts of Ghamid, 'Asir, Sarat, and Ẓahrān, increasing in size and number southward. Starting from about lat. 20 N., a similar series of villages and cultivated tracts extends toward the south at the seaward base of the range, culminating in several large villages in the Jizan basin just north of the Yemen frontier. The topographically higher communities practice terrace cultivation, whereas the Red Sea coastal plain (The Tihamat) and the inland valleys are cultivated by flood-diversion, supplemented in the Jizān area by a modified terrace or basin type, where there is sufficient rainfall. A new dam on Wadi Jizān supplies irrigation water to the area around Abū 'Arish.

About 90 percent of all cultivated land and most of the predominant agrarian communities in Saudi Arabia lie within two belts in the southern Hijaz, 'Asir, and the southern Tihamat; the seaports of Al Lith, Al Qunfudhah, and Jizān serve as outlets for the area. Going eastward toward the desert, the villages are replaced by semi-nomadic and nomadic groups.

Small ports and fishing villages are situated along the Red Sea north of Jiddah at Rabigh, Yanbu' Al Baḥr, Umm Lajj, Al Wajh, and Ḍubā, in general decreasing in size and importance northward. The small village of Aynunah is situated at the northeastern corner of the Red Sea, whereas Maqna and Haql are on the eastern shore of the Gulf of Aqaba. Several other small communities lie in the larger wadi valleys north of Jiddah; there is also a string of settlements in Wadi Fatimah east of Jiddah. These extend as far north as Yanbu' an Nakhl, directly west of Al Madinah, beyond which there are almost no permanent settlements except on the coast; the most

important of the inland villages are Madrakah, Khulays, Ḫamamah, Ḫaqqaq, Ar Rayyān, Badr Ḫunayn, Al Hamrā', and Al Musayjid. In the upland of the Hisma, the only settlements of any size are at Al ʿUlā and Tabūk, although Khaybar and Al ʿUlā are on the edge of the upland. Al Badʿ in Wadi ʿIfal, which forms a valley in Jabal ash Shifā' east of the Gulf of Aqaba in northwestern-most Saudi Arabia, has a small settled community.

Inland on the crystalline desert plateau are palm oases and farms at Qalʿat Bishah, Turabah, Khurmah, and Ranyah, all separated by wide expanses of stony desert. Farther north, in the northern Hijaz, the populated places are smaller and more widely spaced. Of these Ashshara, Al Muwayh, Ad Dafinah, ʿAfif, Al Qāʿiyah, and Ad Dawadimi lie along the At Ta'if-to-Ar Riyāḍ road; Hādhah, Sufaynah, Al Ḫanākiyah, Al Khalf, Al Ḫuwayyiṭ, Al Hayit, and Zarghat are small villages along the eastern edge of the lava fields that extend (where water is available) from near At Ta'if northward to lat. 27° N. The ancient community of Khaybar occupies a similar position on the western edge of the lava fields north of Al Madinah. East of Qalʿat Bishah, beyond the four small villages which extend northward down the wadi for 40 km, there are no permanently inhabited settlements until the constriction of Wadi ad Dawāsir at the east edge of the crystalline plain is reached, some 200 km distant. Northeastward from Bishah no villages are found until Ṣabhā', some 400 km away, is reached. To the north beyond Ṣabhāʾ several villages--Sanam, Ar Ruwayḍah, Muḥayriqah, Quḍayʿān, and 'Arwa', lie at wadi constrictions, where there are slight local increases in ground water supply.

Hā'il, the capital of the Jabal Shammar Province, has a population of about 5,000 and is located where dikes and a wadi constriction impound some ground water beneath a grus plain. Toward Hā'il, in the northeastern corner of the crystalline shield, the most important villages are Dariyah, Miskah, An Nabhaniyah, Al Fawwarah, Samirah, Tahah, Fayd, Al'Uqaylat, Ghazzalah, Mawqaq, and Qufar.

Flora

Acacia, or camel thorn, is the most widespread, and in many places almost the only shrub and small tree of the western desert. The acacia "samr" (Acacia tortilis (Forsk) Hayne), perhaps the hardiest, may be found growing along the wadis or, where rainfall is slightly higher, on the desert plains as isolated flat-topped trees or copses. The acacia "sallam" (Acacia ehrenbergiana Hayne) is also widespread, growing in clumps or thickets along wadi floors, as it requires more water than the samr. In the high mountains the acacia locally called "talh" (Acacia seyal?) probably includes more than one species; it grows into trees larger than "samr" or "sallam". There are several others species, but none of the acacias are true phraeatophytes, indicating land without a permanent water table; most vegetation away from the mountains and seacoast is mesophytic, growing only when rain falls (Vesey-Fitzgerald, 1957).

The most important of the Arabian phraeatophytes are the date palm "nakhla" (Phoenix dactylifera L.); the "sidr" (Zisyphus spina-christi L. Willd), with its lacey foliage and haw-shaped fruit rich in vitamins; the two tamarisks "tarfa" and "ithil" (Tamarix orientalis Forsk and Tamarix macrocarpa (Ehrenb.) Bunge), the "dom" palm (Hyphaene thebaica (Del.) Mart.) and the "rak" (Salvadora persica L.) or "toothbrush shrub" which forms rings of dense

vegetation, often growing on small dunes and maintaining a root system below the sand. The halfa grass (Desmostachya cynosuroides Stapf) is common in the upper stretches of wadis in the southern part of the country.

A distinct flora grows where salty or saline ground water is present, especially along the Red Sea coast, dominant plants being the succulent salt bush Suaeda (represented by two or three species), the sea lavender (Statice axillaris), the mangrove reef fringing copses (Rhizophora sp., Bruguiera sp., or Avicennia marina) are prominent only south of Qunfidah at lat 18°30' N. (Vesey-Fitzgerald, 1955).

In vast stretches of the western desert, where many of the acacias have been burned for charcoal, vegetation is limited to forage shrubs and grass which spring into foliage and flower after rains. The hamdh vegetation is largely Salsola tetrandra Forsk, which grows in saline conditions, but there are also at least five other shrubs. The rimth vegetation is largely Haloxylon schweinfurthii Ascherson, which is favored for camel grazing. Another widely scattered bush is the harmal (Rhazya stricta) or African rue (Peganum harmala). The grasses Panicum turgidum Forsk, and Lasiurus hirsutus (Forsk) Monro are widespread, growing in clumps that furnish forage for camels, sheep, and goats, and are often gathered for hay.

Many unusual plants and trees grow in the Hijaz and 'Asir. Of these the juniper "ar'ar" (Juniperus macropoda Boiss. or Juniperus procera Hochst. (Mandaville, 1973) is the only important conifer in Arabia. It grows in small forests or groves along the crest of the 'Asir where rainfall is 12 in. (4.7 cm) or slightly higher. The largest tree in Saudi Arabia, Acokanthera deflersii Schwein, grows only in the upper foothills east of Jizan (fig. 4). The wild fig (Ficus salici folia Vahl), the tamarind (Tamarindus indicus L.), the poinciana (Delonix elata L. Gamble), the dragon's blood tree (Dracaena ombet Kotschy and Peyr), the sandalwood (Osyris compressa Berg.), the aloes, the 'ishr (Coloptropis sp.) with milky rubber-producing sap, and the Adenium sp. or poison bush with beautiful pink or red flowers, are of special interest. The cactus-like Euphorbia is represented by several species, there being no indigenous cacti on the peninsula, although the prickly pear, Opuntia sp., has been imported for its fruit.

Food crops in Arabia are grown mostly in the 'Asir where the mountain slopes are terraced to hold the rain, along wadis draining the 'Asir and Hijaz, and in scattered isolated oases where ground water sustains the date palm, grains, fruit trees, vegetables, and hay. The most important by far are dates; wheat and barley; the nonsaccarine sorgums, dhura and dukhn; corn; and alfalfa. Fruit besides dates include olive, fig, orange, lemon, lime, pomegranate, grape, cactus apple, apricot, banana, and guava. The vegetables currently cultivated include beans, squash, eggplant, okra, tomato, lettuce, cabbage, onion, carrot, pepper, and potato. Three varieties of truffle grow wild in the desert following fall and winter rains, and several varieties of melons are hauled to the markets in season.



a) Acokanthera deffersii schwein



b) Tamarix macrocarpa

Figure 4. a) Acokanthera deffersii schwein - largest indigenous tree in Arabia. Junction Wadi Qaah (Yithrib) and Wadi Shini near Jallat al Mawt. b) Tamarix macrocarpa (Ehrenb) Bange, c) Zisyphus spini-christi, L. Willd, and, d) Tamarindus indica. These are examples of a few phreatophytes, indicating permanent ground water.



c) Zisyphus spini-christi



d) Tamarindus indica

Relation of flora to rainfall

by J. D. Tothill [1]

Field work for a study of the floral zones of the Coastal Plain or Tihamat, between Jiddah and the Yemen frontier, and of the 'Asir Mountains was done in 1950 and 1951 when the Food and Agriculture Organization of the United Nations was examining the possibility of supplementing the existing irrigation systems of the coastal plain in Jizan Province. From time immemorial, primitive to well developed irrigation systems were employed on the principal rivers that rise in the 'Asir Mountains and form desert deltas on the Tihamat. With the increase of population and need for more food, both for mankind and domestic animals, some reinforcements by means of barrages had become necessary.

The size and number of barrages that would be required depends on the rainfall in the catchment areas, and an estimate of rainfall accurate enough to use as a basis for the size of the barrage projects was urgently needed. No rainfall records had ever been kept for the area, and it was not practical to wait for a decade or longer for meteorological observations to be made. In these circumstances it was decided to test the possibility of defining natural floral zones based on rainfall on the mountains. Seven zones were eventually distinguished and a rainfall estimate made for each (fig. 2).

The plan was to make three widely separated traverses down the face of the mountains, to establish as many zones as could be easily recognized by the coming in or disappearance of readily identified definitive, or index, plants, and then to determine rainfall for each zone. The area of each zone would be calculated from an aerial survey map by joining up the zone contours for the three traveres.

Despite the wild ruggedness, precipitate steepness, and inaccessibility of the upper 2,000 ft of the western face of the mountains, the plan worked out quite well. Seven easily recognized zones were eventually defined and their definitions, extent in the 'Asir area, and probable rainfall are given below. The project proved to be of considerable practical value as its findings were used as the rainfall basis for designing the required barrages.

The traverses of the western face of the 'Asirs were made by the ascent of Jabal Fayfa, Wadi Baysh, and Wadi Itwad.

During the field work on the coastal plain, I had the stimulating companionship of Dr. Van der Plas. For the three traverses of the 'Asir, I was most happily accompanied by Thomas Smallwood [1], a specialist in water supplies for irrigation purposes. For the journey down Wadi Ga'a and into the main Wadi Baysh I am deeply indebted to Dr. Glen Brown, a geologist of the U. S. Geological Survey whose friendship and stimulating ideas I came greatly to value.

[1] Deceased

The Saudi Arabians were both our hosts and friends, and it is a pleasure to acknowledge the many acts of courtesy and kindness shown us by a long list of local residents from the late King Abdul Aziz ibn Saud and his sons, the late Kings Saud and Faisal, down through all walks of life to humble folk who helped us in our daily tasks.

Plant specimens were determined through the kindness of Dr. Taylor, then Custodian of the Herbarium and Head of the Botanical Department of the British Natural History Museum. Miss D. Hillcoat did most of the determinations and to her I owe a special debt of gratitude.

Basic plant collections in southwest Arabia have been made by Scott and Britton of the Expedition sponsored by the British Natural History Museum, and in recent years Vesey-Fitzgerald has added important collections both from the coastal plain and the mountains. My own collection of some 170 named species supplements those made by Scott, Britton, and Vesey-Fitzgerald and was made from the somewhat narrower point of view of discovering and delineating floral zones. In a few cases material was insufficient or inadequate for sending to the Museum, and it was necessary to make provisional determinations. This applies particularly to the free form of Acacia etbaica Schweinf. and to Commiphora africana (A. Rich.) Engler.

The seven zones

As there are no names in general use that fit the seven zones, it seemed best to use names that could easily be learned and understood by anyone working in Arabia. The country people of Saudi Arabia are good botanists and have Arabic names for all the index plants used, and they will naturally use these names instead of the few Latin names that have seemed necessary here.

The zone-defining plants were identified as a result of making a collection of every species that was in blossom or in seed or in a recognizable condition of any kind. This was done on all the journeys made, and the distribution of each plant was noted. The collection was eventually handed to the Botanical Department of the British Natural History Museum for determination, because its herbarium is particularly rich in material from Arabia and the Middle East: this proved to be a most happy arrangement.

The rainfall estimates are based partly on the known isohyet limits of definitive plants that also happen to occur in the Sudan where there has been a long history of botanical collecting, culminating in the three fine volumes on "The Flowering plants of the Sudan" by Dr. F. W. Andrews, and where rainfall statistics have also been compiled for many years.

For the barley zone, the estimates are based on the known minimum requirements for crops in the Soluch area near Bengazi; for the agricultural zone the estimates represent the writer's personal opinion of the rainfall required to produce regular good yields of barley, wheat, lentil, and alfalfa on that sort of soil and in that climate. In all cases the definitive plants or crops are supposed to be growing as pure rain crops unblessed by added water from a dry wadi, or by run-off water collected naturally or by human wit.

In order to fit the seven zones into their places, it seems both logical and useful to commence the discussion with three of the driest zones in Arabia, which, however, are not represented on the western face of the 'Asir Mountains.

Ar Rub al Khali zone.--The driest of all zones in Arabia coexists with the geographical Ar Rub al Khali, or literally The Empty Quarter, and as this name is so widely known, it seems proper to use it for the driest of the floral zones. It is too dry to support trees or shrubs, and vegetation is limited to grasses and other plants that spring to life after receiving rain from one of the rare and sporadic showers that may occur.

Throughout the zone there are dry wadis, and the large ones may carry ground water for many miles. The best of these intruding tongues support the vegetation of wetter zones, and although these tongues occur in the geographical Ar Rub al Khali, they are here excluded from the floral zone of that name.

The rainfall for the zone can be estimated to be only a trace in the driest part, ranging to a shade less than 2 inches at the boundary with the next zone. The 2-inch limit is fixed by the fact that in the northern Sudan the boundary-defining shrub samr, Acacia tortilis, disappears as one proceeds northward into the Sahara at approximately the 2-inch isohyet.

The zone occurs in many pockets outside Ar Rub al Khali of the maps, as for instance in the hills behind the port of Al Wajh which include the ancient mine workings of Al Hurayrah.

The samr desert zone.--This zone is marked by the fact that the conspicuous bush Acacia tortilis (Forsk) Hayne, known universally by Arabs on both sides of the Red Sea as samr, is dominant. It grows sparingly to abundantly depending on soil, but there is no other bush that remotely resembles it. The zone is extended into wetter areas to the point where the bush Acacia ehrenbergiana Hayne, universally known to Arabs as sallam, puts in an appearance.

In the Sudan the northern limit of distribution for sallam practically coincides with the 4-inch isohyet, so the samr zone extends from the 2- to the 4-inch isohyet. The zone is widespread in Saudi Arabia but on the coastal plain does not occur south of Jiddah.

The sallam desert zone.-This zone is characterized by the presence of the two well known acacias samr and sallam, and by the absence of Commiphora and Euphorbia cuneata. The acacias are about equally common.

On the Tihama the dry edge of the zone begins a few miles south of Jiddah where sallam comes, at first sparingly, onto the scene. For the next 200 miles there are many samr but few sallam, indicating a continuation of the dry edge. Between Wadis Hali and Itwad, however, the rainfall increases so that sallam becomes well grown and as abundant as samr. The zone extends for another 10 miles south until it becomes wet enough for Commiphora africana, or qaffal, and Euphorbia cuneata, known locally as 'maz.'

Nowhere in this zone can the grain dukhn, Pennisetum purpureum, be grown as a rain crop. In the Sudan 6 inches of rain are required for the poorest crop that is worth growing, so this affords a basis for assessing the wet boundary of this zone at a little less than 6 inches or perhaps 5 inches.

The Asak-Commiphora-desert zone.-The name calls attention to two of the index plants, Acacia asak, one of the thorn bushes called hashab by Arabs; and on the coastal plain Commiphora africana or "qaffal". The other two index plants are Anisotes trisulcus of the foothills, and the nonprickly Euphorbia cuneata of the Tihama which is widely used for supporting the thatch of village houses.

The two acacias samr and sallam reach their maximum development in this zone, as do the two important tufted grazing grasses of the samr and sallam zones, Lasiurus hirsutus Boiss. and Panicum turgidum Forsk. On the coastal plain this zone commences a little south of Wadi Itwad and extends through the Jizan Province to beyond the Yemen frontier. As to rainfall, the northern boundary was estimated to receive 5 inches.

Nothing in the vegetation indicates the rainfall for the southern boundary, but as one proceeds south through the zone, one finds that the millet dukhn, P. purpureus, is grown as a rain crop at about the latitude of Port Jizan, thus indicating a rainfall of 6 inches there. As this comes at about the middle of the zone, the southern boundary can be assessed by proportion as having rainfall of 7 inches.

A check on these estimates is that in the Sudan, Commiphora africana first appears as one proceeds south in Andrews' Acacia-desert-scrub region, fairly close to the northern boundary at about the 5-inch isohyet. This Commiphora is probably the same as, and certainly the ecological representative of, the coastal plain species of the Jizan.

The Kleinia-Pastoral zone.--This is a well-marked zone commencing on the western escarpment at about 5,000 feet, varying a little with aspect, where Anisotes and Acacia asak fade out. At this boundary the succulent composite herb Kleinia violacea, locally 'thuriya,' becomes an index plant, but it is not so common on the steep mountain slopes as on the plateau lands above.

Associated with it, however, is Acacia etbaica, or qarad of the Arabs. On the escarpment this takes the form of a vigorous bush or small tree as much as 15 feet high, but on the better lands above the scarp, it takes the form of a well-grown tree as much as 30 feet high.

The upper limit of the zone, at about 7,500 feet, is marked both by the appearance of Euryops and by the point at which barley comes to be grown as a purely rain crop. This zone is important, as it embraces the finest pastoral lands in southwest Saudi Arabia. The rainfall at the upper limit of the zone is that required for the growing of barley as a rain crop. Statistics are available for the Soluch area of Cyrenaica, Libya, situated on the coastal plain to the westward of Bengazi. The precipitation at this place is 7 inches, some 5.8 inches of which fall in the barley growing season. Barley is here regularly grown as a subsistance crop and this seems to show that 6 inches of rain is the minimum needed for this crop in

a Mediterranean climate. In tropical Arabia where barley is similarly grown on marginal lands, the sun is hotter and it seems reasonable to raise the estimate to 8 inches.

Barley is grown only in the long rains in this zone and for 8 inches of long rains, one must add 2 for the short rains, making a total of 10 inches. On this basis the Kleinia-pastoral zone begins at the 7-inch and extends to the 10-inch isohyet.

The Euryops-Barley zone.--This is preeminently the zone in which barley and wheat, where suitable lands are available, are regularly grown as subsistance crops on true rain lands that receive no additional subsoil or runoff waters. It is also marked by the conspicuous presence of the composite Euryope arabicus Steud, locally 'jabur,' which can be recognized from a distance even when not in bloom because it bears remarkable resemblance to a 2-ft high seedling of Scotch or similar pine. The herb is stiff as a pine and has a similarly symmetrical arrangement of branches, and completes the deception by having 2-inch long leaves so narrow as to suggest needles. The dominant, and only, acacia, Acacia etbaica Schweinf; finds optimum conditions in this zone and becomes a well grown(?) tree as much as 30 feet tall.

The upper limit of the zone is sharply marked by the lower altitude limit of the conspicuous and only conifer, Juniperus macropoda Boiss., which is likewise the lower limit for the bush Dodonaea viscosa Jacq.

We came upon fragments of this zone on Jabal Fayfa at what we estimated to be 4,000 to 4,500 feet; at El Ga'am on top of the escarpment 35 miles south of Abha at 7,500 feet by altimeter; near Aqabat al Alb on the Yemen frontier at 7,700 feet; and finally a fragment between Abha and Jabal Sawdah where it began and ended at 7,500 and 8,200 feet, respectively.

As to rainfall for the zone, the dry edge coincides with the minimum required for the regular cultivation of wheat and barley as rain crops which was estimated above to be 10 inches annually.

The wet edge is the boundary line for juniper. In the account by Hugh Scott and Everard B. Britton in the British Natural History Museum's "Expedition to South West Arabia 1837-38," vol. 1, no. 1-8, this species is recorded as occurring on Jabal Gelal some 25 miles south of Sana'a', Yemen. The rainfall at Sana'a' averaged 11.78 inches from 1938 to 1947 inclusive, and this suggests a minimum moisture requirement of 12 inches for this bush or tree.

At the same edge the ubiquitous shrub Dodonaea makes its appearance. At Erkowit in the Sudan this Erkowit privet, as it is there called, makes a first appearance as one approaches from the desert. The Kassala isohyet of 300 mm, or 12 inches, passes through or very close to Erkowit, which also suggests the 12-inch isohyet as being the upper limit for this zone.

The rose-juniper-agricultural zone.--The rainfall in this zone affects the flow of water to the coastal plain to only a minor extent, both because the zone is so very limited in extent, and because the plateau waters from a line usually about half a mile from the edge of the scarp flow eastward to

the Ar Rub al Khali. Wadi Baysh and wadis to the south of it receive practically no waters from this zone. Wadi Itwad receives a little; and Wadi Hali receives a substantial quantity.

Literally dozens of definitive plants could be used for index purposes, but Rosa abyssinica R.Br. and Juniperus macropoda Boiss. are outstanding and suffice for practical purposes. The zone is confined in the Asir region to the top of Jabal Fayfa; to a trace at the heads of Wadi Ga'a; and to Jabal Sawdah from above the 8,200 ft (2,500 m) contour up to the summit at 9,425 feet (3,000 m). There is no precise method of estimating rainfall for this zone, but for reasons given above, the lower limit can with some degree of confidence be estimated at 12 inches.

At an elevation of 9,200 feet (2,928 m) was a field owned and farmed by Sheikh Mohammad bin Mohammad bin Said who was a brother of the Naib or Headman of the village of Sawdah. Mohammad gave me the following cropping history for the field, sown in December and harvested in May:

Year	Crop	Yield	Average
1952	Wheat	fair	
1951	Barley	good	240 kilograms, or 528 lbs per feddan or acre
1950	Wheat	fair	
1949	Barley	fair	
1948	Wheat	good	

Mohammad stated that during his 50 years of active farming at the village, there had never been a crop failure; that the crops could be grown only in the long rains; and that in the short or monsoon rains moisture was sufficient only for the freshening of forage grasses and for the healthy maintenance of the widely grown alfalfa. The Sheikh also said that when crops of wheat and barley began to deteriorate, it was the custom to take a crop of Lens esculenta, or lentil, as a rejuvenator.

As on Jabal Fayfa, the effectiveness of the rainfall must be substantially enhanced by the regular appearance of moist cloud, or shabura, which we experienced on several occasions during our 10-day visit. The area covered by shabura is as much as a mile wide on the plateau and is marked by festoons of Spanish moss that drape the branches of the juniper trees.

This is a good agricultural area that has a very regular rainfall sufficient for the production of a fair to good crop of barley, wheat, lentil, or alfalfa. It is believed that such crops together with juniper trees, some of which attain a height of 40 feet, seem to require a rainfall of at least 14 inches. The village land has an altitude of 9,200 feet so the upper limit would have by proportion an annual rainfall of 15 inches. For total rainfall, one must then add a correction of 12 percent at the Jabal Sawdah latitude for the summer, or monsoon, rains, making a total annual rainfall of 16.8 inches at the top of the mountain.

The error in this opinion may not be very great because Mr. Eric Mackinnon, after a very long experience in the Sudan, records for the Blue Nile Province (Agriculture in the Sudan, J. D. Tothill, Oxford University Press, p. 804) that "In general it may be said that the production of successful rain crops requires a rainfall of 400 mm, 16 in., or more." The hotter sun at the lower elevation of that province, coupled with the absence of shabura (mist) would tend to equate the 16 inches with a little less on Jabal Sawdah.

The estimates of rainfall for the zone are therefore 12 inches at the lower boundary and 16.8 inches at the top, with an average of 14.4 inches.

Table 2. Summary of rainfall estimates (in inches)

Name of zone	Estimated rainfall: Dry edge	Wet edge	Mean
Ar Rub al Khali	trace	2	1
Samr desert	2	4	3
Sallam desert	4	5	4.5
Asak-Commiphora desert	5	7	6
Kleinia-pastoral	7	10	8.5
Euryops-barley	10	12	11
Rose-Juniper-agricultural	12	16.8	14.4

Summary of zone characteristics

Name of Zone	Characteristics	Distribution
Ar Rub al Khali	Plant growth insufficient to produce camel forage.	The Empty Quarter.
		Parts of coastal range north of Jiddah.
Samr desert	Rain sufficient for samr but not for sallam.	On coastal plain from Jiddah to Al Wajh
Sallam desert	Samr and sallam both common. Good growth of the tufted forage grasses Lasiurus hirsutus Boiss. and Panicum turgidum Forsk. Commiphora and Euphorbia cuneata absent.	On coastal plain from Jiddah to Wadi 'Itwad.
		East of the Scarp Mountains a narrow strip from near Aṭ Ṭā'if to the Yemen.
Asak-Commiphora desert	Samr and sallam attain optimum growth and both common.	On Tihama from Wadi 'Itwad to the Yemen.
	On Tihama Commiphora africana and Euphorbia cuneata are definitive. On foothills Acacia asak and Anisotes trisulcus definitive.	On the 'Asir foothills up to 5,000 feet.

Kleinia-pastoral	On western face of Asirs, Anisotes, E. cuneata, and juniper all absent. Acacia etbaica, or qarad, common as a bush, becoming bigger and better near the upper limit. Occasional Kleinia.	On western slopes of 'Asir extends from 5,000 to 7,000 feet.
	On the plateau above the scarp, Kleinia violacea is common. Acacia etbaica finds optimum conditions and has become a well grown tree.	On Asir plateau from Abha and Khamis Mushayt north to Sahra and south to El Ga'am; and generally up to 7,500 feet.
Euryops-barley	Kleinia has disappeared. Euryops has become a definitive plant. Wheat and barley are grown regularly as rain crops.	A fragment on Jabal Fayfa.
	Acacia etbaica is common as a tree and the conditions for it remain optimum.	A fairly extensive area commencing 35 miles south of Abha and extending to Aqabat Al Alb.
	Juniper and Dodonaea absent.	Another fragment between Abha and Jabal Sawdah starting at 7,500 and ending at 8,200 ft.
Rose-juniper-agricultural	Many definitive plants but Rosa abyssinica and Juniperus macropoda are conspicuous. The juniper becomes a 40-foot tree in favorable sites.	Confined in the Asir region to Jabal Sawdah above the 8,200 foot contour; and to traces at the heads of Wadi Baysh.
	The only Acacia is etbaica which has shrunk to become a bush.	
	Euryops has faded out.	
	Good crops of wheat barley, lentil, and alfalfa are regularly grown.	
	There are a number of permanently flowing, spring fed streams.	

The rock units mapped in reconnaissance fashion on the geologic map of the Arabian Peninsula (USGS-ARAMCO 1963) were at that time described mostly in field terms, and the map was based largely on interpretation of aerial photographs. Although the map was planned only as general guide for ore and water search, at an early stage lithostratigraphic groups were recognized to range from unmetamorphosed sediments and volcanics to greenschist and amphibolite metamorphic facies, and to change lithologically in short distances along the strike of the volcanogenic and related rocks. Because the resolution of stratigraphic problems would require detailed work during many years, the units were described only in general terms on the map legend. We have attempted to correct and amplify the earlier reconnaissance mapping with current knowledge from numerous contributors (annotated bibliography, Ministry of Petroleum and Mineral Resources bulletin, 19, 20, 27, 1977, 1980, 1981).

Historic geologic divisions

In the first published attempts at division of the basement rock, Karpoff (1955, 1957b) described two series--the Medina and the Wadi Fatima, in the central part of the shield. We had begun our reconnaissance study 5 years earlier at the Yemen border and had worked northward. In 1960, extending our general rock assemblages into the areas described by Karpoff (1960), wherein we tentatively recognized eight units exclusive of plutonic rocks. Of these, six were equivalent to parts of the older Medina Series of Karpoff, and two were equivalent to and coordinate with his younger Wadi Fatima Series. By 1963, after mapping seven quadrangles (3° x 4° at a scale of 1:500,000) and segments of three others--about 36 percent of the Kingdom--we compiled a map at 1:2 million scale which was combined with the mapping of the Arabian American Oil Company (ARAMCO) and various others into the composite map of the Arabian Peninsula (USGS-ARAMCO, 1963). By that time we recognized a total of 33 units among the basement rocks, of which 20 were given rock-term names without formal reference to geographic localities. Of the 14 names based on geographic localities, two were regional, namely the Halaban and Shammar. The Halaban was named for Halaban ridge and the region around the Halaban pass near the southern end of the ridge in the east-central part of the shield, and the Shammar was named for Jabal Shammar, the regional name for the area around Ha'il in the northeastern part of the shield.

Some explanation of the first use of these names is desirable. The first geologist to describe layered rocks near the Halaban ridge was Bogue (1953) of the USGS. He considered that the dioritic and andesitic greenstone and related rocks of the region were probably the same as the "Shawaq volcanics" that he had earlier described as being at Wadi Shawaq in the Jabal ash Shifa' region 900 km northwest from Halaban and near the northwestern edge of the shield. We felt that even though the lithology and metamorphism appeared to be similar, the units were separated by too great a distance of unmapped terrain to justify correlation until the areas were mapped in more detail. Accordingly, G. F. Brown and R. O. Jackson (1960) chose the name "Halaban Andesite" for Bogue's "Shawaq volcanics"; later the term "Halaban formation" was used, because it was known that rock types other than andesitic greenstone were in the section and that an assemblage of at least group rank would be found if it were mapped in any detail.

Likewise the name "Shammar Rhyolite" was used (Brown and Jackson, 1960) to designate the largely unmetamorphosed and silicic volcanic rocks associated with sedimentary rocks cropping out in the northern part of the shield, in order to distinguish these younger rocks from older rhyolite and related volcanogenic beds farther south.

The six other names published in 1960 (Brown and Jackson, 1960) were, from oldest to youngest, the Hali Schist, Baish Greenstone, and Lith Complex below the Halaban; and the Murdama, Fatima, and Ablah formations above the Halaban and below the Shammar Rhyolite. Later we described (USGS-ARAMCO, 1963) the Jiddah Greenstone, which is intruded by the Mecca Granite; the Hibshi formation, dominantly a clastic-volcanic formation that disconformably overlies a gray biotite granite and underlies at least part of the Murdama phyllite in the Jabal Shammar region; the Hadiyah Slate in the northwestern part of the shield; and the iron-bearing Silasia formation. Units were individually named because field information was insufficient to warrant closer correlation over large areas. Names of large wadis or coastal towns were used to avoid giving a specific type locality until the units could be mapped in detail and the best type sections and localities could be chosen. The Murdama and Hibshi Formations are exceptions; both have excellent sections on the mountains of those names.

Current geologic divisions

During the past 17 years, more detailed mapping by numerous geologists has begun to elucidate structural complexities, chronologic episodes and sequences, sedimentary and volcanogenic facies changes, and metallogenic epochs. Computer-enhanced imagery from satellite signals supplied a new tool that supplements aerial photographs and standard color composites of satellite-derived scenes (Blodget and Brown, 1982). Airborne magnetic and digital gamma-radiation surveys also helped in interpreting the geology.

As a result of the more detailed mapping, some formations of the USGS-ARAMCO map (1963) were raised to group rank (Schmidt and others, 1973) to include various formations named for specific localities and type sections. Also, because many more radiometric ages have been determined and structural control is better understood, the sequence of groups has been changed somewhat. The rock units, as presently mapped (1982) and named are shown in figure 2.

Ultramafic and ophiolitic rocks

Ultramafic and serpentine rocks and associated mafic volcanic and plutonic rocks, chert, slate, and marble are widespread, but sparsely distributed throughout the shield. Ultramafic rocks associated with the older marine beds of the Baish-Bahah, were described by Hadley (1975b) as an ultramafic complex in part "conformably interbedded in the Baish group and in part intrusive into it" (Qunfudhah quadrangle, lat. 19°10' N.). Greenwood (1975c) has mapped a serpentine-talc belt at the base of the Baish group farther northeast in the Biljurshi quadrangle at lat. 19°55' N. At Jabal Wask (Al 'Ays area) a mafic-ultramafic dome has been studied intensely for its chromite potential (Kahr, 1961; Johnson and Trent, 1966; Bakor and others, 1976; Kemp and others,

1980; Kemp, 1981). Samples collected by Viktor Kahr, who recognized the domal rocks as belonging to the ophiolite suite, were studied by T. P. Thayer who identified peridotite, alpine gabbro (with alteration to prehnite and other minerals of the rodingite suite), and "...albitized volcanic breccia commonly associated with albite granite of the end member of the alpine mafic magma stem,"...all identified with ophiolite. Kemp and others (1980) report a Pb/U age of 882 $\pm$ 12 m.y. B.P. from zircon in plagiogranite of the ophiolitic complex. Bakor, Gass, and Neary (1976) consider the ophiolite dome to have formed in a back arc environment. As these ultramafic rocks are on the southwest flank of the youngest fault zone (part of the Najd fault system of the shield) and on the northeast flank of the Wadi Kamal domal complex, it appears that the upper mantle-basal oceanic layers of the Wask ophiolite were exposed either by Najd faulting and subsequent erosion, or by uplift of circumferential younger granites--or by some combination of the two processes. This interpretation is strengthened by the fact that the tectonics follow the pattern of equal-intensity aeromagnetic lines (Andreasen and Petty, 1974).

Farther north and 38 km southeast of Wajd, black schists are exposed for 1 km along the track (von Gaertner and Schurenburg, 1954). The carbonaceous schist extends northward at least as far past Al Wajh as the southeast border of Jabal Liban at lat. 26°30' N., where the older metamorphosed flows and sediments produce a bluish hue on enhanced satellite imagery (Blodget and Brown, 1982). These beds as mapped by the Japanese Geological Survey include metagabbro, metabasalt, metadiabase, cherty slate, and limestone (marble). Serpentinite is exposed along an overthrust fault at the eastern edge of the Wajd segment, but may not represent the ultramafic base of a possible Wajd ophiolite suite (Japanese Geological Mission, 1965), although it is in a structural position similar to that of the ophiolite fragments along sutures displaced from the southeast by Najd transverse faulting.

Other ophiolitic suites, generally incomplete as ophiolite was defined at the Penrose Conference (Anonymous 1972) as a classical stratigraphic section of ocean floor above mantle rocks, occur in fault zones at junctions considered plate or island arc boundaries within the shield. The most complete but fragmented ophiolite is at J. Ess (26°20' N. lat., 38° E. long.); the largest exposures are around Jabal al Wask (fig. 5) within the Al 'Ays region northwest of Yenbu at 25° N. lat., 37°30'-38°10' E. long. The longest outcrop of ultramafic and related rocks of probable ophiolitic origin follows the Nabitah fault zone from the Yemen border northward to the Najd fault zone at 21° N. lat. where it is offset 120 km left laterally along the Najd fault zone to the northwest (in various fragments), the northwesternmost being the Tuluhah belt north of 25°30' N. lat. (Frisch and Al-Shanti, 1977). The easternmost ophiolitic zone occurs along the front of the Al-Amar-Idsas fault near the east edge of the shield. Other than the Al 'Ays ophiolite, the ages of other ultramafic and serpentinized suites are not known to us.

If these rocks are dismembered ophiolites, they should be structurally, not stratigraphically, related to--and of different age than--adjoining rocks. If the island-arc accretion model is accepted, the ophiolite rocks might be expected to become progressively younger eastward; they should be somewhat older than the island-arc rocks with which they are structurally associated.

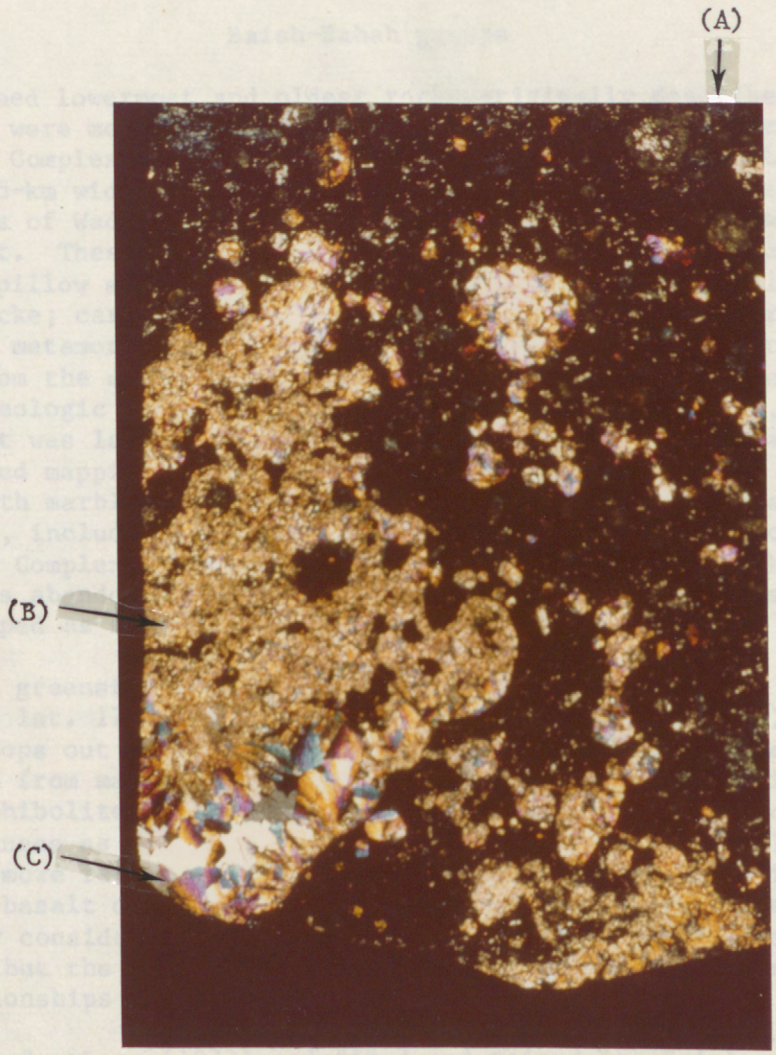

Figure 5. Amygdaloidal metabasalt at the Jabal Ess ophiolite complex at 24° 21' N. lat., 34°44' E. long. The groundmass is equigranular completely chloritized clinopyroxene (?) and basic feldspar (A) with two generations of amygdules, the oldest fine-grained and filled with secondary calcite, (bent twinning planes) quartz, chlorite, and prehnite. The multi-mineral vesicle filling (B) was later transected by coarse-grained calcite (C). Described by S. Block.

Baish-Bahah groups

The presumed lowermost and oldest rocks originally described in the Arabian Shield were metadiorite, metagabbro, and amphibolite formerly named the Lith Complex and occupying a one-degree square at Al Lith. Similarly, a 55-km wide belt of metamorphosed lavas and sedimentary rocks along the banks of Wadis Hali and Tayyah at lat. 18°44' N. and were named the Hali schist. These rocks consist of basalt and andesitic basalt containing local pillow structure, interbedded marine volcaniclastic and sedimentary wacke; carbonaceous and graphitic schists, and minor marble and chert, all metamorphosed to the greenschist facies and generally retrograded from the amphibolite facies. Both of these units were originally shown on the geologic map of the Arabian Peninsula (USGS-ARAMCO, 1963). The Hali schist was later redefined (Schmidt and others, 1973) as a result of more detailed mapping and described as quartz-biotite-garnet schist interbedded with marble, stretched-pebble conglomerate, and metamorphosed volcanic rocks, including the older, more metamorphosed "Lith Complex". The name "Lith Complex", shown on the 1963 map as the basal rock unit of the shield, was abandoned because it included diverse rock types that were later mapped as separate units.

The Baish greenstone was first described from exposures in cliffs along Wadi Baysh, at lat. 17°40' N. (Brown and Jackson, 1959 and 1960), where spilitic pillow lava crops out (fig. 6) as massive greenstone or sericite-chlorite schist derived from mafic igneous rocks. In addition, metadiorite, metagabbo, and amphibolite with subordinate siliceous slate were included. The original thickness as measured along the western limb of a syncline was 12,000 m, but more recent work suggests a synclinal structure with 6,700 m of tholeiitic basalt on one limb (George Simmons, USGS, oral commun.). The unit was originally considered to overlie the Hali schists downstream in the Baysh canyon, but the structure is complicated by tight folds and faults, and the relationships are still not clear.

Schmidt and others (1973) redefined and raised the Baish greenstone to group rank, placed it immediately above the Hali group, and split off the upper schistose part from the marine sediments containing metabasalt cobbles above a disconformity (Greenwood, 1975b) to form the Bahah group, although the lithologic description remained much the same. Baish and Bahah groups form the "metabasalt graywacke-chert assemblage" of Greenwood (1975b) or the "basaltic assemblage" of Fleck and others (1980).

The two groups have the following common components but in different proportions they justify their separate names: pillow metabasalt, marble, chert, carbonaceous or graphitic schist, and some meta-andesite--quite distinct from the overlying andesitic lavas and volcanogenic sedimentary rocks of the Jiddah and younger groups (Schmidt and others, 1973; Hadley 1975a, b; Greenwood and others, 1976).



Figure 6a. Metasedimentary schists in the Jabal Aya quadrangle formerly believed to be of Baish-Bahah age. These beds are now believed to belong in the younger Jiddah (Samran) group, having been overthrust from the east. View south along the top of the An Nimas escarpment. The beds dip east.



Figure 6b. Glaucophane schist near Ad Darb in Bahah Group indicates high pressure in the low glaucophane schist facies beneath overthrusts from the east.

The Bahah group named from the village of Al Bahah in the Jabal Ibrahim quadrangle (Schmidt and others, 1973; Greenwood, 1975b) includes formations considered in this report to be structurally above the Baish group. The marine Bahah group includes paraschists of clastic or tuffaceous origin with distinct ferruginous quartzite, metachert, and carbonaceous and arkosic members. Marble, stretched-pebble conglomerate, and metabasalt make up less conspicuous beds. Carbonaceous beds common in both the Baish and Bahah groups appear to owe the carbon to algal growth in water within the photic zone, probably less than 250 m depth (Jackaman, 1972; Kiilsgaard and others, 1978). A similar assemblage of rocks including metabasalt, carbonaceous or graphitic schists, and jasper or chert extending intermittently on promontories of the crystalline shield as far north as Al Wajh at lat. 26°16' N. has been questionably remapped as part of a younger epoch. At Wadi Fatimah, paraschist, jasper, and keratophyre (including minor marble, and epidosite) are intruded by "pyroxene granite" (Richter-Bernburg and Schott, 1954) and were contact-metamorphosed to amphibolite facies. Northwest of Yenbu at lat. 24°20' N., gneiss comprising amphibolite, quartzite, and leptite is intruded by the Wadi Kamal complex of norite, orthoamphibolite, anorthosite, and ultramafic (serpentinized) rocks which were tentatitively referred to the Hali by Baubron and others (1976).

Three samples of metabasalt near Al Lith at Wadi al Fagh, lat. 20°23' N., gave an age of 1165 $\pm$ 110 m.y. from a total-rock Rb-Sr isochron (Fleck and others, 1980, p. 31) in contrast to more recent work in another laboratory which resulted in Rb-Sr dates of 836 $\pm$ 60 Ma and 830 $\pm$ 9 Ma for metabasalt in Wadi Sadijah in the western part of the Al Lith area, presumably from rocks considered Baish ("Lith") age (Reischmann, 1981). Minimum age for the layered rocks based on total rock Rb-Sr isochrons of intrusive quartz diorite near Biljurshi (lat. 19°52' N.) and Al Lith, are about 850 and 890 m.y. respectively (Fleck and others, 1980, p. 46); farther north Aldrich (Aldrich and others, 1978) measured a K-Ar 40 age of 1190 Ma from horneblende in amphibolite at the northwestern corner of Jabal Shar, lat. 27°20' N. And still farther north carbonaceous slate containing fossil blue-green algae in southeastern Sinai yielded isochron Rb/sr date of 934 $\pm$ 80 m.y. (Shimron and Horowitz, 1972; Shimron and Brookins, 1974).

Jiddah (Samran) group

First shown on the peninsular geologic map (USGS-ARAMCO, 1963) as the Jiddah greenstone, the meta-andesite in the foothills east of Jiddah, where it is intruded by the Mecca granitoid intrusive, was described as andesite and andesite porphyry metamorphosed to the greenschist facies; in many places it is schistose but includes some diabase, gray slate, conglomerate, dacite, and marble. The first radiometric dates determined for the Mecca granodiorite range from 965 to 1025 Ma for Rb-Sr ages and 720-760 Ma for K-Ar ages as determined by Aldrich (in Brown and others, 1963a; Aldrich and others, 1978), utilizing the decay rates adopted by the 25th International Geological Congress (1976). For this reason the Jiddah greenstone was considered to be among the oldest rocks of the shield and was placed beneath the Baish greenstone and above the Silasia Iron formation of northwestern Arabia, as described by Bogue.

Bhutta (1970) recognized two units within the Jiddah greenstone: a lower series of metamorphosed flows and pyroclastic rocks (andesite, diabase, andesite porphyry, rhyolite, and greenstone) and an upper younger sequence of slate, metaconglomerate, tuff, quartzite, and marble (fig. 7). The unit was further defined and named the Jiddah group (Schmidt and others, 1973) following more intensive field work and an extended field conference that covered 11 30-minute quadrangles in the southern part of the shield. The relationship between the Baish-Bahah and the Jiddah group is not clear but possibly the Baish-Bahah is slightly older in that metamorphosed clasts of the older rocks were reported in the basal units of the Jiddah group (Greenwood and others, 1976) and in turn overlain, with angular unconformity by the 'Ablah group. This is the stratigraphic position we had earlier assigned to the meta-andesitic and related rocks exposed within the southern Hejaz quadrangle (Brown and others, 1962).

The Jiddah consists of a lower volcanic formation, the Qirshah andesite, and an upper clastic, predominately immature arkosic and volcaniclastic wacke, the Khutnah formation (Greenwood, 1975c). The Qirshah andesite named for Wadi Qirshah, a tributary to Wadi Ranyah at lat. 20°10° N., consists predominantly of andesitic pyroclastic and flow rocks and includes dacite breccia, ignimbrite, marble, and some pillow basalt, suggesting a marginal marine origin similar to the calcalkaline suite of island-arc volcanics in contrast to the more mafic (calcic) volcanic rocks and deeper marine beds of the Baish-Bahah groups. Much of the sedimentary and volcaniclastic schist of the Jiddah (Samran) is graphitic and includes beds of chert and minor basalt, thus resembling the upper Bahah group. Within the Aqiq quadrangle and west of the Ablah graben, the Jiddah group includes spilitic mafic flows, tan and brown marble, andesite with blobs of serpentine, and fine-grained pyroxenite(?), the ultramafic suite of G. Eijkelboom (oral commun.).

More recent work extending northward along the coast indicates that meta-basalt, meta-andesite, and graphitic schists that were mapped as Jiddah as far north as Al Wajh lithologically resemble the Baish-Bahah (Blodget and Brown, 1982) and are the same beds named Samran by Smith and Kehr (unpub. data) later adopted by several authors and finally defined by Shiba (1984). Some metavolcanic and metasedimentary rocks in the southeastern part of the shield, that were considered Jiddah group by Schmidt and others (1973) and by Greenwood and others (1980) also resemble the Baish-Bahah groups so that on the basis of chemical analyses, as well as on the basis of structural relations and metamorphism, these rocks are shown to be similar to the Hali schist as it was originally mapped in 1969 (Brown and Jackson). The most striking evidence of the Bahah-Hali (now Bahah) affinity is the cherty and carbonaceous or graphitic schists that crop out on both flanks of the gneiss in the 'Asir highlands. In contrast, the Jiddah greenstone as originally mapped was mostly meta-andesite in greenschist facies. The more extensively mapped Jiddah group, however, does contain contain cherty and carbonaceous facies and in fact any island-arc terrane, regardless of age, might be expected to contain this facies; the facies is not group diagnostic. The Jidda group as shown on figure 2 also includes andesitic rocks mapped on the Samran series in the area of Jabal Samran (Nebert, 1969).

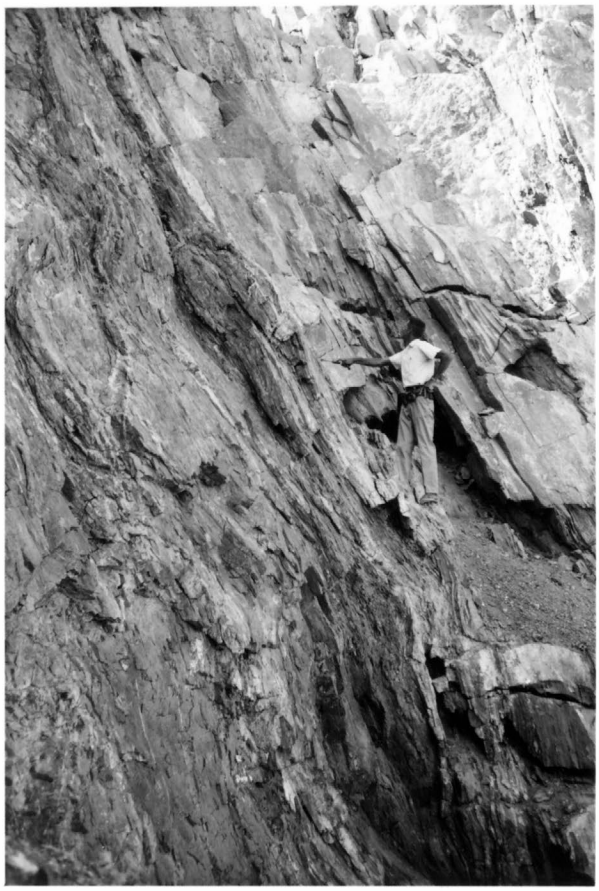

Figure 7a. Hornblendite interbedded with pink marble of the Jiddah (Samran) group in Wadi Fatimah. Two periods of folding are apparent.



Figure 7b. Pillow lava in basalt formerly considered to be in the Baish group, Hilwa area, on north wall of Wadi Baysh gorge. Now believed to belong to the Jiddah (Samran) group.

A tentative reported age for the volcanic rocks of the Jiddah Group comes from a roof pendant on the An Nimas batholith where Fleck and others (1980) found an apparent age of 912 ± 76 Ma from Rb-Sr, a whole-rock isochron. The rocks were considered part of the lower Jiddah Qirshah meta-andesite (Greenwood, 1979).

Concurrent with and subsequent to the accumulation of the Jiddah group, calcic and calc-alkalic plutonic rocks of a comagmatic suite ranging from gabbro through quartz diorite to trondhjemite and granodiorite but mostly diorite and quartz diorite, were synkinematically intruded into the Baish-Bahah and Jiddah groups during the period 890 ± 67 to 848 ± 28 Ma according to Rb-Sr isotopic ratios (Fleck and others, 1980). Some of these plutonic rocks were locally reactivated during the period 797 ± 15 to 763 ± 4 Ma (Cooper and others, 1979) into orthogneiss domes ranging in composition from tonalite to granodiorite; thus they define a minimum Jiddah age. The intrusions and the concomitant orogenies have raised locally the metamorphic rank of the older litho-stratigraphic assemblages to amphibolite facies.

Recent more detailed study of the granitoid intrusives in the Jiddah-Makkah area at the type locality of the Jiddah group gives ages of 763 ± 159 Ma from whole-rock isochrons of samples including quartz diorite and qranodiorite gneiss intruded into the calc-alkaline meta-andesite of the Jiddah group (Fleck, 1981) which, if correct, establishes a younger minimum age for the group than determined by Aldrich, and corresponds in general to the K-Ar ages of Aldrich for the same samples yielding Rb-Sr ages 965 to 1025 Ma. Thus it appears that the major gneiss doming of the subsequent Ablah orogeny at about 763 Ma reset the intrusive dates, and the relative ages of the Jiddah (Samran) and Baish-Bahah groups and remains uncertain.

Ablah group

The name Ablah was first used for the Ablah formation (fig. 8), and applied to a belt of sedimentary rocks exposed in a graben extending south-southwest from Jabal Rafa (lat. 22°30' N., long. 42° E.) past a fluorspar pipe at Ablah which was mined during the time of the Abbasid Caliphate (Brown and Jackson, 1960). The basal polymict conglomerate, quartzitic wacke, red sandstone, stromatolitic limestone, arkose, and purple shale rest nonconformably on Jiddah Group metavolcanic and plutonic rocks. They are folded into a series of asymmetric anticlines and they dip predominantly to the east. Theobold and Thompson (1972), in a detailed study in the vicinity of a native copper occurrence at Jabal Rumur in the southeastern part of the Aqiq quadrangle, described a sequence of red laminated siltstone and gray crossbedded sandstone, containing some conglomerate lenses on disconformities within the sediments which grade upward into ferruginous wacke and andesitic breccia. Andesite flows and feeder dikes occur in the midsection. Some of the coarser grained sedimentary rocks contain fluorite, seemingly epigenetic and coeval with the Ablah fluorite pipe; the copper is stratabound, possibly syngenetic, and structurally related to the contemporaneous andesite flows and dikes.



Figure 8. Oblique aerial view to northwest across the Ablah and Jiddah groups. The boundary is the fault line in the lower third of the scene at the edge of the folded Ablah sediments. Wadi Ranyah flows northeast in the foreground, bisects Tertiary, probably Pliocene flood basalt outliers, and the folded and faulted Ablah group. Wadi Qirshah in the middle distance and Wadi Thurat beyond flow across andesitic meta volcanic rocks of the Jiddah group. Older dioritic rocks intrude the volcanogenetic rocks in a belt east of the oasis of Aqiq, the small light-colored plain in the distance.

The Ablah rocks extend southward discontinuously from the Ablah mine area in a narrow faulted belt in which the rocks are found as roof pendants in, or as grabens between, the diorite-granodiorite-trondjhemite batholiths of the 'Asir and Tihamat ash Sham (Greenwood, 1975c,d; Bayley, 1972; Anderson, 1979; Hadley 1975a). Thin beds of stromatolitic marble thicken southward from two horizons in the Ablah beds at Ablah (calcite and siderite cement are common at several horizons); the beds become metamorphosed progressively southward to a greenchist facies in the northern part of the Wadi Yiba quadrangle and to almandine-amphibolite and sillimanite facies at lat. 19° N. (Bayley, 1972; Hadley, 1975a) in the Wadi Hali quadrangle. At the north end of the infolded graben at Ablah, Greenwood (1975d) divided the Ablah group into three formations: a basal polymict conglomerate-wacke-marble series metamorphosed to greenschist, his Rafa formation; a middle unit composed essentially of calc-alkaline flows but including rhyolite, quartz latite, some basaltic extrusives with pillow structure, marble and pyroclastic rocks, his Jerub formation; and the younger beds comprising the original Ablah formation, his Thurat formation. Greenwood (1975d) gives a thickness of the Thurat as 1100-1300 meters, but the lower units and their southward extension in the Ablah graben are so folded and faulted as to make thickness estimates unreliable. The Ablah group appears to extend southward to and across the Yemen border at lat. 17°30' N., mostly as paraschist, marble, conglomerate, and quartzite or slate beds (Anderson, 1979). The basal polymict conglomerate is discontinuously exposed from Ablah to Jallat al Mawt on the Yemen border, where the pebbles and cobbles are gray gneissic quartz diorite or granite, quartzite, and chloritic hornfels.

Hadley (1975a) divided the Ablah group in the Wadi Hali quadrangle into two formations, as the correlation with the three formations defined by Greenwood in the Aqiq quadrangle is tenuous because of depositional and metamorphic facies changes. These are the Sarban formation, mostly paraschist and marble metamorphosed to the amphibolite facies, and the overlying Hadab, likewise amphibolite schist but retrogressively metamorphosed and including gneiss (Hadley, 1975a). However, the group comprises a definite sequence of shallow-water and nonmarine beds (fig. 9) overlain by calc-alkalic lavas and stromatolitic limestone and marble above a widespread nonconformity. The basal conglomerates contain boulders of the Jiddah trachytoidal and amydaloidal andesites, and related rocks as well as some rocks from the older Baish-Bahah groups.

Fatima group

The Fatimah group (fig. 10) exposed in the hills north of Wadi Fatimah as originally described by Karpoff (1955, 1957b) is remarkably similar to the Ablah group as it rests nonconformably on the Mecca granodiorite and includes red and green immature clastics, stromatolitic limestone, tuffaceous sediments, andesite and basalt flows (Goldsmith, 1966; Nebert and others, 1974). However, the uppermost flows come from feeder dikes which transect the lower sediments and are younger than the sedimentary rocks. The thickness as measured by Goldsmith is about 1,000 m and is comparable to the Thurat formation at Ablah. The age of the Ablah-Fatimah groups may fall somewhere within the timespan from 816 $\pm$ 3 MA (Kemp and others, 1982) for the Mahad adh Dhahab area, and 763 $\pm$ 55 Ma for the Bagarah gneiss dome of Ablah belt (Fleck and others, 1980).



(a)



(b)

Figure 9a, b. Infilled desiccation cracks (a) in gray siltstone and (b) symmetrical ripple marks in associated red siltstone. At type locality of Ablah group, 7.5 km upstream from the junction in Wadi Kirshah. Al Aqiq quadrangle.



Figure 9c. Small thrust fault in Ablah group at the type locality. Siltstone at lower left underlies red faulted sandstone. Thrust is from the east at the junction of Wadis Kirshah and Ranyah. Al Aqiq quadrangle.



Figure 9d. Parasediments of the Ablah group intensely folded into a plunging syncline at Wadi Yiba. View northwest.



Figure 10. Fatimah group, north Wadi Fatimah. Folds in stromatolites and clastics.

Both the Fatimah and the Ablah are intruded by post-orogenic magma; an andesite sill and a basalt flow at the top of the exposed section of sedimentary rocks in Wadi Fatimah are dated at 592 ± 23 and 576 ± 28 Ma, respectively, by K-Ar whole rock analyses (Aldrich and others, 1978); however, both the andesite and basalt are hydrothermally altered and the ages could be reset. At Ablah an intrusive basalt plug which pierces the upper Ablah-Thurat sedimentary rock is dated at 585 ± 39 Ma. However, stromatolites described by Karpoff are Collenia and Corophyton, which together in general appearance, led him to consider the Fatimah as upper Precambrian in accordance with the age assignment in Africa. More recently a sample of one stromalolite collected by D. L. Schmidt was examined by Preston Cloud (USGS) and S. M. Awramik (written commun., 1978), who consider the form to be close to the morphology of Kussiella, a characteristically lower Riphean form of 1350 to 1650 Ma (glauconite age). However, they report at least one record of Kussiella from the upper Riphean or within the time span of 675-950 Ma (glauconite). Thus it appears that the Fatimah sedimentary rocks could be coeval with the Ablah. These sedimentary rocks constitute a typical molasse assemblage, in contrast to the underlying Jiddah, Baish, and Bahah groups, which are predominantly island-arc assemblages.

Silasia formation

Farther north near lat. 28° N., the iron-bearing Silasia formation is associated with spilitic and diabasic greenstone. The formation was named by Richard Bogue (1953) and described as consisting of mostly shale, locally sandy, calcareous, or conglomeratic, and enclosing thinbedded limestone and thin alternate beds of jasper and hematite in the upper part with a thickness of not less than 1400 m (fig. 11). The typical iron formation-banded jaspilite-hematite layers, best seen in Wadi Sawawin at lat. 28° N., are exposed in pods interbedded with slate, limestone, tuffs, agglomerate, and conglomerate, all of which are intruded by diorite, and intensely deformed. Bogue believed that the spilitic greenstone, which he named the Shawaq greenstone from the ancient town and wadi 80 km southeast of Wadi Sawawin, overlay the iron formation, but he further stated that the iron-bearing beds are highly folded and in places overturned. Later Johnson and Trent (1967) considered that the greenstone underlay the Silasia clastics. The Japanese Geological Survey in 1967 correlated the beds with the Hali schist, and Liddicoat (1975) measured a thickness of 919 m for the upper sedimentary section. The Silasia and Shawag formations remain enigmatic to this day; on fig. 2 the Shawaq Greenstone is mapped as part of the Jiddah group and the Silasia formation is retained as a younger volcanogenic metasedimentary unit equivalent to the Ablah type, following the concept that many of the beds formerly named Hali schist are of Ablah age.

Halaban (Hulayfah) group

In the eastern part of the Arabian shield, Bogue (1953) briefly described "a variety of both intrusive and extrusive rocks . . . mostly andesite and fine-grained diorite but gabbro, basalt, and basalt porphyry are not uncommon," --igneous rocks he considered as possibly equivalent to the Shawaq volcanics of northwestern Arabia. Our subsequent mapping suggested that the calc-alkaline volcanic rocks and associated plutonic and hypabyssal intrusives in the eastern regions were most likely somewhat younger than the Shawaq volcanics, although both are regionally metamorphosed, the Shawaq to a somewhat higher grade.



Figure 11. Silasia formation showing siliceous hematite outcrops intruded by diorite at Wadi Sawawin.

Accordingly, we proposed the name Halaban andesite, choosing a regional name for the area where Bogue described widespread outcrops in the region around the Halaban Pass and the water well near the southern end of the 50-km northwest-trending ridge, Samra Halaban, and where Shaib Halaban, a tributary to Wadi as Sirrah, affords an east-west caravan route. As we could not designate a type section for a formation, it was necessary to use a rock name in accordance with the rules of nomeclature, choosing what Bogue considered the dominant rock in his description (Bogue, 1953). The formation (fig. 12) as mapped included, besides andesite, agglomerate, quartzite, graywacke, interbedded marble and rhyolite, and a somewhat younger series of epidiorite, diorite, diabase, gabbro, and serpentinite (Brown and Jackson, 1960; Jackson and others, 1963). Most of the rocks are metamorphosed to the lower and middle greenschist facies, but locally higher grades of metamorphism are found.

Later BRGM (Eijkelboom, 1966; Vincent, 1968) mapped the Halaban region in considerable detail and began to elucidate the lithologic units where we had shown all as Halaban formation (Jackson and others, 1963). Although BRGM did not assign relative ages and specifically avoided describing a sequence of events, designating only lithologic units, the sequence shown on their maps includes ultramafic rocks, mostly pyroxenite and harzburgite much serpentinized, at the base. As part of an ophiolite suite these ultramafic rock are generally older than the andesite-dioitic basement which they structurally overlie. The calc-alkalic Halaban rocks are variously metamorphosed, mostly in the greenschist facies (chlorite-epidote-zoisite-albite) and are overlain by metamorphic tuffs and sedimentary rock. Some subvolcanic fine-grained diorite intrudes the uppermost metavolcanics and metasedimentary rocks. The structure is complex; in places a melange occurs within the section and complicates the stratigraphy, so the suggested sequence might be changed with further study. Vincent raised the Halaban to group status. Eijkelboom separated the volcanic and subvolcanic rocks east of the Al Amar-Idsas fault--the easternmost exposed segment of the Arabian shield--because the flow rocks, namely andesite and dacite, including rhyolite, tuff, agglomerate, volcanoclastic conglomerate, breccia, albitophyre, keratophyre, and some marble and greywacke, are different from the volcanic and subvolcanic rocks west in the vicinity of Halaban.

BRGM later divided the Halaban into four units, including basal ophiolitic melange (BRGM, 1966, Eijkelboom, 1969). Bois (1971), separated the rocks exposed along the northeast edge of Halaban Ridge into ultramafic and gabbroic rocks of an ophiolite suite, and an overlying unit, the Ar Ridaniyah formation, consisting of volcaniclastic rocks, chert, and marble beds metamorphosed to the amphibolite facies. Later the upper units were collectively called the Pyroclastic Halaban in contrast to the underlying Andesitic Halaban (Bounny, 1973). Still later the Halaban rocks were formally named the Afna and Nuqrah formations (Delfour, 1975) and assigned to the Hulayfah group, named for Wadi Hulayfah and the town on the wadi where both formations are exposed; the type locality (lat. 26°N.) is midway between al Madinah and Hail. The younger Nuqrah formation was named for the ancient mining site on the al Madinah-Qasim road 75 km southeast of Hulayfah where it has been studied extensively.



Figure 12. View north along the strike of Wassat stratabound gossan in Halaban group volcanoclastic sediments and cut by late Halaban quartz diorite; locally gneissic from upward movement during culminate orogeny.

More recently Delfour (1979a) has recompiled the earlier BRGM mapping of the Halaban quadrangle and with additional field work in 1975 and 1977, reinterpreted the geology. He separates the Halaban as mapped earlier into four units: three groups above an older basement composed of granite, orthogneiss, and diorite. The groups, in ascending order are the Ajal, composed of biotite schist, gneiss, and amphibolite; Urd, consisting of two formations, a lower ophiolitic complex and upper Abt schist; and the Hulayfah Group here consisting only of the upper formation of the group, the Nuqrah. The Nuqrah is composed of silicic volcanics and volcanoclastic sediments as well as andesite, marble, and jasper, the rocks first described by Eijkelboom as the Al Amar-Idsas formation.

Also more recently BRGM has recompiled the 'Afif quadrangle (Letalenet, 1979), extending the detailed mapping west from the Halaban region. There the formations originally shown as Halaban are divided into five formations grouped into three units besides intrusive diorite, gabbro, ultramafic rocks, and serpentinite. The oldest unit, mostly of sedimentary origin, of schist, gneiss, amphibolite, quartzite, metarhyolite, and meta-andesite, is shown only along the western edge of the quadrangle and has been dated in xenoliths in diorite at 825 m.y. B.P. (Baubron and others, 1976; Letalenet, 1979). The remaining formations above these older rocks are calc-alkalic to silicic flows and volcanoclastic sedimentary rocks in general becoming more alkalic and silicic in the uppermost beds, which seem to be similar to the Hulayfah group of the Nuqrah quadrangle (Delfour, 1977).

Hadley (1973) followed the BRGM classification but omitted the lower ophiolitic complex, and assigned formation names within the Sahl al Matran quadrangle in northwestern Arabia (lat. 26°00'-26°30' N. and long. 38°00' E.) as follows: the lowermost 2,550 m of metaclastic rocks and marble, he named the Thaa formation from exposures on Wadi Thaa in the southeastern part of the quadrangle; the middle 3,950 m of metabasalt, meta-andesite and pyroclastics exposed in the hills around the central Matran plain are the Matran formation; and the upper 3,900 m of lavas, mostly alkalic, and associated pyroclastic rocks, are the Jizl formation, named from the exposures on the flanks of the Wadi Jizl in the southeastern part of the quadrangle.

Subsequently, the ophiolite suite, Ar Ridaniyah formation, and the overlying Abt schist, were taken together to form the Urd group for Jabal al Urd at lat. 24°05' N. and long. 44°50' E. (Delfour, 1977). As most of the Jabal al Urd region is underlain by the Abt schist, which we now believe to be clastic deposits of the Murdama group metamorphosed to paraschists by underthrusting along the Al Amar-Idsas fault and by later granitic intrusions, we suggest abandoning the group name.

The southern extension of the Halaban (Hulayfah) rocks includes two formations in the Juqjuq quadrangle at lat. 21°00'-21°30' N., and long. 43°30'-44°00' E. (Hadley, 1976); a lower volcanic formation composed of andesite, basalt, and conglomerate, the Juqjuq formation (from Wadi Juqjuq, a tributary to Wadi Dawasir), and an upper formation, the Arfan, from Jabal Arfan north of Wadi Juqjuq in the northwestern part of the quadrangle. The Juqjuq formation is more than 13,100 m thick at the type locality,

and the Arfan formation was estimated to be more than 7,600 m thick (Hadley, 1976; Schmidt and others, 1978). Subsequently, it has been suggested by C.R. Ramsey and N.J. Jackson (oral commun., 1980), that some of the rocks of the Arfan formation belong to the Murdama group.

Delfour (1977) on the Nuqrah quadrangle reported 6,500 m of the Afna formation in two units, a lower 2,500 m of conglomerate, marble, tuffs, and siltstone, and an upper 4,000 m of predominantly andesite and basalt but including diabase sills and some rhyolitic tuffs and flows at lat. 25°-26° N., and long. 40°30'-42° E. The Nuqrah formation at the type locality is 4,000 m thick and composed of three members, a lower rhyolitic tuff and rhyolite with less abundant andesite; a middle unit of marble, graphitic tuff, and sulphide minerals associated with breccia, cherty tuffite, bedded chert, jasper, rhyolite, and subordinate andesite; and an upper unit of conglomerate, ignimbrite, rhyolite, and tuffite.

The Halaban (Hulayfah) group (Brown and Jackson, 1979) covers large areas in the eastern and northern part of the shield and was considered a possible supergroup (Brown and Jackson, 1979) but this is deferred, needing further elucidation. The outcrops extend in folded and faulted belts for at least 800 km in a north or northwesterly direction and extend laterally as much as 40 km in the type region. The early mapping limited the outcrops almost entirely to the region north and east of the southernmost Najd fault. Geochronologic dates range from about 785 and 775 Ma for volcanic rocks (Rb-Sr) to 729 (Zircon) and 724 Ma (Rb-Sr) for tonalite intrusive into the volcanic rocks (Fleck and others, 1980; Aldrich and others, 1978; Cooper and others, 1979). Thus the dominant calc-alkalic rocks include a stratigraphic unit that contains uppermost rhyolitic flows, ignimbrite, and tuffaceous sedimentary rocks--in all a typical island-arc assemblage. This assemblage makes up the Halaban group (Brown and others, 1972; Brown and Jackson, 1979), here comprising the Hulayfah group, of the northeastern shield and the Halaban as widely mapped in recent years in the southeastern shield.

The granite Delfour includes in the older basement extends into and appears to be part of the large granite batholith which extends through the Dawadami area. It is about 1400 km^2 in area and, according to Al-Shanti (1976), composed mostly of two major types, a syntectonic monzogranite in the western part, and a late tectonic, evenly grained monzogranite containing xenoliths of the syntectonic granite in the eastern part. A minor part is post-tectonic monzogranite and alkalic granite in small stocks and dikes. These phases appear to have one calc-alkaline magmatic source with granite intrusion beginning during the tectonic phase and continuing after tectonism ceased. As the batholith and related stocks are intruded into the Abt Schist and the invasion culminated at about 570 Ma according to numerous K-Ar dates (tables 8, 10), consideration of interpreting the Abt schist coeval with the Murdama group seems plausible even though regionally metamorphosed in front of the Al Amar-Idsas overthrust fault.

Murdama group

The Murdama formation was named after Jabal Murdama 30 km southeast of 'Afif, a type locality (fig. 13) suggested by Bogue (1954) after his reconnaissance of the eastern shield area. Slate, phyllite, quartzite, graywacke, and conglomerate were seen in a traverse across the north end of the mountain. The contact with the underlying metavolcanic rocks seemed to be conformable at the northwest corner of the mountain (Brown and Jackson, 1960). Later, when the peninsular map was compiled, it became known from additional information that at least some paraschists cropping out along the Najd faults are of Murdama age. The Hadiyah slate was tentatively correlated by Brown and others (1963 b) with the type section of the Murdama formation, even though the sandstone-siltstone of the Hadiyah slate was first seen 500 km northwest of Jabal Murdama at the Hadiyah station on the Hejaz railroad. The correlation was made on the basis of lithologic similarity, thickness, degree of metamorphism, and an apparent stratagraphic position above rocks considered to be Halaban. Subsequently, the original Murdama formation was measured in detail by J. Letalenet (1974) on the western flank of Jabal Murdama, where he found a polygenic conglomerate resting on andesite of the Halaban and extending 2,700 m upward as graywacke, siltstone, and sandstone to a reddish-brown rhyolite porphyry overlying a polymict conglomerate. Letalenet (1974) considered the rhyolite to be part of the Murdama because the conglomerate beneath the rhyolite did not contain clasts of the underlying clastics of the Murdama. Earlier we had dated the rhyolite by K-Ar whole-rock methods at 561 $\pm$ 25 Ma and 560 $\pm$ 20 Ma (samples 141a, 141b, table 4, Aldrich and others, 1978). The samples are rhyolite crystal tuff and rhyolite porphyry which are deuterically altered, according to Salman Block. And more recently samples from the same locality average 544 Ma, utilizing conventional interpretations of K-Ar corrected to the Sydney decay constants (Baubron and others, 1976). Flows southwest of Al Madinah near the top of a similar thick clastic section gave an age of 633 $\pm$ 15 Ma by Rb-Sr whole-rock isochron (Hedge in Aldrich and others, 1978). These ages are concordant with those reported by Baubron and others (1976) for the Hibshi formation. Baubron and others (1976) considered the younger ages that they obtained for the Murdama to result from rehomogenization of the argon. We are inclined to consider the rhyolite at the center of Jabal al Murdamah as disconformable above the Murdama and belonging to the younger Shammar group which is dominantly alkalic flows. The Murdama formation was raised to group rank by Delfour, (1977) to include basal conglomerate and flows (Hibshi formation), limestone and marble (Farida formation), and the upper sandstone-siltstone facies (Hadiyah Formation).

East of Jabal al Murdamah in Jabal al 'Alam, the Murdama includes 500-800 m of fine-grained andesite at the core(top) of the Maslum syncline. The syncline is bisected by a post tectonic calc-alkalic granite which, although not isotopically dated, is similar to granites throughout the northeast shield with K-Ar dates of about 600 Ma. The Murdama has schistosity indicating two episodes of folding, an earlier episode resulted in low-grade greenschist facies and a later compression during the Najd faulting at about 550 Ma. A third possibly older tectonic epoch involves the Abt paraschists which conformably overlie the Ar Ridaniyah calcareous unit in the Ad Dawadami district at the eastern edge of the shield (Al Shanti, 1976). The lower part of the Ar Ridaniyah



Figure 13a. Type locality of Murdamah group, view to the southeast. The sediments of the Murdamah group lie in a syncline plunging to the southeast in the middle distance. It rests disconformably on the meta-andisite and metarhyolitic tuffaceous volcanics of the Halaban (Hulayfah) group exposed in the foreground.



Figure 13b. Slate and shale of the Hadiyah group beneath the flaggy Cambrian Siq Sandstone which in turn underlies the pinnacled Ram Umm Sahm sandstone. North edge of the Arabian Shield.

is gneissic and quartz-feldspathic schist which can be correlated with the Hibshi formation, at least in part, whereas the upper calcareous metasedimentary rocks is most likely the metamorphosed extension of the Farida marble underneath the Al Amar-Idsas fault. These beds all dip east except where invaded by posttectonic quartz monzonite and granite or local folds reverse the dip. The Farida marble in outcrop has been squeezed out of a stratigraphic position above basal conglomerate and graywacke, in places transgressing tectonically over the older Halaban crystalline rocks to overlap the Hibshi conglomerate.

Chitinozoan-like microfossils from dolomite at Jabal Rokham tentatively correlated with the Murdama group are similar to forms in the upper Riphean of Greenland and suggest that the span 638-600 m.y. B.P. for the Murdama group from K-Ar ratios is reasonable (Binda and Bokhari, 1980; Vidal, 1979).

Shammar group

The younger alkalic and peralkalic volcanic rocks (fig. 14) of the Shammar rhyolite and associated gently folded sedimentary beds were considered (Brown and Jackson, 1960) to be the youngest Precambrian rocks in the shield. The sialic, essentially unmetamorphosed volcanic rocks, including flows and tuffs, that are increasingly younger toward the northern edge of the shield, have been divided into two formations (Delfour, 1967). In the northwest Hejaz area, Brown and others (1963b) later recognized sedimentary rocks interbedded with and above the Shammar, as well as rhyolite and fine-grained granite in dikes and stocks that intrude the Shammar. The younger sedimentary beds including some flow rocks were later separated and assigned to the Jubaylah group by Delfour (1967, 1970a), who found the outcrops restricted to long narrow shear zones or grabens of the northwest-trending Najd fault system.

The radiometric time span was not closely defined by our early work (Brown and Jackson, 1960). If the age 633 $\pm$ 15 Ma obtained by Hedge (Aldrich and others, 1978) is considered the end of the Murdama epoch, the Shammar could represent volcanism from that time until about 555 $\pm$ 25 Ma, the date obtained for the Shammar by Baubron and others (1976, fig. 5) utilizing Rb/Sr data. The rhyolite (560 $\pm$ 20 Ma and 561 $\pm$ 25 Ma whole-rock K-Ar) at the center of the Jabal Murdama syncline is most likely post-Murdama and later phase of the Shammar rhyolitic volcanism but hydrothermal alteration found in one sample may have caused argon loss and a deceptive young age. The interval of 633 Ma to about 555 Ma was also a period of widespread plutonic activity: older calc-alkalic monzogranitic batholiths; younger transgressive plugs and stocks of increasing alkalinity to peraluminous and peralkalic intrusive rocks including ring dikes; and a comagmatic series ranging from about 620 Ma to about 550 Ma (Aldrich and others, 1978; Fleck and others, 1976; Schmidt and others, 1979). This activity appears to have culminated about 570 Ma.

In the region southwest of Ha'il in the Nuqrah quadrangle, Delfour (1977) found two formations in the Shammar--the basal Kuara formation with a basal conglomerate, upper clastic, rhyolite and andesite; and the upper Malha formation, mostly rhyolite flow and ignimbrite. The oldest reported age, 621 $\pm$ 25 Ma came from the Malha formation from six Rb-Sr measurements (Baubron



Figure 14a. Shammar group. Jabal Garra'ah is composed of a lithic tuff and andesite in foreground; rhyolite dike in background. Jibalah group sediments and thin flows overlie these beds on the left (northern) flank.



Figure 14b. Jibaylah group at Jebal Nadah. Sahl al Matran quadrangle at 26°25' N. long., 38°13' E. lat., view SE. Andesite on lower slope, in the Jibaylah yielded a K40Ar cooling date of 528± 20 m.a. from biotite (table 8) whereas the underlying rhyolite on right below the Jibaylah layered rocks yielded an average of 574± 6.7 m.a. from biotite for the underlying Shammar volcanics (Fleck and others, 1976).



Figure 14c. The Jibalah group at Jabal Antaq near the north end of the Halaban Ridge and near the east edge of the shield at lat. 24° N. A pebble conglomerate at the base underlies sandstone, siltstone, and shale here dipping east. Andesite interbedded at the type locality 380 km northwest is dated at 558± 66 m.a. (40Ar/39ASr) at the end of the Precambrian. Geochronology by J. F. Sutter.

and others, 1976; Delfour, 1977), thus indicating that the Murdama and the older portions of the Shammar groups are essentially of the same age, eruptions of Shammar volcanics continuing to the end of the Precambrian.

Jubaylah group

Sedimentary beds and flows originally mapped above and interbedded with the Shammar rhyolite (Brown and others, 1963) were later separated and recognized as a distinct unit above an unconformity (Delfour, 1967). They comprise the youngest rocks involved in the diastrophism of the Arabian Shield.

Outcrops are along and on top of the three principal Najd fault zones in the northern part of the shield, where underlying schistose rocks have been eroded to form troughs or faulted to form graben. Subsequent horizontal movement and some vertical movement has folded the Jubaylah beds into taphrogeosynclinoria, in which steeper limbs on the northeast flanks reflect the sinistral movement of the Najd faults (Delfour, 1970; Hadley, 1974). The thicknesses of exposures are variable, owing in part to subsequent erosion; the range from 155 m at Wadi Murdan (lat. 27°40' N.) near the northwest corner of the shield where the group dips under the Siq Sandstone, to 750–850 m at the Mashhad area (Hadley, 1974) (fig. 15a), and to 2,300 m at Qal'at as Sawrah (Hadley, 1975c) west of Harrat Khaybar could also be explained by irregular, fault-controlled deposition and presence of tuffs and volcanic flows. At the type locality east of Harrat Khaybar, the thickness of two formations of the Jubaylah Group is more than 3,300 m (Delfour, 1977). The group extends discontinuously southeast to Jabal Umm Taq on the west flank of Samra Halaban at long. 44°10' E., lat. 23°50' N. along the northeast Najd shear zone and to long. 44° E., lat. 22°40' N. along the middle Najd zone where the thickness is about 320 m.

The Jubaylah group was divided informally by Delfour (1967) at the type locality east of Harrat Khaybar into three units, a basal conglomerate; andesite, basalt, and welded silicic tuff; and a cherty limestone containing stromatolitic structures. Later he named two units, the basal Umm al 'Aisah and the upper Jifn Formations, but did not assign a formal name to the volcanics, recognizing that flows and ejecta occurred at various horizons in the section (Delfour, 1977). West of Harrat Khaybar, Hadley (1973) found a similar sequence which he named, from base upward, the Rubtayn (conglomerate and fine clastics), Badayi' (andesite), and Muraykhah (limestone and shale). West of the Mashhad area described by Hadley near Al 'Ula, the Jubaylah crops out in small areas along Wadi Falqah which follows a Najd fault zone where the following section is exposed: about 100 m of polymict conglomerate; andesitic tuff and agglomerate; siliceous beds with calcareous concretions and lithographic limestone; intraformational conglomerate containing clasts of the limestone; and an uppermost tuffaceous green shale. Fifty km farther northwest in Wadi Jizl west of Harrat al 'Uwayrid, 85 m of the lower part of the Jubaylah crops out beneath a rhyolite agglomerate thrust block. The beds are red sandstone and polymict conglomerate. Fifteen kilometers east of the above exposure, the basal conglomerate and sandstone are 64 m thick below 118 m of thin-bedded and fetid limestone, paper shale, siltstone, and chert. Ripple and rain splatter marks in the upper beds suggest a shallow-water and beach environment of deposition.

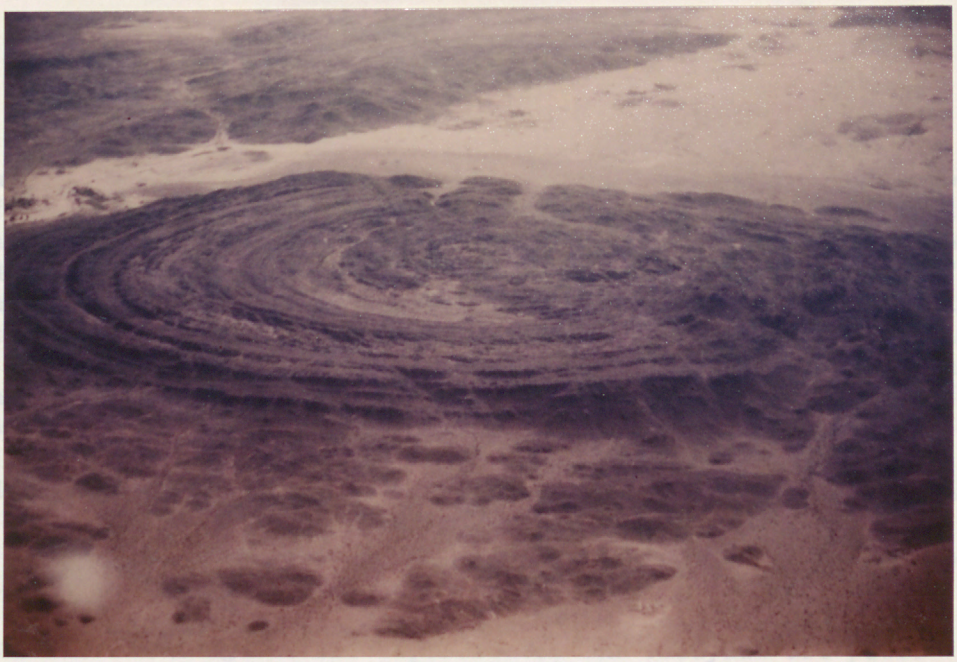

Figure 15a. Jabal Sha'i layered gabbro pluton in the southeastern shield near the village of Khaybar at lat. 18°47' N., long. 42°53' E. This carefully studied and drilled pluton yielded and age of 616 m.a. from 40Ar/39/Ar ratio in hornblende with a heating event at about 510 m.a. (Coleman and others, 1977)



Figure 15b. Aerial view to the southeast of Jabal Huassan at the east edge of the shield. The arcuate antiformal ridge is composed of Halaban metasediments graded through epidote schist to amphibolite around the Al Mizil orthogneiss (tonalite-trondhjemite) which underlies the central plain. The dome probably represents anatectonic reactivation of Halaban crust at about 600 m.a. or possibly younger (Fleck and Hadley, 1982).

One hundred fifty kilometers farther northwest at Wadi Murdan and beyond in Ash Shifa, the beds are polymict conglomerate and trachytoidal andesite porphyry; along the southwestern flank of Wadi As Sirr in the middle zone of the Najd fault system near where it intersects the Red Sea at lat. 27° N., thick red and green shale and fine-grained sandstone overlie a thick polymict conglomerate wherein are clasts from all the older rocks. Originally mapped as Shammar (Brown and others, 1963), the strata are probably of Jubaylah age, even though schistosity in some zones approaches that of the underlying Murdama group.

Toward the southeast end of Jubaylah outcrops near the eastern edge of the shield at Jabal Umm Taq (900 km southeast of the ash Shifa), wacke, shale, and siltstone dip 25°-30° E. above gray and red ripple-marked sandstone and a basal conglomerate of white quartz pebbles.

The lava flows throughout the exposures of the Jubaylah are petrographically different from older outpourings and are of interest for possible radiometric dating of the Jubaylah group. They are composed of andesite, alkalic basalt (mugearite), and rhyolite or lithic tuffs (minor), are generally porphyritic, often with large (2 cm) plagioclase phenocrysts (An 40-60), and are amygdaloidal. Amygdule minerals include quartz (cristobalite ?), and calcite. Delfour (1970) found rarer barite, celestite, and nepheline. Hadley (1974) described devitrified glass and chlorite, chlorophoenicite, epidote, and calcite; opaque iron-rich minerals are common in all sections except the crystal tuffs. Chlorite, epidote, and zeolites are products of hydrothermal alteration in one rock (see no. 67, an altered andesite, table 8).

Two samples (67, 69, table 8), from Delfour's type locality gave whole rock K-Ar ages of 299 $\pm$ 11 Ma for the lower hydrothermally altered flow containing deuteric calcite (R. Marvin, written commun.), and 548 $\pm$ 18 Ma for the dacite or alkalic andesite flow. The younger apparent age is most certainly unreliable, probably due to reheating during hydrothermal alteration. To check the possible validity of the 548 $\pm$ 18 Ma apparent age for the fresh andesite (no. 69, table 8), John Sutter (written commun., 1983) kindly made an 40 Ar/39 Ar age spectrum analysis of the andesite (table 9) and comments as follows: "40 Ar/39 Ar age spectrum plateau age = 558 $\pm$ 6.6 m.y. where 6.6 Mi error is reported at the 2 level of confidence (95 percent). The 40 Ar/39 Ar total gas age is 534 Ma which should be essentially equivalent to the K/Ar age for this sample.

"The age spectrum indicates loss of ^{40} Ar from the sample by volume diffusion from potassium-bearing mineral phases. I suggest that the major potassium-bearing phase is a feldspar and if so the apparent age of the first two temperature steps on the age spectrum (350-425° C), about 465 Ma, represents the last time the sample cooled through 100-150° C, the temperature range below which feldspars tend to retain most of their radiogenic argon." A whole-rock K/Ar age (fig. 16) of 515 $\pm$ 17 Ma (no. 22b, table 8) from a potassium-rich mafic flow could be reliable but could also be low due to argon loss. The chemical analysis is that of an oxidized mugearite (oligoclase andesine basalt) according to George Phair (USGS, written commun.). At the Mashhad area, Fleck and others (1976) determined K/Ar ages of 567 $\pm$ 6 and 581 $\pm$ 7 Ma for biotite in rhyolite of the Shammar group

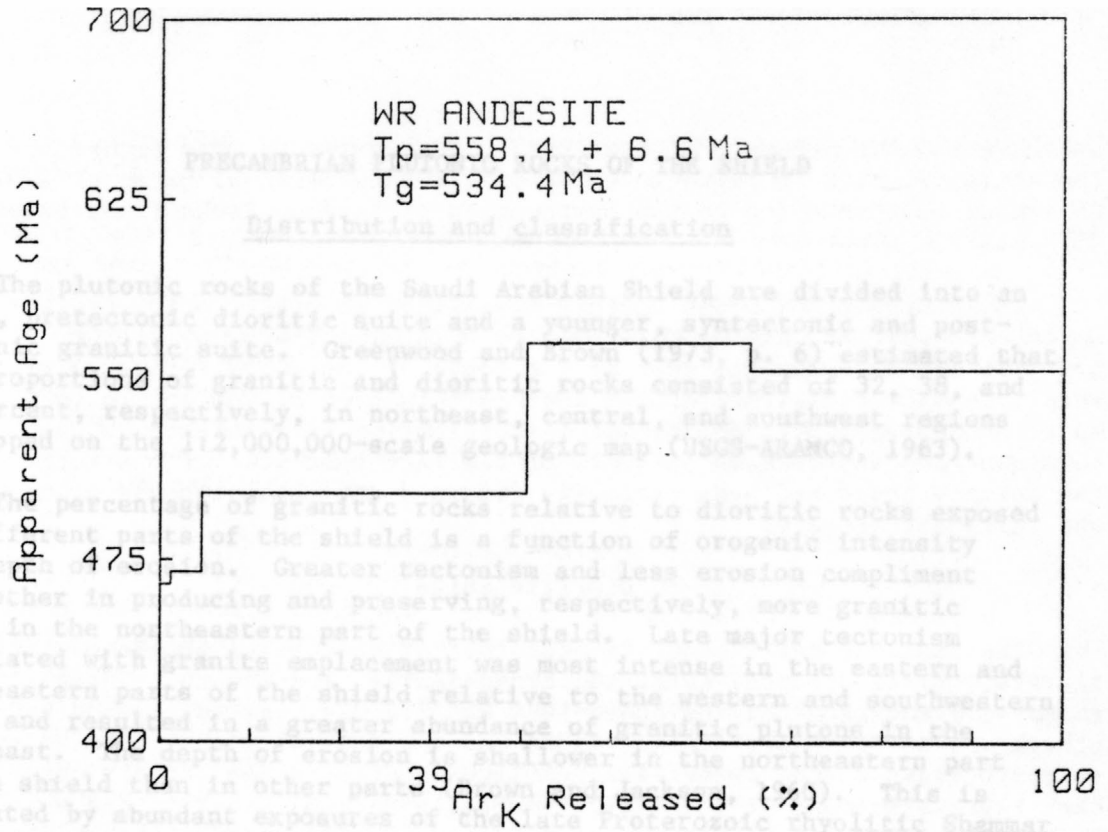

AGE SPECTRUM DATA

TEMP	40-Ar / 39-Ar	37-Ar / 39-Ar	36-Ar / 39-Ar	39-Ar % OF TOTAL	40-Ar* %	39-Ar (mole)	APPARENT K/Ca mole/mole	APPARENT AGE MA
350	278.124	5.184E-01	8.234E-01	1.2	12.5	1.34E-13	1.00E+00	464.90+- 98.90
425	66.237	3.015E-01	1.048E-01	3.4	53.3	3.67E-13	1.72E+00	469.89+- 8.64
500	45.951	3.477E-01	2.669E-02	35.9	82.9	3.90E-12	1.50E+00	502.55+- 3.14
850	45.840	4.055E-01	7.577E-03	24.7	95.2	2.69E-12	1.28E+00	565.27+- 3.25
FUSE	48.075	1.355E+00	1.898E-02	34.7	88.5	3.77E-12	3.84E-01	553.44+- 3.31
TOTAL GAS								534.43
PLATEAU AGE								558.37+- 3.28

G.BROWN: B1157 whole rock andesite
J = .008435 SAMPLE WT. = .2383g

Figure 16. Incremental 39-ArK of Jubaylah andesite at type locality of Jubaylah Group. By John Sutter.

ostensibly underlying the Jubaylah Group, although a fault separates the beds (Hadley, 1973). A sample of biotite from andesite at the Mashhad area +5ve a K/Ar age of 528 ± 20 Ma presumably from a flow in the Jubaylah, but the stratigraphic position is not certain. Also a K/Ar age of 532 ± 15 Ma was determined for a whole-rock sample from a basalt dike 41 km east of the Mashhad area where the dike crops out beneath the unconformity below the Siq Sandstone of probable Late Cambrian age. Finally, Baubron, Delfour, and Vialette (1976) measured whole rock K/Ar ages of 502 and 512 m.y. B.P. for flows from the Jubaylah; Delfour suggests that these dates are too low and reflect heating and argon loss during subsequent eruptions. Certainly almost all the samples we have examined show some hydrothermal alteration, but the question of whether this alteration was penecontemporaneous with the eruptions or was related to some later episode remains uncertain even though much of the evidence points to early hydrothermal metamorphism. The alteration of the lavas studied raises questions about the geological accuracy of the radiometric ages.

The Jubaylah group as now exposed appears to be of local derivation, even though the sequence in general is similar from basin to basin. Deposition began with coarse fluvial clastics, probably fanglomerate, ended with stromatolitic shallow-water marine beds, and was interrupted at various levels by flows of basalt, andesite, and rhyolite or lithic tuffs.

Stromatolitic mats in chert from the Jubaylah group at Jabal Umm al 'Aisah was studied and found to contain filaments of the blue-green algae Obruchevella parva, Reitlinger, a conical stromatolite, Conophyton, and unicells of uncertain affinity (Cloud and others, 1979). This meagre fauna suggests that the Jubaylah group is near the lower boundary of the Phanerozoic or latest Precambrian (Vendian). The disconformable stratigraphic position below the Siq Sandstone, which in turn is subjacent to or part of fossiliferous sandstone considered Upper Cambrian by Seilacher (1970), allows room for the radiometric dates to be true time of deposition and volcanic eruption, but the Ediacarian fauna in the cherty upper beds of the group together with the hydrothermal alteration and possible argon loss in the volcanic samples argue for an earlier, possibly earliest Cambrian or latest Precambrian age. Subsequent to the above reported age estimates, Pier Binda and C. R. Ramsay (1980) point out from BRGM work (Baubron and others, 1976) that the Jubaylah is disconformable above the Jabal ar Rahadah granite, which is dated at 577 ± 15 Ma by a 7-point Rb-Sr whole rock isochron (corrected to the Sydney constants). The granite is intruded into the Murdama group. Binda (1981) concludes that the Jubaylah group is probably uppermost Vendian (600-570 Ma old). A minimum age younger than 570 Ma does not invalidate Cloud's and Binda's conclusions, and the spectral age of 558 ± 6.6 Ma of Sutter seems a most logical date from all the evidence.

PRECAMBRIAN PLUTONIC ROCKS OF THE SHIELD

Distribution and classification

The plutonic rocks of the Saudi Arabian Shield are divided into an older, pretectonic dioritic suite and a younger, syntectonic and post-tectonic granitic suite. Greenwood and Brown (1973, p. 6) estimated that the proportions of granitic and dioritic rocks consisted of 32, 38, and 13 percent, respectively, in northeast, central, and southwest regions as mapped on the 1:2,000,000-scale geologic map (USGS-ARAMCO, 1963).

The percentage of granitic rocks relative to dioritic rocks exposed in different parts of the shield is a function of orogenic intensity and depth of erosion. Greater tectonism and less erosion compliment each other in producing and preserving, respectively, more granitic rocks in the northeastern part of the shield. Late major tectonism associated with granite emplacement was most intense in the eastern and northeastern parts of the shield relative to the western and southwestern parts and resulted in a greater abundance of granitic plutons in the northeast. The depth of erosion is shallower in the northeastern part of the shield than in other parts (Brown and Jackson, 1960). This is indicated by abundant exposures of the late Proterozoic rhyolitic Shammar group; in places, as at Jabal Aja', granitic intrusive rocks are still preserved in direct, subvolcanic contact with the Shammar volcanic rocks (Stoeser and Elliot, 1980). In the central part of the shield, in a belt about 200 km wide and including the major Najd fault zones, late orogeny was intense and the erosional level is moderately shallow in that many late granitic plutons are exposed with few cogenetic rhyolitic rocks of the Shammar group. The southern part of the shield is deeply eroded and was less deformed during the late major orogeny so that this region has the smallest area of granitic plutons and only rare exposures of Shammar-type volcanic rocks.

This deepening of erosion from north to south is well portrayed on the total-intensity aeromagnetic map of the shield, where the intensity of magnetization distinctly increases from north to south across the Shield (Blank, 1980).

In addition to the granitic and dioritic suites, a mafic-ultramafic suite is characterized by serpentinite in association with ultramafic, gabbroic, basaltic, and diabasic rocks. The mafic-ultramafic suite is confined mostly to narrow belts in large fault zones, is independent of the dioritic-suite rocks, and makes up less than one percent of the Precambrian plutonic rocks of the shield. The mafic-ultramafic suite is ophiolite that rarely is complete at any one locality and that probably represents tectonic remnants of oceanic crust of different ages in different places (Frisch and Al-Shanti, 1977; Delfour, 1979b; Bakor and others, 1976; Al-Rehaili and Warden, 1980).

In general, the plutonic rocks of the dioritic and granitic suites are petrographically easily classified into standard rock types. In this report granitic refers to lencocratic plutonic rocks containing more than 5 percent modal potassium feldspar and more than 20 percent modal quartz, thus

avoiding the broader term of granitoid. Rock names in this report are those of the classification of plutonic rocks of the International Union of Geological Sciences, Subcommission on the Systematics of Igneous Rocks (Strecheisen, 1973, 1976).

The plutonic rocks are further classified as pretectonic, syntectonic, and posttectonic in reference to a culminant orogeny (about 650 $\pm$ 25 Ma) during which most of the rocks of the early (primary) crust were intensely tectonized during the cratonization of the shield (675 Ma to 560 Ma ago). This tectonic classification in reference to the culminant orogeny is used in spite of the fact that most of the rocks of the primary crust had been variously deformed and metamorphosed prior to the culminant orogeny.

Dioritic suite

The dioritic suite consists, in order of decreasing abundances, of diorite, quartz diorite, tonalite, trondhjemite, and gabbro. These rocks were emplaced between about 1000 and 700 m.y. age (Greenwood and others, 1976; Fleck and others, 1980) and together with their equivalent volcanic rocks of the andesite assemblage constitute the primary crust that represents most of the early (precratonization) crust of the shield. Rocks of the dioritic suite are pretectonic in reference to the culminant orogeny.

The plutonic rocks of the dioritic suite are commonly medium grained and hypidiomorphic granular. The diorite contains hornblende with or without variable amounts of biotite and quartz. The quartz diorite and tonalite are quartz-biotite rocks with or without hornblende, and the trondhjemite is a quartz-biotite rock. The gabbro commonly contains clinopyoxene, partly altered to hornblende, and hornblende, partly altered to biotite. In many places, all these plutonic rocks have finer and coarser grained phases and their overall heterogeneous character suggests a shallow level of intrusion. In particular, the diorite commonly has mineral compositions and textures that are variable and heterogeneous even at outcrop and hand-specimen scale and suggest that some of the diorite was hypabyssal and subvolcanic to overlying andesitic volcanic rocks. The trondhjemite is locally graphic or granophyric and some contains enhedral quartz phenocysts and suggests that some trondhjemite is hypabyssal and subvolcanic to overlying dacitic volcanic rocks.

These early rocks were mostly well tectonized, pervasively sheared to a commonly north-trending foliation, and metamorphosed to the greenschist facies before the culminant orogeny and cratonization when they were tectonically mixed with their volcanic equivalents, the andesitic assemblage, and abundantly intruded by rocks of the granitic suite.

Many of the low-density, more silicic rocks of the dioritic suite such as the trondhjemites and some tonalites are found in large gneiss domes or antiforms where they had been metamorphosed to amphibolite facies, conspicuously shear foliated, and converted to orthogneisses. These gneiss domes rose gravitationally in response to heating and tectonic thickening

during the culminant orogeny. The orthogneisses are tectonically associated with migmatitic and plutonic rocks of the granitic suite.

During past mapping, many granitic gneisses and orthogneissic rock units have been variously mapped as basement rocks older than rocks of the adjoining dioritic suite in any given area. However, none of the isotopic ages of these gneisses have proven to be older than the associated dioritic suite and andestic assemblage rocks, and where well dated, all yield dates related to orogenies that are younger than the dioritic suite in their respective regions. The orthogneisses are in gneiss domes or large fault structures and most were tectonized and mobilized during the culminant orogeny.

Granitic suite

The granitic suite consists, in order of decreasing abundance, of granodiorite, granite, alkali-feldspar granite, and peraluminous-peralkalic granite, as well as gabbro. The rocks of the granitic suite are exposed throughout the Precambrian shield and are most abundant in the northeastern half of the shield, with the exception that alkali-feldspar granite and peralkalic granite have not been foud in the southwestern part of the shield (Stoeser and Elliott, 1980). Most of these rocks were emplaced during cratonization after about 675 Ma ago. Many granitic rocks are slightly to extensively tectonized and partly metamorphosed through pervasive cataclastic shear and are classified as syntectonic; these were intruded during the culminant orogeny. Other granitic rocks were intruded in a posttectonic setting from after the culminant orogeny to about the end of the Precambrian; they commonly produce contact metamorphic aureoles in the adjacent wall rock. A relatively few granitic rocks in the western half of the shield were intruded earlier than the culminant orogeny, during more spacially restricted orogenies, for example, about the time of the deposition of the Ablah group of rocks.

The syntectonic granitic rocks commonly form large batholiths of predominantly biotite granodioritic composition and are commonly associated with the large gneiss domes of tonalitic and trondhjemitic orthogneiss. The batholithic granodiorite is mostly conspicuously flow foliated as well as cataclastically sheared in response to late orogenic processes.

Early in the posttectonic setting, biotite granite (monzogranite and syenogranite) was intruded as large, irregularly shaped plutons. Presumably with increasing depth of erosion and the resulting increasing brittle fracture at shallow crustal levels, circular plutons of biotite-perthite granite, a few km to as much as 10 km in diameter, were emplaced somewhat later, about 600 Ma ago. Many of these are ring structured where they intruded preexisting structure or perhaps where some late orogenic forces controlled their emplacement. Some of these circular and elliptical plutons are composed of biotite-perthite alkali-feldspar granite and sodic amphibole peralkalic granite; some are peraluminous granites. Not all the late, small granitic plutons are circular or layered, but circular layered masses are conspicuous in most parts of the Shield.

The posttectonic granitic magmas were bimodal; some layered granite plutons contain partial concentric layers or irregular intrusive bodies of synchronously intruded basaltic, diabasic, or moderately mafic hybrid rocks. In addition, circular layered plutons of gabbro, commonly leucocratic from a few km to 10 km in diameter, are conspicuous throughout the shield. These gabbroic rocks are late, nonmetamorphosed, and in a few places can be seen to cut late granite plutons. That the late gabbro and the diabasic intrusions are intricately and synchronously associated with the circular granitic intrusions indicates that immiscible gabbroic magma was associated with granitic magma deep in the crust during cratonization.

The latest and shallowest granitic rocks of the Precambrian Shield are granite to alkali-feldspar granite in small plutons or stocks in or adjacent to the Najd fault zone. Those in the Najd fault zone are readily dated 1) as being slightly younger than the Najd faulting where they cut the strongly sheared rocks of the fault zone and commonly form small circular stocks less than several kilometers in diameter, or 2) as having been intruded during Najd faulting where the small plutons are greatly elongated (some elongation ratios to about 1:10) in the fault zone and where the granitic rock is highly flow foliated and sheared. These latter, synkinematic rocks are conspicuous granitic gneisses that often were mapped in the past as granitic orthgneisses of an old basement.

Many dikes of diabase and fewer dikes of rhyolite fill conjugate and secondary fractures complimentary to the Najd faults in large areas between the Najd faults (Moore, 1979). Large swarms of diabasic dikes are most common in the large granitic batholiths. For example, granodioritic batholiths were systematically fractured in contrast to the dioritic plutons in which strains were relieved by ductal yield along pre-existing structural grain. A few diabasic, gabbroic, and syenitic plugs less than 1 km in diameter intruded the Najd fault zones after fault movement had ceased.

CHEMISTRY OF THE PRECAMBRIAN CRYSTALLINE ROCKS

Introduction

The analysed rock samples were collected during reconnaissance geologic mapping, mostly prior to the more detailed, 1:100,000-scale mapping. The samples are from localities (fig. 2) well distributed over the entire shield and are listed in numerical order in table 3. The last two samples, numbers 501 and 502, are of Precambrian crystalline rocks from the bottom of two deep drill holes through the Phanerozoic sedimentary rocks in the Eastern Province of Saudi Arabia about 400 km east of the eastern edge of the shield; they are not shown on figure 2. Chemical and normative analyses of 199 Precambrian rocks of the Saudi Arabian Shield are given in table 4.

Most of the analyses were done in the U.S. Geological Survey laboratory, Washington, D.C., under the direction of F. J. Flanagan and Leonard Shapiro using the single-solution, rapid rock analysis method (Shapiro, 1967). Most of the samples had been analyzed previously in the DGMR-USGS laboratory in Jiddah, but because the laboratory at that time was set up for the routine analysis of minor metals in samples collected for mineral exploration, these early whole-rock analyses proved inadequate and most of the samples were re-analyzed in Washington.

The normative analyses were calculated on the USGS Multex System (Honeywell 6880 computer) using a graphic normative analyses program (Bowen, 1971) as modified by Stuckless and VanTrump (1979). The computer liaison was done by George VanTrump, Jr. The analyses were not corrected for the effects of hydration, oxidation, and introduction of CO_2 (Irvine and Baragar, 1971). For most samples for which CO_2 and H_2O are given, these effects can be discounted without significantly affecting the results.

In table 3 petrographic data are given and each sample is classified by igneous type, name, age, and tectonic region in order to compare the chemistry of the various categories of rocks. The rock names given in the classification part of the table are those recommended by the International Union of Geological Sciences Subcommission (IUGS) (Streckeisen, 1973, 1976, 1979). Each rock name is a consensus or a best compromise of the available petrography and of the normative mineralogy, but for consistency the naming strongly emphasizes the classification schemes of the IUGS Subcommission and of Irvine and Baragar (1971). Where naming proved difficult, a further check was made by using weight-percent chemical data directly in the classification of Church (1975).

Table 3. Description and classification of crystalline rocks of the Arabian Shield for which chemical analyses are given in table 4.

No. on fig. 2	Field number	Location[1] (lat.-long.)	Rock-unit symbol on Plate 1[2]	PETROGRAPHY: Color	Grain size[3]	Normative color index 4	Mafic content (percent)[5]	Plagioclase composition[6]	Normative An content[7]	Potassium feldspar type[8]	Rock texture-structure[9]	Rock name[10] (field or petrography)	Remarks	CLASSIFICATION: Igneous type[11]	Rock name[12] from chemistry	Age[13]	Region[14]	Reliability of analysis[15]
1	8712(ALD1)	28/35NW	mgd	Gray	--	(16)	3,Bi	Olig	(30)	Or,Pth	Cataclastic, Mr	Granodiorite	--	Plutonic	Granodiorite	C(S?) +	N	
3	B1813	"	*[gr](ju)	--	--	(53)	--	--	(58)	--	--	Amphibolite	Jabal Maglah; contact metamorphic, volcanic	Metam.(volc)	Amphibolite (basalt)	H	N	
4A	ALD3	"	gr	--	mg	(2)	2,Bi,Hb	Olig	(11)	Or,Pth	Minor catacl.	Granite	Near Jabal Lawz; rock similar to 4B	Plutonic	Granite	M +	N	
4B	B1815	"	gr	--	--	(2)	2,Bi	Olig	(11)	Or, Pth	Minor catacl.	Granite	Near Jabal Lawz; rock similar to 4A	Plutonic	Granite	M	N	
8	B1016(ALD7)	27/35NE	gp	--	--	(2)	1,Hb	--	(0)	Pth,Mc,Or	--	Granite	Jabal Harb; 0.5 km inside west border of pluton	Plutonic	Peralkalic granite	S, N? +	N	
9	B1011	"	*[jd](gp)	Red	mg	(7)	5,Mt	--	(0)	Pth	--	Granite	Small satellitic plug related to pluton of 13	Plutonic	Peralkalic granite	S, N?	NN	X
13	B1022	"	gp	Gray	fg-mg	(6)	20,Hb,Bi,Mt	--	(0)	Pth	Graphic, Mr	Granite	Center of large pluton in Najd fault zone, Jabal Shar	Plutonic	Peralkalic granite	S, N?	NN	X
14A	B1008C	"	gp	Red	--	(7)	--	--	(0)	--	--	Granite	Near contact, same pluton as 13, Jabal Shar	Plutonic	Peralkalic granite	S, N?	NN	X
14B	B1008	"	gp	--	fg-mg	(3)	3,Bi,Hb,Mt	--	(0)	Pth,Mc	Myrmekitic	Granite	Same pluton as 13, Jabal Shar	Plutonic	Peralkalic granite	S, N?	NN	X
14XA	B1009A	27/35SE	nsy	--	--	(3)	--	--	(3)	--	--	Syenite	Circular pluton in Najd fault zone	Plutonic	Alkalic quartz syenite	N	NN	
14XB	B1009B	"	nsy	--	--	(1)	--	--	(0)	--	--	Syenite	Same pluton as 14XA	Plutonic	Peralkalic quartz syenite	N	NN	
15	B1023	27/35NE	gp	--	fg	(2)	2,Mt	--	(0)	Mc,Pth	Micrographic	Granite	Jabal Shar; large sill or laccolith on Najd fault	Hypabyssal	Peralkalic granite	S, N?	NN	X
17	B1007	"	gp	Red	mg	(1)	1,Hm	--	(0)	Mc,Pth,Or	Micrographic	Granite	Jabal Shar; same pluton as 13	Plutonic	Peralkalic granite	S, N?	NN	X
18	B1044	27/36NW	rt	Red	fg	(3)	--	--	(4)	--	Porphyritic	Rhyolite porph.	Intrudes greenstone; intruded by diabase dikes	Hypabyssal	Rhyolite	S	N	
19	B1046	"	nj	--	--	(23)	--	--	(37)	--	Trachytoidal	Andesite	Associated with Najd fault; basaltic andesite?	Volcanic	Alkalic basalt	K	N	
20	B1052	"	nj	--	--	(7)	--	--	(32)	--	Welded tuff	Rhyolite	Clast in basal conglomerate on Najd fault	Volcanic	K-r olite?	S	N	X
21	B1047	"	gp	Dark-red	mg	(5)	Hm	--	(3)	Or,Pth	--	Granite	Appears disconformable below Jubaylah	Plutonic	Alk-feldspar granite	S	N	X
22A	B1062B	27/36SE	nj	--	--	(2)	Oxidized Rieb?	--	(6)	--	Lithic fragm.	Rhyolite tuff	Flow, 1 m thick, in Jubaylah Group	Volcanic	Na-rhyolite?	K	NN	X
22B	B1062C	"	nj	Dark-green	Crypto.	(18)	26Px (alt'd)	Olig-And	(21)	Or	Porph, amygd	Basalt	Flow in Jubaylah; oxidized mugearite?	Volcanic	Alkalic basalt	K +	NN	
23	B1059	26/36NW	gb	Gray	--	(10)	14, Hb,Bi	--	(3)	--	--	Leucogabbro	Small pluton in Najd fault zone	Plutonic	Trondhjemite	H(N?)	WN	
24	B1037	"	ga	Red	mg	(3)	6,Bi,Mt	--	(8)	Pth,Mc	--	Granite	Jabal Liban; large granite pluton; 1% modal fluorite	Plutonic	Alk-feldspar granite	S +	WN	
25A	B1823	26/37NW	gr	--	--	(6)	5,Hb,Bi	Olig	(21)	Or	--	Granodiorite	10 x 20 km elliptical pluton,	Plutonic	Granodiorite	S	NN	

Sample number Plate 1	Field number	Location[1] (lat.-long.)	Rock-unit symbol on Plate 1[2]	PETROGRAPHY: Color	Grain size[3]	Normative color index 4	Mafic content (percent)[5]	Plagioclase composition[6]	Normative An content[7]	Potassium feldspar type[8]	Rock texture-structure[9]	Rock name[10] (field or petrography)	Remarks	CLASSIFICATION: Igneous type[11]	Rock name[12] from chemistry	Age[13]	Region[14]	Reliability of analysis[15]
25B	B1823A	"	*[gr](nj)	--	vfg	(19)	?,Hb	--	(53)	--	--	Andesite	Small plug or dike in Najd fault zone, similar to 28A	Hypabyssal	Quartz andesite	K?	NN	
27	B1824	"	Sr	--	--	(3)	--	--	(3)	--	--	Rhyolite	Shammar? structurally above Jubaylah in Najd fault	Volcanic	Alk-feldspar rhyolite	S	NN	
28A	B1822	"	*[mh](di)	--	vfg	(22)	Cpx,Hb	And	(41)	--	--	Microdiorite	Contact zone of satellite near 25B	Hypabyssal	Diorite	K?	NN	
28B	B1822A	"	*[mh](gm)	--	--	(7)	?,Hb,Bi	Olig	(24)	Pth	--	Adamellite	Small pluton, 2.5 km across, satellitic to pluton at 25A	Plutonic	Granodiorite	S	NN	
29	B1825	"	ay(gp)	Red	fg	(2)	?,Hm	--	(4)	Pth,Mc	Micrographic	Granite	Granite on Najd fault	Plutonic	Alk-feldspar granite	S, N?	NN	
30	B1831	26/37SW	npg	--	--	(2)	?,Bi	--	(9)	Mc,Or,Pth	Hypidiomorphic	Granite	In Najd fault zone	Plutonic	Granite	S	WN	
31	B1826	"	nog	--	--	(3)	?,Bi	--	(11)	--	Flaser gneiss	Granite	Jabal Ghalal, in Najd fault zone	Gneiss	Trondhjemite	C	WN	
32	B1829	"	*[ngn](gm)	--	fg-mg	(3)	?,Bi	--	(16)	--	Hypidiomorphic	Adamellite	Jabal Ghalal, in Najd fault zone	Plutonic	Granite	C	WN	
33	B1827	"	*[npg](gm)	--	cg	(2)	3,Bi,Hb	Olig	(8)	Pth,Mc	Hypidiomorphic	Granite	Jabal Ghalal, in Najd fault zone	Plutonic	Alk-feldspar granite	S	WN	
36	B1126	26/37SE	Sr	Dark-red	fg	(10)	?,Hm	--	(17)	--	Micrographic	Felsite	Related to subvolcanic intrusion, Shammar age	Dike	Dacite	S	NN	
37	B1125	26/38SW	*[jq](mgd)	--	--	(6)	10,Bi,Hb	Olig	(22)	Or	Mod. catacl.	Adamellite	In quartz diorite-diorite body	Plutonic	Granodiorite	C, S?	NN	
38	B1805	26/37SE	nj	--	--	(2)	?,Bi	--	(19)	Or	Welded tuff	Rhyolite	In Jabaylah sedimentary section	Volcanic	K-rhyolite	K	NN	Y
39	B1806	"	nj	--	--	(3)	--	--	(12)	--	Pyroclastic	--	Highly calcic tuff or calcarenite	Sedimentary	Calcic tuff	K	NN	ZX
41	B1109	26/38SE	*[ay](gm)	--	--	(5)	--	--	(4)	--	Minor catacl.	Granite	Qalat as Sawrah quad., unit includes granophyre	Plutonic	Alk-feldspar granite	S	NN	
42	B1107	"	asy	--	--	(7)	?,Bi,Hm	--	(18)	Micro Pth	--	Granite	Qalat as Sawrah quad., weathered	Plutonic	Granite	A	NN	
43	B1804	"	gr	Red	cg	(2)	1,Bi	Olig	(10)	--	--	Adamellite	Qalat as Sawrah quadrangle	Plutonic	Granite	S	NN	
45	B1106	26/38SE	*[agr](agb	--	--	(34)	Hb,Bi	--	(41)	--	--	Diorite	Part of Jabal abu Safiyah complex	Plutonic	Qtz. diorite	A	NN	
46	B3906A	"	agd	--	--	(2)	1,Bi	Ab-Olig	(2)	Mc	Cataclastic	Granite gn.	Qalat as Sawrah quadrangle	Gneiss	Alk-feldspar granite	A?	NN	
47	B1104	"	agr	Red	fg	(1)	Bi	And	(3)	--	Porphyritic	Granite	Qalat as Sawrah quad., highly altered	Plutonic	Alk-feldspar granite	S (N?)	NN	
48	B1840	25/37NW	gr	--	--	(2)	2,Bi	Olig	(9)	Pth,Mc	Hypidiomorph.	Adamellite	Cavernous weathering; in Najd fault zone	Plutonic	Alk-feldspar granite	S	WN	
49	B1845	"	gr	--	mg	(2)	2,Bi	Olig	(0)	Mc,Pth	Hypidiomorph.	Adamellite	--	Plutonic	Granite	S	WN	
50	B1839	"	gr	--	mg	(1)	1,Bi	Olig	(2)	Pth,Mc	Hypidiomorph.	Adamellite	Cavernous weathering	Plutonic	Granite	S	WN	

Sample number Plate 1	Field number	Location[1] (lat.-long.)	Rock-unit symbol on Plate 1[2]	PETROGRAPHY Color	Grain size[3]	Normative color index 4	Mafic content (percent)[5]	Plagioclase composition[6]	Normative An content[7]	Potassium feldspar type[8]	Rock texture-structure[9]	Rock name[10] (field or petrography)	Remarks	CLASSIFICATION Igneous type[11]	Rock name[12] from chemistry	Age[13]	Region[14]	Reliability of analysis[15]
51	B1838	"	*[agd]	Black	--	(27)	50,Hb	--	(65)	--	Diabasic	Diabase	Wadi Hamdh	Dike	Leuco. diabase	N	WN	
52	B1835	25/37NE	nog	--	fg	(2)	4,Bi	--	(20)	--	Gneissic	Trondhjemite	Basement on Najd fault	Gneiss	Trondhjemite	J (N?)	WN	
54	S1GPB	25/38NW	ngn	--	fg-mg	(4)	7,Bi	--	(20)	Or	Gneissic	Granite	Wadi al Jizl, in Najd fault zone	Gneiss	Granodiorite	C?(N?)+	NN	
55	B1123	25/38NE	agb	--	--	(52)	--	--	(55)	--	--	Gabbro	Part of Jabal abu Safiyah complex	Plutonic	Gabbro	A	NN	
56	B1843B	25/37SW	jgb	--	--	(7)	?,Bi	--	(27)	--	--	Qtz. diorite	--	Plutonic	Trondhjemite	J	WN	
57	B1630	24/38SW	jt	--	--	(14)	20,Hb,Px,Bi	An_{30}	(46)	--	Gneissic	Qtz. diorite	Yanbu	Plutonic	Tonalite	J	WC	
58	B1312	27/41NW	gp	Gray	fg	(8)	5,Bi,Hb	--	(0)	Pth	Micrographic	Granite	Jabal Aja, gr-gp batholith	Plutonic gn.	Peralkalic granite	S	NE	
61A	B1310	27/41SW	*[gr](gp)	Red	--	(1)	--	--	(10)	--	--	Granite	Jabal Aja, layered, layer adjacent 61B; altered	Plutonic	Granite	S	NE	
61B	B1311	"	gp	Red	mg	(1)	Hm, Na-amph?	--	(6)	Pth	Hypidiomorph.	Granite	Jabal Aja, layer adjacent to 61A	Plutonic	Alk-feldspar granite	S	NE	
62	B1308	26/41NE	gp	--	--	(7)	Hb (Na-amph?)	--	(3)	Pth	Cataclastic	Granite	Jabal ar Rumman, gp batholith	Plutonic gn.	Alk-feldspar granite	S	NE	
63	B1103	26/39SW	ay	--	--	(1)	--	--	?(73)	--	Agglomeratic?	Rhyolite?	Jabal as Safran, not evaluated	Altered?	--	S?	NN	X
64	B1325	26/41SE	*[hq](gr)	Red	fg	(1)	Mt	--	(6)	--	--	Granite	--	Hypabyssal	Granite	S	NE	
65	17,827	25/39NW	*[ay](jq)	Gray	--	(17)	14,Hb,Bi	Olig	(36)	Or	--	Qtz. diorite	Old basement	Plutonic	Tonalite	J	NN	
66	B1154	25/40NE	hc	--	--	(26)	Bi	--	(47)	--	--	Phonolite	Nuqrah quad, under Jubaylah conglomerate	Volcanic	Andesitic basalt	H (K?)	HN	
67	B1155	"	nj	--	vfg	(30)	14	Ab-Olig	(31)	--	Amygdaloidal	Andesite	Nuqrah quad, flow above Jubaylah conglomerate	Volcanic	Basaltic andesite	K +	HN	
68A	JD1714	"	hc	--	--	(8)	--	--	(12)	--	--	Rhyolite	Nuqrah quad, from drill core	Volcanic	Na-dacite	H +	HN	
68B	JD1713	"	hc	--	--	(6)	--	--	(3)	--	--	Rhyolite	Nuqrah quad, from drill core, Nuqrah formation	Volcanic	Na-rhyolite	H	HN	
69	B1157	"	nj	Red-brown	fg	(18)	35,Hm,Epi	And	(30)	--	--	Andesite	Nuqrah quad, flow	Volcanic	Andesite?	K +	HN	
70	B1145	"	hc	--	--	(9)	12,Mt	Olig	(12)	--	Porphyritic	Rhyolite	Nuqrah quad, flow in pyroclastic section	Volcanic	Na-dacite	H	HN	
71	JD1711	25/41NW	hc	--	Micro-cryst.	(7)	Mt?	Olig	(6)	Or	Porphyritic	Rhyolite	Nuqrah quad, from drill core	Volcanic	Na-rhyolite	H +	TN	
73	B2078	24/40NE	mh, ar	--	--	(3)	--	--	(25)	--	Breccia	Felsite	Jabal Shida	Volcanic	K-rhyolite	S	HC	Y
74	B1137	"	*[nj]ngb	--	--	(35)	Px,Opx	Lab	(51)	--	--	Gabbro	Intrusive into Jubaylah with granophyre	Plutonic	Gabbro	K	HC	
75	B1138	"	nj	--	--	(19)	--	--	(39)	--	--	Magearite	Hanakiyah	Volcanic	Andesite	K	HC	

Sample number Plate 1	Field number	Location[1] (lat.-long.)	Rock-unit symbol on Plate 1[2]	PETROGRAPHY Color	Grain size[3]	Normative color index 4	Mafic content (percent)[5]	Plagioclase composition[6]	Normative An content[7]	Potassium feldspar type[8]	Rock texture-structure[9]	Rock name[10] (field or petrography)	Remarks	CLASSIFICATION Igneous type[11]	Rock name[12] from chemistry	Age[13]	Region[14]	Reliability of analysis[15]	
76	S2GFB	24/39SW	gm	--	mg	(2)	3,Bi	Olig	(13)	Pth,Mc	Cataclastic	Granite	SW of Medina, batholith cut by Najd faults	Plutonic	Granite	M	WC		
77	S3GFB	24/39SE	*[gm]ga	Red	mg	(3)	3,Mc,Bi	Olig	(3)	Pth,Mc	Minor catacl.	Granite	Medina, from quarry, small granite body	Plutonic	Alk-feldspar granite	M +	HC(NN)		
78A	ALD9	27/42SW	gp	Gray	mg	(1)	2,Bi	Olig?	(6)	Pth,Mc	Hypidiomorph.	Granite	Jabal Selma, near 78B	Plutonic	Alk-feldspar granite	S +	NE		
78B	B1316	"	gp	Red	--	(2)	--	--	(7)	--	--	Granite	Jabal Selma, near 78A	Plutonic	Alk-feldspar granite	S	NE		
80	B1339	26/42SW	hq	Gray	--	(29)	--	Olig?	(36)	--	Gneissic	Qtz. diorite	Gneiss below Hibahi conglomerate	Gneiss	Qtz. diorite	H	NE		
81A	B1338A	"	[mi](gr)	Gray	cg	(3)	Bi	Olig	(19)	--	Hypidiomorph.	Adamellite	Jabal Hibahi, granite boulder from Hibahi conglomerate	Plutonic	Granite	M	NE		
81B	B1338B	"	[mi](gr)	Red	fg	(1)	--	--	(11)	--	--	Granite	Jabal Hibahi, granite boulder from Hibahi conglomerate	Plutonic	K-granite	M	NE		
82A	ALD10	"	mgd	Red	--	(15)	12,Hb,Bi	Olig	(26)	Or	Hypidiomorph.	Granite	Jabal Tin	Plutonic	Granodiorite	C +	NE		
82B	B1330	"	mgd	--	--	(13)	--	--	(29)	--	--	Granite	Jabal Tin	Plutonic	Granodiorite	C	NE		
83A	B1333	26/42SW	gr	Gray	--	(12)	--	--	(27)	--	--	Granite	Granitoid, possibly intrudes Hibahi formation	Plutonic	Quartz monzodiorite	M	NE		
83B	B1334	"	mi	--	--	(5)	--	--	(15)	--	--	Dacite	Flow in upper Hibahi fm	Volcanic	Dacite	S	NE		
84	B1301	25/42NW	gp	White	--	(2)	Na-amph?	Olig	(8)	Pth,Or	--	Granite	Jabal Qutn, 15-km circular pluton, intrudes mu	Plutonic	Alk-feldspar granite	M - S	NE		
85	B1302	"	gr	Gray	mg	(5)	Bi	--	(29)	Pth,Mc	--	Granite	East of Qutn, 5-km circular pluton, intrudes mu	Plutonic	Granodiorite	M - S	NE	Y	
86	B1317	"	gr	Gray	--	(6)	--	--	(29)	--	--	Granite	East of Qutn, 4-km circular pluton, intrudes mu	Plutonic	Granodiorite	M - S	NE		
87	B1318	25/42NE	gr	Gray	mg	(9)	--	--	(30)	--	--	Granite	East of Qutn, 3-km circular pluton, intrudes mu	Plutonic	Granodiorite	M - S	NE		
88	B1340	25/43SE	mgd	--	--	(9)	7,Bi	--	(34)	--	--	Adamellite	Intrudes Murdama formation	Plutonic	Granodiorite	S	NE		
89	B1341	"	mgd	--	--	(10)	19,Bi,Hb	And	(32)	Mc,Or	--	Adamellite	Intrudes Murdama formation	Plutonic	Granodiorite	S +	NE		
90A	ALD12	24/43NE	mgd	--	--	(11)	11,Bi,Hb	And	(28)	Or	Cataclastic	Granite	Intrudes Murdama and Abt formations	Plutonic	Granodiorite	S +	NE		
90B	B1342A	"	mgd	--	--	(3)	--	--	(25)	--	--	Granite	Intrudes Murdama and Abt formations, similar to 90A	Plutonic	Granodiorite	S	NE		
91A	ALD13	"	gp	--	--	(1)	3,Bi(Fl)	Ab-Olig	(11)	Pth,Mc	Minor catacl.	Granite	Circular pluton 7-km diameter, intrudes Abt fm.	Plutonic	Granite	S +	NE		
91B	B1345	"	gp	--	--	(2)	--	--	(14)	--	--	Granite	Circular pluton 7-km diameter,	Plutonic	Granite	S	NE		
93A	Q13064	24/44SW	gb	--	--	(47)	--	--	(58)	--	--	Gabbro	Jabal al Jilani, elliptical gabbro; intruded by Dawadimi batholith, nos. 88-90.	Plutonic	Gabbro	E?	NE		
93B	Q11464M	"	gb	--	--	(39)	--	--	(59)	--	--	Gabbro	Jabal al Jilani, elliptical gabbro	Plutonic	Gabbro	E?	NE		

Sample number Plate 1	Field number	Location[1] (lat.-long.)	Rock-unit symbol on Plate 1[2]	PETROGRAPHY Color	Grain size[3]	Normative color index 4	Mafic content (percent)[5]	Plagioclase composition[6]	Normative An content[7]	Potassium feldspar type[8]	Rock texture-structure[9]	Rock name[10] (field or petrography)	Remarks	CLASSIFICATION Igneous type[11]	Rock name[12] from chemistry	Age[13]	Region[14]	Reliability of analysis[15]
93C	Q22A64	"	gb	--	--	(34)	--	--	(61)	--	--	Gabbro	Jabal al Jilani, elliptical gabbro	Plutonic	Gabbro	E?	NE	
93D	Q22645	"	gb	--	--	(37)	--	--	(59)	--	--	Gabbro	Jabal al Jilani, elliptical gabbro	Plutonic	Gabbro	E?	NE	
93Z	B1439	24/44SE	gm	--	--	(22)	--	--	(37)	--	--	Granodiorite	Jabal al Hasraj, small gr pluton, intrudes Aht fm.	Plutonic	Qtz. monzodi.	S	NE	
94	B1163	23/39NE	ju (fa)	--	vfg	(13)	Bi	Olig	(0)	Or	--	Rhyolite	Small intrusive into conglomerate of Fatima formation, see 106	Hyabyssal	Na-rhyolite?	S(Fa) +	WC	Y
98	JD1712	23/40NE	hc	--	vfg	(9)	--	And	(76)	--	flow banded	Rhyolite	Jabal Sayid, near Najd fault and gp pluton; K metasom.	Volcanic	K-dacite?	H +	HC	Y
102	B215	23/41NW	hc	--	vfg-glassy	(11)	Hm	And	(16)	Or?	Porphyritic	Dacite	Associated with rhyolite, dacite, red andesite flows	Volcanic	Na-dacite?	H +	HC	
103	B216	"	*[gr]	--	fg	(44)	27,Hb,Cpx, Opq	Lab	(46)	--	--	Diabase	Near Najd fault, Najd? age	Dike	Diabase	N +	HC	
104	B1497 (ALD15)	23/41NE	gb	Dark	--	(41)	--	--	(76)	--	Mod. gneissic	Diorite	Jabal al Hamam, Halaban or Jiddah basement	Plutonic	Gabbro	H +	HC	
105	B1498	"	hc	Light	fg	(3)	10?,Bi,Hb?	Olig?	(21)	Or?	Cataclastic	Granodiorite	5 km SE of Jabal al Hamam	Plutonic	Granodiorite	C?	HC	
106	B1165	23/39SE	fa	--	fg	(3)	--	Olig	(11)	Or?	Porphyritic	Latite	Flow or sill at top of Fatima section, see 94	Volcanic	Na-rhyolite	Fa +	WC	
111	B1611	22/39SW	jq	Gray	mg	(6)	Hb,Bi	--	(25)	--	--	Granodiorite	Dahaban, syntectonic intrusion	Plutonic	Granodiorite	A?	WS	
113	B1610	21/39NW	agr	Gray	fg	(2)	--	--	(0)	--	Granophyric	Granite	North of Jiddah, subvolcanic to Fatima silicic volc.	Plutonic	Alk-feld. gr.	Fa	WS	
114A	B1600, (ALD18)	"	*[jd](agr)	Gray	mg	(2)	1,Bi,Mu	Olig	(13)	Pth, Or	Gneissic	Granite	Quarry east of Jiddah airport	Plutonic (gn)	Granite	A +	WS	
114B	B1600A	"	*[jd](agd)	Gray	fg-mg	(14)	6,Bi,Hb,Mu	Olig	(25)	Or	Mod. catacl.	Granite	Quarry east of Jiddah airport	Gneiss	Granodiorite	A	WS	
114C	B1600B	"	*[jd](agd)	Gray	--	(5)	9,Ep,Chl	Olig-and	(21)	Or	Cataclastic	Granite	Quarry east of Jiddah airport	Gneiss	Granodiorite	A	WS	
115	B1601	"	*[jd](agd)	--	--	(4)	--	--	(29)	--	Cataclastic	Granite	East of Jiddah airport	Gneiss	Granodiorite	A	WS	
116	B1606A	"	*[jt]	Dark	fg	(24)	--	--	(57)	--	--	Diabase	North of Jiddah, dike in metadiorite	Dike	Qtz. diabase	Fa? N?	WS	
117A	B900	21/39NE	fa	Dark	--	(42)	Ol?,Px?,Opq	And-Ab?	(3)	--	Porphyritic	Basalt	Jabal Mukassar, 2-m sill, 10 m below top, upper fa.	Sill	Na-andesite?	Fa-S? +	WS	
117B	B901	"	fa	Dark	vfg	(18)	Bi,Hm	Olig?-And	(20)	--	Porphyritic	Dacite	Jabal Sidr, 30-m sill on top, intrudes limestone	Sill	Na-andesite?	Fa-S? +	WS	
122	B1629	21/39SW	*[jd](ju)	Dark-green	--	(6)	--	--	(18)	--	--	Dacite	Greenstone quarry south of Jiddah	Volcanic	Na-dacite	J	WS	
123	B1625	"	*[agd](agr)	Red	--	(3)	--	--	(7)	--	--	Granite	Small pluton east of Jiddah, north of Makkah road	Plutonic	Na-granite	Fa	WS	
124A	ALD19	21/39SE	jq	Gray	--	(10)	18,Bi,Hb	And	(39)	--	Cataclastic	Trondhjemite	Fresh rock from pipeline ditch, east of Makkah	Gneiss	Tonalite	J +	WS	

Sample number Plate 1	Field number	Location[1] (lat.-long.)	Rock-unit symbol on Plate 1[2]	PETROGRAPHY									Rock name[10] (field or petrography)	Remarks	CLASSIFICATION				
				Color	Grain size[3]	Normative color index 4	Mafic content (percent)[5]	Plagioclase composition[6]	Normative An content[7]	Potassium feldspar type[8]	Rock texture-structure[9]				Igneous type[11]	Rock name[12] from chemistry	Age[13]	Region[14]	Reliability of analysis[15]
124B	B1603	"	jq	--	--	(4)	--	--	(27)	--	--		Trondhjemite	Similar to 124A	Gneiss	Trondhjemite	J	WS	
125	ALD21	21/40SW	agm	--	--	(3)	--	--	(14)	--	--		Granite	Taif, small gr pluton, from quarry	Pluton	Granite	S +	B	
126	ALD23	10/41NW	jt	--	--	(10)	--	--	(39)	--	--		Qtz. diorite	Wadi Shuqub quad, small outlier to large batholith	Plutonic	Tonalite	J +	B	
127A	ALD22	"	gp	Pink	cg	(2)	--	--	(6)	--	--		Granite	Jabal Qunah pluton, outer ring granite	Plutonic	Alk-feldspar granite	S +	B	
127B	9B	"	gp	--	--	(2)	--	--	(8)	--	--		Granite	Similar to 127A	Plutonic	Alk-feldspar granite	S	B	
133	B1702	20/41SE	jd	--	--	(16)	--	--	(64)	--	--		Diorite	Aqiq quadrangle, complex diorite batholith	Plutonic	Qtz. diorite	J	B	
134	B1703	"	ab	--	--	(9)	--	--	(1)	--	--		Rhyolite	Aqiq quad, Ablah belt, flow near base	Volcanic	Na-rhyolite	A	J	
138	B1725	"	ab	--	--	(24)	--	--	(28)	--	--		Andesite	Aqiq quad, Ablah belt, sill near gr. stock	Sill	Andesite	A	J	
139	B1726	"	*[ab]	--	--	(2)	--	--	(7)	--	--		Rhyolite	Aqiq quad, Ablah belt, 10 m thick sill	Sill	Alk-feldspar rhyolite	S	J	
141A	B230A	23/43NW	mu	Dark	ultra-fg	(13)	Bi,Cpx	And	(23)	--	Flow,porph.		Dacite	Jabal al Murdamah; flows above upper cgl., = Shammar	Volcanic	Dacite-andesite?	S(M) +	TN	
141B	B230	"	mu	Red-brown	--	(3)	Cpx,Hb	Olig	(14)	Or,Microph	Flow,porph		Rhyolite	Jabal al Murdamah; flows above upper cgl., = Shammar	Volcanic	Rhyolite	S(M) +	TN	
141C	B229	"	mu	"	ultra-vfg	(3)	Hb?,Bi	Olig	(18)	Or	Flow,porph		Rhyolite	Jabal al Murdamah; flows above upper cgl., = Shammar	Volcanic	Na-dacite?	S(M)	TN	
141D	B1368B	"	mu	"	--	(3)	--	--	(5)	--	Flow, porph		Rhyolite	Jabal al Murdamah; flows above upper cgl., = Shammar	Volcanic	Rhyolite	S(M)	TN	
142	B233A	23/43NE	mu	--	vfg	(10)	--	--	(29)	--	--		Dacite	Afif quadrangle, flow above Murdama, = Shammar	Volcanic	Dacite	S(M)	TN	
143	B247	"	hd	--	--	(15)	--	--	(31)	--	--		Microdiorite	Afif quadrangle, greenstone under Farida marble	Volcanic	Dacitic andesite	H?	TN	
144A	ALD14	23/44NE	ga	--	--	(2)	Bi	--	(10)	Pth	--		Granite	Jabal Zaabah, ring-structured, intrudes Abt fm.	Plutonic	Alk-feldspar granite	S(N?) +	NE	
144B	B1362	"	ga	--	--	(6)	13,Bi,Hb	Olig	(20)	Pth,Mc	Hypidiomorph.		Granite	Jabal Zaabah, ring-structured, intrudes Abt fm.	Plutonic	Granite	S(N?)	NE	
145	B1432	23/44SE	um	--	--	(31)	--	--	(65)	--	--		Gabbro	Fault associated, pre-Halaban ophiolite?	Plutonic	Gabbro	pre-H	NE	
146	B1512	22/42NE	hu(mu)	--	--	(1)	--	--	(4)	--	--		Rhyolite	Rhyolite boulder from Murama cgl. (mapped as hu), 146 rhy similar 147A gm = Shammar	Volcanic	Alk-feldspar rhyolite	M = S?	TC	
147A	B1513A	"	*[gm](mog)	Gray	--	(1)	--	--	(6)	--	--		Granite	Foliated granite intrudes Halaban? of 147B	Plutonic	Alk-feldspar granite	M?	TC	
147B	B1513B	"	*[gm](hu)	--	--	(29)	Px	--	(60)	--	Flow		Basalt	Flow in Halaban?, intruded by 147A	Volcanic	Quartz basalt	H	TC	

Sample number Plate 1	Field number	Location[1] (lat.-long.)	Rock-unit symbol on Plate 1[2]	PETROGRAPHY: Color	Grain size[3]	Normative color index 4	Mafic content (percent)[5]	Plagioclase composition[6]	Normative An content[7]	Potassium feldspar type[8]	Rock texture-structure[9]	Rock name[10] (field or petrography)	Remarks	CLASSIFICATION: Igneous type[11]	Rock name[12] from chemistry	Age[13]	Region[14]	Reliability of analysis[15]
149A	ALD17	22/44NE	gm	--	mg	(2)	2,Bt	Olig	(10)	Pth	Porphyritic	Granite	Jabal Zan, near contact with Halaban? (Ar Ridaniyah fm)	Plutonic	Granite	S +	TN	
149B	B1346	"	gm	--	--	(4)	--	--	(16)	--	--	Granite	Similar to 149A	Plutonic	Granite	S	TN	
149X	B1347A	22/44SE	*[hu](ngb)	--	--	(21)	--	--	(38)	--	--	Diabase	Ain Umm Wizir, 1-km plug of diabase in Najd fault	Hypabyssal	Diorite	K +	TN	
150	B1481	22/42SW	mog	--	--	(29)	Hb	--	(53)	--	Lineated	Tonalite	Basement gneiss in Najd fault zone	Gneissic	Tonalite	H-N	TC	
152	B1493	22/42SE	mog	Gray	--	(18)	--	--	(45)	--	Lineated	Tonalite	Basement gneiss in Najd fault zone	Gneissic	Tonalite	H-N	TC	
154	B1457	22/44SW	gr	--	cg	(2)	Bt	Olig	(12)	Mc,Pth	--	Granite	Young granite	Plutonic	Granite	S	TC	
155	B1492	21/42NE	gr	--	--	(2)	Hb	--	(3)	--	--	Granite	Circular, ring-structured granite cut by Najd fault	Plutonic	Alk-feldspar granite	S(N?)	TC	
157	B1469	21/43NW	*[Qu](gp)	--	fg	(1)	Hb	--	(4)	--	Lineated	Granite	Uruq Subay, syntectonic intrusion in Najd fault	Plutonic	Na-Alk-feld. granite	N	TC	
158	B1461	21/44NW	gm	--	--	(1)	Hb,Bt	--	(6)	--	--	Granite	Subvolcanic Shammar? intrusion	Plutonic	Alk-feld.gr.	S	TC	
159A	B1460	"	ga	--	fg	(3)	Hb,Bt	--	(15)	--	--	Granite	?Ring dike of Shammar ga, adjacent to Najd fault zone	Hypabyssal	Qtz. syenite	S(N?)	TC	
159B	B1460A	"	ga	--	--	(2)	--	--	(4)	--	--	Granite	In contact with 159A, circular ga intrusion?	Plutonic	Alk-feldspar granite	S	TC	
160	B1459	"	ga	--	--	(6)	--	--	(0)	--	--	Granite	0.5-km wide dike of syenitic ga; similar to 159A?	Hypabyssal	Alk-feld. qtz. syenite	S(N?)	TC	
161	B1458	"	mgd	--	--	(3)	Hb,Bt	--	(22)	Or	Gneissic	Granite	Late syntectonic batholith	Plutonic	Granodiorite	C	TC	
162	B1487	21/42SE	gp	--	--	(5)	--	--	(2)	--	--	Granite	North of Ranyah, large north-trending red gr. batholith	Plutonic	Alk-feldspar granite	S	HS	
163	B1488	"	gm	--	--	(4)	--	--	(3)	--	--	Granite	Similar to 162, near contact with orthogneiss	Plutonic	Alk-feldspar granite	S	HS	
164	B1489	21/43SW	mgd	--	--	(23)	Hb	--	(32)	--	Migmatitic	Gneiss	Migmatized basement, reoriented in Najd fault zone	Gneissic	Quartz monzodiorite	(H)-C-(N)	HS	
166	B1462	21/44SE	ga	Red	--	(3)	--	--	(8)	--	--	Granite	10-km east of Jabal Khidah, large pluton	Plutonic	Alk-feldspar granite	S	TC	
167A	B1463	"	an	Gray	--	(27)	--	--	(67)	--	--	Anorthosite	Jabal Mahail, 11 x 30 km, intrusive vs tectonic?	Plutonic	Leucogabbro-norite	E?,C?	TC	
167B-H	11666-11670, 11679	"	an	Gray	--	(3 to 10)	Bt,Hb,Px?	Lab	(51 to 65)	--	Some cataci.	Anorthosite	7 analyses on same anorthosite body as 167A	Plutonic	Anorthosite	E?,C?	TC	
170A	B1463A	21/44SE	gm	Red	--	(3)	?,Bt	Olig	(22)	Mc,Or	Hypidiomorph	Granite	Intrusive into anorthosite body no. 167, near contact	Plutonic	Granite	H	TC	
171	ALD25	20/42SW	agd(jd?)	Gray	mg	(4)	Bt	--	(15)	--	Lineated	Granodiorite	Thamiyat quad., An Nimas batholith complex	Plutonic	Na-grano-diorite	A,C? +	J	
172	1724	"	agd(jd?)	Gray	mg	(3)	Bt	--	(24)	--	Gneissic	Granodiorite	Thamiyat quad., An Nimas batholith complex	Plutonic	Na-grano-diorite	A,C?	J	

Sample number Plate 1	Field number	Location[1] (lat.-long.)	Rock-unit symbol on Plate 1[2]	PETROGRAPHY: Color	Grain size[3]	Normative color index 4	Mafic content (percent)[5]	Plagioclase composition[6]	Normative An content[7]	Potassium feldspar type[8]	Rock texture-structure[9]	Rock name[10] (field or petrography)	Remarks	CLASSIFICATION: Igneous type[11]	Rock name[12] from chemistry	Age[13]	Region[14]	Reliability of analysis[15]
174	B1700	"	agd(jd?)	--	--	(7)	--	--	(20)	--	--	Qtz. diorite	Thaniyat quad., An Nimas-batholith complex	Gneissic	Na-granodiorite	A,C?	J	
175	B528	"	gb	Dark	mg	(43)	37,Cpx,Ol, Opx	Lab(And)	(36)	--	--	Gabbro	Thaniyat quad, 5-km diameter, layered intrusion	Plutonic	Olivine gabbro	J?,S?	J	
177	B-DS1	20/42SE	*[mu]	Red-brown	vfg	(2)	Px,Amph	--	(3)	Or	Spherulitic	Rhyolite	Rhyolite from mixed rhyolite-diabase, intrudes mu	Dike	Rhyolite	S(N?)	HS	
178	B-DS8	"	gb	Black	mg	(33)	--	--	(75)	--	--	Gabbro	Jabal Sidan, 4 x 10 km, eliptical, layered gabbro	Plutonic	Leuco. olivine norite	S	HS	
186	B1456, (AL016)	23/45SW	mgd	Gray	--	(5)	5,Bi	And	(34)	Or	Cataclastic	Granite	Old basement from east of Idsas-Al Amar fault	Gneissic	Trondhjemite	E +	E	
194	B19	19/41NE	jt	Dark-green	--	(30)	24,Hb,Cpx, Opq	Lab	(50)	--	Hypidiomorph,	Gabbro	Diorite basement, augite-hypersthene quartz diorite	Plutonic	Qtz. leuco-gabbro-norite	J +	J	
195	B15	"	jt	Gray	--	(9)	--	--	(47)	--	Lineated	Tonalite	Biljurshi quad., late diorite basement rock	Gneissic	Trondhjemite	J	J	
196	B17	"	jt	Gray	--	(5)	Hb,Bi,	--	(27)	--	--	Qtz. diorite	Biljurshi quad., part of An Nimas batholith	Plutonic	Trondhjemite	A	J	
197	B10	19/41SE	agd	Pink	mg	(2)	Bi	--	(8)	Mc	Some foliation	Granite	Jabal Tharban, intrudes Ragarah gneiss (763 m.y.)	Plutonic	Alk-feldspar granite	S	J	
198	B33	"	sy	Dark	--	(7)	--	--	(10)	--	--	Syenite	Jabal Tawi (Lakathah), outer circular pluton, 10-km diam.	Plutonic	Syenite	S,A?	J	
198Z	B34	"	*[jc][gr]	--	--	(2)	--	--	(11)	--	--	Granite	Granite, G_3?, west of Lakathah, Wadi Yiba quad.	Plutonic	Granite	A,S?	J	
199	B950	"	gb	Black	--	(40)	--	--	(59)	--	--	Gabbro	Jabal Tawi (Lakathah), core of circular pluton, 6-km diam.	Plutonic	Leucogabbro olivine	S,A?	J	
200	Birk-2	18/41NE	*[ab](ba)	--	--	(40)	--	--	(73)	--	--	Amphibolite	--	Metamorphic	Ol. norite?	B	B	
201A	B1705	19/42NW	jt	Gray	--	(18)	Bi,Hb	And	(42)	--	Gneissic	Qtz. diorite	Wadi Tarj quad., An Nimas batholith	Gneissic	Tonalite	A, early	J	
201B	B1706	"	jt	Light-gray	mg	(2)	Bi	Olig	(24)	--	Gneissic	Trondhjemite	Wadi Tarj quad., An Nimas batholith	Gneissic	Trondhjemite	A, early	J	
202	B1704	"	*[aog](gb)	Dark-gray	mg	(39)	Cpx,Ol,Hb	Lab	(62)	--	Subophitic	Gabbro	Jabal Uthaynat, 1-km diam. layered gabbro, outer layer	Plutonic	Olivine norite	S,A?,late	J	
203A	B1708	19/43NW	hd	Gray	fg	(2)	Bi(Ga)	Olig	(29)	Mc,Or	Cataclastic	Granodiorite	Part of large gneiss dome complex, orthgneiss	Gneissic	Trondhjemite	H(C)	HS	
203B	B1709	"	[hd]mgd	Gray	fg	(3)	--	--	(14)	--	Cataclastic	Granodiorite	Same locality as 203A, magmatitic gneiss	Gneissic	Granodiorite	C	HS	
204	B1722	"	gp	Red	fg	(1)	Bi	--	(7)	Mc	Hypidiomorph,	Granite	Center, Jabal Al Hassir elliptical layered pluton	Plutonic	Alk-feldspar granite	S	HS	
205	B1723	"	gp	Red	cg	(1)	Bi	Olig	(5)	Pth,Mc	Hypidiomorph,	Granite	Outer ring, J. Al Hassir elliptical layered pluton	Plutonic	Alk-feldspar granite	S	HS	

Sample number Plate 1	Field number	Location[1] (lat.-long.)	Rock-unit symbol on Plate 1[2]	PETROGRAPHY: Color	Grain size[3]	Normative color index 4	Mafic content (percent)[5]	Plagioclase composition[6]	Normative An content[7]	Potassium feldspar type[8]	Rock texture-structure[9]	Rock name[10] (field or petrography)	Remarks	CLASSIFICATION: Igneous type[11]	Rock name[12] from chemistry	Age[13]	Region[14]	Reliability of analysis[15]
206	B1710	"	mog	--	--	(3)	--	--	(26)	--	Cataclastic	Granodiorite	Part of large gneiss dome complex, orthogneiss	Gneissic	Trondhjemite	H(C)	HS	
207	B1716	19/43NE	mgd	--	--	(4)	--	--	(26)	--	Lineated	Granodiorite	Large syntectonic batholith, complex	Gneissic	Granodiorite	C	TS	
208	B1713	"	hd	--	--	(28)	--	--	(47)	--	--	Qtz. diorite	Diorite basement of Halaban age	Plutonic	Qtz. diorite	H	TS	
209	1721	19/43SW	gp	Red	cg	(4)	Hb,Bi	--	(7)	Mc,Pth	Hypidiomorph.	Granite	Outer ring, J. Al Hassir elliptical layered pluton	Plutonic	Alk-feldspar granite	S	HS	
212	B1719	19/43SE	gb	--	--	(48)	--	--	(68)	--	--	Gabbro	Jabal al Ashsha, SW end, elliptical layered gb complex	Plutonic	Olivine gabbro	S	TS	
214	B1720	"	gb(um)	--	--	(94)	Ol	--	(90)	--	--	Serpentinite	Jabal al Ashsha, center, elliptical layered gb complex	Plutonic	Hartzburgite	S	TS	
215	B1718	"	*[06w]hq	--	--	(10)	--	--	(38)	--	--	Qtz. Diorite	Basement rock outlier in Wajd sandstone	Plutonic	Qtz. Diorite	H	TS	
217	B-WP-1	18/42NW	jv	--	--	(43)	--	--	(56)	--	--	Basalt	On Wadi Tayyah road	Volcanic	Qtz. basalt	J	J	
218	B-WP-1	"	jc	--	--	(46)	--	--	(62)	--	--	Schist	On Wadi Tayyah road	Volcanic	Basalt	J	J	
223A	B1707E	18/43NE	mog	--	mg	(8)	Hyp,Hb	And	(39)	Or	--	Enderbite	Granulite-facies rock along Najd fault zone	Metamorphic	Trondhjemite?	H(N)	TS	Z,Y
223B	B1707W	"	nog	--	--	(64)	--	--	(70)	--	--	Charnockite	Granulite-facies rock along Najd fault zone	Metamorphic	Metabasalt?	H(N)	TS	Z
223C	B-SW402	"	nog	--	--	(4)	--	--	(19)	--	--	Charnockite	Granulite-facies rock along Najd fault zone	Metamorphic	Metagranite?	H(N)	TS	Z
224	GF8151	18/42SW	gm	--	--	(1)	1,Bi	Olig	(16)	Mc	Foliated	Granite	Young, large granite pluton	Plutonic	Granite	A(S?) + J		
227	B140	18/42SE	mog	Dark-green	mg	(34)	Hb,Bi	--	(37)	--	--	Diorite	On Abha-Khamis Mushayt road, basement diorite	Plutonic	Qtz. diorite	H	HS	
237	B125	17/42NE	mgd	Gray	--	(6)	Bi	--	(29)	--	Some gneissic	Granite	Elliptical pluton, east of Wadi Bayah	Plutonic	Granodiorite	C(A?)	HS	
241	B120	17/43SW	aog	Gray	mg	(7)	--	--	(30)	--	Gneissic	Granite	Jabal al Harisi, syntectonic granitoid complex	Gneissic	Granodiorite	C(A?)	HS	
501	--	?	?	--	--	--	--	--	--	--	--	Graywacke?	Eastern Province, Shagar #1, drill core, top of PB	Sedimentary?	Basaltic andesite?	?	EE	Z,X
502	--	?	?	--	--	--	--	--	--	--	--	Graywacke?	Eastern Province, Shamasiyah #1, drill core, top of PB	Sedimentary?	--	?	EE	Z,X

Table 3.--Description and classification of crystalline rocks of the Saudi Arabian Shield for which chemical analyses are given in table 4.

1/ Location by 30-minute quadrangle; latitude and longitude are for southwest corner of one-degree quadrangles that are further subdivided into 30-minute quadrants.

2/ Asterisk indicates map-unit outcrop, representative of the sample, is too small to show at map scale (plate 1). The rock-unit symbol shown on the map is listed in brackets; the most probable correct rock-unit symbol for the sample is in parentheses.

3/ Grain sizes are standard for plutonic and volcanic rocks: vf, very fine grained; fg, fine grained; mg, medium grained; cg, coarse grained.

4/ NCI, normative color index in parentheses (Irvine and Baragar, 1971, p. 527), is sum of normative mafic minerals (milar data).

5/ Mafic minerals (modal data) listed in order of decreasing abundance; Bi, biotite; Hb, hornblende; Rieb, riebeckite, Amph, amphibolite; Px, pyroxene; Cpx, clinopyroxene; Opx, orthopyroxene; Hyp, hypersthene; Ol, olivine; Mt, magnetite; Hm, hematite; Opq, opaque minerals; Mu, muscovite; Ga, garnet; Fl, fluorite; Chl, chlorite; Epi, epidote.

6/ Ab, albite; Olig, oligoclase; And, andesine; Lab, labradorite.

7/ NPC, normative plagioclase composition in parentheses (Irvine and Baragar, 1971, p. 527) is 100 An/(An+Ab+5/3Ne) (molar data).

8/ Potassium-feldspar minerals, listed in order of decreasing abundance; Or, orthoclase; Pth, perthite; Mc, microcline.

9/ Mr, Myrmekitic; frags, fragments; porph, porphyritic; amygd, amygdaloidal; catacl, catclastic; foli, foliation; mod, moderately.

10/ Porph, porphyry; gn, gneiss; qtz, quartz.

11/ Several nonigneous rocks are listed as sedimentary. Metam, metamorphic; volc, volcanic; gn, gneiss.

12/ Names where possible are according to Streckeisen (1976, 1979). Rhy, rhyolite; and, andesite; ba, basalt; gr, granite; sy, syenite; monzodi, monzodiorite; gbnorite, gabbronorite; amph, amphibolite; peralk, peralkalic; alk, alkalic; alk-feld, alkalic-feldspar; leuco, leucocratic; qtz, quartz, ol, olivine.

13/ Age symbols represent stratigraphic and tectonic intervals: B, Bahah (about 1,100 m.y.?); J, Jiddah (950-800 m.y.); A, Abhah (about 765 m.y.); H, Halaban (800-650m.y.); C, culminant (collisional?) orogeny (650-625 m.y.); M, Murdama (650-580? m.y.); S, Shammar (600-580? m.y.); N, Najd faulting event (Najd orogeny) (580-560? m.y.); K, Jubaylah (about 570 m.y.). Symbol, +, indicates a geochronological determination on sample, see tables.

14/ Tectonic regions, see figure 1 for symbols, Divisions were made in an attempt to observe chemical variations and trends across the Shield.

15/ General categories of rocks for chemical comparison: Gp, peralkalic granite; Ga, alkalic-feldspar granite; Gr, granite; Gd, granodiorite; Th, trondhjemite and tonalite; Gb, gabbro, diorite quartz diorite, anorthosite, and ultramafic; Mv, mafic volcanic and dike rocks: diabase, basalt, andesite, dacite; Lv, leucocratic volcanic and dike rocks: rhyolite and dacite; Z, rocks with unusual chemistry including 3 sedimentary rocks. A few rock analyses are nondefinitive (x) and have not been used in the comparative chemical plots; others (y) are of uncertain use.

The total-rock sample is biased toward granitic rocks represented by 101 analyses in comparison to 50 analyses of dioritic and gabbroic rocks, and 49 analyses of volcanic rocks as well as a few dike rocks. Most of the rocks have calc-alkalic compositions that fit normal distributions in any of the three classification schemes used. A majority of the rocks were classified preliminarily on the Q-Or-(An+Ab) ternary diagram using the IUGS classification. On this diagram, compositions of granite and granodiorite generally separate well. The subdivision of the rocks of granite composition constitutes a major problem (the feldspar problem of normative analyses; Irvine and Baragar, 1971; Le Maitre, 1976) in determining the amount of normative Ab-molecule to allocate to normative anorthite and potassium feldspar.

Peralkalic granite is defined by molar data where the $(Na_2O+K_2O)/Al_2O_3$ ratio is greater than 1; the norm of these granites contain acmite and(or) sodium silicate. The separation of alkali-feldspar granite and granite on the basis of chemical data is not defined in any of the classifications named above; the allocation of albite in the normative analysis makes it impossible to directly use either the Q-Or-(An+Ab) or the Q-(Or+Ab)-An ternary diagrams. For this report alkali-feldspar granite is arbitrarily separated from granite on the basis of molar data in which the $(Na_2O+K_2O)/Al_2O_3$ ratio was greater than 0.850. This separation of alkali-feldspar granite is well demonstrated on the ternary diagram Al_2O_3-CaO-(Na_2O+K_2O) which also separates the peralkalic and peraluminous rocks. The granitic compositions are well separated on Q-OrT-AnT, where T equals (Or+Ab+An)/(Or+An) (Le Maitre, 1976), and on the Q-Or-An diagram, but statistical boundaries for naming the granitic rocks on these diagrams are not available.

For purposes of synthesizing the chemistry of the 199 rock analyses, all the rocks were divided into categories of region, igneous rock type, and age (table 4). Throughout the chemical examination, a fourth category of quality of the chemical analysis (listed in table 4) was constantly considered. The regional divisions are tectonic provinces shown on figure 17. Because the rocks as collected have a shield-wide distribution, it is reasonable to look for regional chemical differences in rocks of the same type and age.

All the rocks were divided into either plutonic or volcanic categories. A few rocks are of other types, but after examination of field descriptions, petrography, and chemistry, they were studied as part of either the plutonic or volcanic categories. Nine rocks from dikes and sills were best examined under the volcanic category and nine rocks from hypabyssal intrusive bodies were examined under the plutonic category. All the 23 gneisses appear to be orthogneiss and migmatite and were classified as plutonic; five highly metamorphic rocks were divided into either plutonic or volcanic categories, according to the available data. Three sedimentary rocks were not included in the chemical study.

All the rocks were further classified according to an assigned age category. Each age category is a stratigraphic interval with the exception of age categories that correspond to the culminant orogeny and the Najd faulting event. From the oldest to youngest the age categories are: Baish-Bahah, Jiddah (Samran), Ablah, Fatimah, Halaban (Hulayfah), culminant orogeny, Murdama, Shammar, Jubaylah, and Najd faulting event. These age

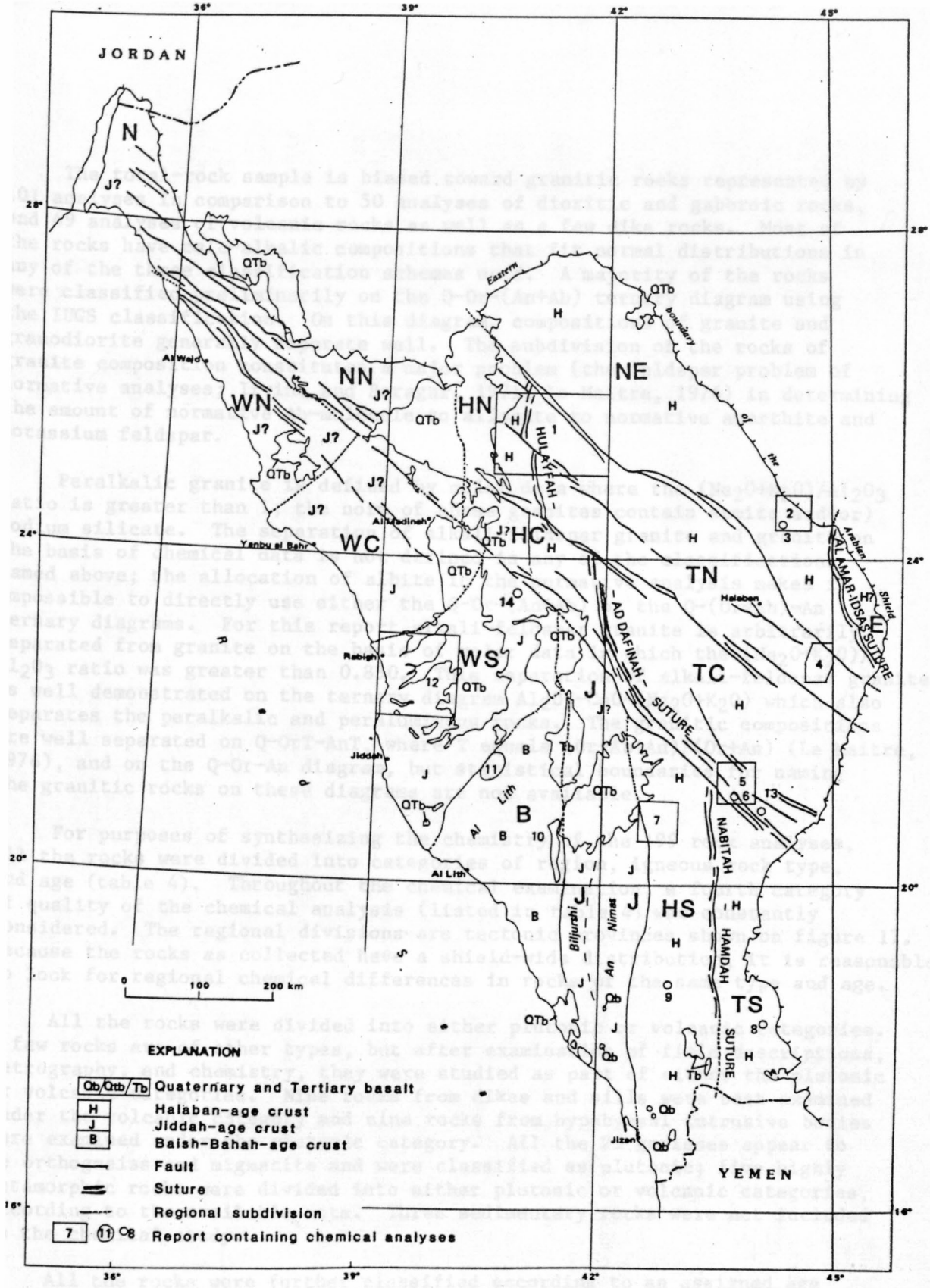

Figure 17. Map showing subdivision of the Precambrian Arabian Shield into broad tectonostratigraphic belts from which chemical analyses of volcanic and plutonic rocks have been used in this report. Numbers indicate quadrangles and areas from which published analyses have been used: 1, Nuqrah quadrangle (Delfour, 1977) 2 and 3, Ad Dawadimi district (Al-Shanti, 1974 and 1976); 4, Jaba al Hawshah (Kanaan, 1979); 5, Bir Juqjuq quadrangle (Dodge and others 1979); 6, Bir Juqjuq quadrangle (Kroner and others, 1979); 7, Wadi a Miyah (Schmidt, 1980a); 8, Wadi Wassat (Jackaman, 1972); 9, Jabal Sha (Coleman and others, 1977); 10, Wadi Bidah (Jackaman, 1972); 11. Taif (Nasseef and Gass, 1977); 12, Khulays quadrangle (Skiba, 1980; W. J. Skiba and C. F. Gilboy, written commun., 1975); 13, Jabal Yafikh quadrangle (Schmidt, 1981b).

Table 4. Chemistry and normative analyses of crystalline rocks of the Arabian Shield.

No. on fig. 2	1	3	4A	4B	8	9	13	14A	14B	14XA	14XB	15
SIO2	64.00	48.40	72.20	75.00	76.40	70.00	75.50	76.00	80.00	65.00	68.00	77.00
AL2O3	15.40	15.50	14.70	13.40	11.60	7.60	9.45	9.83	7.18	17.70	15.90	8.50
FE2O3	1.60	1.60	0.69	0.74	1.30	3.33	0.78	2.43	1.41	3.34	2.68	2.38
FEO	2.90	9.20	0.56	0.60	1.00	3.10	1.80	1.90	1.20			0.36
MGO	3.10	7.40	0.21	0.20		0.06	0.08	0.43	0.09	0.11	0.03	0.04
CAO	4.20	11.00	1.00	0.95	0.04	0.55	0.66	0.92	0.29	0.46	0.04	0.97
NA2O	4.00	2.40	4.00	3.80	4.20	11.32	7.00	5.80	5.90	6.36	6.90	6.70
K2O	2.90	0.40	5.20	4.20	4.60	4.55	3.81	3.61	4.09	5.38	4.60	3.54
TIO2	0.81	1.10	0.15	0.21	0.12	0.33	0.17	0.44	0.18	0.15	0.05	0.17
P2O5	0.26	0.11	0.02	0.04	0.03			0.07		0.11	0.06	
MNO	0.07	0.21	0.02	0.04	0.03	0.05	0.03	0.02	0.01			0.01
CO2	0.05	0.05	0.08	0.05	0.02							
H2O+	0.70	1.30	0.42	0.65	0.46							
H2O-	0.11	0.08	0.12	0.10	0.03							
TOTAL	100.62	99.58	99.73	100.46	100.13	101.08	99.59	101.61	100.61	98.61	98.26	100.73
NORMATIVE MINERALS												
Q	16.446		27.056	34.909	34.508	26.669	35.586	33.086	47.437	6.671	10.913	39.365
C			0.917	1.096						0.853		
OR	17.259	2.428	31.092	25.012	27.363	26.650	22.678	21.028	24.085	32.240	27.664	20.988
AB	34.089	20.857	34.248	32.404	34.283	13.639	27.595	30.029	14.112	54.575	57.169	24.092
AN	15.611	31.158	4.376	4.168						1.585		
AC					1.315	9.549	2.273	6.930	4.065		1.983	6.908
NS						16.400	6.863	2.440	7.221			5.806
WO	1.397	9.948				1.129	1.377	1.690	0.599			2.016
EN	7.776	13.127	0.529	0.502		0.148	0.201	1.056	0.223	0.278	0.076	0.100
FS	2.816	10.076	0.251	0.220	0.940	5.194	3.103	2.760	1.918			0.400
FO		4.065										
FA		3.439										
MT	2.336	2.383	1.012	1.081	1.239							
HM										3.387	2.042	
IL	1.549	2.146	0.288	0.402	0.229	0.621	0.325	0.824	0.341			0.324
RU										0.152	0.051	
AP	0.620	0.268	0.048	0.095	0.072			0.163		0.264	0.073	
CC	0.115	0.117	0.184	0.115	0.001							
SD					0.052							
TOTAL	100.014	100.009	100.001	100.003	100.002	100.001	100.000	100.004	100.000	100.006	99.971	100.000

	17	18	19	20	21	22A	22B	23	24	25A	25B	27
SIO2	80.00	70.70	48.40	77.00	73.50	82.40	48.00	74.00	76.90	66.20	59.40	70.40
AL203	8.58	15.30	17.00	7.18	10.25	8.50	15.40	12.00	12.20	17.10	16.70	12.60
FE203	2.27	2.10	10.50	6.22	3.08	1.70	13.50	1.18	0.70	0.40	2.10	3.60
FEO	0.40	0.12	1.50	0.72	0.68	0.80	0.84	1.60	1.00	2.00	4.70	0.08
MGO	0.05	0.38	4.20	0.36	0.17	0.09	2.50	0.60	0.15	1.00	3.60	0.15
CAO	0.28	0.70	6.00	0.53	0.82	0.42	4.00	2.00	0.70	2.70	6.00	1.60
NA20	3.20	4.90	4.00	0.50	2.90	3.83	4.80	6.20	4.10	4.60	2.80	3.80
K20	3.91	3.80	2.40	4.58	4.82	0.34	3.10	1.01	4.00	3.90	0.66	4.70
TI02	0.16	0.35	3.10	0.47	0.47	0.10	3.10	0.42	0.10	0.51	0.96	0.25
P205		0.17	0.38	0.08	0.06		0.74	0.04		0.22	0.19	0.01
MNO	0.02		0.13	0.18	0.11		0.20	0.06		0.05	0.16	0.06
C02		0.06								0.11	0.02	1.10
H20+		0.78								0.64	1.10	0.39
H20-		0.36								0.16	0.34	0.24
TOTAL	99.39	100.53	100.16	99.24	98.92	98.75	99.99	99.80	100.24	100.12	99.71	99.45
NORMATIVE MINERALS												
Q	47.668	26.611		56.346	38.183	58.858		30.315	35.663	17.191	20.970	30.188
C		2.434		0.642		1.087				1.198	0.999	0.940
OR	23.369	22.779	14.530	27.668	29.406	2.046	19.046	6.022	23.673	23.328	4.009	28.240
AB	22.620	42.060	34.676	4.325	25.334	33.009	42.229	52.934	34.745	39.401	24.353	32.694
AN		2.011	21.866	2.154	0.739	2.122	11.768	1.947	3.076	11.400	29.189	0.934
AC	4.199											
WO	0.587		0.626		1.276			3.257	0.168			
EN	0.126	0.960	7.933	0.917	0.437	0.228	2.319	1.508	0.374	2.521	9.216	0.380
FS								1.394	1.095	2.625	5.764	
FO			1.951				2.911					
MT	0.901			1.580	1.227	2.331		1.726	1.016	0.587	3.130	
HM	0.223	2.130	10.757	5.269	2.334	0.124	14.036					3.660
IL	0.307	0.257	3.531	0.913	0.922	0.193	2.289	0.805	0.190	0.980	1.874	0.302
TN			3.232				2.704					
RU		0.220					0.916					0.095
AP		0.408	0.922	0.194	0.147		1.822	0.096		0.327	0.463	0.024
CC		0.138								0.253	0.047	2.544
TOTAL	100.000	100.009	100.022	100.007	100.005	100.000	100.042	100.003	100.000	100.012	100.012	100.001

	28A	28B	29	30	31	32	33	36	37	38	39	41
SIO2	52.60	67.30	74.80	73.60	75.40	72.00	75.30	65.20	68.00	76.10	36.20	68.60
AL203	17.70	15.80	12.30	14.10	12.70	14.90	13.50	15.40	14.60	13.50	3.80	13.50
FE203	2.10	1.10	1.40	0.48	1.40	0.20	0.70	2.20	1.40	1.20	0.49	4.70
FEO	3.80	2.00	0.08	0.48	1.00	1.30	0.96	1.60	1.00	0.08	0.24	0.76
MGO	4.00	1.10	0.05	0.20	0.25	0.45	0.05	2.30	1.30	0.46	0.86	0.05
CAO	10.40	2.60	1.10	0.90	1.20	1.50	0.80	2.10	2.40	1.60	30.70	1.10
NA20	4.30	4.20	4.80	4.30	4.80	3.80	4.30	4.90	4.40	1.00	0.50	4.70
K20	0.56	3.60	3.50	4.30	1.00	4.10	4.60	2.70	2.90	3.10	1.00	4.80
TI02	0.63	0.50	0.10	0.09	0.16	0.19	0.09	0.69	0.42	0.12	0.06	0.26
P205	0.52	0.13		0.01	0.01	0.05		0.17	0.15	0.01	0.09	
MNO	0.11	0.04		0.02	0.06	0.02	0.02	0.07		0.02		0.07
C02	2.50	0.05	0.32	0.06	0.02	0.06	0.08			0.91	23.90	
H20+	0.97	0.56	0.32	0.35	0.53	0.65	0.33			1.80	1.20	
H20-	0.64	0.13	0.10	0.13	0.15	0.14	0.13			1.10	0.74	
TOTAL	102.02	99.56	99.16	99.35	99.14	99.88	101.18	99.70	98.42	103.14	101.22	99.80
NORMATIVE MINERALS												
Q	4.611	21.814	32.816	30.371	41.380	30.172	30.504	19.384	25.527	57.919	28.527	21.618
C		0.705		0.912	1.643	1.768	0.177	1.033	0.226	7.872	1.701	
OR	3.335	21.615	21.008	25.786	6.030	24.580	27.074	16.393	17.746	18.674	6.040	28.785
AB	36.671	36.110	41.256	36.925	41.445	32.621	36.240	42.600	38.554	8.626	4.324	40.359
AN	27.555	11.922	1.705	4.080	5.879	6.833	3.449	9.563	11.315	2.161	0.644	1.586
WO	2.126		0.728									1.650
EN	10.040	2.784	0.126	0.505	0.635	1.137	0.124	5.885	3.353	1.168	2.189	0.126
FS	4.442	2.045		0.379	0.538	1.974	1.069	0.114				
MT	3.069	1.620		0.706	2.071	0.294	1.011	3.277	2.077		0.613	1.953
HM			1.422						0.017	1.223	0.078	3.423
IL	1.206	0.965	0.172	0.173	0.310	0.366	0.170	1.346	0.826	0.216	0.116	0.501
TN			0.028									
RU										0.009		
AP	1.241	0.313		0.024	0.024	0.120		0.414	0.368	0.024	0.218	
CC	5.730	0.116	0.739	0.138	0.046	0.138	0.181			2.110	55.554	
TOTAL	100.028	100.007	100.000	100.001	100.001	100.003	100.000	100.010	100.008	100.001	100.005	100.001

	42	43	45	46	47	48	49	50	51	52	54	55
SIO2	73.80	75.10	55.20	73.70	77.60	73.20	73.30	72.40	49.20	77.90	70.11	45.30
AL203	9.30	14.00	15.70	13.70	12.50	14.50	14.10	14.80	19.20	12.00	15.57	14.30
FE203	7.80	0.71	0.21	2.00	0.78	0.69	0.22	0.34	5.50	0.73	0.89	5.10
FEO	0.48	0.20	7.00		0.16	0.56	0.80	0.40	4.60	0.52	1.20	10.10
MGO	0.08	0.29	4.60	0.20	0.10	0.22	0.24	0.18	4.80	0.23	0.66	6.20
CAO	0.70	0.82	7.40	0.25	0.20	1.00	1.70	1.00	9.20	2.00	2.64	9.20
NA20	1.80	3.60	3.70	4.30	4.10	4.80	4.00	4.60	2.30	4.20	4.67	2.40
K20	3.30	4.70	1.10	4.70	3.90	4.40	3.60	4.40	1.00	0.66	3.17	0.80
TIO2	0.26	0.09	1.60	0.19	0.15	0.14	0.10	0.03	0.55	0.14	0.39	4.70
P205		0.01	0.30	0.02		0.02	0.02		0.24	0.01	0.29	0.22
MNO	0.04	0.01	0.13	0.27		0.04	0.04	0.02	0.17	0.02	0.04	0.58
C02		0.04		0.02		0.06	0.56	0.08	0.06	0.06	0.14	
H20+		0.49		0.54		0.37	0.64	0.49	1.40	0.29	0.39	
H20-		0.31		0.28		0.07	0.12	0.24	0.32	0.11	0.08	
TOTAL	98.57	100.96	98.51	100.76	100.01	100.35	99.93	99.50	99.67	99.15	100.55	99.98
NORMATIVE MINERALS												
Q	50.310	34.269	5.634	30.175	38.445	26.151	33.742	26.882	5.628	47.158	25.023	0.421
C	1.532	1.623		1.186	1.176	0.211	1.903	0.852		0.917	0.677	
OR	19.988	27.894	6.705	27.955	23.164	26.097	21.558	26.464	6.103	3.961	18.776	4.780
AB	15.612	30.594	32.297	36.623	34.871	40.767	34.300	39.617	20.101	36.091	39.607	20.534
AN	3.560	3.766	23.707	0.990	0.997	4.468	4.827	4.535	40.396	9.625	10.341	26.171
WO			5.069						1.976			7.735
EN	0.204	0.725	11.818	0.501	0.250	0.550	0.606	0.456	12.347	0.582	1.648	15.613
FS			10.605			0.303	1.213	0.449	3.420	0.160	0.901	7.736
MT	0.947	0.418	0.314	0.333	0.081	1.004	0.323	0.502	8.236	1.075	1.293	7.477
HM	7.342	0.425		1.784	0.728							
IL	0.506	0.172	3.135	0.363	0.286	0.267	0.192	0.058	1.079	0.270	0.742	9.026
AP		0.024	0.733	0.048		0.048	0.048		0.587	0.024	0.688	0.527
CC		0.091		0.046		0.137	1.291	0.185	0.141	0.139	0.319	
TOTAL	100.001	100.001	100.018	100.005	100.000	100.002	100.002	100.000	100.015	100.001	100.016	100.019

	56	57	58	61A	61B	62	63	64	65	66	67	68A
SIO2	69.90	62.70	71.50	77.30	76.70	73.10	80.20	75.30	64.43	46.20	48.50	70.60
AL2O3	14.60	16.20	12.20	12.20	12.20	12.20	11.90	13.80	15.51	17.00	14.93	12.90
FE2O3	1.70	2.40	2.04	0.42	1.40	1.30	0.52	0.39	1.73	13.10	12.04	2.50
FEO	2.60	3.40	1.40	0.32	0.16	3.00	0.20	0.24	3.12	0.88	1.20	2.70
MGO	0.74	2.60	0.48	0.20	0.04	0.05	0.15	0.15	3.27	3.10	4.73	0.85
CAO	3.30	5.30	1.44	0.50	0.43	0.50	0.90	0.55	4.98	8.10	6.02	1.30
NA2O	4.60	3.30	4.45	2.40	3.70	4.30	0.18	4.30	4.02	3.40	4.23	5.00
K2O	0.55	1.40	4.72	4.50	4.50	4.40	1.90	4.10	1.29	1.30	1.54	2.30
TIO2	0.43	0.58	0.24	0.07	0.07	0.45	0.10	0.09	0.68	2.40	2.50	0.52
P2O5	0.09	0.10					0.01	0.04	0.25	0.38	0.53	0.06
MNO	0.12	0.05	0.05			0.09		0.01	0.09	0.07	0.17	
CO2	0.02								0.02			
BAO									0.05			
H2O+	0.66								0.91			
H2O-	0.10								0.14			
TOTAL	99.89	99.33	99.38	99.75	99.93	99.59	98.99	99.87	101.16	99.67	99.33	100.13
NORMATIVE MINERALS												
Q	32.296	22.170	25.543	45.646	37.274	28.844	72.619	33.655	20.432	2.911	1.592	28.285
C	0.709			2.525	0.464		8.260	1.399				
OR	3.295	8.439	28.311	27.159	26.806	26.160	11.688	24.480	7.666	8.008	9.441	13.766
AB	39.457	28.485	37.023	20.742	31.561	36.609	1.586	36.764	34.208	29.990	37.134	42.853
AN	15.871	25.763		2.533	2.150	0.999	4.580	2.493	20.581	28.442	17.846	6.039
AC			1.055									
WO		0.164	3.028			0.625			1.080	2.499	2.516	0.040
EN	1.868	6.605	1.213	0.509	0.100	0.125	0.389	0.377	8.190	8.048	12.221	2.144
FS	2.923	3.464	0.892	0.128		3.883			3.363			2.060
MT	2.499	3.550	2.474	0.622	0.315	1.896	0.369	0.551	2.522			3.671
HM					1.194		0.287	0.014		13.656	12.491	
IL	0.828	1.124	0.463	0.136	0.134	0.860	0.198	0.173	1.299	2.094	3.007	1.000
TN										3.434	2.480	
AP	0.216	0.242					0.025	0.096	0.595	0.938	1.302	0.144
CC	0.046								0.046			
TOTAL	100.006	100.006	100.001	100.000	100.000	100.001	100.001	100.002	99.982	100.021	100.031	100.003

	68B	69	70	71	73	74	75	76	77	78A	78B	80
SIO2	71.30	54.40	65.80	75.60	76.10	47.50	53.50	72.80	69.20	74.20	73.90	58.80
AL203	13.10	14.00	13.90	11.90	11.80	17.19	15.50	14.11	14.47	13.80	13.70	16.25
FE203	3.30	12.60	4.00	0.40	2.10	4.54	10.90	0.95	1.29	0.44	1.10	1.37
FEO	2.50	1.50	2.30	1.30	0.24	5.80	1.50	0.82	1.25	0.60	0.56	3.80
MGO	0.32	1.00	1.00	1.70	0.38	4.31	1.20	0.21	0.01	0.10	0.23	3.24
CAO	0.23	5.60	1.80	0.65	0.72	9.09	7.80	1.43	1.77	0.63	0.50	7.69
NA20	3.60	3.90	5.60	5.30	1.00	3.12	3.70	4.18	4.60	4.80	3.90	4.18
K20	1.70	2.00	1.90	0.21	5.60	1.45	1.40	4.44	4.41	4.50	5.10	1.43
TIO2	0.38	2.40	0.76	0.16	0.25	2.60	3.00	0.27	0.48	0.07	0.22	0.64
P205	0.04	1.10	0.11		0.04	0.47	1.00	0.20	0.20	0.02		0.13
MNO		0.10	0.11	0.02	0.04	0.11	0.08	0.03	0.05	0.06		0.05
CO2					0.05			0.04	0.98	0.05		
H20+					0.80			0.35	0.83	0.47		
H20-					0.14			0.06	0.13	0.10		
TOTAL	96.47	99.52	98.60	98.65	99.86	98.43	100.65	100.15	100.28	100.21	100.07	98.96
NORMATIVE MINERALS												
Q	43.987	15.141	21.733	40.321	47.796	0.876	13.288	28.790	25.081	27.620	30.525	9.524
C	5.199			1.822	3.047			0.402	1.682	0.052	0.862	
OR	10.413	11.986	11.542	1.276	33.657	8.909	8.308	26.374	26.400	26.787	30.377	8.660
AB	31.577	33.469	48.711	46.120	8.606	27.449	31.440	35.555	39.433	40.915	33.263	36.247
AN	0.912	14.997	7.380	3.316	3.046	29.754	21.641	5.564	1.296	2.698	2.500	21.883
WO		1.546	0.443			5.821	2.637					6.824
EN	0.826	2.526	2.560	4.354	0.963	11.160	3.001	0.526	0.025	0.251	0.577	8.269
FS	1.282			1.882		2.923		0.333	0.537	0.740		5.003
MT	4.960		5.725	0.596	0.183	6.844		1.385	1.895	0.643	1.176	2.036
HM		12.779	0.164		2.010		10.946				0.297	
IL	0.748	3.430	1.484	0.312	0.483	5.134	3.353	0.515	0.924	0.134	0.421	1.246
TN		1.541					3.060					
AP	0.098	2.642	0.268		0.096	1.157	2.379	0.476	0.480	0.048		0.316
CC					0.116			0.091	2.258	0.115		
TOTAL	100.002	100.059	100.007	100.000	100.003	100.027	100.053	100.011	100.011	100.002	100.000	100.008

	81A	81B	82A	82B	83A	83B	84	85	86	87	88	89
SIO2	68.80	75.20	65.30	65.60	62.40	69.00	76.40	70.70	70.30	66.30	68.90	66.00
AL203	16.20	13.40	15.40	15.80	17.53	14.90	12.50	15.68	16.60	16.60	15.80	15.70
FE203	1.10	0.37	1.10	1.00	1.64	3.40	0.10	1.92	1.75	0.60	0.30	1.10
FEO	0.68	0.40	2.60	2.60	2.30	0.64	0.92	0.60	1.30	2.40	3.00	1.90
MGO	0.63	0.15	2.80	2.60	1.91	0.59	0.05	0.93	1.19	1.70	1.50	2.10
CAO	2.00	0.53	3.90	3.90	4.20	1.70	0.60	2.25	2.85	3.50	3.20	4.10
NA2O	4.30	2.30	4.40	4.20	4.74	4.80	3.70	2.99	3.67	4.10	3.30	3.90
K2O	4.60	6.90	2.80	2.90	3.60	3.70	4.60	3.30	2.82	3.10	2.20	2.90
TIO2	0.25	0.08	0.62	0.52	0.50	0.52	0.06	0.30	0.30	0.48	0.39	0.67
P2O5	0.11	0.03	0.28	0.24	0.24	0.10		0.07	0.11	0.19	0.13	0.36
MNO			0.08	0.03	0.04	0.02			0.01	0.05	0.03	0.01
CO2			0.05									
H2O+			0.45									
H2O-			0.07									
TOTAL	99.87	99.86	100.18	99.98	99.68	99.95	99.64	99.46	101.72	99.77	99.48	99.30
NORMATIVE	MINERALS											
Q	21.557	34.225	16.830	17.642	9.728	22.824	35.609	35.112	30.108	19.822	30.817	21.168
C	0.785	1.264				0.148	0.347	3.308	2.569	0.597	2.515	
OR	27.549	41.037	16.658	17.242	21.467	22.003	27.477	19.749	16.516	18.500	13.165	17.356
AB	36.876	19.587	37.483	35.757	40.473	40.874	31.647	25.623	30.778	35.036	28.277	33.422
AN	9.327	2.449	14.095	15.791	16.068	7.830	3.009	10.842	13.300	16.282	15.216	16.982
WO			1.346	0.876	1.409							0.516
EN	1.590	0.376	7.020	6.515	4.800	1.479	0.126	2.346	2.937	4.276	3.783	5.297
FS		0.299	3.011	3.165	2.137		1.524		0.460	3.244	4.732	1.512
MT	1.487	0.540	1.606	1.459	2.399	0.625	0.147	1.078	2.515	0.879	0.440	1.615
HM	0.089					2.991		1.201				
IL	0.481	0.153	1.185	0.994	0.958	0.994	0.115	0.577	0.565	0.921	0.750	1.289
AP	0.264	0.072	0.668	0.572	0.574	0.238		0.168	0.258	0.454	0.312	0.864
CC			0.114									
TOTAL	100.006	100.002	100.016	100.013	100.013	100.005	100.000	100.004	100.006	100.011	100.007	100.019

	81A	81B	82A	82B	83A	83B	84	85	86	87	88	89
SIO2	68.80	75.20	65.30	65.60	62.40	69.00	76.40	70.70	70.30	66.30	68.90	66.00
AL203	16.20	13.40	15.40	15.80	17.53	14.90	12.50	15.68	16.60	16.60	15.80	15.70
FE203	1.10	0.37	1.10	1.00	1.64	3.40	0.10	1.92	1.75	0.60	0.30	1.10
FEO	0.68	0.40	2.60	2.60	2.30	0.64	0.92	0.60	1.30	2.40	3.00	1.90
MGO	0.63	0.15	2.80	2.60	1.91	0.59	0.05	0.93	1.19	1.70	1.50	2.10
CAO	2.00	0.53	3.90	3.90	4.20	1.70	0.60	2.25	2.85	3.50	3.20	4.10
NA20	4.30	2.30	4.40	4.20	4.74	4.80	3.70	2.99	3.67	4.10	3.30	3.90
K20	4.60	6.90	2.80	2.90	3.60	3.70	4.60	3.30	2.82	3.10	2.20	2.90
TIO2	0.25	0.08	0.62	0.52	0.50	0.52	0.06	0.30	0.30	0.48	0.39	0.67
P205	0.11	0.03	0.28	0.24	0.24	0.10		0.07	0.11	0.19	0.13	0.36
MNO			0.08	0.03	0.04	0.02			0.01	0.05	0.03	0.01
CO2			0.05									
H20+			0.45									
H20-			0.07									
TOTAL	99.87	99.86	100.18	99.98	99.68	99.95	99.64	99.46	101.72	99.77	99.48	99.30
NORMATIVE MINERALS												
Q	21.557	34.225	16.830	17.642	9.728	22.824	35.609	35.112	30.108	19.822	30.817	21.168
C	0.785	1.264				0.148	0.347	3.308	2.569	0.597	2.515	
OR	27.549	41.037	16.658	17.242	21.467	22.003	27.477	19.749	16.516	18.500	13.165	17.356
AB	36.876	19.587	37.483	35.757	40.473	40.874	31.647	25.623	30.778	35.036	28.277	33.422
AN	9.327	2.449	14.095	15.791	16.068	7.830	3.009	10.842	13.300	16.282	15.216	16.982
WO			1.346	0.876	1.409							0.516
EN	1.590	0.376	7.020	6.515	4.800	1.479	0.126	2.346	2.937	4.276	3.783	5.297
FS		0.299	3.011	3.165	2.137		1.524		0.460	3.244	4.732	1.512
MT	1.487	0.540	1.606	1.459	2.399	0.625	0.147	1.078	2.515	0.879	0.440	1.615
HM	0.089					2.991		1.201				
IL	0.481	0.153	1.185	0.994	0.958	0.994	0.115	0.577	0.565	0.921	0.750	1.289
AP	0.264	0.072	0.668	0.572	0.574	0.238		0.168	0.258	0.454	0.312	0.864
CC			0.114									
TOTAL	100.006	100.002	100.016	100.013	100.013	100.005	100.000	100.004	100.006	100.011	100.007	100.019

Crystalline Rocks of Arabian Shield

	90A	90B	91A	91B	93A	93B	93C	93D	93Z	94	98	102
SIO2	66.20	71.80	76.20	75.20	53.20	50.80	50.20	48.30	62.20	74.00	73.20	62.10
AL203	15.60	15.40	13.00	13.60	16.70	18.20	20.10	18.40	16.00	6.23	12.40	14.00
FE203	0.87	0.40	0.23	1.17	1.40	2.50	0.60	2.30	1.00	2.35		5.20
FEO	2.30	1.00	0.70	0.84	5.30	5.30	6.00	6.80	3.80	1.30	2.00	2.30
MGO	2.20	0.54	0.10	0.15	8.20	7.40	8.30	8.70	4.20	0.76	1.90	1.50
CAO	3.80	2.40	0.85	1.30	10.80	9.80	9.80	9.40	5.80	2.00	3.10	4.10
NA20	4.30	3.90	3.50	3.80	2.70	2.80	2.90	2.80	4.10	5.55	0.55	5.40
K20	2.80	3.00	4.60	4.80	0.14	0.22	0.27	0.34	1.30	0.78	2.60	0.97
TIO2	0.74	0.23	0.08	0.06	0.42	0.70	0.67	1.40	0.51	0.01	0.08	1.40
P205	0.34	0.01	0.02	0.03	0.06	0.11	0.09	0.52	0.27	0.01		0.59
MNO	0.10		0.03		0.11	0.13	0.07	0.13	0.05		0.03	0.15
CO2	0.05		0.05		0.08	0.09	0.11	0.08				1.20
H20+	0.63		0.55		0.44	1.50	0.73	0.60				1.40
H20-	0.07		0.03		0.17	0.32	0.14	0.16				0.18
TOTAL	100.44	99.47	100.29	101.48	100.15	101.06	100.54	100.44	99.90	99.43	98.93	101.48
NORMATIVE MINERALS												
Q	19.444	31.619	36.228	31.369	2.565	1.503			14.308	45.996	51.052	21.129
C		1.416	0.887								3.176	0.814
OR	16.663	17.965	27.358	28.098	0.835	1.326	1.610	2.026	7.742	4.957	16.028	5.795
AB	36.642	33.442	29.807	31.852	23.052	24.164	24.759	23.891	34.962	29.791	4.855	46.197
AN	15.101	11.999	3.794	5.820	33.331	37.167	41.398	36.940	21.580		16.043	8.998
AC										7.311		
NS										2.889		
WO	0.555			0.156	8.277	4.637	2.656	2.567	2.355	4.426		
EN	5.518	1.363	0.251	0.370	20.606	18.796	12.114	13.356	10.541	2.035	4.936	3.777
FS	2.486	1.141	1.026	0.472	8.159	6.887	5.594	5.250	5.445	2.549	3.752	
FO							6.127	5.951				
FA							3.118	2.578				
MT	1.270	0.588	0.336	1.680	2.048	3.697	0.878	3.363	1.461			3.887
HM												2.576
IL	1.415	0.443	0.153	0.113	0.805	1.356	1.284	2.681	0.976	0.020	0.158	2.688
AP	0.811	0.024	0.048	0.070	0.143	0.266	0.215	1.242	0.644	0.025		1.413
CC	0.115		0.114		0.184	0.209	0.252	0.183				2.759
TOTAL	100.019	100.001	100.001	100.002	100.005	100.007	100.006	100.029	100.015	100.001	100.000	100.033

	103	104	105	106	111	113	114A	114B	114C	115	116	117A
SIO2	52.50	46.70	72.60	75.40	70.50	75.50	75.20	66.50	69.50	73.30	52.20	50.70
AL203	15.30	20.70	14.90	13.70	14.10	12.90	13.70	13.87	14.00	13.80	18.70	16.40
FE203	2.60	1.70	1.00	0.70	1.30	1.30	0.43	0.59	0.75	1.30	3.40	1.90
FEO	6.80	5.90	1.20	0.52	1.80	0.36	0.70	1.80	0.76	1.00	5.70	8.30
MGO	5.80	9.40	0.42	0.32	1.00	0.08	0.40	0.72	0.30	0.73	4.10	9.40
CAO	9.50	12.60	1.80	1.50	2.20	0.08	1.20	7.56	7.63	2.40	8.00	1.20
NA20	3.40	1.70	3.60	6.10	3.60	4.40	4.10	4.32	4.40	3.50	3.00	2.10
K20	0.27	0.20	4.10	1.10	3.50	3.60	3.10	1.80	2.64	2.80	0.55	1.40
TIO2	1.50	0.16	0.22	0.11	0.55	0.14	0.19	0.28	0.13	0.24	1.10	1.60
P205	0.24	0.14	0.05		0.03	0.28	0.04	0.01	0.09	0.06	0.24	0.19
MNO	0.09	0.10	0.01	0.03	0.01		0.05	0.04			0.10	0.03
C02	0.06						0.05					0.64
H20+	1.70						0.73					
H20-	0.13						0.04					
TOTAL	101.01	100.19	100.68	100.98	99.25	99.30	100.39	98.32	100.81	99.72	98.57	99.85
NORMATIVE MINERALS												
Q	4.163		31.189	32.220	29.856	36.507	36.554	21.931	22.707	36.314	8.029	14.682
C			1.388		0.468	1.789	1.643			0.799		11.918
OR	1.627	1.190	24.252	6.534	20.978	21.567	18.474	10.911	15.569	16.691	3.348	8.814
AB	29.339	14.486	30.493	51.886	30.898	37.745	34.987	37.496	37.157	29.876	26.146	18.932
AN	26.196	48.600	8.612	6.787	10.872		5.421	13.476	10.632	11.615	37.011	0.710
WO	8.301	5.607		0.290				10.408	11.089		0.940	
EN	14.731	8.224	1.047	0.801	2.526	0.202	1.005	1.839	0.746	1.834	10.517	24.942
FS	8.188	3.285	1.034	0.252	1.361		0.715	2.493	0.560	0.369	6.208	11.811
FO		10.758										
FA		4.736										
MT	3.844	2.482	1.451	1.020	1.912	0.765	0.629	0.877	1.085	1.901	5.077	2.935
HM						0.790						
IL	2.905	0.306	0.418	0.210	1.060	0.270	0.364	0.545	0.246	0.460	2.152	3.238
AP	0.580	0.334	0.119		0.072	0.146	0.096	0.024	0.213	0.143	0.585	0.479
CC	0.139						0.115					1.551
TOTAL	100.014	100.009	100.003	100.000	100.002	99.781	100.003	100.001	100.005	100.003	100.014	100.011

	117B	122	123	124A	124B	125	126	127A	127B	133	134	138
SIO2	59.90	67.80	73.40	63.40	72.40	73.40	66.70	74.30	75.20	60.40	65.70	54.20
AL203	15.60	14.90	13.30	17.40	15.70	14.50	16.20	13.50	13.00	17.50	15.30	14.30
FE203	2.80	3.30	1.70	1.20	0.30	0.53	0.92	0.17	0.90	2.80	3.80	3.80
FEO	5.50	1.70	0.76	3.90	1.60	0.70	2.80	0.60	0.82	4.10	1.40	7.30
MGO	2.90	0.55	0.31	1.00	0.60	0.50	2.10	0.10	0.13	2.90	1.60	3.50
CAO	3.20	2.30	0.83	5.20	3.20	1.20	4.60	0.65	0.77	6.60	0.86	3.80
NA20	5.20	5.60	4.80	4.00	4.50	3.70	3.80	4.30	4.00	2.00	6.60	4.10
K20	0.57	1.40	2.30	1.20	0.76	4.20	1.30	5.10	4.30	0.58	1.10	2.00
TIO2	1.20	0.44	0.21	0.50	0.13	0.19	0.42	0.09	0.16	0.42	0.81	2.10
P205	0.42	0.04	0.13	0.36	0.13	0.06	0.10		0.03	0.14	0.23	0.58
MNO	0.13	0.07	0.05	0.20	0.02	0.03	0.10	0.06	0.06	0.17	0.09	0.21
C02	0.20			0.05		0.05	0.05	0.05	0.05	0.02	0.30	0.08
H20+				1.00		0.46	0.72	0.24	0.45	2.30	1.20	2.80
H20-				0.05		0.05	0.26	0.05	0.02	0.05	0.10	0.27
TOTAL	99.81	99.33	99.38	100.09	99.84	99.89	100.75	99.40	100.17	101.36	99.89	100.93
NORMATIVE	MINERALS											
Q	15.642	24.703	35.591	21.804	35.019	32.835	25.521	28.345	33.773	26.967	20.801	8.252
C	2.130	0.088	1.755	1.061	1.981	1.963	0.538		0.556	2.011	3.000	0.058
OR	3.450	8.433	13.898	7.206	4.521	25.054	7.753	30.466	25.558	3.511	6.647	12.315
AB	45.074	48.303	41.534	34.394	38.331	31.605	32.450	36.783	34.044	17.334	57.109	36.150
AN	12.156	11.365	3.342	23.503	15.126	5.295	22.052	2.499	3.327	32.471	0.887	15.168
WO								0.184				
EN	7.399	1.396	0.790	2.531	1.504	1.257	5.278	0.252	0.326	7.398	4.075	9.083
FS	6.194			5.809	2.529	0.595	3.910	0.934	0.613	4.956		7.490
MT	4.159	4.518	2.049	1.768	0.438	0.776	1.346	0.249	1.313	4.158	2.514	5.741
HM		0.248	0.325								2.152	
IL	2.335	0.852	0.408	0.965	0.249	0.364	0.805	0.173	0.306	0.817	1.573	4.156
AP	1.019	0.097	0.315	0.866	0.310	0.143	0.239		0.071	0.340	0.557	1.431
CC	0.466			0.116		0.115	0.115	0.115	0.114	0.047	0.698	0.190
TOTAL	100.024	100.003	100.007	100.021	100.007	100.003	100.006	100.001	100.002	100.010	100.013	100.034

	139	141A	141B	141C	141D	142	143	144A	144B	145	146	147A
SIO2	76.10	57.70	73.20	75.70	71.00	66.00	63.70	74.70	70.00	49.70	76.10	75.80
AL203	11.90	17.50	13.60	12.30	14.25	15.00	15.50	13.30	14.50	21.30	12.70	13.80
FE203	1.50	4.90	1.80	1.70	1.82	2.90	2.20	0.21	0.41	0.50	1.40	0.52
FEO	0.60	1.20	0.36	0.20	0.52	1.10	2.40	0.90	2.60	3.80	0.20	0.36
MGO	0.05	1.90	0.54	0.58	0.53	2.40	2.20	0.10	0.55	10.20	0.06	0.02
CAO	1.00	4.80	1.40	2.00	0.60	3.00	4.70	0.78	2.00	9.80	0.36	0.55
NA2O	4.60	5.30	3.80	3.80	4.61	3.60	4.00	3.60	3.80	2.70	4.20	4.60
K2O	2.90	3.20	3.20	1.50	4.14	3.60	2.90	5.20	3.80	0.12	4.30	4.20
TIO2	0.10	0.89	0.33	0.15	0.32	0.44	0.63	0.11	0.38	0.22	0.16	1.00
P2O5	0.01	0.32	0.16	0.04	0.10	0.12	0.31		0.19	0.04	0.04	0.03
MNO	0.02	0.11	0.10	0.04	0.04	0.06	0.12	0.04	0.01	0.02		0.11
CO2	0.08	0.66	0.05	0.34		0.15	0.05	0.05				
H2O+	0.89	1.30	0.57	0.66		1.00	1.10	0.57				
H2O-	0.11	0.13	0.13	0.07		0.08	0.07	0.05				
TOTAL	100.49	100.79	99.70	99.53	98.22	100.11	100.59	99.99	98.55	98.61	100.32	101.68
NORMATIVE MINERALS												
Q	36.940	4.945	36.162	44.481	27.110	22.391	17.539	31.873	27.527		34.633	31.535
C			1.866	1.700	1.362	0.368		0.452	0.971		0.581	0.751
OR	17.335	19.202	19.190	9.013	24.982	21.626	17.361	31.042	22.858	0.721	25.532	24.576
AB	39.373	45.539	32.631	32.694	39.833	30.967	34.289	30.773	32.731	23.218	35.711	38.542
AN	3.295	14.733	5.667	7.637	2.372	13.369	15.980	3.590	8.836	46.387	1.532	2.508
WO	0.478	1.289					2.200			1.151		
EN	0.126	4.805	1.365	1.469	1.348	6.076	5.551	0.252	1.394	12.053	0.150	0.049
FS							1.796	1.386	3.895	2.960		
FO										9.645		
FA										2.610		
MT	1.729	1.673	0.538	0.346	0.898	2.507	3.231	0.308	0.605	0.737	0.182	
HM	0.325	3.822	1.456	1.490	1.239	1.219					1.281	0.515
IL	0.192	1.716	0.636	0.290	0.621	0.850	1.212	0.211	0.735	0.425	0.305	0.986
RU												0.471
AP	0.024	0.770	0.385	0.096	0.242	0.289	0.744		0.458	0.096	0.095	0.070
CC	0.184	1.524	0.115	0.786		0.347	0.115	0.115				
TOTAL	100.001	100.018	100.010	100.003	100.006	100.007	100.018	100.000	100.010	100.002	100.002	100.003

	147B	149A	149B	149X	150	152	154	155	157	158	159A	159B
SIO2	52.20	75.50	74.70	56.80	57.00	65.40	74.90	76.30	74.80	76.50	66.00	73.00
AL2O3	18.30	13.50	13.20	15.70	16.10	15.00	13.70	12.50	13.20	12.80	17.70	14.40
FE2O3	6.50	0.29	0.30	2.10	3.08	2.40	0.80	1.10	0.25	0.39	0.94	1.10
FEO	3.60	1.00	1.10	6.70	6.40	4.00	0.44	0.60	0.24	0.40	1.40	0.80
MGO	5.10	0.20	0.39	3.00	3.80	2.50	0.23	0.10	0.06	0.04	0.32	0.04
CAO	9.60	0.78	1.60	5.10	7.40	5.80	1.10	0.76	1.20	0.50	1.90	0.63
NA2O	2.80	3.20	3.50	3.50	2.80	3.10	3.90	4.10	5.60	4.10	5.30	4.70
K2O	0.12	4.60	4.80	2.70	1.10	1.30	4.40	4.30	2.90	4.30	5.10	4.70
TIO2	0.08	0.12	0.20	1.80	0.44	0.60	0.31	0.12	0.09	0.06	0.69	0.15
P2O5	0.34	0.02	0.08	0.74	0.15	0.18	0.09	0.38	0.02	0.01	0.16	0.24
MNO	0.03	0.04		0.12	0.20	0.09					0.07	0.02
CO2		0.10		0.02								
H2O+		0.51		0.49								
H2O-		0.07		0.15								
TOTAL	99.17	100.30	100.09	99.35	98.47	101.08	100.07	100.94	98.36	99.15	99.88	99.78
NORMATIVE MINERALS												
Q	9.652	37.214	31.851	9.714	13.222	25.540	32.974	35.199	29.730	35.268	11.247	26.843
C		2.132					0.738	0.627		0.521	0.391	1.012
OR	0.719	27.360	28.401	16.234	6.601	7.654	26.035	25.344	17.423	25.641	30.264	27.835
AB	24.012	27.255	29.655	30.134	24.061	26.135	33.044	34.603	48.176	35.008	45.036	39.858
AN	37.509	3.127	6.139	19.489	28.550	23.089	4.875	1.284	2.354	2.437	8.416	1.561
WO	3.552		0.537	0.504	3.230	1.840			1.489			
EN	12.873	0.501	0.973	7.602	9.611	6.203	0.574	0.248	0.152	0.101	0.800	0.100
FS	1.180	1.483	1.444	7.956	8.991	4.522			0.087	0.316	0.788	0.351
MT	9.551	0.423	0.436	3.098	4.535	3.467	0.520	1.582	0.369	0.571	1.369	1.598
HM							0.442	0.006				
IL	0.154	0.229	0.380	3.478	0.849	1.135	0.590	0.227	0.174	0.115	1.316	0.286
AP	0.816	0.048	0.190	1.783	0.361	0.425	0.213	0.898	0.048	0.024	0.381	0.570
CC		0.229		0.046								
TOTAL	100.018	100.002	100.004	100.040	100.010	100.010	100.005	100.020	100.001	100.000	100.009	100.013

	160	161	162	163	164	166	167A	167B	167C	167D	167E	167F
SIO2	65.50	71.40	73.70	74.30	62.60	73.30	51.70	48.00	50.00	49.10	42.50	48.80
AL203	15.11	15.20	13.20	13.10	15.70	12.90	21.00	28.30	28.40	29.44	17.00	28.20
FE203	4.19	0.76	1.80	1.94	1.60	1.60	0.94	5.04	2.12	2.20	9.34	3.23
FEO	0.36	0.76	1.00	1.40	3.10	0.92	5.90					
MGO	0.35	0.55	0.33	0.06	4.10	0.23	4.40	3.32	0.49	1.16	12.82	2.82
CAO	0.70	2.30	1.20	0.60	4.90	0.83	10.40	10.35	11.47	12.03	10.98	11.94
NA2O	4.42	4.20	4.70	4.50	3.80	4.30	2.50	3.60	4.70	4.40	1.04	3.76
K2O	7.20	3.40	4.70	4.90	3.30	4.20	0.35	0.61	0.54	0.47	0.11	0.33
TIO2	0.37	0.30	0.24	0.20	0.61	0.25	0.56					
P2O5	0.07	0.12		0.03	0.02	0.03	0.04					
MNO			0.02		0.06	0.03	0.06					
TOTAL	98.42	99.03	100.89	101.58	101.03	99.14	98.74	100.62	99.62	100.60	97.39	100.48
NORMATIVE MINERALS												
Q	11.231	28.715	26.141	27.874	11.513	30.699	4.329					
C		0.723						2.922				
OR	43.296	20.297	27.529	28.660	19.542	25.174	2.114	3.633	3.265	2.811	0.693	1.968
AB	38.059	35.902	39.419	37.690	32.222	36.906	21.619	30.702	31.495	26.902	9.383	27.695
AN	0.127	10.735	1.030	1.063	16.069	3.543	46.034	51.750	56.078	59.910	44.134	59.643
NE									4.986	5.841		2.393
WO	1.228		2.034	0.705	3.407	0.181	2.683		0.899	0.207	5.823	0.059
EN	0.887	1.384	0.815	0.148	10.233	0.581	11.199	0.246	0.777	0.179	20.565	0.051
FS		0.275		0.631	3.482	0.011	9.448					
FO								5.668	0.331	1.924	9.444	4.931
MT	0.089	1.113	2.570	2.784	2.325	2.353	1.393					
HM	4.202		0.012					5.080	2.169	2.227	9.958	3.260
IL	0.715	0.576	0.452	0.376	1.161	0.482	1.087					
AP	0.169	0.287		0.070	0.047	0.072	0.097					
TOTAL	100.004	100.006	100.000	100.002	100.002	100.002	100.003	100.000	100.000	100.000	100.000	100.000

	167G	167H	170	171	172	174	175	177	178	186	194	195
SIO2	49.50	48.80	73.70	72.20	73.40	71.10	47.70	75.20	44.80	69.90	54.60	71.20
AL2O3	30.80	31.40	14.20	14.60	14.50	13.60	16.30	13.00	22.10	15.80	17.00	13.80
FE2O3	2.24	3.23	0.20	1.30	1.00	1.80	3.20	0.49	1.90	1.20	3.00	1.60
FEO			1.00	1.00	0.72	2.50	7.30	1.20	2.80	1.60	5.40	2.90
MGO	0.76	0.65	0.43	0.80	0.38	0.92	7.40	0.12	12.40	0.85	4.80	1.30
CAO	9.54	11.75	1.80	1.80	2.90	2.20	8.90	0.36	9.80	3.80	8.50	4.50
NA2O	5.03	3.49	3.40	5.00	4.40	4.50	4.20	3.80	1.80	4.00	3.40	2.80
K2O	1.01	0.28	4.10	1.70	1.40	1.40	1.50	4.60	0.08	1.20	0.31	0.35
TIO2			0.18	0.41	0.14	0.49	2.40	0.14	0.12	0.25	1.10	0.25
P2O5			0.06	0.12	0.06	0.13	0.59	0.03	0.04	0.08	0.43	0.02
MNO				0.14	0.04	0.14	0.14	0.03	0.07	0.06	0.08	0.12
CO2				0.05	0.23	0.01		0.08	0.07		0.05	0.05
H2O+				0.47	0.65	0.85		0.77	3.60		1.30	1.00
H2O-				0.22		0.06		0.02	0.31		0.02	0.06
TOTAL	100.28	99.90	99.07	100.30	100.20	100.25	99.63	100.31	102.29	99.34	100.76	100.59
NORMATIVE MINERALS												
Q		1.286	33.591	32.162	36.615	33.113		34.434		32.517	9.019	40.904
C	4.133	4.008	1.050	1.680	1.160	1.029		1.386	1.555	1.219		0.806
OR	6.036	1.661	24.455	10.135	8.342	8.374	8.897	27.443	0.493	7.182	1.857	2.091
AB	32.822	29.650	29.040	42.684	37.543	38.544	24.861	32.463	15.869	34.279	29.158	23.959
AN	47.864	58.526	8.618	7.899	12.646	10.124	21.272	1.095	49.921	18.563	30.616	22.123
NE	5.538						5.856					
WO							8.007				3.738	
EN		1.625	1.081	2.010	0.954	2.319	5.358	0.302	10.541	2.144	12.116	3.274
FS			1.387	0.349	0.342	2.586	2.052	1.639	1.196	1.666	5.848	3.857
FO	1.341						9.208		15.161			
FA							3.887		1.896			
MT			0.293	1.902	1.462	2.642	4.657	0.717	2.870	1.762	4.408	2.346
HM	2.265	3.243										
IL			0.345	0.786	0.268	0.942	4.575	0.268	0.237	0.481	2.117	0.480
AP			0.143	0.287	0.143	0.312	1.403	0.072	0.099	0.192	1.032	0.048
CC				0.115	0.527	0.023		0.184	0.166		0.115	0.115
TOTAL	100.000	100.000	100.003	100.008	100.004	100.009	100.032	100.002	100.003	100.005	100.024	100.003

	196	197	198	198Z	199	200	201A	201B	202	203A	203B	204
SIO2	71.70	72.90	62.70	74.60	41.20	45.60	59.80	71.40	47.20	73.40	70.40	75.20
AL2O3	14.60	13.20	18.20	13.50	17.20	19.30	16.50	16.50	18.70	15.80	16.10	13.60
FE2O3	1.50	1.30	1.40	0.64	5.30	1.60	2.40	1.10	1.20	0.68	0.64	0.53
FEO	1.20	0.42	1.90	0.78	6.80	7.40	3.70	0.36	7.10	0.56	0.96	0.44
MGO	1.00	0.22	1.00	0.10	5.30	13.00	3.30	0.13	12.20	0.24	0.54	0.04
CAO	3.20	1.80	1.90	1.00	12.80	9.40	5.80	3.20	9.00	3.40	1.70	0.62
NA2O	4.60	4.90	6.70	4.00	2.60	1.80	3.80	5.30	2.60	4.40	5.00	4.00
K2O	1.00	3.50	4.40	4.50	0.36	0.12	1.10	0.49	0.16	0.40	3.40	4.80
TIO2	0.30	0.24	0.94	0.17	3.70	0.26	0.82	0.10	0.64	0.10	0.36	0.08
P2O5	0.05	0.02	0.25	0.05	1.90	0.06	0.24	0.08	0.08	0.06	0.12	0.02
MNO	0.08	0.09	0.13	0.06	0.15	0.12	0.08	0.02	0.12	0.04	0.02	0.01
CO2	0.05	0.76	0.05	0.05	0.03	0.08	0.04	0.03	0.07	0.06	0.01	0.04
H2O+	0.64	0.41	0.42	0.27	2.10	1.10	1.50	0.53	0.74	0.74	0.58	0.62
H2O-	0.05	0.04	0.05	0.03	0.08	0.12	0.13	0.06	0.10	0.02	0.05	0.07
TOTAL	100.39	100.08	100.33	99.94	100.82	100.72	100.21	99.67	100.44	100.35	100.27	100.50
NORMATIVE MINERALS												
Q	33.003	29.207	1.904	31.939			16.158	32.371		39.131	24.096	32.426
C	0.370			0.469				1.716		2.249	1.425	0.843
OR	5.952	20.818	26.113	26.739	2.185	0.718	6.661	2.933	0.954	2.384	20.243	28.541
AB	39.206	41.734	56.938	34.034	22.602	15.425	32.952	45.433	22.207	37.555	42.628	34.058
AN	15.343	3.710	6.619	4.342	35.132	44.792	25.329	15.361	39.246	16.236	7.644	2.709
WO		0.130	0.371		7.164	0.638	0.957		2.024			
EN	2.509	0.551	2.501	0.250	5.622	7.402	8.423	0.328	5.234	0.603	1.355	0.100
FS	0.622		1.026	0.739	0.970	2.757	3.696		1.932	0.379	0.682	0.258
FO					5.563	17.791			17.824			
FA					1.058	7.304			7.249			
MT	2.191	0.958	2.039	0.933	7.894	2.349	3.566	0.948	1.756	0.994	0.935	0.773
HM		0.648						0.461				
IL	0.574	0.459	1.793	0.325	7.219	0.500	1.596	0.192	1.227	0.192	0.689	0.153
AP	0.119	0.048	0.595	0.119	4.623	0.144	0.583	0.192	0.191	0.143	0.286	0.048
CC	0.115	1.740	0.114	0.114	0.070	0.184	0.093	0.069	0.161	0.138	0.023	0.092
TOTAL	100.004	100.002	100.015	100.003	100.103	100.005	100.014	100.004	100.006	100.004	100.006	100.001

	205	206	207	208	209	212	214	215	217	218	223A	223B
SIO2	75.50	70.80	70.80	58.70	72.90	49.00	35.30	63.30	51.40	46.70	68.00	49.40
AL203	13.10	16.60	14.70	15.20	12.60	18.40	1.40	17.70	15.20	15.20	14.50	13.70
FE203	1.00	0.75	0.88	3.10	1.70	1.00	11.70	0.67	3.00	1.70	3.60	2.70
FEO	0.40	0.68	1.20	4.20	1.80	5.20	2.80	3.30	6.80	9.00	2.40	8.70
MGO		0.44	0.77	4.60	0.17	10.70	33.20	1.70	7.50	10.30	0.88	9.80
CAO	0.48	3.20	3.30	6.90	0.62	12.00	1.40	5.60	8.20	7.40	4.40	11.50
NA2O	4.10	4.90	3.80	3.00	3.80	2.10	0.02	4.50	2.40	2.00	3.30	1.40
K2O	4.30	1.00	2.30	1.40	5.00	0.16	0.12	1.00	1.10	0.92	0.28	0.24
TIO2	0.10	0.12	0.31	0.54	0.32	0.37	0.08	0.67	0.90	1.10	0.38	0.37
P2O5		0.08	0.14	0.27	0.04	0.05	0.08	0.39	0.22	0.26	0.13	0.08
MNO	0.01		0.02	0.16	0.09	0.10	0.17	0.08	0.18	0.20	0.06	0.21
CO2	0.04	0.01	0.56	0.07	0.07	0.07	0.76	0.04	0.05	0.08	0.30	0.07
H2O+	0.55	0.49	0.82	1.40	0.64	0.82	9.99	0.77	2.40	3.80	0.82	1.30
H2O-	0.04	0.02	0.06	0.08	0.07	0.05	0.86	0.10	0.06	0.23	0.07	0.10
TOTAL	99.98	99.39	100.20	100.51	100.26	100.55	106.64	100.37	100.86	101.32	99.67	100.42
NORMATIVE MINERALS												
Q	34.612	31.462	33.553	15.170	29.950			18.093	3.798		38.442	0.912
C	0.930	1.880	1.612		0.068		0.740	0.060			1.807	
OR	25.659	5.994	13.759	8.430	29.812	0.954	0.815	5.972	6.705	5.731	1.684	1.445
AB	35.033	42.060	32.552	25.866	32.443	17.922	0.194	38.482	20.947	17.840	28.427	12.067
AN	2.149	15.510	12.064	24.326	2.393	40.653	1.860	25.246	28.317	31.394	19.426	30.955
WO				3.468		7.772			4.942	2.081		10.930
EN		1.112	1.941	11.674	0.427	13.387	35.645	4.279	19.267	17.220	2.231	24.862
FS		0.437	1.014	4.644	1.554	4.168		4.597	9.136	9.181	0.934	13.777
FO						9.453	41.599			6.883		
FA						3.244				4.045		
MT	1.042	1.103	1.292	4.580	2.487	1.462	10.739	0.982	4.487	2.598	5.314	3.988
HM	0.291						6.037					
IL	0.192	0.231	0.596	1.045	0.613	0.709	0.175	1.286	1.763	2.202	0.735	0.716
AP		0.192	0.336	0.652	0.096	0.119	0.218	0.934	0.537	0.649	0.313	0.193
CC	0.092	0.023	1.289	0.162	0.161	0.161	1.986	0.092	0.117	0.192	0.695	0.162
TOTAL	100.000	100.004	100.008	100.016	100.003	100.004	100.007	100.021	100.014	100.017	100.008	100.007

	223C	224	227	237	241	501	502
SIO2	69.70	74.90	55.70	69.20	65.30	51.60	38.70
AL203	15.30	14.40	15.10	15.70	17.30	21.30	17.80
FE203	0.84	0.29	1.50	1.00	1.00	9.86	19.10
FEO	1.80	0.32	5.10	1.60	1.80		
MGO	0.41	0.17	5.40	0.96	1.20	3.10	7.55
CAO	2.00	1.50	7.70	3.50	3.90	7.02	0.62
NA20	4.10	4.00	3.90	4.40	4.40	4.76	0.08
K20	4.70	3.00	1.20	2.20	2.80	1.25	4.04
TIO2	0.50	0.07	1.70	0.41	0.66	0.50	3.50
P205	0.15	0.05	0.58	0.11	0.36	0.26	0.73
MNO		0.05	0.10	0.04	0.07		
CO2	0.07	0.05	0.24	0.05	0.05		
H20+	0.49	0.41	0.92	0.77	0.60		
H20-	0.05	0.11	0.08	0.10	0.06		
TOTAL	100.44	99.67	99.83	100.59	99.91	99.65	99.62
NORMATIVE MINERALS							
Q	22.868	37.262	6.527	26.234	19.533	0.215	12.506
C	0.355	2.106		0.097	0.929		14.433
OR	27.894	17.943	7.220	13.109	16.740	7.413	25.916
AB	34.843	34.258	33.599	37.543	37.669	40.419	0.735
AN	8.536	6.881	20.517	16.465	16.876	33.177	
WO			5.417				
EN	1.026	0.429	13.693	2.411	3.024	7.748	20.412
FS	1.793	0.329	5.605	1.522	1.537		
MT	1.223	0.426	2.214	1.462	1.467		
HM						9.895	20.734
IL	0.954	0.135	3.287	0.785	1.268		
TN						0.047	
RU						0.482	3.799
AP	0.357	0.120	1.399	0.263	0.863	0.618	1.210
CC	0.160	0.115	0.556	0.115	0.115		
TOTAL	100.008	100.003	100.032	100.006	100.020	100.013	99.745

Table 3.--Chemical and normative analyses of crystalline rocks of the Saudi Arabian Shield

1/ Laboratory and analytical method:

A. USGS, Washington, D.C., rapid rock analyse, single-solution method, Leonard Shapiro (ref., 1967); analysts: Paul Elmore, Sam Botts, Lowell Artis (Nov., 1964); S. M. Berthold (July, 1965); Paul Elmore, Sam Botts, Lowell Artis, H. Smith, John Glenn, G. Chloe, D. Taylor (Dec., 1965, Jan., 1966, Aug., 1966); Lowell Artis (June, 1973); Paul Elmore (Sept., 1973).

B. USGS, Washington, D.C., rapid rock analyses, single-solution method, Leonard Shapiro (ref., 1967); analysts: Herbert Kirshenbaum (Oct., 1973) and Sam Botts, John Glenn (May, 1973); CO_2 not determined, H_2O from DGMR-USGS lab., Jiddah.

C. USGS, Denver, Co., colorimetric and atomic absorption analyses, Claude Huffman, Jr.; analysts: G. T. Burrow, Wayne Mountjoy (July, 1974).

D. DGMR-USGS, Jiddah, atomic absorption, volumetric, and gravimetric methods, W. L. Campbell, technical advisor; analysts: Ibrahim Baradja, Souhar Al Farouki, Adel Hakeem, Mahmond Ashy, Abdulaziz Masoud, and others (July 1972); FeO, Ti_2O, P_2O_5, MnO, USGS lab., Washington, analysts: Sam Botts, John Glenn (May, 1973). Of the 20 "D" analyses, eight in brackets, [D], were not used in the chemical synthesis and plot figures of this report.

E. DGMR-USGS, Jiddah, atomic absorption, volumetric, and gravimetric methods, W. L., Campbell, technical advisor; analysts: Ibrahim Baradja, Souhar Al Farouki (Oct., 1971).

2/ Where only one H_2O is given amount is for total water as loss on ignition.

3/ Minerals: Q, quartz; C, corundum; OR, orthoclase
AB, albite; AN, anorthosite; NE, nepheline; AC, acmite;
NS, sodium metasilicate; WO, wollastonite
EN, enstatite; FS, ferrosilite; FO, forsterite;
FA, fayalite; MT, magnetite; HM, hematite;
IL, ilmenite; TN, titanite; RU, rutile; AP, apatite;
CC, calcite; SD, siderite

categories relate to stratigraphy discussed earlier in this report and in various reports summarizing the stratigraphy, plutonism, tectonism, and cratonization of the Arabian Shield (for example, Greenwood and others, 1980; Schmidt and others, 1979; Schmidt and others, 1973) and with some changes in terminology and nomenclature to the summary report of Delfour (1979b).

The Baish-Bahah age category is defined for those primitive volcanic rocks from the Wadi Bidah region (B, fig. 17) as defined by Schmidt and others (1973) and modified by Greenwood and others (1980); Baish-Bahah groups have been defined in the Wadi Bidah-Bahah area by Greenwood (1975b) even though the name Baish is from Wadi Baysh in the southwestern part of the shield where the "Baish" rocks of Wadi Baysh have been subsequently mapped as Jiddah rocks (fig. 2). The Jiddah-age category is defined for volcanic and plutonic rocks of the andesite assemblage and dioritic suite from the Biljurshi-An Nimas region (J, fig. 17). Jiddah rocks were originally named by Brown (USGS-ARAMCO, 1963) for rocks in the vicinity of the city of Jiddah but the rocks of the Jiddah group have been defined subsequently in more detail in the Biljurshi-Aqiq area east of Wadi Bidah by Greenwood (1975b and c), and the Jiddah age rocks (region J on figure 17) are defined herein in Biljurshi and Aqiq quadrangles. The Ablah-age category is defined for rocks of the Bidah and Biljurshi-An Nimas regions (B and J, fig. 17) that are younger than the Jiddah-age rocks, but are older than the culminant orogeny. The Halaban(Hulayfah)-age category is defined for andesitic assemblage rocks and dioritic-suite rocks from the Nuqrah quadrangle (Delfour, 1977) (area 1, fig. 17) and Juqjuq quadrangle (Hadley, 1976; Dodge and others, 1979) (area 5, fig. 17) from the eastern half of the shield.

The culminant-orogeny age category is defined for the gneiss domal and batholithic granodiorite rocks of the Jabal al Qarah and Junaynah quadrangles (Schmidt 1981a, 1980a) (Bishah area). These syntectonic rocks are well represented throughout the eastern half of the shield and are younger than Halaban (Hulayfah) rocks and are synchronous with the early Murdama and Shammar rocks. Many large gneiss domes (antiforms) formed during the culminant-orogeny, but these orthogneisses are tectonized older plutonic rocks, and for chemical comparison, they are classified according to their intrusive age rather than the age of tectonism (their tectonic age is generally shown in parentheses after their plutonic age in table 3). In contrast, these orthogneisses are mapped on figure 2 according to their tectonic age.

The Murdama-Shammar age category is defined for posttectonic plutonic, hypabyssal, and volcanic rocks, that intruded at least some Murdama, or are stratigraphically within, the Murdama and Shammar groups. The Murdama-Shammar rocks are designated as either Murdama age or Shammar age depending on local stratigraphy, and in general those rocks classified as Shammar-age are slightly younger than those classified as Murdama-age. The Jubaylah-Najd age category includes those volcanic, dike, and hypabyssal rocks stratigraphically within or intrusive into the Jubaylah Group in the Najd fault system and those intrusive rocks associated with or slightly post-dating the Najd faulting event.

Because the 199 chemically analyzed rocks of this report are widely distributed (diluted in space) and are divisable into many age categories (diluted in time), it is desirable to control or compare the chemistry of rocks of this report with the published chemistry of rocks from local areas where stratigraphy and age relations are well known. Twelve such control areas are shown on figure 17. About 300 control analyses have been examined using the same computed normative program and plots as was used for the 199 analyses reported herein.

Chemical variation of volcanic and plutonic rocks

Volcanic rocks

The Na_2O-CaO-K_2O (NCK) ternary diagram shows the spread or chemical separation of the analyzed rocks as well as, or better than many of the other ternary diagrams examined. For the normative data, the nearly comparable Ab-An-Or diagram does almost as well. Figures 18A, 18B, and 18C show the distribution of control rocks for the metavolcanic rocks of the shield. Figure 18A shows the distribution of the low-K_2O, mafic volcanic rocks of Baish-Bahah age from Wadi Bidah (control area 10). The similarily consistently low-K_2O rocks of wide compositional range from basalt to dacite and sodic rhyolite (at least some quartz keratophyre) of the Samran group from the Rabigh area (control area 12) have been mapped on figure 2 as Jiddah-age rocks. Figure 18B shows the distribution of Halaban rocks which include many low in K_2O, but overall they differ from the Baish-Bahah and Jiddah rocks of figure 18A in having many rocks that range to higher K_2O. These Halaban control samples are from the Nuqrah quandrangle, area 1, Wadi Miyah quandrangle, area 7, and Wadi Wassat, area 8.

Figure 18C shows the distinctly high K_2O, low CaO, dacitic to rhyolitic rocks of the Murdama and Shammar groups, as well as the less potassic, more mafic rocks of the Jubaylah rocks, from the Nuqrah quadrangle (area 1) and Wadi Miyah quandrangle (area 7). On this diagram, Murdama, Shammar, and Jubalah rocks separate with little compositional overlap.

Figure 19 shows the metavolcanic rocks analyzed for this report along with the rock-group boundary lines drawn from the control samples of figure 18. On figure 19, the Shammar and Murdama volcanic rocks are clearly separated by their high K_2O content from the older volcanic rocks. The Jubaylah volcanic rocks form a cluster that extends toward a composition that is more calcic than the control set, but this is emphasized partly by three diabasic dikes rocks (symbol N, fig. 19) of Najd age. The 10 Halaban rocks shown scatter widely between the CaO and Na_2O corners and have variable K_2O content within the range of the Halaban control rocks (fig. 18B). Three Jiddah-age rocks are as potassic as the most potassic of the Jiddah control group (fig. 18A).

Three analyses of Fatimah rocks from the Jiddah-Rabigh region (WS, fig. 17) are on the potassic side of the Jiddah control rocks from the Rabigh area (12), whereas one is as potassic as the Shammar rocks. The Fatimah rocks rest unconformably on rocks of the Samran (Jiddah?) group of the Rabigh area and are distinctly younger (Skiba, 1980). Three Ablah-age rocks have highly variable potassic contents and plot on the sodic side of the diagram. These

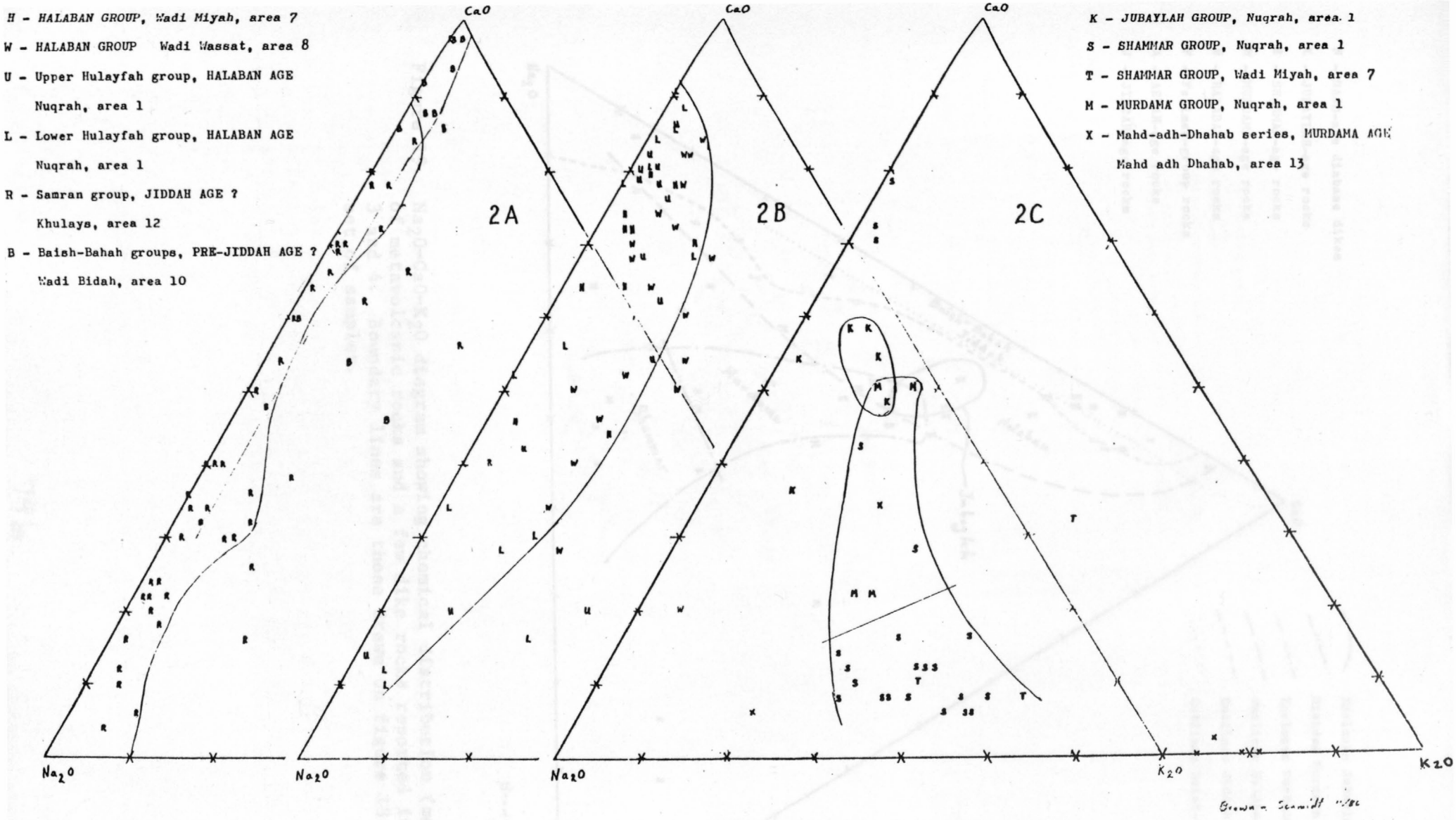

Figure 18. N_2O-CaO-K_2O diagram showing the chemical distribution (molar data) of control samples of metavolcanic rocks from rock groups: Baish-Bahah, Jiddah, Halaban, Murdama, Shammar, and Jubaylah. The samples are from local areas where these stratigraphic units have been described and chemically analyzed. The chemistry of rocks of the Baish-Bahah and Samran (Jiddah?) groups is shown on figure 18A; of the Halaban group, figure 18B; and of the Murdama, Shammar, and Jubaylah Jubaylah groups, figure 18C.

79a

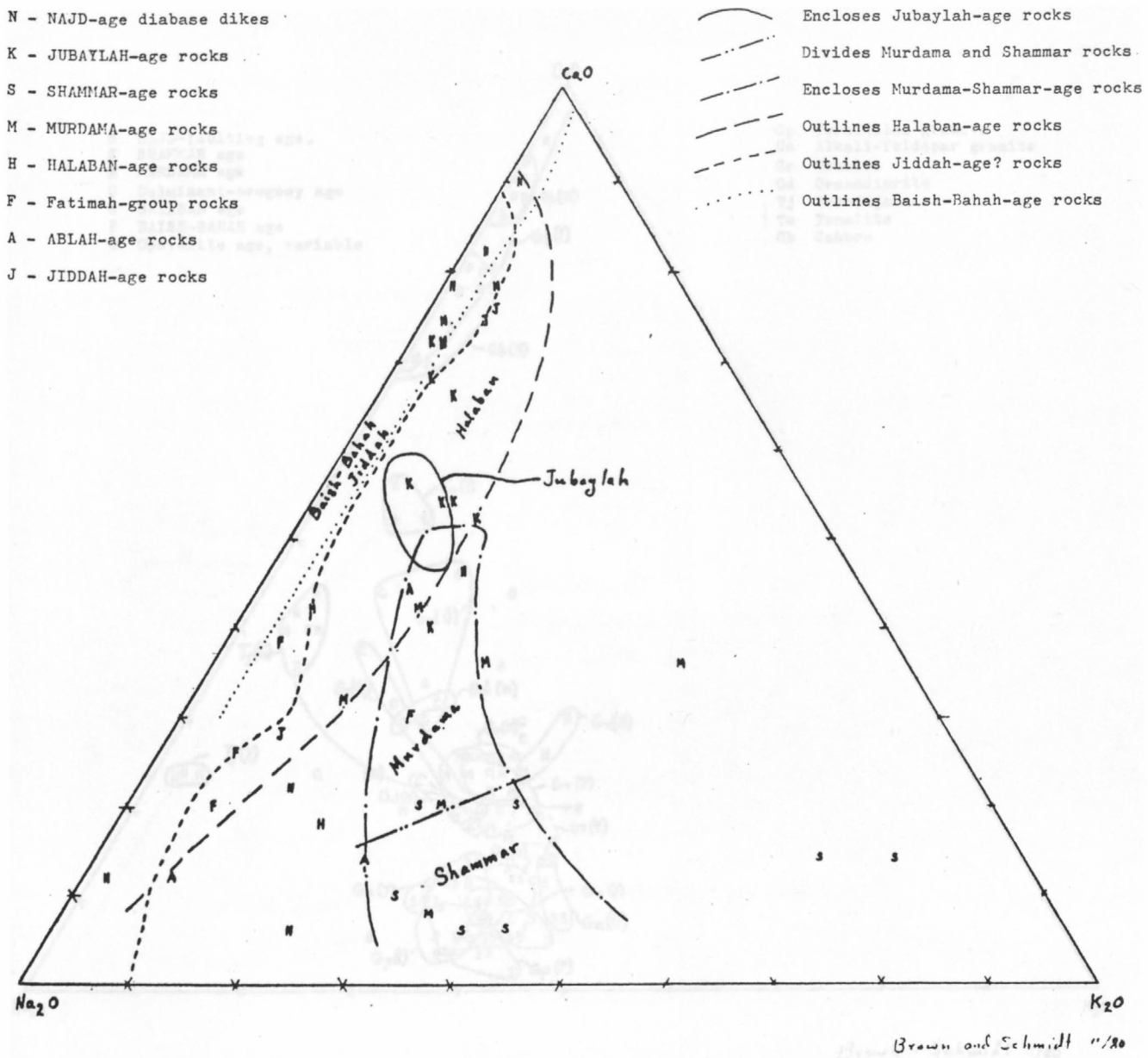

Figure 19. Na_2O-CaO-K_2O diagram showing chemical distribution (molar data) of metavolcanic rocks and a few dike rocks reported in tables 3 and 4. Boundary lines are those drawn on figure 18 for control set of samples.

few samples of Fatimah and Ablah rocks distinctly suggest rock chemistry that is more mature than that of the calc-alkalic rocks of the Jiddah (Samran) and Halaban (Hulayfah) groups. The scant chemistry does not distinguish between Fatimah and Ablah, but does strongly suggest that neither is correlative with either the Murdama or the Shammar rocks.

The consistently low K_2O content of the Baish-Bahah rocks (Bidah area 10) and the Samran rocks (Jiddah group?, Rabigh area 12) in figure 18A suggests an origin in an intraoceanic (ensimatic), island arc environment. The Halaban (Hulayfah) group rocks in figure 18B are presumably of similar origin, but the Halaban (Hulayfah) rocks in this report are restricted to the eastern half of the shield, a part of the shield that was intruded by late granitic plutons much more abundantly than the western half as represented by control samples of the Rabigh area 12 and Bidah area 10). The inference made here is that many more Halaban (Hulayfah) rocks have been altered by late granitic plutonism, and hence, the Halaban (Hulayfah) rocks show a much larger spread toward K_2O enrichment.

A second factor suggests that late potassic hydrothermal metasometism may have altered many of the Halaban (Hulayfah) rocks because many of the samples, especially the control samples, were collected in mineralized districts, for example, the Nuqrah and Wassat districts. This argument is less forceful however, because hydrothermal alteration may be also prevalent in parts of the Bidah and Rabigh areas. In this regard, 5 samples from the Mahd adh Dhahab mineralized district (area 14, fig. 17) are plotted on figure 18C--two are pyroclastic rocks from near the mine workings and are probably of Murdama (or Shammar) age and two are from a rhyolitic plug within the mine workings. All 4 are highly hydrothermally metasomatized especially in silica and potassium as indicated by petrography as well as the chemistry on figure 18C. A fifth sample from a rhyolite dike 2.5 km northeast of the mine is little altered, has a quartz trachyte composition, and is probably a subvolcanic intrusive of Murdama age. These Mahd adh Dhahab analyses from R. J. Roberts (written commun., 1980) are presented as an extreme case of known potassium hydrothermal metasomatism of one set of igneous rocks.

Still, a third factor suggests that more samples of siliceous and potassic volcanic rocks are represented in the Halaban samples than in the Baish-Bahah and Jiddah samples because the Halaban group is younger and less deformed and therefore less eroded than the Baish-Bahah and Jiddah groups.

Plutonic rocks

The plutonic rocks from the Arabian Shield, for both the control samples (fig. 20) and samples analyzed for this report (fig. 21), are well separated on the Na_2O-CaO-K_2O diagram. Figure 20 shows the chemistry of the control samples from the control areas of figure 17. In this sampling, analyses of the pretectonic rocks of the dioritic suite, especially of rocks of diorite composition, are sparse. Five analyses of amphibolite gneiss from the At Taif area 11 (Nasseef and Gass, 1977) are gabbroic and of very similar composition and may be orthogabbros; they are classified herein as Baish-Bahah age. Four analyses of the ophiolitic suite from the

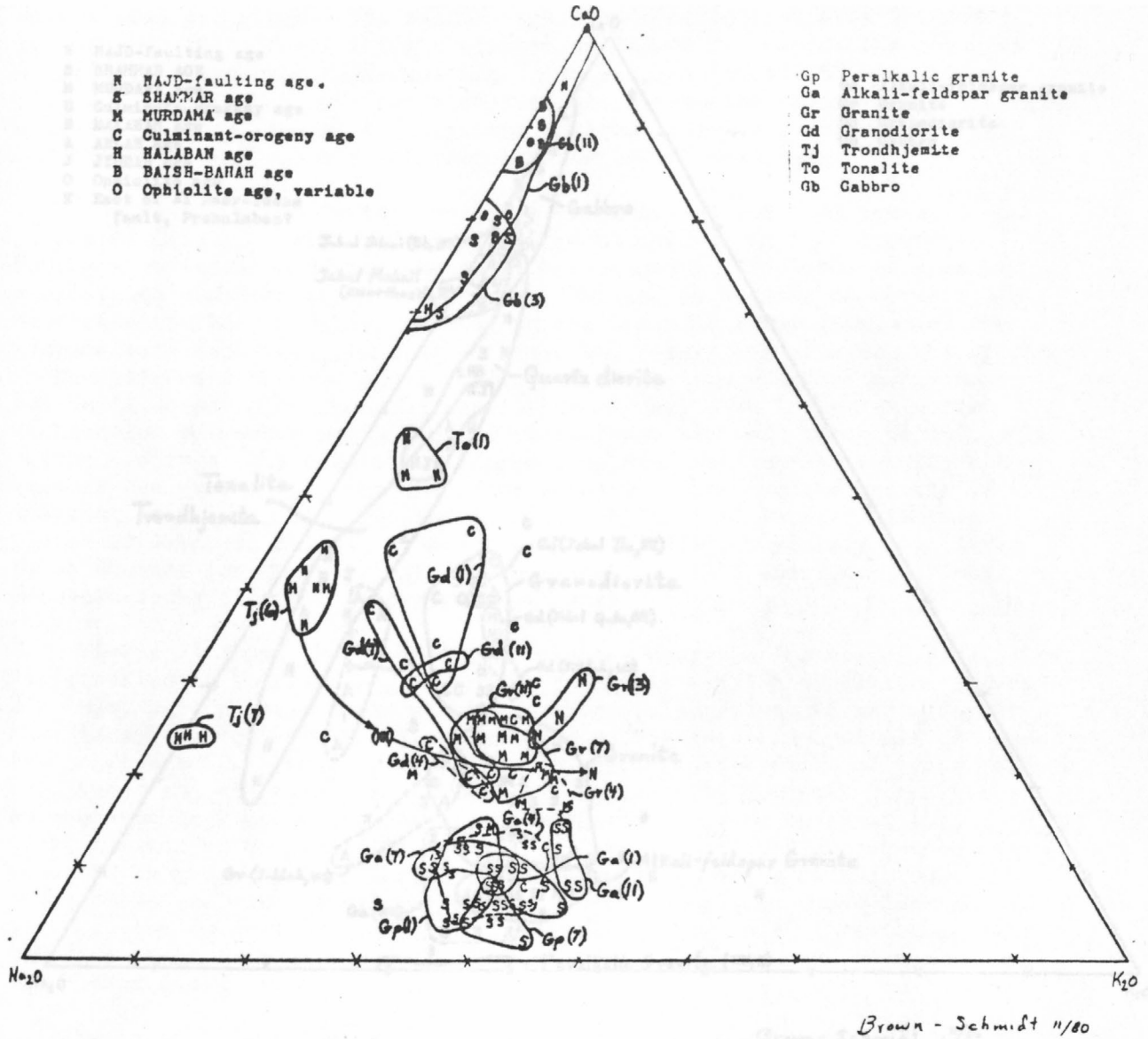

Figure 20. Na_2O-CaO-K_2O diagram showing plutonic-rock chemistry (molar data) of control samples classified by age. Lines enclose representative samples of different composition and age from specific areas (area numbers as on figure 17 in parentheses). The cluster of trondhjemite of Halaban age from area 6 (Tj(6)) consists of orthogeneiss containing migmatitic layers (HN) of mixed Halaban-age and Najd-age rock and granitic layers (N) of Najd age--samples(HN) and N are joined by arrowed tie lines showing compositional trend of migmatization.

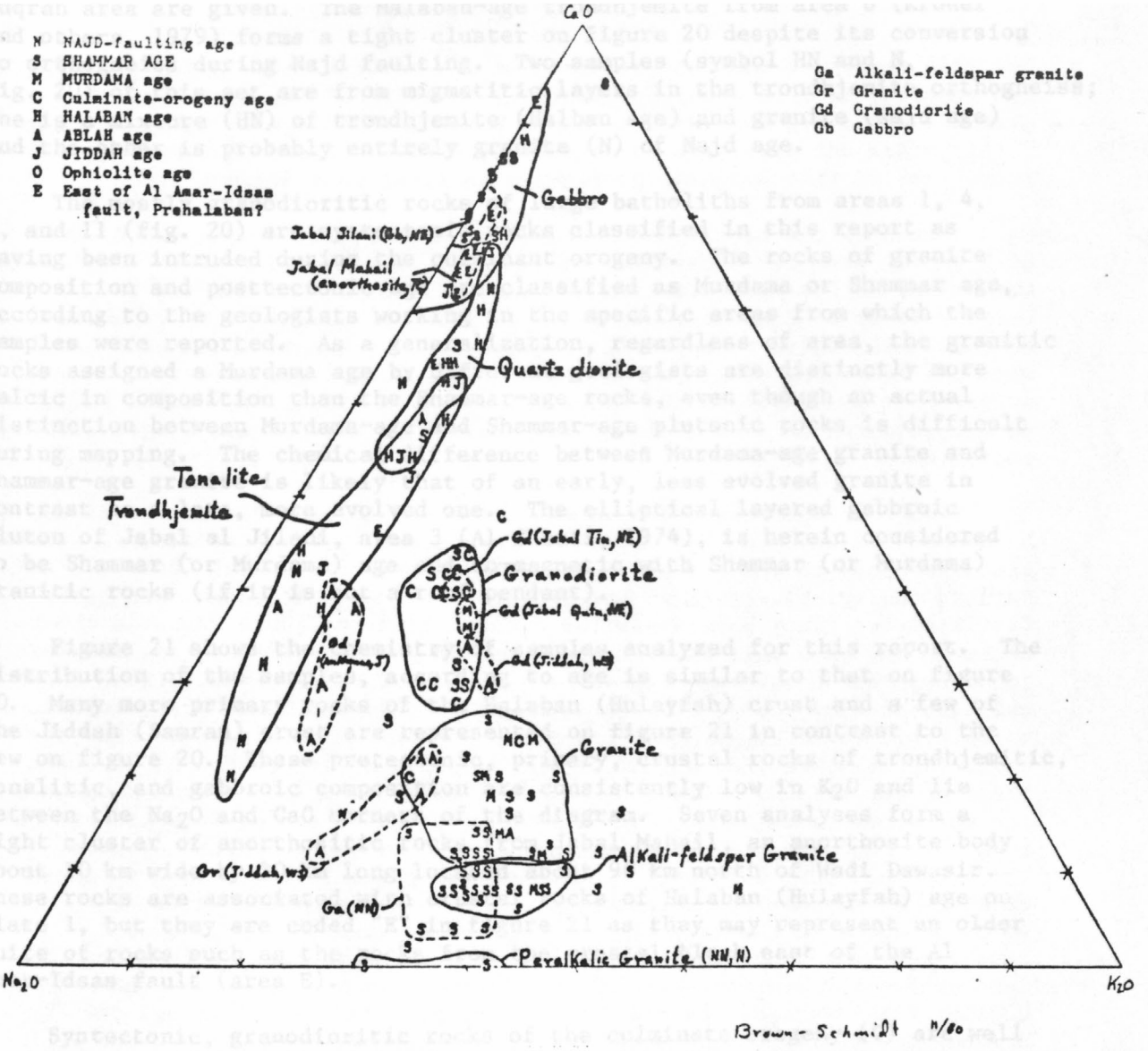

Figure 21. Na_2O–CaO–K_2O diagram showing plutonic-rock chemistry (molar data) of samples reported in tables 3 and 4 and classified by age. Lines enclose representative samples of different rock types. Samples from several specific localities (for region code see figure 17) are enclosed by dashed lines.

Nuqrah area are given. The Halaban-age trondhjemite from area 6 (Kroner and others, 1979) forms a tight cluster on figure 20 despite its conversion to orthogneiss during Najd faulting. Two samples (symbol HN and N, fig. 20) of this set are from migmatitic layers in the trondhjemite orthogneiss; one is a mixture (HN) of trondhjemite (Halban age) and granite (Najd age) and the other is probably entirely granite (N) of Najd age.

The mostly granodioritic rocks of large batholiths from areas 1, 4, 7, and 11 (fig. 20) are syntectonic rocks classified in this report as having been intruded during the culminant orogeny. The rocks of granite composition and posttectonic age are classified as Murdama or Shammar age, according to the geologists working in the specific areas from which the samples were reported. As a generalization, regardless of area, the granitic rocks assigned a Murdama age by different geologists are distinctly more calcic in composition than the Shammar-age rocks, even though an actual distinction between Murdama-age and Shammar-age plutonic rocks is difficult during mapping. The chemical difference between Murdama-age granite and Shammar-age granite is likely that of an early, less evolved granite in contrast to a late, more evolved one. The elliptical layered gabbroic pluton of Jabal al Jilani, area 3 (Al Shanti, 1974), is herein considered to be Shammar (or Murdama) age and co-magnetic with Shammar (or Murdama) granitic rocks (if it is not a roof pendant).

Figure 21 shows the chemistry of samples analyzed for this report. The distribution of the samples, according to age is similar to that on figure 20. Many more primary rocks of the Halaban (Hulayfah) crust and a few of the Jiddah (Samran) crust are represented on figure 21 in contrast to the few on figure 20. These pretectonic, primary, crustal rocks of trondhjemitic, tonalitic, and gabbroic composition are consistently low in K_2O and lie between the Na_2O and CaO corners of the diagram. Seven analyses form a tight cluster of anorthositic rocks from Jabal Mahail, an anorthosite body about 10 km wide by 30 km long located about 90 km north of Wadi Dawasir. These rocks are associated with crustal rocks of Halaban (Hulayfah) age on plate 1, but they are coded "E" in figure 21 as they may represent an older suite of rocks such as the rocks from the crustal block east of the Al Amar-Idsas fault (area E).

Syntectonic, granodioritic rocks of the culminate orogeny (C) are well represented on figure 21 as on figure 20. However, granodioritic rocks classified as Ablah age form a scatter of points that is distinctly more sodic than rocks associated with the culminate orogeny. These granodiorites are presumably associated with a post-Jiddah(Samran)-age orogeny of about Ablah age (Ablah-age orogeny). The lower K_2O content of both the volcanic and plutonic rocks of Ablah age suggests an earlier orogeny in a slightly more primitive, thinner, less cratonized crust than the crust at the time of the culminant orogeny.

The posttectonic plutonic granites of Murdama and Shammar age show a distribution similar to that of the control samples. The greater overlapping distribution of rocks of Murdama and Shammar age in figure 21 may result from greater subjectivity in the age classification of the analysed rocks

for this report in contrast to those of the control set. Only one Najd-age granitic rock is shown on figure 21 in spite of the fact that other granitic rocks are suggested to be of possible Najd age in table 3; field criteria are not available to adequately classify these youngest Precambrian rocks, and on this diagram, preference is given to a Shammar age.

Granodioritic batholithic rocks (samples 88, 89, 90A, and 90B) from the Ad Dawadimi area are classified as youngest Shammar age because they intrude the schist of the Abt formation as well as rocks of the Murdama group. Large volumes of granodioritic rocks as young as Shammar age are unusual in the Shield where batholithic granodioritic rocks are associated consistently with the culminant orogeny. We infer that youthful granodioritic as well as granitic plutonism in the large area west of the Al Amar-Idsas fault is an exception in an area of especially intensive and perhaps longer lasting tectonism.

Figure 22 summarizes the distribution of all plutonic rock analyses classified by age on the Na_2O-CaO-K_2O diagram. Consistently, the pretectonic, dioriticsuite plutonic rocks of the primary crusts of Baish-Bahah, Jiddah (Samran), and Halaban (Hulayfah) ages have low K_2O compositions that range from gabbro to trondhjemite; They have a similar distribution on figure 22 as do the volcanic rocks of the same ages on figures 18 and 19. These plutonic and volcanic rocks together constitute the primary crusts of Baish-Bahah, Jiddah (Samran), and Halaban (Hulayfah) ages. In general, the syntectonic, granodioritic batholithic rocks of the granitic-suite and of the culminant-orogeny age form a distinct cluster that signifies the first abundance of K_2O in plutonic rocks of the shield; equivalent volcanic rocks of the culminant-orogeny age are sparse or nonexistent (fig. 18C). On a lesser scale, some granodioritic rocks of Ablah age did precede the K_2O rocks of the culminant orogeny. The youthful, post-tectonic, granitic-suite plutonic rocks form distinct clusters of Murdama and Shammar age. A comparable distribution of volcanic rocks of the same ages is seen on figures 18C and 19. The alkali-feldspar granites form a tight cluster exclusively within the Shammar-age field. The peralkalic granites form a similarly tight cluster that overlaps the alkali-feldspar granite cluster within the Shammar-age field. These peralkalic granite rocks from areas 1 and 7 are representative of a broad belt of peralkalic granite plutons that parallels the Hulayfah-Ad Dafinah-Nabitah-Hamdah serpentinite fault zone. Many of the alkalic and peralkalic granite plutons of the shield (Stoeser and Elliott, 1980) are associated with this zone of tectonic ophiolite (Frisch and Al-Shanti, 1977; Delfour, 1979; Schmidt and others, 1979b).

The Shammar-age magmatism was bimodal and a distinct cluster of Shammar-age gabbro occurs in the gabbroic field of the diagram (fig. 22). These Shammar gabbros are from concentrically layered plutons that are associated in age with the widespread circular granitic plutons of the shield. The few analyses of Najd-age granite form a distinctive high-K_2O cluster on figure 22.

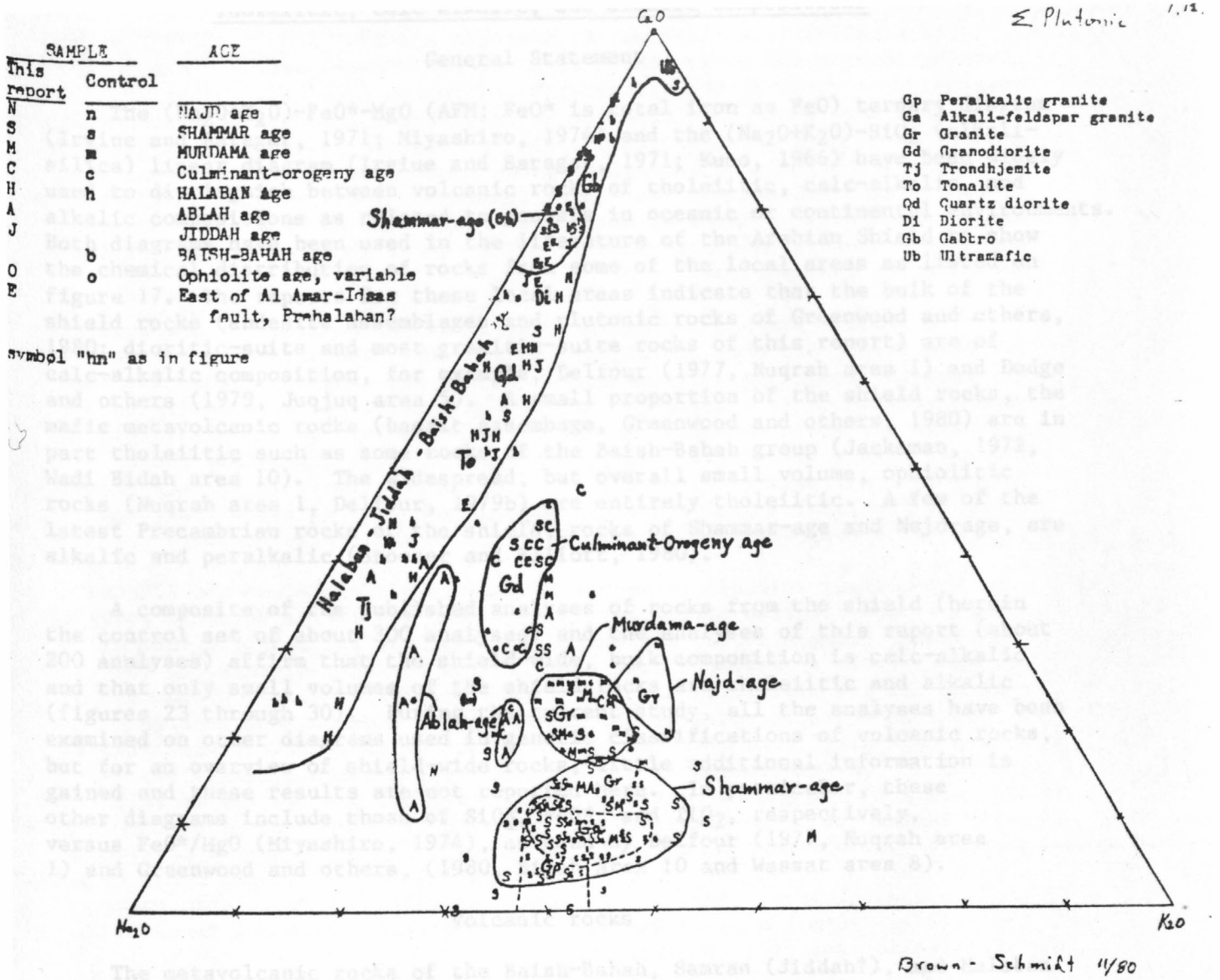

Figure 22. Na_2O–CaO–K_2O diagram summarizing all the plutonic-rock chemistry (molar data) examined in this report (combination of figures 20 and 21). Each sample is classified according to an assigned age. Solid lines enclose clusters of different age. Dashed lines enclose tight clusters of plutonic rocks of alkali-feldspar granite (Ga) and peralkalic granite (Gp) compositions within the sample cluster of Shammar age.

Tholeiitic, calc-alkalic, and alkalic compositions

General Statement

The (Na_2O+K_2O)-FeO*-MgO (AFM; FeO* is total iron as FeO) ternary diagram (Irvine and Baragar, 1971; Miyashiro, 1974) and the (Na_2O+K_2O)-SiO_2 (alkali-silica) linear diagram (Irvine and Baragar, 1971; Kuno, 1966) have been widely used to distinguish between volcanic rocks of tholeiitic, calc-alkalic, and alkalic compositions as related to genesis in oceanic or continental environments. Both diagrams have been used in the literature of the Arabian Shield to show the chemical distribution of rocks from some of the local areas as listed on figure 17. The reports for these local areas indicate that the bulk of the shield rocks (andesite assemblages and plutonic rocks of Greenwood and others, 1980; dioritic-suite and most granitic-suite rocks of this report) are of calc-alkalic composition, for example, Delfour (1977, Nuqrah area 1) and Dodge and others (1979, Juqjuq area 5). A small proportion of the shield rocks, the mafic metavolcanic rocks (basalt assembage, Greenwood and others, 1980) are in part tholeiitic such as some rocks of the Baish-Bahah group (Jackaman, 1972, Wadi Bidah area 10). The widespread, but overall small volume, ophiolitic rocks (Nuqrah area 1, Delfour, 1979b) are entirely tholeiitic. A few of the latest Precambrian rocks of the shield, rocks of Shammar-age and Najd-age, are alkalic and peralkalic (Stoeser and Elliott, 1980).

A composite of the published analyses of rocks from the shield (herein the control set of about 300 analyses) and the analyses of this report (about 200 analyses) affirm that the shield-wide, bulk composition is calc-alkalic and that only small volumes of the shield rocks are tholeiitic and alkalic (figures 23 through 30). During the current study, all the analyses have been examined on other diagrams used in genetic classifications of volcanic rocks, but for an overview of shield-wide rocks, little additional information is gained and these results are not reported here. In particular, these other diagrams include those of SiO_2, FeO*, and TiO_2, respectively, versus FeO*/MgO (Miyashiro, 1974), as used by Delfour (1977, Nuqrah area 1) and Greenwood and others, (1980, Bidah area 10 and Wassat area 8).

Volcanic rocks

The metavolcanic rocks of the Baish-Bahah, Samran (Jiddah?), and Halaban (Hulayfah) groups for the control data on the AFM diagram are shown in figure 23. The chemical distribution scatters widely within the calc-alkalic field (Irvine and Baragar, 1971) but is confined within the outer bounds of the composition of the calc-alkalic rocks of the Cascade Mountains (USA; outer dotted line, fig. 23). These metavolcanic rocks of the andesite and basaltic assemblages completely overlap in distribution and all range well into the tholeiitic field on the basalt side of the diagram. The only within-group stratigraphic data available are for the Hulayfah (Halaban) rocks where chemistry for upper and lower units are reported (Delfour, 1977). However, the upper Halayfah (Hulayfah) rocks consistently straddle the tholeiitic-calc-alkalic line, whereas the lower rocks consistently lie below the line on the calc-alkalic side. This is the opposite that would be expected and we wonder, because of structural complications, whether these rocks can be mapped stratigraphically in the field.

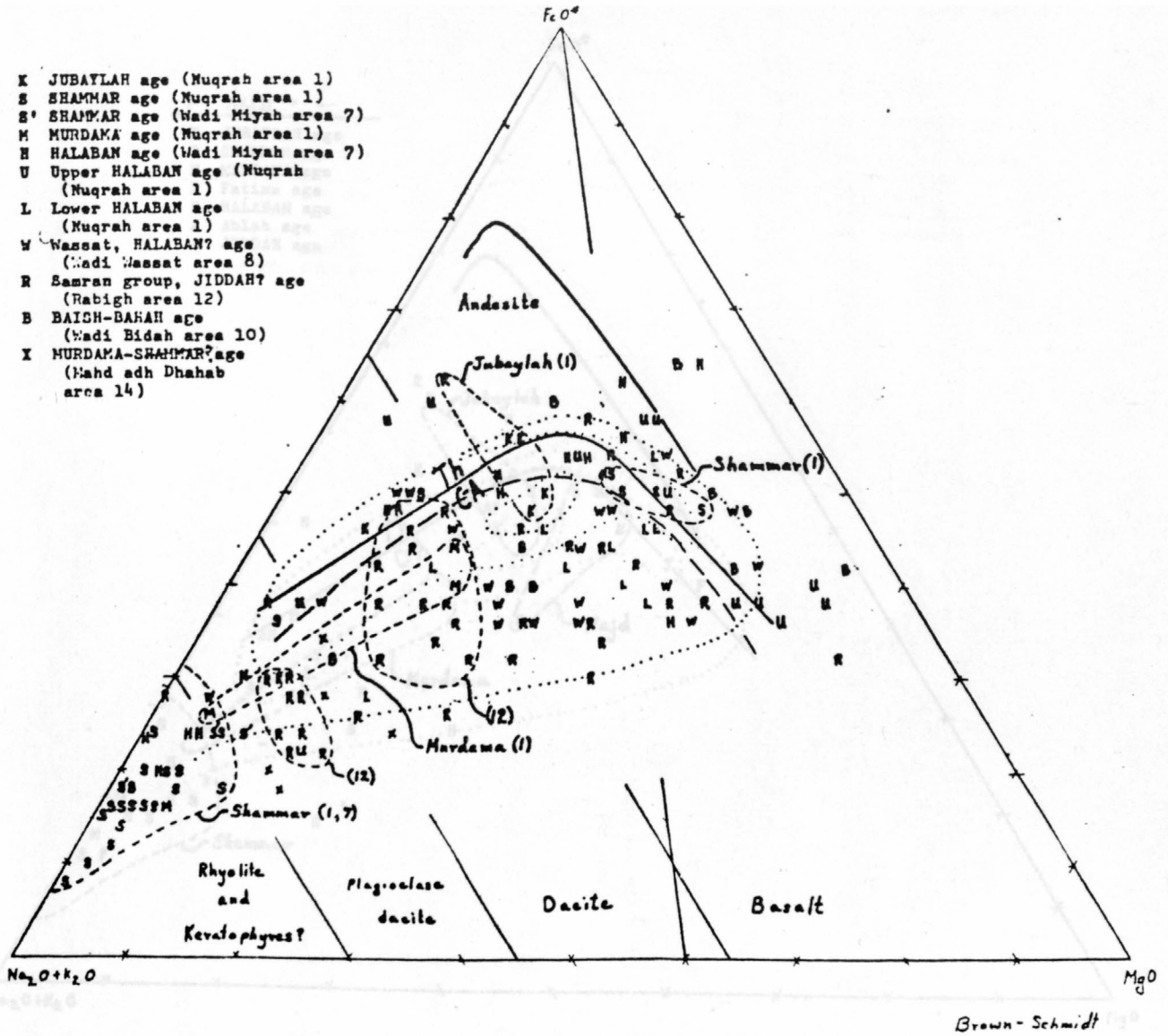

Figure 23. AFM diagram showing metavolcanic-rock chemistry (weight percent data) or control samples classified by age. Samples are from local areas shown on figure 17. Lower solid line separates tholeiitic compositions (above line) and calc-alkalic compositions (below line) according to Irvine and Baragar (1971, p. 528); Upper solid line is the Skaergaard liquid trend. Two inner dotted lines are approximate contours drawn on plotted data of calc-alkalic volcanic rocks from the Aleutians (Irvine and Baragar, 1971, p. 528). Outer dotted line encloses calc-alkalic volcanic rocks from the Cascade Mountains (Irvine and Baragar, 1971, p. 528). Long dashed line separates upper-Hulayfah-group rocks (upper Halaban; above line) from lower-Halayfah-group rocks (lower Halaban; below line) from Nuqrah area 1. Short dashed lines enclose some specific age-area sets as labeled. Rock-type classification approximate is shown by diagonal lines intersecting the sides of the diagram.

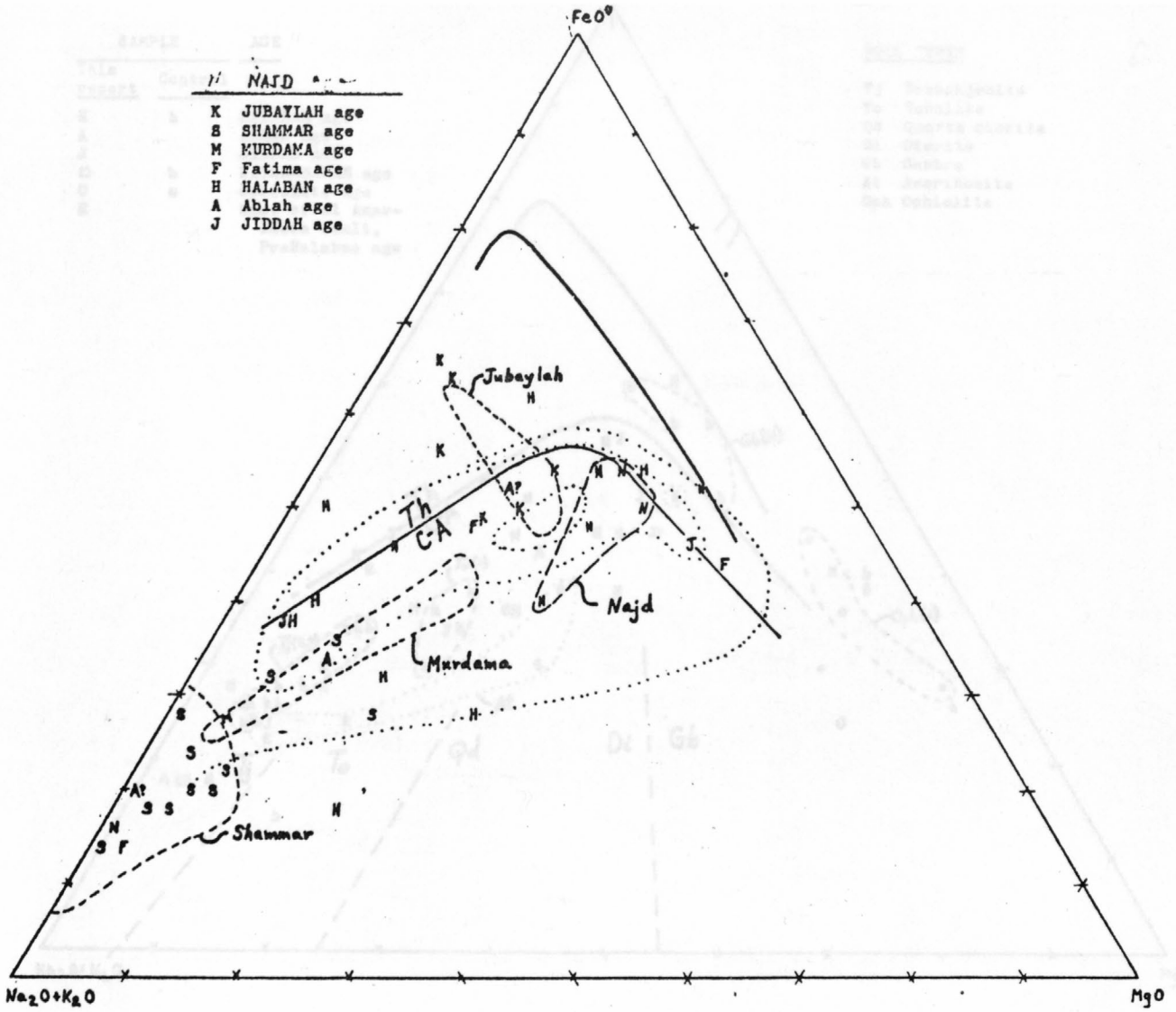

Figure 24. AFM diagram showing chemical (weight percent data) distribution of metavolcanic rocks and a few dike rocks reported in tables 3 and 4. Solid and dotted lines are as in figure 23. Long dashed line encloses andesitic and diabasic rocks in dikes and small plug intrusions associated with Najd faulting.

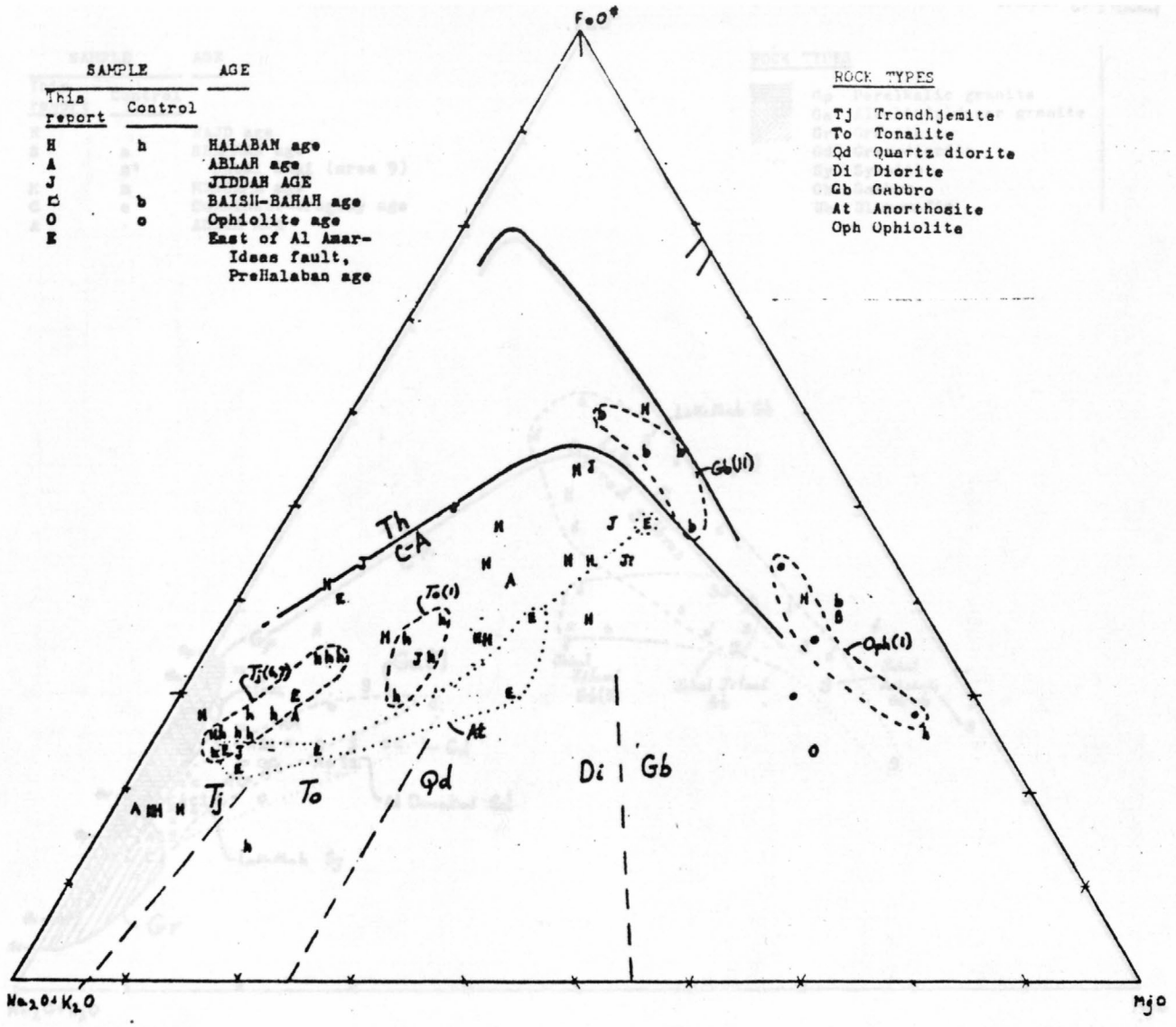

Figure 25. AFM diagram showing chemical (weight percent data) distribution of rocks of the diorite suite from the Saudi Arabian Shield. Analyses are classified by age; lower case symbols are from control analyses; upper case symbols are from analyses of this report. Lower solid line separates tholeiitic (Th) and calc-alkalic compositions (C-A) according to Irvine and Baragar (1971, p. 528); upper solid line is the Skaergaard liquid trend. Short dashed lines enclose specific control samples giving rock type and source area (in parentheses; see figure 17). Dotted line encloses anorthositic rocks (sample locality 167, table 3). Long dashed lines approximately divide diagram into principal rock types of the diorite suite.

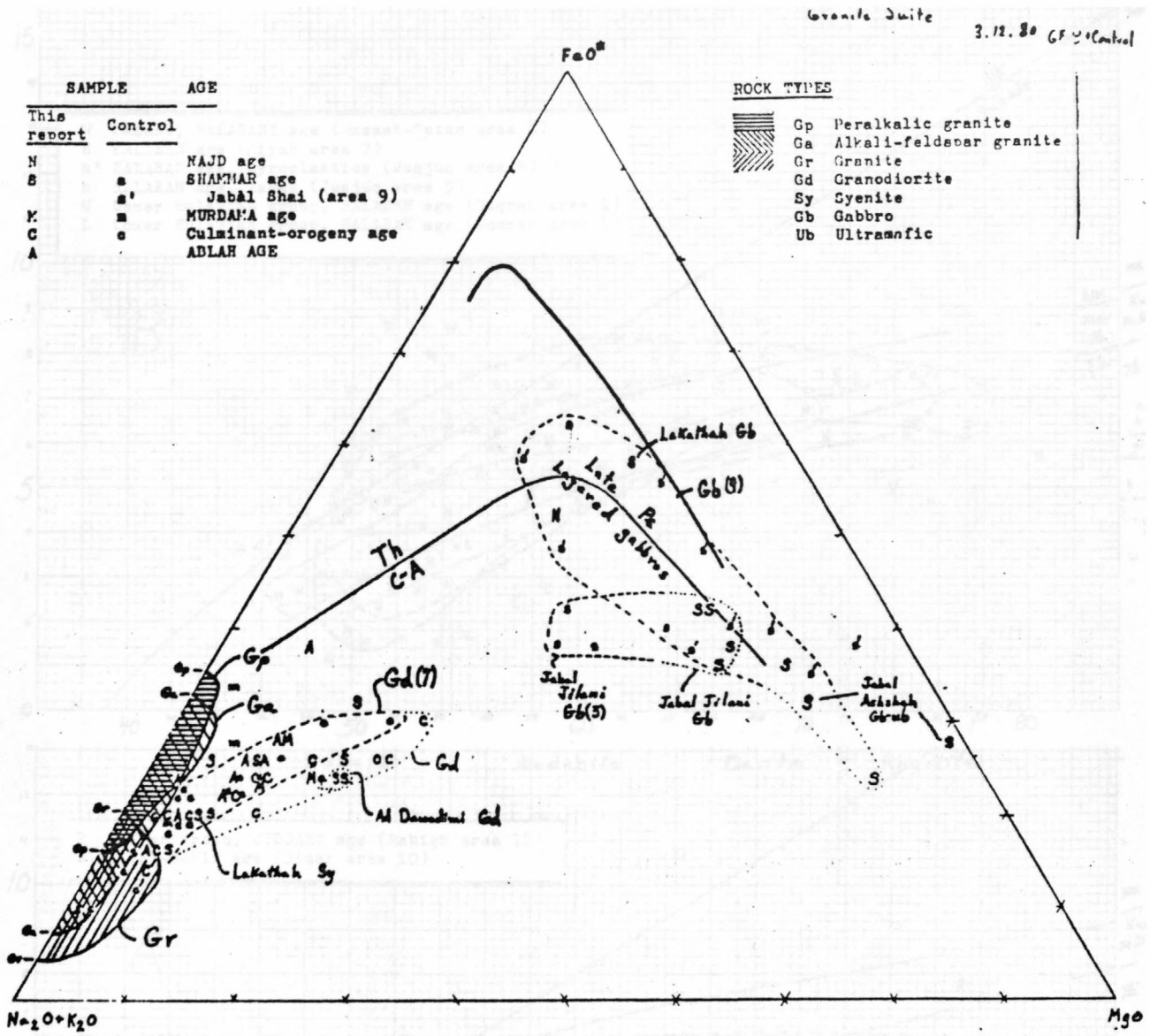

Figure 26. AFM diagram showing chemical (weight percent data) distribution of rocks of the granite suite from the Saudi Arabian Shield. Analyses are classified by age; lower case symbols are from control analyses; upper case symbols are from analyses of this report. Solid lines are as in figure 25. Short dashed lines enclose specific sets of control samples giving rock type and source area (in parentheses; see fig. 17). Dotted lines enclose specific sample sets of this report.

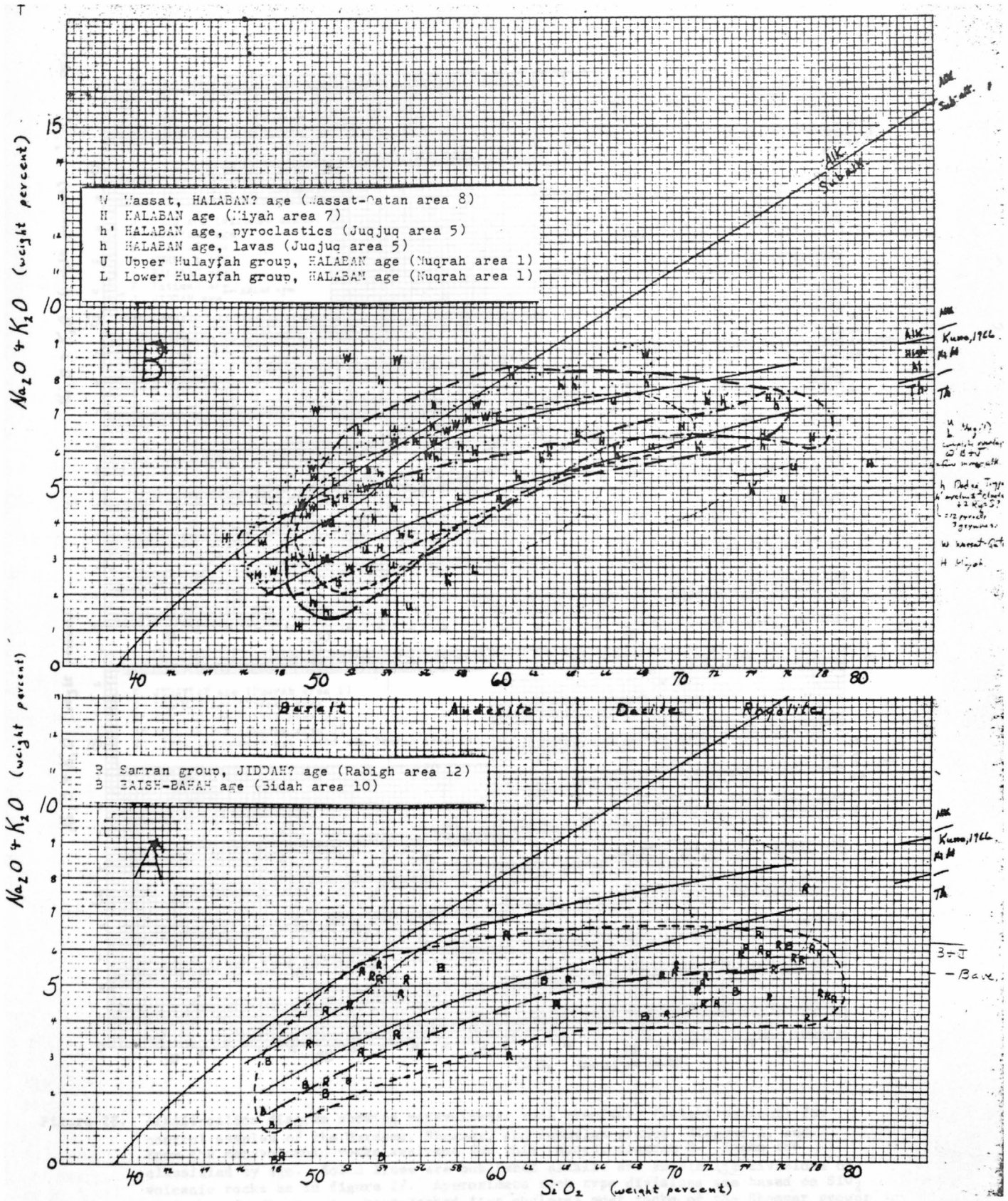

Figure 27. Alkali-silica diagram showing metavolcanic rock chemistry (weight percent) for control samples of the Baish-Bahah and Jiddah basalt according to Kuno (1966). Approximate rock-type divisions are groups, diagram A, and of the Halaban group, diagram B. Rocks are classified by age. Upper solid line divides alkaline and subalkaline fields for Hawaiian data (Irvine and Baragar, 1971) and two lower solid lines divide tholeiite, high-alumina basalt, and alkali olivine based on SiO_2 content. In diagram A, long-dashed line shows trend of Baish-Bahah rocks, and short-dashed line encloses total distribution of Baish-Bahah and Jiddah rock. In diagram B, long-dashed line encloses most Halaban rocks of the Juqjuq area 5; short-dashed line encloses most Halaban rocks of the Nuqrah area 1; dash-dot line encloses most Halaban rocks of the Miyah area 7; and dotted line encloses most Halaban rocks of the Wassat area 8.

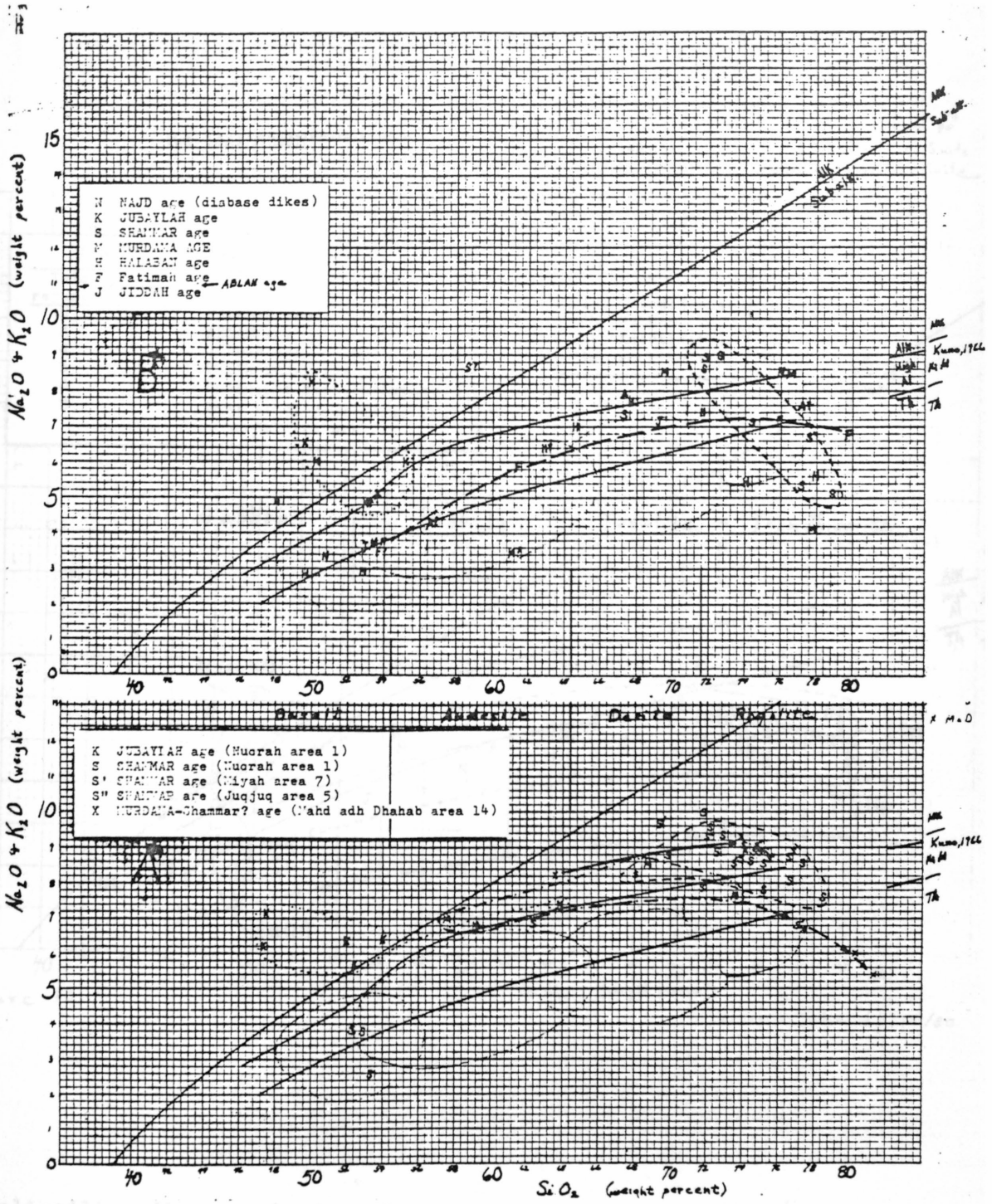

Figure 28. Alkali-silica diagram showing metavolcanic rock chemistry (weight percent) for control samples of the Murdama, Shammar, and Jubaylah groups, diagram A, and from the metavolcanic rocks analyzed for this report, diagram B. Rocks are classified by age. Solid lines are published alkalic and subalkalic divisions of volcanic rocks as in figure 27. Approximate rock type divisions are based on SiO_2 content. In diagram A, short-dashed line encloses most rocks of the Shammar group; dash-dot line encloses rocks of the Murdama group; and dotted line encloses rocks of the Jubaylah group. Solid arrow suggests direction of intense hydrothermal alteration of "rhyolite porphyry" in dikes and a plug in the Madh adh Dhahab area 13 and dashed arrow for pyroclastic rocks of the same area. In diagram B, short-dashed line encloses rocks of the Shammar group; long-dashed line shows trend of rocks of the Fatimah group, and dotted line encloses rocks of the Jubaylah group.

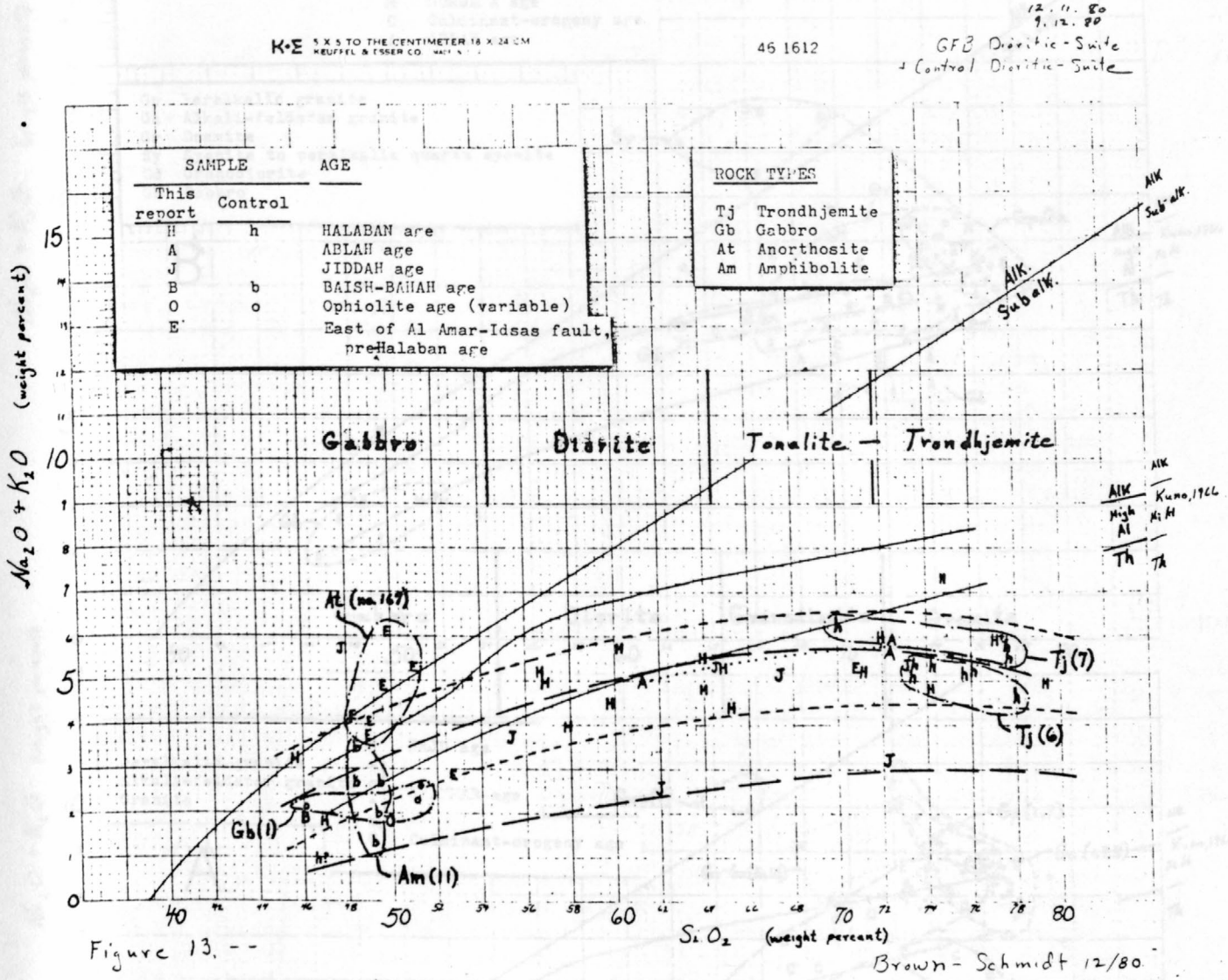

Figure 13. --

Figure 29. Alkali-silica diagram showing plutonic rock chemistry (weight percent data) of dioritic suite for samples of this report and of control set. Rocks are classified by age. Solid lines are alkalicsubalkalic divisions from the literature for volcanic rocks as in figure 27. Approximate rock-type divisions are based on SiO_2 content. Long-dashed lines enclose Baish-Bahah-age and Jiddah-age rocks. Short-dashed lines enclose Halaban-age rocks. Dotted line connects rocks of Ablah age from the An Nimas batholith. Dash-dot lines enclose sample sets from specific areas (area numbers in parentheses from fig. 17; "no. 167" from table 3).

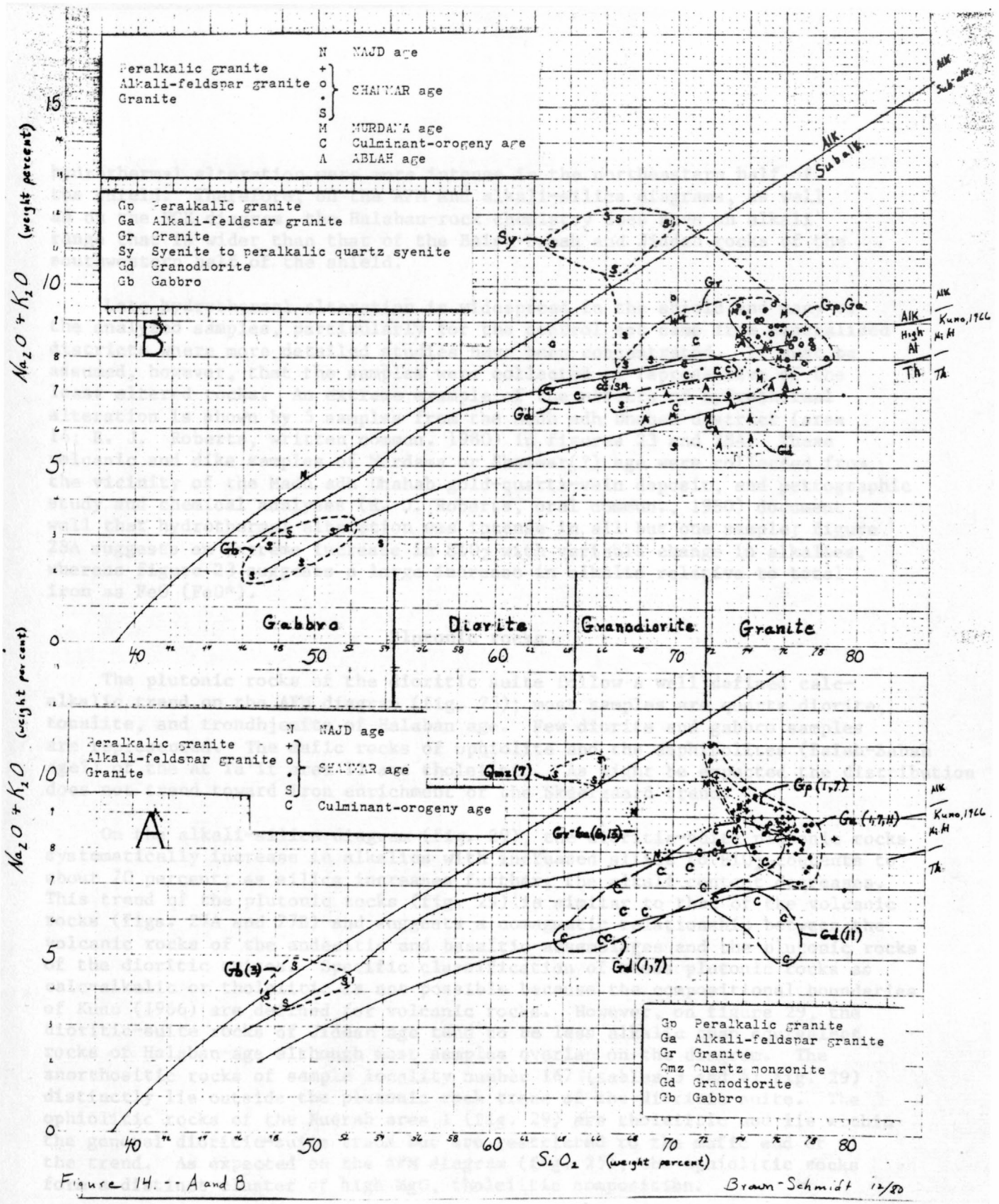

Figure 14. -- A and B

Figure 30. Alkali-silica diagram showing plutonic rockchemistry (weight percent data) of granitic suite; diagram A for samples of control set and diagram B for samples of this report. Rocks are classified by age. Solid lines are alkalic-subalkalic divisions from the literature for volcanic rocks as in figure 27. Approximate rock-type divisions are based on SiO^2 content. In diagram A, lines enclose control samples from specific areas (area numbers in parentheses from fig. 17); longdashed lines enclose Shammar-age rocks of different compositions; and dotted line encloses Najd-age granitic rocks. In diagram B, lines enclose samples of this report of different composition and age; longdashed line encloses rocks of culminant-orogeny age; short-dashed lines enclose various rock compositions of Shammar age; and dotted line encloses rocks of Ablah age.

The alkali-silica diagrams, figures 27A and 27B, show a similar wide distribution for the metavolcanic rocks of the control set. On these two diagrams, the rocks of the Baish-Bahah and Samran (Jiddah?) groups are distinctly more tholeiitic than the rocks of the Halaban group, but overlap of some rocks of each group provides a nearly complete intermixing of the data. The rocks of the Halaban (Hulayfah) group range from tholeiitic to alkalic by Kuno's classification. The Wassat (Halaban?) rocks in particular tend to to be more alkalic. Rocks of all three groups tend to separate into more tholeiitic clusters and more alkalic clusters for those rocks of andesitic and basaltic compositions.

The Jiddah (Samran) and Halaban (Hulayfah) metavolcanic rocks analyzed for this report are shown on figures 24 and 28B. The data show a wide distribution in the calc-alkalic field on the AFM diagram, figure 24; the wide distribution is similar to that of the control-set data on figure 23, even with the small number of data points available. On the alkali-silica diagram, figure 28B, the Jiddah (Samran) and Halaban (Hulayfah) rocks mostly form a linear array of calc-alkalic composition. These metavolcanic rocks of the basaltic and andesitic assemblages have an overall average calc-alkalic composition that extends into the tholeiitic field.

The younger volcanic rocks are distinctly segregated on the AFM and alkali-silica diagrams (figs. 23, 24, 28A, and 28B). The volcanic rocks of the Shammar group are well segregated as rhyolites for both the control set and for the analyses of this report. The Shammar volcanics of the control set are distinctly alkalic by Kuno's classification on figure 28A. A few mafic volcanic rocks of the Shammar group from the Nuqrah area 1 make a calc-alkalic cluster that trends into the tholeiitic field (fig. 23 and 23A). The few samples of the Murdama group available (figs. 23, 24, 28A, and 28B) are mostly calc-alkalic dacites, but are too few to satisfactorily define the trend suggested on figures 23 and 28A. Rocks of the Jubaylah group of both the control set and the set of this report make a distinctive cluster that stradles the tholeiitic and calc-alkalic line for mafic to intermediate compositions (figs. 23, 24, 28A, and 28B). Diabasic dike rocks of the Najd age form a cluster mostly on the tholeiitic line but range to calc-alkalic compositions (fig. 24).

Limited data for metavolcanic rocks of the Ablah and Fatimah groups are available only for analyses of this report (figs. 24 and 28B). On figure 28B, the few Fatimah rocks form a distinct calc-alkalic trend ranging from andesitic to rhyolite composition and the few Ablah rocks tend to follow a similar trend.

The effects of alteration, such as spilitization, non-isochemical metamorphism, and late hydrothermal alteration, are little known for the metavolcanic rocks herein studied. Increase in Na_2O caused by spilitization may be expected for particularly the rocks of the Baish-Bahah group (basaltic assemblage), and mobility of Na_2O may be expected during the widespread greenschist metamorphism. Such alteration of the alkali content in the rocks of the basaltic and andesitic assemblages may account for some of the spread of the analyses across the alkalic to tholeiitic fields on the AFM and alkalies-silica diagrams (figs. 23, 24, 27A, and 27B). As described above, alkalic alteration may be expected to be more intense in the Halaban metavolcanic rocks because late granitic intrusion and late

hydrothermal alteration were more intense in the northeastern half of the shield. Therefore, on the AFM and alkali-silica diagrams, as well as on the NCK diagram, the Halaban-rock chemistry does have an alkali range that is wider than that of the Baish-Bahah and Jiddah rocks of the southwestern half of the shield.

Late hydrothermal alteration is widespread in the shield and many of the analyzed samples, particularly for the control set came from mineralized districts where more detailed studies have been concentrated. It must be assumed, however, that the samples were collected as representive of the least altered rocks. An extreme example of the effects of hydrothermal alteration is shown by 5 samples from the Madh adh Dhahab district (area 14; R. J. Roberts, written commun. 1980) in figures 23 and 28A. These volcanic and dike samples of Murdama or Shammar(?) age were collected from the vicinity of the Madh adh Dhahab gold-quartz-vein deposit, and petrographic study and chemical analyses (R. J. Roberts, oral commun., 1980) document well that hydrothermal alteration was intense in all but one sample; figure 28A suggests an extreme increase in SiO_2 with variable change in alkalies, whereas figure 23 suggests a large increase in alkalis relative to total iron as FeO (FeO*).

Plutonic rocks

The plutonic rocks of the dioritic suite follow a well defined calc-alkalic trend on the AFM diagram (fig. 25); most samples are quartz diorite, tonalite, and trondhjemite of Halaban age. Few diorite and gabbro samples are represented. The mafic rocks of ophiolite and the amphibolites (Baish-Bahah age?) of the At Ta'if area 11 are tholeiitic. As might be expected the distribution does not trend toward iron enrichment of the Skaergaard trend.

On the alkali-silica diagram (fig. 29), the dioritic-suite plutonic rocks systematically increase in alkalies with increased silica to SiO_2 contents to about 70 percent; as silica increases further, the alkali content decreases. This trend of the plutonic rocks (fig. 29) is similar to that of the volcanic rocks (figs. 27A and 27B) and suggests a comagmatic relationship between the volcanic rocks of the andesitic and basaltic assemblages and the plutonic rocks of the dioritic suites. Specific classification of these plutonic rocks as calc-alkalic or tholeiitic is not possible because the compositional boundaries of Kuno (1966) are defined for volcanic rocks. However, on figure 29, the dioritic-suite rocks of Jiddah age tend to be less alkalic than equivalent rocks of Halaban-age although most samples overlap on the diagram. The anorthositic rocks of sample locality number 167 (tables 3 and 4; fig. 29) distinctly lie outside the plutonic rock trend of the dioritic suite. The ophiolitic rocks of the Nuqrah area 1 (fig. 29) are tholeiitic and lie within the general dioritic-suite trend but are restricted to the mafic end of the trend. As expected on the AFM diagram (fig. 25), the ophiolitic rocks form a distinct cluster of high MgO, tholeiitic composition.

The plutonic rocks of the granitic suite are distinctly bimodal in composition on figures 26, 30A, and 30B. The gabbroic rocks, characteristic of the small, circular, layered plutons of youthful Precambrian (Shammar) age, tend toward distinct iron enrichment but much less so than on the Skaergaard trend. On the alkali-silica diagrams (figs. 30A and 30B), the

Shammar gabbros spread across the alkalic to tholeiitic fields of volcanic classifications of Kuno (1966) and Irvine and Barager (1971). The granodiorite and granite rocks of culminant-orogeny age and Shammar age follow a broken calc-alkalic trend that is considerably enriched in total alkalies (figs. 26, 30A, and 30B) relative to the trend of the dioritic-suite rocks on similar diagrams (figs. 25 and 29). The late alkali-feldspar granite and peralkalic granite samples follow a distinctly different trend of total iron enrichment (fig. 26) and of alkali enrichment (fig. 30A and 30B).

The few analyses of Ablah plutonic rocks, mostly granodiorite and granite, follow the calc-alkalic trend of the culminant-orogeny age on the AFM diagram (fig. 26), but are distinctly less alkalic than the rocks of culminant orogeny age on the alkali-silica diagram (fig. 30B). The low total-alkalic content of the Ablah rocks is caused by a low K_2O content that is much lower than in younger granodiorite and granite rocks from elsewhere in the shield; this, in general, is characteristic of the early, precratonization granitic rocks of the western part of the shield. This is more strikingly so, if the control set of granodioritic gneisses from the At Tā'if area (Gd, area 11) of the western shield on figure 30A is considered to be Ablah age rather than of culminant-orogeny age; we have no age data that disputes such a reclassification of these rocks. The distinctive alkalic cluster of syenitic and quartz monzonitic rocks on figures 30A and 30B are common, but not abundant, for rocks of Shammar age from widely separated parts of the shield. They suggest a trimodal distribution for plutonic rocks of Shammar age.

Discussion of chemistry

The chemical variation of the volcanic and plutonic rocks of the Saudi Arabian Shield has been examined regionally by Greenwood and Brown (1973), Greenwood and others (1976), Greenwood and others (1980), and Delfour (1979b) and locally by Jackaman (1972), Delfour (1977), Al Shanti (1974 and 1976), Kanaan (1979), Dodge and others (1979), Nasseef and Gass (1977), Skiba (1980), and others. This report contributes the fact that the chemical evolution of these rocks is systematic with age in any given region and is similar for different regions throughout the entire Shield regardless of age. The chemical data presented above, as well as this discussion of the chemistry, has been summarized in a review paper by Schmidt and Brown (1982).

The major-element chemistry is readily divisible into major categories of age (stratigraphy) that are related directly to the chemical evolution and systematic genesis of the shield. The chemical evolutionary trend for the metavolcanic rocks is summarized on the NCK diagram, figure 19, and for the plutonic rocks on figure 22. The evolutionary trend fits especially well two major categories of crustal development: 1) a primary crust of early, multiple, intraoceanic island-arcs broadly categorized agewise (stratigraphically) as Baish-Bahah, Jiddah, and Halaban; and 2) late cratonization crust categorized agewise (stratigraphically and structurally) as the culminant orogeny, Murdama-Shammar, and Jubaylah-Najd. The chemistry of the early crustal rocks of different ages (Baish-Bahah, Jiddah, and Halaban) is similar regardless of age and is not distinctly subdivided within itself. The chemistry of the late cratonization rocks is more distinctly and readily subdivided within itself.

The primary crust (that is, the first or early crust) of the shield is composed of calc-alkalic metavolcanic rocks and equivalent calc-alkalic plutonic rocks. Most of the metavolcanic rocks are classified as an andesitic assemblage that ranges in composition from basalt to sodic dacite but whose calc-alkalic composition varies little areally or age-wise across the shield. The abundant plutonic rocks are classified in a dioritic suite that ranges in composition from gabbro to trondhjemite and again whose calc-alkalic composition varies little with area or age across the shield. Calc-alkalic volcanic and plutonic rocks of such large volume as is found in the Arabian Shield are characteristic of volcanic-magmatic arcs and might be expected to have more mafic and tholeiitic compositions in their early, immature stages of development and more silicic and calc-alkalic compositions in their later, more mature stages of development (Miyashiro, 1974). This is suggested in the chemical data of the major elements (figs. 27A, 27B, 29, 23, and 25). However, the Arabian Shield is tectonically complex and deeply eroded, and to date, distinctively immature and mature parts of individual volcanic-magmatic arcs have only been proposed and suggested; more detailed mapping, chemistry, and dating is needed. The sparse age data allow divisions into large regions of primary crustal rocks that have been designated as Baish-Bahah, Jiddah, and Halaban ages, but these large regions are in themselves far too large and complex to encompass single volcanic-magmatic arcs. It is likely that each age group actually encompasses several independent arcs that have been collisionally combined at different stages of shield development.

The chemistry of the metavolcanic rocks of the Baish-Bahah, Jiddah, and Halaban groups, each, does contain some tholeiitic rocks (figs. 27A, 27B, and 28B). A slight chemical discrimination toward a more tholeiitic composition for the metavolcanic rocks of the Baish-Bahah group as compared to the Jiddah group can be seen on figure 27A, and a slight discrimination toward a less calc-alkalic composition can be seen for the Baish-Bahah and Jiddah groups as compared to the Halaban group (figs. 27A and 27B). However, sampling is localized and limited in amount considering the tectonic complexity of the shield, and the older age and deeper erosion of the Baish-Bahah and Jiddah rocks may simply mean that more rocks of an immature, lower part of the Baish-Bahah and Jiddah have been sampled in comparison to the Halaban. Also, the Halaban rocks of the eastern part of the shield have been much more intruded by young granitic rocks and may have been subjected to more alteration subsequent to their emplacement.

Syntectonic plutonic rocks of the granitic suite of culminant-orogeny age mostly form large granodioritic batholiths of calc-alkalic composition (figs. 26, 30A and 30B). Within their calc-alkalic composition, these rocks are distinctly more alkalic than are plutonic rocks of similar SiO_2 content of the dioritic suite (figs. 25 and 29). Volcanic equivalents of these syntectonic plutonic rocks have not been recognized in the field, although the few analyses of volcanic rocks of the Murdama group are chemically similar to the granodiorite of the culminant-orogeny age. In general, the Murdama-age volcanic rocks in their association with molassic sedimentary rocks are classified as post-tectonic and early Shammar equivalents, but a sharp distinction between late syntectonic and posttectonic ages of molassic sedimentary rocks cannot be made, especially because this age boundary probably varies slightly from region to region across the shield.

The plutonic rocks of culminant-orogeny age, are deep-seated rocks commonly spacial associated with the orthogneisses of large gneiss domes (antiforms), and it seems likely that little magma was erupted at the paleosurface at that time. This syntectonic granodiorite formed during tectonic thickening of the shield when the shield in many places was hot enough and thick enough for some old trondhjemitic and tonalitic masses to rise gravitationally as gneiss domes. The thickened crust seems related definitely to this first appearance of large volumes of potassic magma within the shield.

The potassic magmatism continued in a posttectonic cratonic environment as represented by the plutonic, granitic-suite rocks of Shammar-age and their volcanic equivalents of the Shammar group. These plutonic and volcanic rocks have a distinctive major-element chemistry that is bimodal in granite-rhyolite and gabbro-basalt (figs. 23, 26, 28A, and 28). Their chemistry is distinctly more potassic than that of the plutonic and volcanic rocks of the dioritic suite and the andesite assemblage. The Shammar rocks formed from calc-alkalic magmas that in part evolved to alkalic magmas (figs. 28 and 30A).

Synorogenic potassic volcanic and plutonic rocks that are older than the culminant-orogeny are those of the Ablah and Fatimah groups from the southwestern shield regions (J, B, and WS, fig. 17). These rocks are distinctly much less potassic than the later culminant-orogeny rocks and are examplified by the An Nimas batholith and the batholith rocks of the Jiddah-Makkah area. The Ablah rocks seem related to an earlier orogeny in a restricted part of the shield that had a thinner, less mature crust than that associated with the later, shield-wide culminant orogeny. On the basis of chemistry, the Fatimah rocks of the Jiddah-Makkah area (region WS, fig. 17) are similar to the Ablah rocks and formed in a similar crustal environment, but on a different crustal block and perhaps at a different time.

These ages represent events in the Pan African orogeny. Older hornblende ages, 710-778 Ma, are from calc-alkaline syngenetic, generally gneissic, quartz monzonite, granodiorite, and granite bodies which are usually exposed in domes. Ages in the span 805-932 Ma were obtained mostly from diorite, quartz diorite, and granodiorite plutons exposed in the scarps and foothills east of the Red Sea and in the southern part of the Arabian Shield.

The Jubaylah-group volcanic rocks form a distinctive assemblage of mafic to intermediate rocks that range from calc-alkalic to alkalic in composition (figs. 28A and 28B). They are the youngest rocks of the Precambrian Shield and their composition is suggestive of the magmatism of a continental rift system. However, no characteristic rift existed at this Najd faulting time. The Jubaylah volcanic rocks erupted during the compressional, transcurrent faulting of Najd age (Moore, 1979), but they erupted only in restricted, tensional parts of the large-displacement, sinuous faults in the complex Najd fault system.

Granite of Najd age is penecontemporaneous and bimodal with Jubaylah volcanic rocks (fig. 30A). The Najd-age granite is exposed in the Najd fault zones at different places than the Jubaylah volcanic rocks. The chemistry of the Najd granite is too sparse and not of high quality, but it seems distinctly alkalic and probably in part overlaps with the Shammar field.

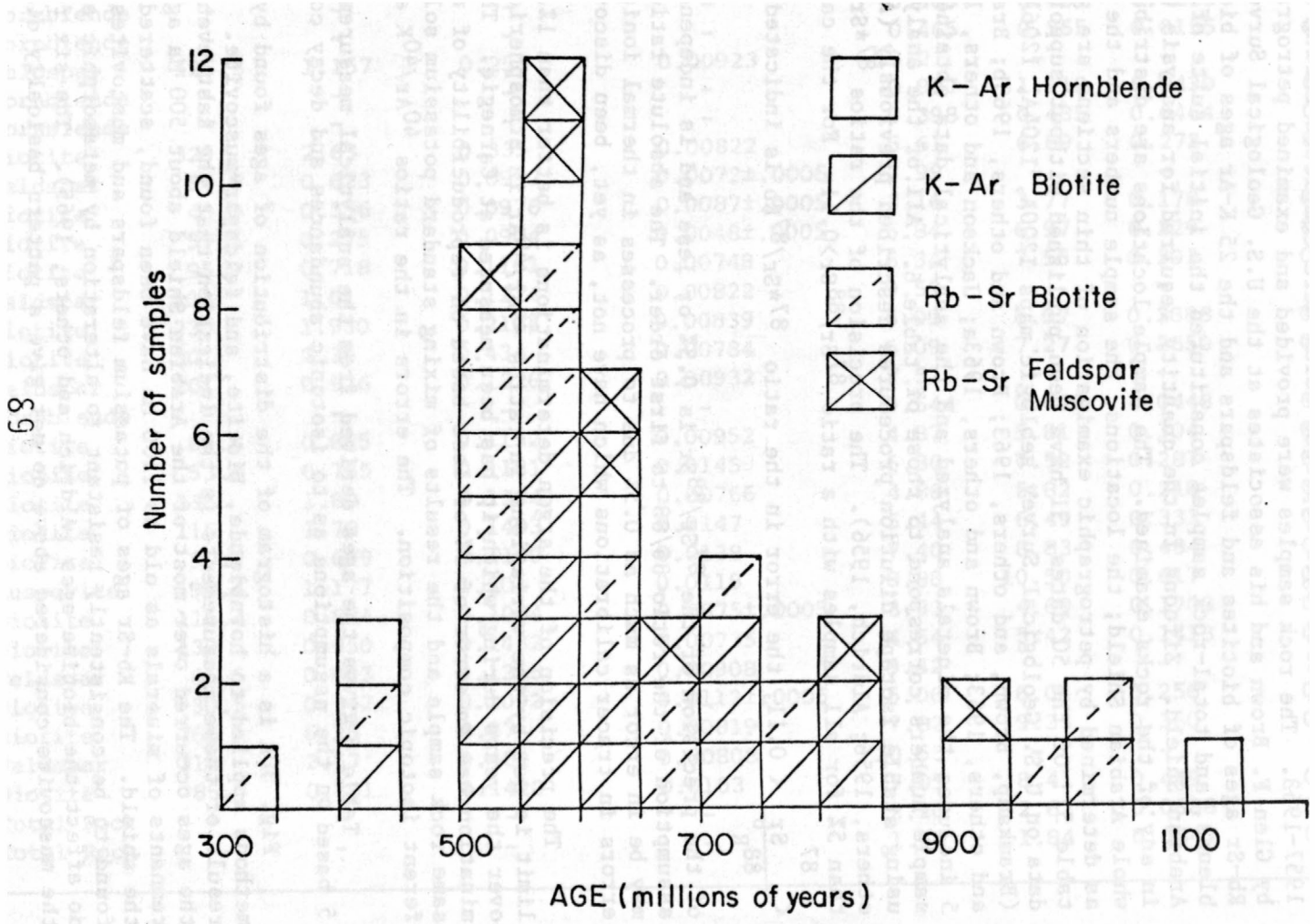

FIG. 30a. Histogram showing distribution of K-Ar and Rb-Sr ages for several minerals.

L. T. Aldrich

GEOCHRONOLOGIC DATA FOR ARABIAN SHIELD

First Radiometric age determinations

by L. Thomas Aldrich

The radiometric ages reported below were completed during the period 1957-1963. The rock samples were provided and examined petrographically by Glen F. Brown and his associates at the U.S. Geological Survey. The 25 Rb-Sr ages of biotites and feldspars and the 25 K-Ar ages of biotites, hornblends, and total-rock samples constituted the initial suite of ages for the Arabian Shield. Zircons in the quantity required for analysis were not found in any of the rocks examined. The sample locations are distributed over the whole Arabian Shield; the locations, the sample numbers and the rock types as determined by petrographic examination of thin sections are given in table 5. Of the 50 dates, 31 have been published without supporting chemical data on U.S. Geological Survey geologic maps I200A, I204A, 1206A, and 1211A. (Bramkamp, Brown, and others, 1963; Brown and others, 1963b; Bramkamp, Ramirez, and others, 1963; Brown and others, 1963a; Jackson and others, 1963). Table 5 includes the minerals analyzed and the analytical data obtained. The sample numbers correspond to those of table 6. All of the analyses were made using stable isotope dilution procedures described previously (Aldrich and others, 1956; Aldrich, 1956). The precision of the ratios $^{87}*Sr/^{87}Rb$ is better than 5% for all samples with a ratio $^{87}Sr/^{88}Sr>0.11$. For the cases when $0.085 < \frac{^{87}Sr}{^{88}R^{b}} < 0.11$, the error in the ratio $^{87}*Sr/^{87}Rb$ is indicated. The precision of the precision of the $^{87}Sr/^{88}Sr$ is 0.3% or less and is independent of the assumption of the ratio 86/88 to first order. The absolute ratio, $^{87}Sr/^{88}Sr$, may be in error as much as 0.5% due to processes in thermal ionization and to errors in tracer calibrations which have not, as yet, been discovered.

The precision of the argon determinations is better than 1%. This upper limit is set by the variations in ratios $^{36}Ar/^{40}Ar$ in atmospheric argon observed over the years during which it has been measured at Carnegie. The ^{40}K determination has an error of 3% or less based on reproducibility of results on the same rock sample and the results of mixing standard potassium solutions of different isotopic composition. The errors in the ratios $^{40}Ar/^{40}K$ are less than 4%.

Table 6 gives the ages derived from the analytical measurements of table 5 based on the assumptions as to isotopic abundances and decay constants stated.

Fig. 30A is a histogram of the distribution of ages found by the different methods applied to hornblende, biotite, and feldspar-muscovite. The first result of these measurements is the indication that the last event affecting the ages occurred over most of the Arabian Shield about 500 Ma ago. Secondly, remnants of minerals as old as 1100 Ma have been found, scattered throughout the shield. The Rb-Sr ages of potassium feldspars and muscovites have been found to be consistently resistant to alteration by metamorphic events which do affect the biotite ages (Aldrich and others, 1965). The six feldspars and the muscovite considered above do not give a pattern basically different from

Table 5. Isotopic chemistry of samples from Saudi Arabia
By L. T. Aldrich

Sample No.	Mineral	^{87}Rb ppm	$^{87}Sr^*$ ppm	$^{87}Sr/^{88}Sr$	$^{87}Sr^*/^{87}Rb$	K (%)	^{40}K ppm	$^{40}Ar^*$ ppm	$^{40}Ar^*/^{40}Ar$ (total)	$^{40}Ar^*/^{40}K$
1.	Hornblende	-	0.590	-	-	0.956	1.14	0.0363	0.74	0.0318
2.	Feldspar	44.8	0.131	0.0901	0.0131	11.0	-	-	-	-
3.	Biotite	221	0.482	0.219	0.00616	5.35	-	-	-	-
4.	Hornblende	-	-	-	-	0.409	0.487	0.0213	0.72	0.0437
5.	Hornblende	-	-	-	-	0.465	0.555	0.0155	0.38	0.0279
6.	Feldspar	125.3	1.157	0.253	0.00923	13.2	-	-	-	-
7.	Hornblende	-	-	-	-	0.937	1.118	0.0430	0.84	0.0384
8.	Hornblende	-	-	-	-	0.398	0.485	0.0464	0.58	0.0977
9.	Biotite	320	2.63	0.335	0.00822	5.61	6.69	0.272	0.67	0.0406
	Feldspar	84.9	0.623	0.0992	0.0072±.0005	7.99	-	-	-	-
10.	Biotite	40.9	0.356	0.0976	0.0087±.0005	3.16	3.77	0.170	0.70	0.0451
11.	Biotite	57.5	0.275	0.0904	0.0048±.0005	5.84	6.97	0.229	0.90	0.0329
12.	Biotite	95.9	0.718	0.1161	0.00748	6.34	7.56	0.303	0.85	0.0401
	Feldspar	123	1.01	0.1274	0.00822	9.59	-	-	-	-
13.	Biotite	230	1.930	0.2104	0.00839	5.09	6.07	0.2388	0.89	0.0393
14.	Biotite	301	2.36	0.434	0.00784	6.09	7.27	0.2650	0.97	0.0365
	Feldspar	101	0.926	0.1226	0.00932	7.52	-	-	-	-
15.	Hornblende	-	-	-	-	0.544	0.649	0.0448	0.90	0.0690
	Biotite	88.5	0.845	0.1152	0.00952	4.87	5.81	0.304	0.94	0.0523
16.	Biotite	53.5	0.765	0.1181	0.0145	6.30	7.52	0.287	0.95	0.0382
17.	Biotite	235	1.80	0.1304	0.00766	4.88	5.82	0.218	0.95	0.0375
18.	Biotite	116	1.70	0.1403	0.0147	5.44	6.49	0.333	0.85	0.0513
19.	Biotite	50.7	0.699	0.1100	0.0138	7.40	8.83	0.484	0.92	0.0548
20.	Muscovite	99.4	1.177	1.301	0.0118	8.88	10.50	0.617	0.86	0.0588
21.	Biotite	116.4	0.874	0.1004	0.0075±.0005	3.93	4.69	0.1703	0.75	0.0393
22.	Biotite	130	0.950	0.1432	0.00735	4.54	5.42	0.1413	0.72	0.0261
	Feldspar	66.5	0.603	0.1256	0.00908	9.42	-	-	-	-
23	Biotite	30.5	0.342	0.1092	0.0112±.0005	5.06	6.04	0.256	0.77	0.0424
24.	Biotite	763	6.25	3.97	0.00819	7.82	9.33	0.360	0.84	0.0386
	Feldspar	319	2.57	0.401	0.00808	10.53	-	-	-	-
25.	Biotite	85.7	0.881	0.1420	0.0103	7.05	8.41	0.449	0.94	0.0534
26.	Total Rock	-	-	-	-	2.20	2.62	0.0686	0.93	0.0261
27.	Total Rock	-	-	-	-	1.54	1.84	0.0647	0.92	0.0352

Table 6. Locations, rock types, and ages of mineral samples from Saudi Arabia

L. T. Aldrich

Map Publication No.	Aldrich Sample No.	Locality Name (J.=Jebel; W.=Wadi)	Longitude (East)	Latitude (North)	Rock Type	Mineral	Rb-Sr age[1] (m.y.)	K-Ar age[2] (m.y.)
1	1.	W. Afal	35°09'17"	28°51'40"	Granodiorite	Hornblende	-	480
2	2.	W. Moss	35°04'18"	28°35'08"	Biotite granite	Feldspar	920 ± 200	-
4	3.	J. Lauz	35°24'35"	28°33'28"	Biotite perthite quartz monzonite	Biotite	430 ±	-
5	4.	Shaib as Siq	35°44'47"	28°02'10"	Diorite	Hornblende	-	630
6	5.	Shaib as Siq	35°47'05"	28°02'26"	Amphibolite schist	Hornblende	-	425
7	6.	J. Harb	35°36'08"	27°55'24"	Microcline granite	Feldspar	645	-
8	7.	J. Harb	35°37'14"	27°55'20"	Quartz syenite	Hornblende	-	565
11	8.	J. Shar	35°42'31"	27°42'42"	Amphibolite	Hornblende	-	1190
78	9.	J. Selma	42°07'22"	27°08'33"	Perthite biotite granite	Biotite	575	590
						Feldspar	505 ± 50	-
82	10.	J. Tin	42°19'24"	26°16'09"	Orthoclase granite	Biotite	610 ± 40	645
53	11.	J. al Aswad	38°13'35	25°33'32"	Albite biotite granite	Biotite	340 ± 70	490
90	12.	J. Um ad Diban	43°51'54"	24°57'25"	Biotite granodiorite	Biotite	525	585
						Feldspar	575	-
91	13.	J. Jabalah	43°55'12"	24°50'00"	Biotite granite	Biotite	590	575
144	14	J. Za'abah	44°48'24"	23°47'42"	Biotite perthite granite	Biotite	550	540
						Feldspar	655	-
104	15.	J. Hamām	41°38'06"	23°41'12"	Granodiorite gneiss	Hornblende	-	915
						Biotite	665	730
186	16.	J. Qusās (Idsas)	45°14'31"	23°18'06"	Granite gneiss	Biotite	1010	560
149	17.	J. Za'n (E. Batholith)	44°55'30"	22°36'16"	Biotite granite	Biotite	540	550
114	18.	Jidda	39°16'06"	21°30'49"	Two-mica granite	Biotite	1025	720
124	19.	Mecca	39°57'12"	21°30'00"	Trondhjemite (quartz diorite)	Biotite	965	760
	20.	Mecca	40°01'52"	21°32'11"	Pegmatite	Muscovite	825	800
125	21.	Taif	40°27'06"	21°13'54"	Biotite quartz monzonite	Biotite	525	535
127	22.	SE J. Qunah	41°16'26"	20°51'49"	Microcline biotite granite	Biotite	515	400
						Feldspar	635	-
126	23.	W. Turaba	41°14'33"	20°43'24"	Quartz diorite	Biotite	785	615
140	24.	J. Rafā'	41°57'30"	20°27'30"	Peralkaline granite	Biotite	575	565
						Feldspar	565	-
171	25.	W. Ranya	42°01'36"	20°21'00"	Calcalkalic granite	Biotite	720	740
238	26.	W. Wahrugh (D-34)	43°07'25"	17°42'13"	Biotite granite	Total Rock	-	400
239	27.	W. Qa'a (D-24)	43°17'30"	17°42'30"	Orthoclase granite	Total Rock	-	525

[1] Ages based on Rb^{87} properties: 0.283 g ^{87}Rb/g ^{87}Rb, $\lambda\beta(^{87}rB) = 1.42 \times 10^{-11}$ yr^{-1}

[2] Ages based on K^{40} properties: 119.3 μg ^{40}K/g K, $\lambda e(^{40}K) = 0.581 \times 10^{-10}$ yr^{-1}

$\lambda\beta(^{40}K) = 4.962 \times 10^{-10}$ yr^{-1}

Table 7. Rhubidium-strontium ages of crystalline rocks of Saudi Arabia
Analysed by Carl Hedge

Sample Locality No.	Age (m.y.)	ppm Rb	ppm Sr	Rb^{87}/Sr^{86}	Sr^{87}/Sr^{86}	Material Analyzed	Rock	Collected by	Location Lat. N.	Location Long. E.
59a	492 ± 15	229	16.4	41.60	0.9968	whole rock	granite	Petty	27° 42'	41° 25'
59b	580 ± 18	169	19.6	25.65	0.9173	whole rock	granite	Petty	27° 42'	41° 25'
68		29.9	58.1	1.491	0.7174	whole rock	rhyolite	Delfour	25° 45'	40° 45'
71	658 ± 40*	5.3	157	0.098	0.7052	whole rock	rhyolite	Delfour	25° 36'	41° 26'
98		45.8	61.3	2.167	0.7245	whole rock	rhyolite	Delfour	23° 51'	40° 56'
77	673 ± 60	119	128	2.701	0.7289	whole rock	granite	Brown	24° 30'	39° 30'
94	633 ± 15*	124	82.6	4.364	0.7440	whole rock	rhyolite	Brown	23° 42'	39° 40'
106		44.7	107	1.211	0.7149	whole rock	latite	Brown	23° 23'	39° 44'
95	520 ± 15	821	53.2	44.61	1.0202	biotite	granite	Goldsmith	23° 36'	40° 32'
96	572 ± 35*	10.0	111	0.263	0.7068	whole rock	porphyritic felsite	Goldsmith	23° 30'	40° 50'
97		85.3	141	1.753	0.7184	whole rock	do	Goldsmith	23° 32'	40° 54'
99	731 ± 15*	13.7	924	0.53	0.7046	whole rock	gneissic qtz. monzonite	Goldsmith	23° 56'	40° 59'
107		54.4	4.3	36.99	1.0841	whole rock	do	Goldsmith	23° 02'	40° 49'
100a		72.1	5.5	38.38	1.077	whole rock	granite	Goldsmith	32° 32'	41° 06'
100b	692 ± 15*	123	5.1	69.25	1.383	K-feldspar	granite	Goldsmith	32° 32'	41° 06'
100c		72.5	13.2	15.90	0.8682	whole rock	granite	Goldsmith	32° 32'	41° 06'
101a		382	21.9	22.05	0.8821	whole rock	granite	Goldsmith	33° 32'	41° 10'
101b	590 ± 10*	659	86.5	50.60	1.1390	whole rock	granite	Goldsmith	33° 32'	41° 10'
101c		320	1.9	494.9	4.857	whole rock	granite	Goldsmith	33° 32'	41° 10'
108	555 ± 15	535	43.5	35.62	0.9699	biotite	granite	Goldsmith	23° 27'	41° 21'

ample ocality o.	Age (m.y.)	ppm Rb	ppm Sr	Rb^{87}/Sr^{86}	Sr^{87}/Sr^{86}	Material Analyzed	Rock	Collected by	Location	
									Lat. N.	Long. E
135a	617 ± 10	98.5	48.2	5.94	0.7587	whole rock	granodiorite	Brown	20° 02'	41° 51'
135b		88.9	24.2	10.73	0.7980	whole rock	granodiorite	Brown	20° 02'	41° 51'
137	582 ± 20	64.5	20.5	9.32	0.7827	whole rock	qtz.monzonite	Brown	20° 11'	41° 52'
169	530 ± 20	496	140	10.33	0.7807	K-feldspar	granite gneiss	Brown	20° 58'	43° 49'
170B	576 ± 25	188	78.8	6.896	0.7603	whole rock	granite	Whitlow	20° 55'	44° 23'
193	583 ± 15	184	49.5	10.77	0.7930	whole rock	granite	Trent	19° 33'	41° 44'
224	549 ± 30	212	131	4.625	0.7421	whole rock	granite	Brown	17° 57'	42° 11'
233	586 ± 35	148	118	3.629	0.7361	whole rock	rhyolite	Overstreet	18° 20'	44° 15'
234	585 ± 10	387	9.3	121.0	1.755	microcline	pegmatite	Overstreet	18° 07'	44° 14'
235	550 ± 20	122	29.2	12.06	0.8040	whole rock	granite porphyry	Overstreet	18° 08'	44° 15'
240	694 ± 30	129	60.6	6.185	0.7653	whole rock	gneissic granite	Brown	17° 26'	42° 54'

Decay constant for Rb^{87}: $\lambda = 1.42 \times 10^{-11}$/yr.

that of the biotites by themselves or from that seen all of the Rb-Sr ages measured. The pattern of hornblende K-Ar ages is also similar to that obtained from the other minerals. The simplest generalized picture of the Arabian Shield from these data is that of a large area of about 1000-1200 Ma old on which has been superposed an even culminating 550 Ma. A particular sequence of samples with geographic proximity is that starting at Jiddah with sample No. 18 and continuing southeast about 300 km. Samples 18, 19, 20, 23, 25 have an age pattern similar to that observed for Precambrian rocks in the Appalachians, which is generally discordant and ranging down from 1050 Ma. Samples 21, 22, and 24 are relatively concordant and may represent younger rocks associated with the event which lowered the age of the other rocks.

These data should be compared with the K-Ar ages obtained in Eastern Egypt as published by Higazy and El-Ramly (1960) in the area between latitude 33°-35° East.

The total-rock argon ages of samples 26 and 27 from the 'Asir are presented, not as a measure of their true age or even an approximation of the time of any "event" in this area, but rather to indicate the minimum age that may be ascribed to these rocks. It must be pointed out that these samples could be older than those in the northern part of the shield and still have this young apparent age, due to argon leakage from the potassium feldspars.

Early tabulation of Rb-Sr and K-Ar ages

by

Glen F. Brown, Carl Hedge [1/], and Richard Marvin [1/]

During the course of initial geologic field work by the U.S. Geological Survey in the Arabian Shield, 101 radiometric ages were determined from rocks in the Precambrian-Cambrian basement. These ages were determined between 1963 and 1970 after the pioneer age-work of L. T. Aldrich (see preceding section) but before the extensive dating of the rocks of the Precambrian Shield after 1972. This tabluation fo the Rb-Sr and K-Ar ages is presented for the benefit of other geologists and geochemists who are presently working in the region. We caution those who use these ages to remember the limitations of Rb-Sr and K-Ar ages.

Carl Hedge analyzed 31 samples (table 7) in the Denver laboratory, U.S. Geological Survey, and obtained 7-Rb-Sr isochron whole-rock ages and 14 Rb-Sr mineral/whole-rock ages. Seven of the 80 K-Ar ages listed in table 8 were determined by Richard Marvin, Harald Mehnert, and Violet Merritt in the Denver laboratory. Thirty-two K-Ar ages were determined by Geochron Laboratories, Kruger Enterprises, Inc., Cambridge, Mass., and 41 K-Ar ages by Teledyne Isotopes, Westwood, New Jersey.

Of the 31 Rb-Sr age determinations by Hedge (Table 7) 19 were used to plot isochron diagrams. The igneous samples used for the plots range from gneissic quartz monzonite to aegerine granite and porphyritic felsite. Tb-Sr isochron ages range downward from 731 Ma for gneissic quartz monzonite to 572 Ma for

---

1/ U.S. Geological Survey, Denver, CO.

Table 8. POTASSIUM-ARGON AGES SAUDI ARABIAN CRYSTALLINE ROCKS

Sample Locality No.	Age (m.y.)	K%	$Ar^{40} \times 10^{-10}$ moles/gm	$\%Ar^{40}$	Ar^{40}/K^{40}	Analyzed by	Material analyzed	Rock	Collected by	Location Lat. N.	Location Long. E.
22b	515 ± 17	2.63 2.67	27.33	94	0.0346	USGS-Marvin Mehnert, Merritt[3]	whole rock	oxidized* muggearite	Brown	27° 45'	36° 10'
26	591 ± 18	6.29 6.34	75.81 77.31	96 89	0.0406	Geochron[2]	biotite	granite	Trent	26° 47'	37° 05'
34	605 ± 18	6.68 6.72	82.07 85.07	98 96	0.0418	Geochron	biotite	granite	Trent	26° 13'	37° 26'
40	528 ± 20	6.53 6.43	68.91	99	0.0356	USGS-Marvin Mehnert, Merritt	biotite	rhyolite	Brown	26° 28'	38° 13'
44	532 ± 15	1.895 1.872	20.19 20.24	63 91	0.0360	Geochron	whole rock	andesite	Brown	26° 20'	38° 37'
54	567 ± 16	6.52 6.36	74.06 74.81	97 98	0.0387	Geochron	biotite	gneiss (?)	Brown	28° 52'	35° 09'
65	827 ± 40	0.385 0.401	7.061 7.231	75 81	0.0609	Geochron	hornblende	quartz	Brown	25° 48'	39° 13'
67	299 ± 11	1.30 1.32	7.393	83	0.0189	USGS-Marvin Mehnert, Merritt	whole rock	andesite (some alteration)	Brown	25° 33'	40° 45'
69	548 ± 18	1.70 1.71	18.95	95	0.0372	USGS-Marvin Mehnert, Merritt	whole rock	andesite	Brown	25° 33'	40° 45'
72	525 ± 16	1.532 1.500	16.11 15.91	81 82	0.0354	Geochron	whole rock	andesite	Brown	24° 52'	39° 11'
89	577 ± 15	7.27 7.29	89.07 82.57	98 97	0.0395	Geochron	biotite	granite	Mytton	25° 01'	43° 48'
92	595 ± 12	6.12 6.10	75.31 74.06	95 97	0.0409	Geochron	biotite	granite	Mytton	24° 30'	43° 19'

96

Locality No.	Age (m.y.)	K%	$Ar^{40} \times 10^{-10}$ moles/gm	$\%Ar^{40}$	Ar^{40}/K^{40}	Analyzed by	Material analyzed	Rock	Collected by	Location Lat. N.	Location Long. E.
102	566 ± 30	1.095 1.126	13.24 12.38	30 80	0.0386	Geochron	whole rock	dacite	Brown	23° 29'	41° 23'
103	506 ± 15	2.180 2.198	22.19 22.17	83 92	0.0339	Geochron	whole rock	diabase dike	Brown	23° 50'	41° 25'
112	585 ± 12	0.50 0.49	5.959 5.915	86 86	0.0402	Isotopes (1)	hornblende	schist	Hanford	22° 24'	39° 24'
117_a	592 ± 23	1.247 1.222	15.11 14.91	88 82	0.0407	Geochron	whole rock	altered basalt	Brown	21° 35'	39° 38'
117_b	576 ± 28	0.550 0.518	6.280 6.280	69 68	0.0394	Geochron	whole rock	andesite	Brown	21° 35'	39° 38'
119	549 ± 20	6.65 6.48	71.56 74.81	74 91	0.0373	Geochron	biotite	granite	Goldsmith	21° 43'	40° 27'
120	577 ± 18	7.10 7.03	82.32 84.32	84 96	0.0395	Geochron	biotite	qtz. monzonite	Goldsmith	21° 41'	40° 40'
121	570 ± 17	7.15 7.22	83.82 83.32	97 98	0.0390	Geochron	biotite	granite	Goldsmith	21° 41'	40° 41'
128	827 ± 16	0.32 0.33	5.829 5.995	82 73	0.0609	Isotopes	hornblende with 5% impurities	diorite	Brown	20° 32'	41° 25'
129_a	932 ± 46	0.489 0.440	9.858 9.808	82 86	0.0709	Geochron	hornblende	diorite	Brown	20° 32'	41° 31'
	821 ± 16	0.49 0.50	8.865 8.994	95 95	0.0604	Isotopes	hornblende with 5% impurities	diorite			
129_b	912 ± 18	0.44 0.45	9.240 9.070	91 90	0.0689	Isotopes	hornblende with 5% impurities	quartz diorite	Brown	20° 32'	41° 31'

Locality No.	Age (m.y.)	K%	$Ar^{40} \times 10^{-10}$ moles/gm	$\%Ar^{40}$	Ar^{40}/K^{40}	Analyzed by	Material analyzed	Rock	Collected by	Location Lat. N.	Location Long. E.
130	805 ± 16	0.25 0.24	4.301 4.323	90 92	0.0590	Isotopes	amphibole with 15% impurities	quartz diorite	Brown	20° 26'	40° 26'
131	595 ± 12	3.72 3.52	44.86 43.75	90 97	0.0410	Isotopes	muscovite	paraschist	Brown	20° 26'	40° 49'
132	717 ± 18	0.42 0.42	6.312 6.517	90 94	0.0512	Isotopes	hornblende	gneiss	Brown	20° 28'	40° 56'
136	585 ± 39	0.43 0.43	5.150	87	0.0401	USGS-Marvin, Mehnert, Merritt	whole rock	basalt	Brown	20° 10'	41° 52'
141a	561 ± 25	3.646 3.635	42.78 40.28	97 98	0.0382	Geochron	whole rock	andesite	Brown	23° 39'	43° 08'
141b	560 ±20	2.162 2.277	24.92 25.67	94 94	0.0382	Geochron	whole rock	dacite (?)	Brown	23° 39'	43° 08'
148	574± 12	5.32 5.24	62.58 62.62	98 99	0.0393	Isotopes	biotite (+60 mesh)	granite	Brown	22° 53'	44° 56'
86	585 ± 12	5.10 4.98	60.08 60.66	99 99	0.0401	Isotopes	biotite (-60 mesh)	granite			
149x	513 ± 17	2.66	22.73	95	0.0345	USGS-Marvin, Mehnert, Merritt	whole rock	gabbro chilled rim	Brown	22° 28'	44° 34'E
149y	458 ± 15	5.87	44.09	93	0.0303	"	biotite	gabbro	Brown		
151	644 ± 23	6.44 6.47	86.65	95	0.0450	USGS-Marvin, Mehnert, Merritt	biotite	grabbro	Hanford	22° 19'	42° 24'
153	496 ± 12	0.48 0.49	4.721 4.876	76 26	0.0331	Isotopes	plagioclase and quartz	granite	Brown	22° 25'	43° 48'
165	596 ± 12	0.69 0.71	8.485 8.664	77 87	0.0410	Isotopes	hornblende with 20% impurities	qtz. monzonite	Brown	21° 15'	43° 57'

Locality No.	Age (m.y.)	K%	$Ar^{40} \times 10^{-10}$ moles/gm	$\%Ar^{40}$	Ar^{40}/K^{40}	Analyzed by	Material analyzed	Rock	Collected by	Location	
										Lat. N.	Long. E.
168_b	710 ± 16	0.092 0.096	1.418 1.421	63 70	0.0506	Isotopes	whole rock	troctolite	Brown	20° 32'	42° 32'
169	539 ± 20	0.38 0.36	4.034 4.022	29 31	0.0365	Isotopes	plagioclase and quartz	gneiss	Brown	20° 58'	43° 49'
173	826 ± 16	4.18 4.21	74.99 77.31	98 97	0.0608	Isotopes	biotite with 10% impurities	granite	Brown	20° 17'	42° 08'
	711 ± 30	0.39 0.36	5.762 5.564	27 24	0.0506	Isotopes	hornblende	granite			
175	484 ± 10	0.12 0.11	1.119 1.097	78 79	0.0323	Isotopes	whole rock	leuco gabbro	Brown	20° 16'	42° 28'
180_a	598 ± 12	5.11 5.03	63.07 61.51	99 99	0.0412	Isotopes	biotite	granite	Brown	23° 58'	45° 01'
180_b	584 ± 12	6.48 6.40	77.00 77.17	99 99	0.0401	Isotopes	biotite	granite	Brown	23° 58'	45° 01'
181	597 ± 12	6.49 6.54	80.17 79.67	99 99	0.0411	Isotopes	biotite	grano-diorite	Brown	23° 58'	45° 05'
183	597 ± 12	7.75 7.81	94.63 96.41	99 99	0.0411	Isotopes	biotite	grano-diorite	Brown	23° 41'	45° 08'
184	583 ± 12	6.51 6.51	77.71 77.62	98 98	0.0400	Isotopes	impure biotite	grano-diorite	Brown	23° 53'	45° 07'
	546 ± 5	0.50 0.51	5.580 5.580	89 89	0.0370	Isotopes	hornblende	granite			
187	589 ± 12	7.88 7.97	95.88 95.57	99 99	0.0405	Isotopes	biotite	granite	Brown	23° 01'	45° 29'
188	619 ± 12	5.27 5.40	68.69 67.94	99 99	0.0429	Isotopes	biotite	granite	Brown	23° 01'	45° 33'
	629 ± 12	1.38 1.40	18.04 18.23	95 98	0.0437	Isotopes	hornblende	granite			

Locality No.	Age (m.y.)	K%	$Ar^{40} \times 10^{-10}$ moles/gm	$\%Ar^{40}$	Ar^{40}/K^{40}	Analyzed by	Material analyzed	Rock	Collected by	Location Lat. N.	Location Long. E.
189	632 ± 12	4.96 4.92	63.87 65.79	97 99	0.0440	Isotopes	biotite with minor hornblende	qtz. diorite	Brown	22° 36'	45° 07'
	611 ± 12	0.75 0.74	9.418 9.373	92 92	0.0422	Isotopes	hornblende	qtz. diorite			
190	759 ± 20	7.41 7.55	123.1 121.6	98 98	0.0548	Geochron	biotite	granite	Trent	19° 55'	41° 33'
191_a	646 ± 12	0.86 0.87	11.62 11.69	89 80	0.0451	Isotopes	hornblende with 10% impurities	granite gneiss	Brown	19° 53'	41° 37'
191_b	759 ± 31	0.931 0.978	15.71 15.54	91 93	0.0548	Geochron	hornblende	granite gneiss	Brown	19° 53'	41° 37'
	694 ± 14	1.03 1.01	15.09 14.88	98 97	0.0492	Isotopes	hornblende with 20% impurities	granite gneiss			
192	607 ± 12	0.88 0.88	10.88 11.15	96 97	0.0419	Isotopes	hornblende	gneiss	Brown	19° 52'	41° 43'
194	676 ± 28	0.408 0.398	5.830 5.630	84 82	0.0476	Geochron	plagioclase	qtz. diorite	Brown	19° 35'	41° 53'
213_a	578 ± 12	0.10 0.10	1.214 1.148	82 60	0.0396	Isotopes	whole rock	gabbro	Brown	19° 09'	43° 48'
213_b	516 ± 10	0.084 0.083	0.8735 0.8548	77 77	0.0347	Isotopes	whole rock	gabbro	Brown	19° 09'	43° 48'
219_a	656 ± 14	0.090 0.102	1.319 1.318	87 79	0.0460	Isotopes	whole rock	norite	Brown	18° 45'	42° 53'
219_b	484 ± 10	0.15 0.15	1.443 1.448	86 83	0.0323	Isotopes	whole rock	norite	Brown	18° 45'	42° 53'

Locality No.	Age (m.y.)	K%	$Ar^{40} \times 10^{-10}$ moles/gm	$\%Ar^{40}$	Ar^{40}/K^{40}	Analyzed by	Material analyzed	Rock	Collected by	Location Lat. N.	Location Long. E.
221_b	422 ± 8	0.12 0.12	0.9806 0.9967	92 92	0.0276	Isotopes	whole rock	norite	Brown	18° 56'	43° 02'
225_a	655 ± 12	7.14 6.98	95.38 97.80	99 98	0.0458	Isotopes	biotite	diorite	Brown	18° 13'	42° 32'
	615 ± 12	0.98 1.02	12.73 12.67	91 92	0.0425	Isotopes	hornblende	diorite			
225_b	686 ± 14	4.86 4.70	68.34 70.03	98 98	0.0485	Isotopes	biotite with 20% impurities	diorite	Brown	18° 13'	43° 32'
228_a	649 ± 23	6.72 6.70	90.83	97	0.0453	USGS-Marvin, Mehnert, Merritt	biotite	gabbro	Brown	18° 24'	42° 42'
228_b	615 ± 12	8.50 8.49	106.9 109.2	93 94	0.0426	Isotopes	muscovite	pegmatite	Brown	18° 24'	42° 42'
229_a	588 ± 17	1.970 2.008	24.17 23.82	95 95	0.0404	Geochron	whole rock	(drill core	Brown	18° 08'	44° 07'
229_b	577 ± 16	2.17 2.13	25.40 25.27	94 90	0.0395	Geochron	whole rock	andesite (drill core	Brown	18° 08'	44° 07'
229_c	572 ± 15	2.15 2.07	24.37 24.92	94 94	0.0391	Geochron	whole rock	andesite (drill core	Brown	18° 08'	44° 07'
229_d	571 ± 15	2.61 2.63	30.80 30.25	94 93	0.0390	Geochron	whole rock	andesite (drill core	Brown	18° 08'	44° 07'
229_e	595 ± 18	2.179 2.194	26.87 26.57	76 83	0.0409	Geochron	whole rock	andesite (drill core	Brown	18° 08'	44° 07'
230	544 ± 15	3.282 3.192	36.18 35.18	90 85	0.0369	Geochron	whole rock	andesite	Overstreet	18° 24'	44° 11'
231_a	519 ± 15	3.608 3.503	36.65 37.56	93 93	0.0350	Geochron	whole rock	andesite	Overstreet	18° 22'	44° 14'

Locality No.	Age (m.y.)	K%	$Ar^{40} \times 10^{-10}$ moles/gm	$\%Ar^{40}$	Ar^{40}/K^{40}	Analyzed by	Material analyzed	Rock	Collected by	Location Lat. N.	Location Long. E.
231b	579 ± 22	0.485 0.450	5.454 5.604	68 67	0.0396	Geochron	whole rock	andesite	Overstreet	18° 22'	44° 14'
232	575 ± 15	2.232 2.204	25.57 26.52	83 87	0.0393	Geochron	whole rock	andesite	Overstreet	18° 20'	44° 15'
234	600 ± 24	1.087 1.015	13.09 12.86	83 83	0.0414	Geochron	whole rock	diorite	Overstreet	18° 06'	44° 15'
236	565 ± 16	3.624 3.701	42.48 41.73	96 95	0.0385	Geochron	whole rock	felsite dike	Overstreet	18° 07'	44° 15'

Constants $^{40}_{K}\lambda e = 0.581 \times 10^{-10}$/yr $\lambda\beta = 4.962 \times 10^{-10}$/yr Atomic abundance $^{40}K = 1.167 \times 10^{-4}$

1/ Isotopes, Inc., later Teledyne Isotope, Westwood, NJ.
2/ Geochron Laboratories, Inc., Cambridge, MA.
3/ USGS Analysts, R.F. Marvin, H.H. Mehnert, and Violet Merritt.

the porphyritic felsite. Samples from the aegerine granite gave an isochron age of 590 Ma. Where they could be precisely determined, the initial Sr^{87}/Sr^{86} ratios were relatively low (0.703-0.705). An initial ratio of 0.704 was therefore used to calculate the individual ages reported in table 7. Rhyolite sills or flows in the upper beds of the Murdama Group gave an age of 633 Ma, whereas the underlying and older Hulafah (Halaban) gave a minimum age of 651 Ma from rhyolite near the tope of the group. The latter is especially significant as they rhyolite samples came from drill cores in strata-bound ore deposits syngenetically deposited above the middle Hulayfah (Halaban) andesite and in the lower part of the uppermost rhyolite of the Halaban Group.

The K-Ar ages range from 299 to 932 Ma. The ages younger than about 500 Ma undoubtedly reflect some severe resetting caused by late Precambrian hydrothermal alteration and some resetting caused by uplift and deep erosion. In places, some resetting may have been caused by heating by Neogene volcanism associated with the formation of the Red Sea. Hornblende ages, which are least susceptible to resetting (argon loss), cluster around 550 and 570 Ma and from 590-660 Ma. These ages represent events in the Pan African orogeny. Older hornblende ages, 710-778 Ma, are from calc-alkaline syngenetic, generally gneissic, quartz monozonte, granodiorite, and granite bodies which are usually exposed in domes. Ages in the span 805-932 Ma were obtained mostly from diorite, quartz diorite, and granodiorite plutons exposed in the scarps and foothills east of the Red Sea and in the southern part of the Arabian Shield. Following the earlier geochronological work (tables 6, 7, 8) an intensive study was begun in 1972 with geochronologists working in the field parties. Early analyses of the intensive program were limited to K-Ar determinations (Fleck and others, 1976) but when analytical work became more accurate for low rubidium values, attention was directed to rubidium-strontium determinations (Fleck and others, 1980). It became apparent that many K-Ar ages gave cooling dates when magmas cooled below the point where the daughter argon was retained in the rock--especially in the biotite and feldspar fractions. Thus many K-Ar dates at about 550 m.a. in schist belts of the Najd fault zones suggest that an important period of fault movement occurred at or near the end of cratonization. A later cooling event, possibly representing erosion, of cover rocks and upper crust of the shield during Middle to Late Cambrian, was recorded at 520-535 m.a. (Fleck and others, 1974). This event was further verified by a "fission track" age on four grains of sphene from a diorite in southwestern Arabia (C. W. Naeser, written commun.) which gave an average of 510 $\pm$ 52 m.a. as a cooling date when the tracks stopped annealing. The K-Ar age of the hornblende from the diorite was 615 $\pm$ 12 m.a.

Also, later work utilizing zircon and measuring daughter leads from uranium and thorium decay in zircons have helped define the two earlier major orogenies where the zircons were palingenetically new--the Ablah and culminant orogenies at 797-763 $\pm$ m.a. and 660-666 m.a. (Cooper and others, 1979, and fig. 39.) Also in recent years the French (B.R.G.M.) have made numerous analyses (more than 360 samples) in their laboratory at Orleans (Baubon and others, 1976.) Likewise analyses have been reported from the University of Leeds (A. Kroner and others, 1979) and at the Department of Geology, Nottingham, and the Institute of Geological Sciences in London (Duyverman and others, 1982.)

Crustal history of the Precambrian Shield

General Statement

The evolutionary history of the Precambrian Arabian Shield must be evaluated grossly across a structural width of more than 1000 km or a total of more than 1500 km, if the Nubian Shield of Egypt and Sudan is included. Across these widths, the crustal rocks of the Arabian or Arabian-Nubian Shield are grossly similar in petrology, chemistry, structure, and age. Across either Shield, the crustal rocks were made and cratonized in about 450 million years from about 1000 Ma to about 550 Ma ago.

No continental crust older than about 1 Ga has been found in the Arabian Shield despite a concerted effort to find "old" continental crustal rocks. In the easternmost part of the Shield, a 2100-Ma-old continental crust may be nearby as recent lead-isotope studies indicate that some of the youthful Precambrian granitoid rocks here contain old leads (Stacey and others, 1980). At this time, it is not resolved whether the crustal block of the Ar Rayn region east of the Al Amar-Idsas fault (region E, fig. 17) is actually part of this old crust or whether the old crust is still farther east beneath the Phanerozoic sedimentary rocks.

An initial stratigraphy for the shield was based on reconnaissance mapping and petrology (Brown and Jackson, 1960; USGS-ARAMCO, 1963). The stratigraphy was modified by more detailed mapping and petrography (Schmidt and others, 1973) and has been better defined by additional mapping by BRGM, Ministry, and USGS geologists since 1973 and particularly by Rb-Sr geochronology in the southern part of the shield (Fleck and others, 1980). For the most part, the initial stratigraphic names and sequence still stand, although the areas where some of the units had been defined (type area) have been changed. Some of these changes have not strictly followed standard stratigraphic nomenclature procedures but are justified for the complex Precambrian rocks, to provide a common set of stratigraphic names over a long period of study.

The shield has been subdivided (fig. 17) on the basis of the early crustal stratigraphic groups, the Baish-Bahah, Jiddah (Samran), and Halaban (Hulayfah). The actual rock boundaries between these groups are not easily mapped because the overall lithologies of each group are similar. The boundaries on figure 17 are drawn largely along major north-trending structures that bound early crustal volcanic and plutonic rocks of similar age. The north-trending stratigraphic belts, are strongly offset by the Najd faults of youngest Precambrian age. The volcanic and plutonic rocks of the late cratonization history are superimposed upon the early crustal rocks and, hence, do not effect the subdivisions on figure 17.

The Wadi Bidah region (B, fig. 17) contains the type reference area of the Baish-Bahah groups (basaltic assemblage). In the Biljurshi region (J, fig. 17) early crustal rocks of the Jiddah group (andesite assemblage), are described and dated between 900 m.y. and about 850 m.y.. This region also contains the type locality of a younger group, the Ablah group, that is dated at between 850? m.y. and about 750 m.y. The type area for the Halaban group is centered around Halaban in region TN (fig. 17). Correlatives of the Halaban rocks are well described as the Hulayfah group in region HN

in the Nuqrah quadrangle (Delfour, 1977) and as the Halaban group in region TC in the Bir Juqjuq quadrangle. The Tathlith regions, TN, TC, and TS, and the northeast region, NE, are largely underlain by crust of Halaban age of about 800 m.y. to 725 m.y. old. The western boundary is the long serpentinite fault zone of Hulayfah-Ad Dafinmah-Nabitah-Hamdah. The regions HS, HC, and HN form a western belt that at least in large part or entirely consists of Halaban crustal rocks.

The early crustal rocks in the western and northern regions have not been named consistently in the literature or well dated. The initial type area of the Jiddah group is in the vicinity of the townsite of Jiddah, and the available dates suggest that the regions, WS, WC. and perhaps WN, may be underlain by crustal rocks of Jiddah (Samran) age. A Jiddah age is not denied by the available dates from the Eastern Desert of Egypt (Hashad, 1980), which was an integral part of the Arabian Shield. Region NN is highly faulted by the convergence of the Najd fault system and, for the time being, the early crust of this northern Najd fault region, NN, and of the northern region, N, is considered also as Jiddah age. Region E, east of the Al Amar-Idsas fault, has been most commonly mapped as consisting of Halaban rocks, but it may be older as suggested earlier in this chapter.

The primary crustal rocks of the shield consist of metavolcanic and metasedimentary rocks of a basaltic assemblage and an andesitic assemblage and of plutonic rocks of a dioritic suite; in addition, subordinate tectonic remnants of ophiolitic rocks are scattered throughout much of the shield. These rock groupings are based on petrology, petrography, and chemistry (Greenwood and others, 1976; Dodge and others, 1979; Delfour, 1979) and on Rb-Sr and Pb isotopic studies (Fleck and others, 1980; Baubron and others, 1976; and Stacey and others, 1980). Most of these rocks are of the andesitic assemblage and dioritic suite that formed in intraoceanic island arcs as volcanic-magmatic arcs. The basaltic assemblage of the Baish-Bahah group as sampled in the Wadi Bidah area has a distinctly more tholeiitic composition then the andesite-assemblage rocks and may have an oceanic crust affinity. More likely the Baish-Bahah rocks are simply an early and basal, more tholeiitic part of the Jiddah andesitic assemblage and of Jiddah age because the basaltic assemblage rocks all across regions J and B (fig. 17) are interspersed with andesite assemblage rock of the Jiddah Group and diorite-suite rock that consistently date between 900 and 800 Ma.

The problem of the age and origin of the Baish-Bahah rock clearly points out the fact that the study of the Precambrian shield has barely begun to decipher individual volcanic-magmatic arcs as well as other specific constructional blocks that form the composite early crust as it is known today. Each of the early stratigraphic groups is broadly bounded by a meaningful age range, but each likely consists of more than a single constructional block within that age range.

The following early and late crustal history of the shield outlines one possible sequence of events that in each event might be expected to be much more complex than described. This crustal history has been summarized in a review paper by Schmidt and Brown (1982).

Early crustal history

The early, primary crust of the Saudi Arabian Shield is a composite of several intraoceanic, island arcs, and subordinate remnants of oceanic crust (ophiolite). These primary constructional blocks have been combined at different times in different places during several subduction and collisional events from about 1000 Ma to about 700 Ma ago. Especially the older constructional blocks have been tectonized and the combined crust has been tectonically and magmatically thickened during these early collisional events. Throughout most parts of the shield, compressional structures are consistently north-trending and it is presumed that the original island arcs trended generally northward and that subduction may have been both westward and eastward under different arcs at different times. Deep erosion during the late crustal history, discussed below, means that, for the most part, we see today the deep magmatic parts of the volcanic-magmatic arcs. Most of the metavolcanic and metasedimentary rocks exposed adjacent to these deeply eroded magmatic arcs were originally deposited marginally to the volcanic-magmatic arcs. Therefore, the early layered rocks exposed throughout the shield contain a large proportion of pyroclastic and immature clastic metasedimentary rocks derived from the island-arc volcanic rocks. The original andesitic volcanic piles in the upper part of the magmatic arcs are less commonly preserved, except where they have been thrust into adjacent basins prior to the deep erosion of the volcanic arc.

The early, primary crust consists predominantly of an andesitic assemblage of metavolcanic and metasedimentary rocks and comagmatic plutonic equivalents of dioritic suite. These primary crustal rocks have been well dated in the southern part of the Shield between about 900 Ma and 700 Ma old (Fleck and others, 1980). In a broad western belt about 250 km wide between Al Lith and Qalat Bishah (regions B and J, fig. 17), rocks of the dioritic suite as well as those of the andesite assemblage date between 900 Ma and 800 Ma Rocks of similar composition are dated between 800 Ma and 700 Ma in a broad eastern belt, about 250 km wide, between Qalat Bishah and the eastern edge of the exposed shield (regions HS and TS, fig 17). The andesitic assemblage rocks of the western belt are mapped mostly as Jiddah group as characterized in the Biljurshi quadrangle (Greenwood, 1975c). The andesitic assemblage rocks of the eastern belt are mapped mostly as Halaban rocks as characterized in the Bir Juqjuq quandrangle (Hadley, 1976). Both of these belts, one of early primary crust of Jiddah age and the other, of late primary crust of Halaban (Hulayfah) age are tectonically complex, and undoubtedly each is composed of more than one constructional block of interoceanic, island-arc materials.

The Jiddah-age crust in regions B and J can be further subdivided by age along the 42d meridian. To the east of the 42d meridian, dioritic-suite rocks of the An Nimas batholith (fig. 31) are dated between about 850 and 800 Ma. The An Nimas batholithic complex (Anderson, 1977) consists of plutons of diorite, quartz diorite, tonalite, and trondhjemite, as well as subordinate gabbro and small screens of metavolcanic rocks. The complex is about 70 km wide and extends 150 km from latitude 19°00' northward to 20°30' to where it is covered by the Harrat al Buqum. The An Nimas batholithic complex is probably the deeply eroded core of a volcanic-magmatic arc and is just one

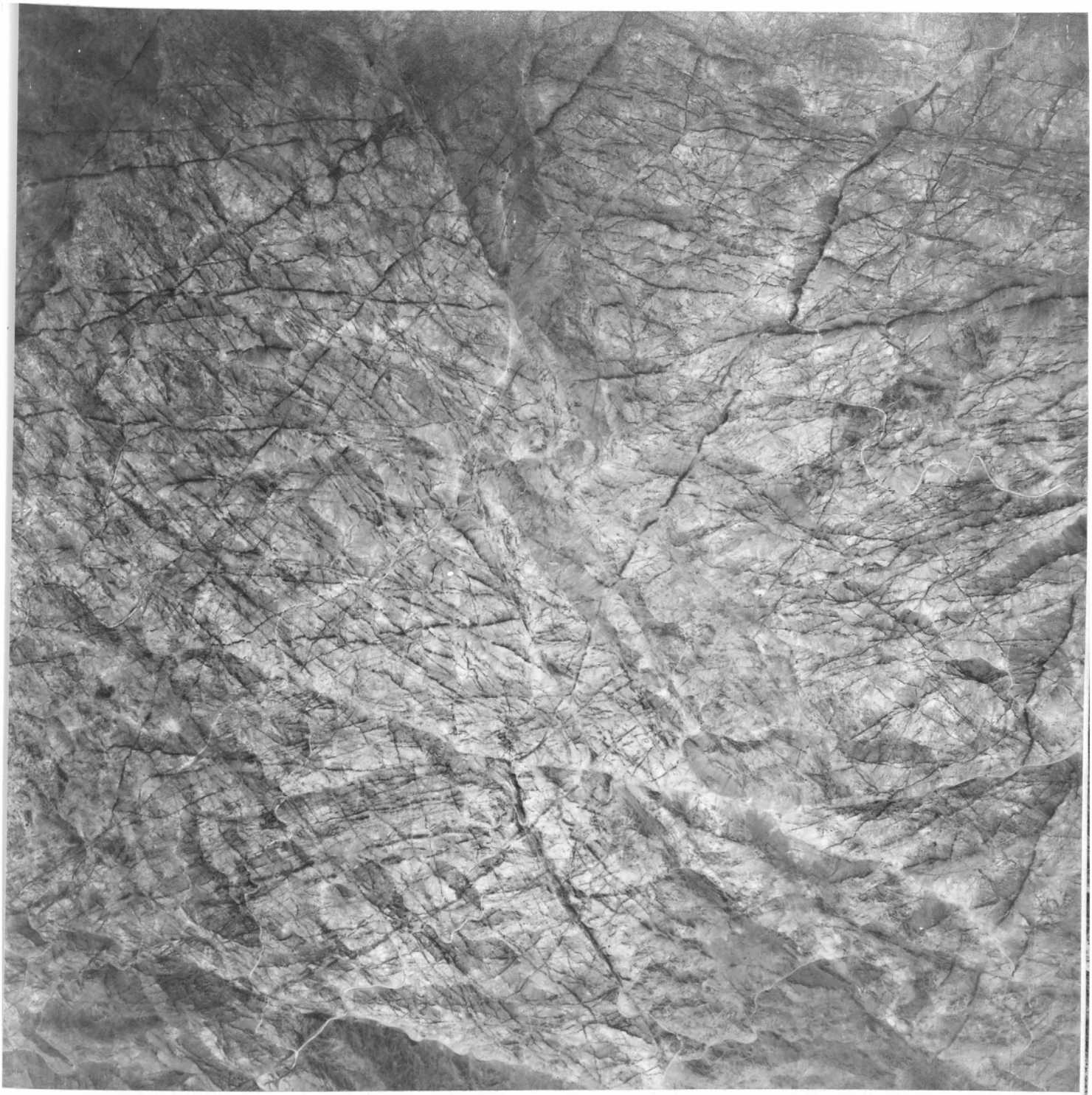

Figure 31. Vertical aerial photograph of the northern portion of the An Nimas batholith possibly the oldest plutonic rocks heretofore dated in the Arabian Shield (816± 4 my, Cooper and others, 1979; 837± 50 my. Fleck and others, 1980). The syntectonic batholith ranges in composition from diorite to tonalite with much interlayered quartz diorite. The darker areas represent diorite or mixed rocks. The terrain is crisscrossed with metabasalt and meta-andesite dikes following lineations--faults and joints from at least two and possibly three orogenic episodes. At least some conjugate dikes were formed during the Nejd orogeny. (Geology after Greene, 1981)

integral constructional block within the Jiddah-age crust. At one locality within the batholithic complex, metaandesitic and metadacitic rocks are dated 912 ± 76 Ma (initial $^{87}Sr/^{86}Sr$ = 0.7024, Fleck and others, 1980) which is about 60 Ma to 100 Ma older than the age of the comparable quartz dioritic and trondhjemitic rocks; the 912 Ma date may be too old and must be substantiated by further studies.

To the west of the 42d meridian for about 200 km, the plutonic rocks of the dioritic suite are dated consistently between 900 and 850 Ma old and are interspersed with andesitic assemblage rocks mapped as Jiddah (Samran) group as represented in the Biljurshi quandrangle (Greenwood, 1975c) and basaltic assemblage rocks mapped as Baish-Bahah groups as represented in the Jabal Ibrahim quadrangle (Greenwood, 1975b). Because the dioritic-suite rocks are dated uniformly and consistently from 900 to 800 Ma across the entire belt, the basaltic assemblage Baish-Bahah group rocks are possibly a more tholeiitic, basal, and immature part of the predominantly calc-alkalic andesite assemblage of the Jiddah (Samran) group rather than being remnants of oceanic crust as has been suggested in the literature. The 200-km-wide belt is intensely folded, faulted, and probably thrust faulted as well. On the west side of the belt near Al Lith, metabasalts mapped as Baish group are dated 1165 ± 110 Ma (initial $^{87}Sr/^{86}Sr$ = 0.7029, Hadley and Fleck, 1980a), yet are intruded by quartz dioritic rocks dated at 895 ± 173 Ma (initial $^{87}Sr/^{86}Sr$ = 0.7025). Again, as in the An Nimas batholithic complex, the metavolcanic rocks seem to date too old for the presumably comparable plutonic rocks. An alternative, less likely, explanation is that the volcanic rocks of an older constructional block are tectonically mixed with the Jiddah-age crustal rocks.

The andesitic-assemblage rocks in the vicinity of Jiddah townsite, the original type area for the Jiddah greenstone, are possibly Jiddah age (as defined in the Biljurshi quadrangle) on the basis of some dated plutonic rocks (table 5, this report). Fifty to 100 km north of Jiddah and east of Rabigh (region WS), andesitic-assemblage rocks of the Samran group of (Skiba, 1980) are calc-alkalic and trend toward a tholeiitic composition (fig. 27A). These rocks may be correlated tentatively with those at Jiddah, but ages have not been determined. Still farther northwestward along the western edge of the shield, rock ages on early crustal rocks also have not been determined. Support for early crustal rocks of Jiddah (Samran) age can be extrapolated from dates on the dioritic-suite rocks from the southern part of the Eastern Desert of Egypt where six Rb-Sr, whole-rock dates range from 987 to 830 m.y. (Hashad, 1980, p. 41). The areal distribution of these rocks in Egypt extrapolates to Saudi Arabia from south of Yambu al Bahr to north of Al Wajh.

The Halaban(Hulayfah)-age crust in the regions HS and TS (fig. 17) are subdivided structurally by the serpentinite belt of Hulayfah-Ad Dafinah-Nabitah-Hamdah into at least 2 constructional blocks. The belt of Halaban crust west of the serpentinite belt, region HS, contains andesitic-assemblage rocks that are dated between 785 ± 96 Ma (initial $^{87}Sr/^{86}Sr$ = 0.7025) and 746 ± 16 Ma (initial $^{87}Sr/^{86}Sr$ = 0.7021) and quartz diorite to tonalite plutonic rocks of the dioritic suite that are dated 723 ± 107 Ma (initial $^{87}Sr/^{86}Sr$ = 0.7025) and 724 ± 93 Ma (initial $^{87}Sr/^{86}Sr$ = 0.7027) (Fleck and others, 1980). The belt of Halaban (Hulayfah) east of the serpentinite belt (region TS) contains Halaban

(Hulayfah) andesitic-assemblage and dioritic-suite rocks that have not been satisfactorily dated, but which suggest ages between 800 and 700 Ma. These two belts of Halaban(Hulayfah)-age crust can be extended, using the serpentinite belt, northward across the shield through the type area of the Hulayfah group (Halaban equivalent; Delfour, 1977) and through the Halaban type area in the vicinity of Halaban ridge.

In summary, the early, primary crust of the shield is a combination of several constructional blocks, of which each is an intraoceanic island arc consisting of an andesitic assemblage of metavolcanic rocks and a dioritic suite of plutonic rocks. For the convenience of discussion, these rocks are lumped into a primary crust of Jiddah-age (900 to 800 Ma old) and a primary crust of Halaban-age (800 to 700 Ma old).

Early collisional orogeny

In the southern part of the Shield, several widely spaced gneiss domes of tonalitic-trondhjemitic orthogneisses are indicative of crustal heating, tectonism, metamorphism, and the gravitational rise of less dense plutonic parts of the primary crust of Jiddah (Samran) age. Syntectonic intrusion of granodioritic batholiths accompanied the rise of orthogneisses and represent the first large volumes of potassic plutonic rocks in the early crust at any given locality. The best documented example is the Baqarah gneiss dome in the southern end of the An Nimas batholith, where tonalitic and trondhjemitic orthogneisses are accompanied by synkinematic granodioritic gneissic batholithic rocks that are dated at 763 $\pm$ 53 Ma (initial $^{87}Sr/^{86}Sr$ = 0.7032; Fleck and others, 1980)(fig. 32). A similar gneiss domal complex at the northern end of the An Nimas batholith gives less reliable K-Ar dates between 740 and 711 Ma (table 8, this report). Interpretation suggests that, while the early, primary, Halaban-age crust was forming somewhere to the east, the older Jiddah-age crust was subjected to combination and consolidation by early collisional tectonism involving tectonic and magmatic crustal thickening, gneiss doming, and granodiorite intrusion.

The orogenic mountains were eroded and resulted in deposition of molassic sedimentary rocks that, along the west side of the An Nimas batholith are mapped as the metasedimentary rocks of the Ablah group. These voluminous graywacke deposits of the Ablah group are commonly quartz bearing and contain even some quartz sandstones which indicate derivation from large volumes of quartz diorite, tonalite, and trondhjemite of the Jiddah crust. These quartzose sedimentary rocks together with thick marble deposits indicate deposition from a deeply eroded crust and in a semi-stable basin that together were indicative of a nearly continental environment. However, the generally low K_2O, calc-alkalic volcanism associated with the Ablah rocks indicate that the continental crust had not uniformly established full thickness.

Other gneiss domes and molassic metasedimentary rocks superposed elsewhere upon Jiddah-age crust in the western Shield may be related to the same early collisional orogeny and may be correlatives of the Baqarah orthogneiss and Ablah group rocks or may represent other early collisional orogenies of slightly different age and place. Another example is the metasedimentary rocks mapped

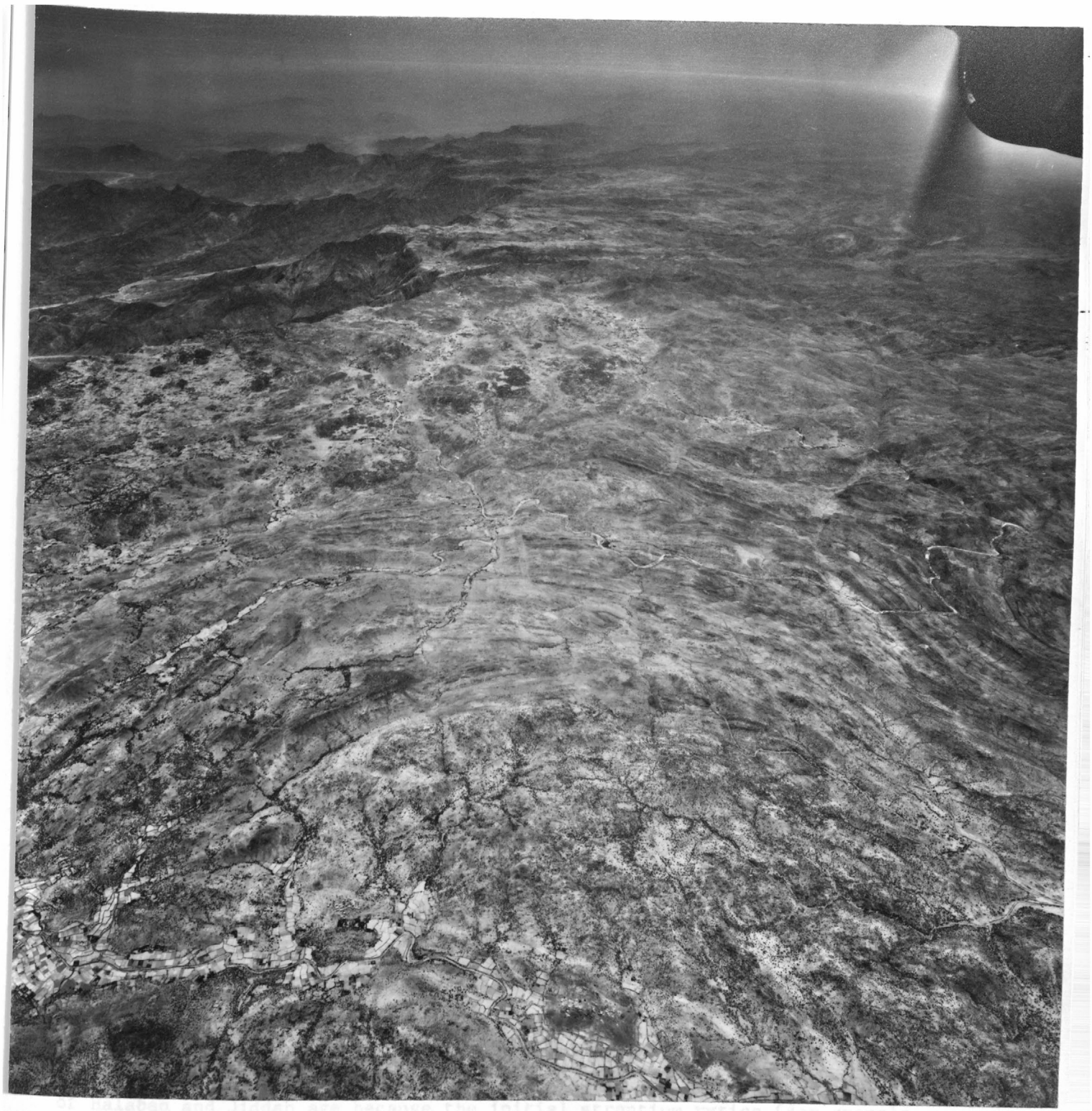

Figure 32. Aerial oblique view to the northwest of orthogneiss dome enfolded into amydaloidal metabasalt flows of the Baish group. K-Ar age of hornblende in the gneiss yielded an age estimate of 759+31my.B.P. Total fusion 782±35 my.B.P. (Fleck and others, 1976). The town of Baljarshi rests on the northwestern flank of the arch and overlooks the Asir escarpment. The dome represents rejuvenation of quartz diorite estimated to have first solidified at 890±67 ma.

as Ablah group west of a large gneiss domal complex in the adjoining quadrangles of Jabal Afaf (Hadley and Fleck, 1980b) and Jabal Ibrahim (Greenwood, 1975b) (fig. 33). The Fatimah group and abundant adjacent orthogneisses and intrusive granodiorites, dated at the Jiddah airport at 763 ± 159 Ma (initial $^{87}Sr/^{86}Sr$ = 0.7026; Fleck and others, 1980), is Ablah age and may represent the same or perhaps a different early collisional orogeny.

Late crustal history

Culminant orogeny and post-tectonic granites

The late crustal history of the Arabian Shield began sometime after 700 Ma ago and involved the final combining, consolidation, and cratonization of the Shield as a whole. The major orogeny associated with this late crustal history is rightly called the culminant orogeny; it was the ultimate orogeny involved in the cratonization of the entire Shield. The late crustal history is characterized by many gneiss domes (gneiss antiforms), granodioritic batholiths, and granite plutons that in general became progressively more potassic with decreasing age (fig. 34). The syntectonic and posttectonic, granodioritic and granitic, rocks constitute about 50 percent of the eastern part of the shield and diminishes in abundance westward across the western Shield.

The culminant orogeny began probably slightly before 650 Ma ago and extended to about 620 Ma ago. The histograms of rock ages on figure 35 show a distinct secondary mode between 650 and 620 Ma. One, presumably late, syntectonic granodiorite batholith associated with the large gneiss dome east of Qalat Bishah in the Jabal al Qarah quadrangle (Schmidt, 1981a) gives a high-quality, Rb-Sr isochron of 623 ± 18 Ma (initial $^{87}Sr/^{86}Sr$ = 0.7033; Fleck and others, 1980).

During the culminant orogeny widespread crustal heating caused amphibolite-facies metamorphism in the primary crustal rocks at intermediate crustal depths. Under these conditions, large, low-density bodies of trondhjemite and tonalite became gravitationally unstable adjacent to denser diorites and metaandesitic-assemblage rocks, and the trondhjemites and some tonalites rose as orthogneisses in elongated gneiss domes with north-trending axes. Rb-Sr dating of these massive orthogneisses at amphibolite facies indicates that many of them retained their original plutonic age (Halaban or Jiddah age). Large volumes of granodioritic magma with associated granodioritic migmatite accompanied or shortly followed the rise of the orthogneiss and was emplaced at about the same crustal level as the gneiss domes. The granodioritic magma, however, originated presumably from a crustal source that was deeper than the crustal level from which the trondhjemite orthgneiss rose because the orthogneisses rarely show but the slightest evidence of having been partially melted. The granodiorite magma may have partially melted from deep lower crustal rocks of Halaban and Jiddah age because the initial strontium ratios (for example, 0.7033) of the granodiorite normally would be expected from primitive rocks whose ^{87}Rb had evolved over 100 or at least over less than several 100 Ma.

The very widespread, culminant orogeny is believed to be caused by collision between the Halaban (Hulayfah) crust and an older continental crust at the east edge of--or somewhat farther east of--the exposed shield. Such collisional orogeny resulted in the final combining of the various

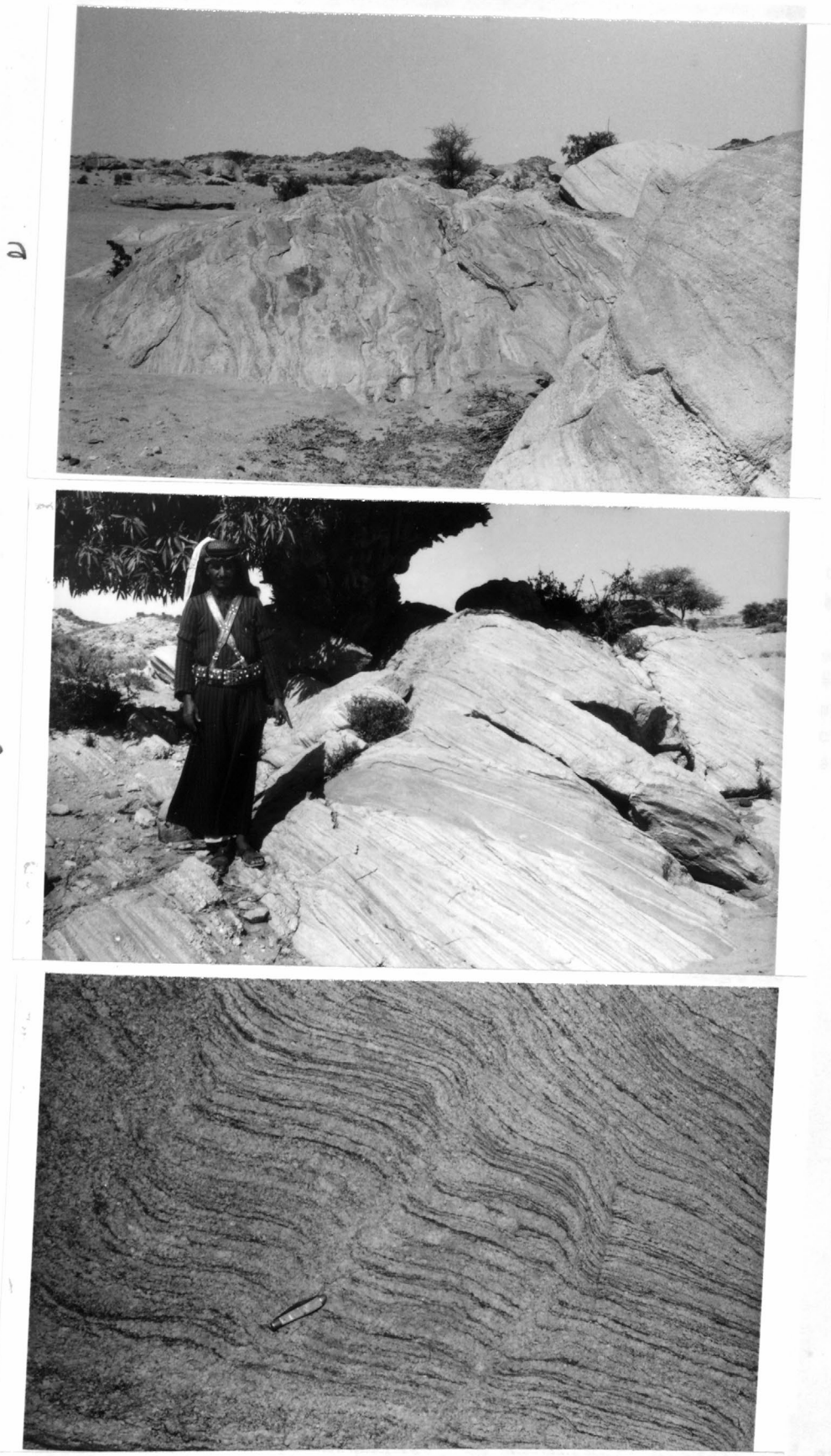

Figure 33. Schistose gneiss at Wadi Dhuqiyah 65km southeast of Al Ta'if The lineation dips east. (a), Biotite albite zenolithic fragment above pegmatite stringers (b), detailed drag folds in the gneiss limestone N 20°E sinestral movement (c), gneiss is considered to have been formed by the doming at the end of the Ablah cycle (1760), the crenulation later during Nejd time (± 570).



Figure 34a. Aerial view south of the eastern edge of the Khamis Mushayt gneiss dome flanked by paragneiss which in turn has subsequently been intruded by the Tindahah monzogranite. The Khamis Mushayt gneiss dome of 664±9 m.a.(Rb/Sr age) has metamorphosed volcanoclastic sediment of Halaban age (785-665 m.a.) or possibly of Jiddah age (780-850 m.a.). Subsequent to the doming of the Tindahah monzogranite batholith it was post-tectonically intruded on the eastern flank (K-Ar cooling age about 563). The village of Tindahah is in middle distance on right. (Fleck and others 1976; Fleck and others 1980)



Figure 34b. Jabal al Hidab at 19°40'N.lat., 42°45'E.long. Alkalic red granite gp intruded into paragneiss and amphibolite gneiss dome composed of Halaban rocks in a syntectonic dome formed during culminant orogeny. (mpa). The alkalic granite is post tectonic with a biotite K-40 Ar age of 595± 9 M.A. (Fleck)

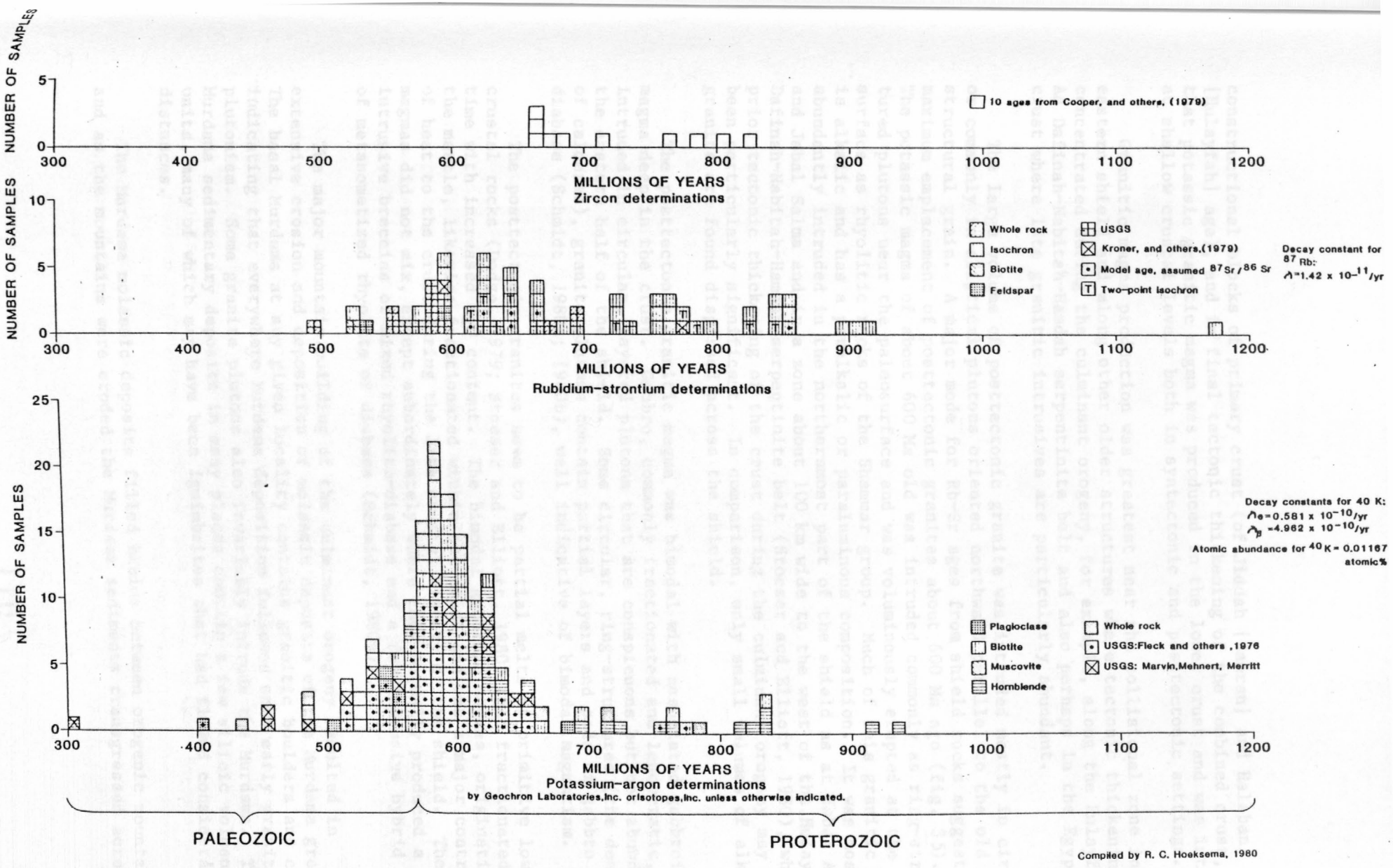

Figure 35. Geochronologic analysis of Paleozoic and Precambrian rocks.

constructional blocks of primary crust (of Jiddah [Samran] and Halaban [Hulayfah] age), and in final tectonic thickening of the combined crust, such that potassic granitic magma was produced in the lower crust and was intruded at shallow crustal levels both in syntectonic and posttectonic settings.

Granitic magma production was greatest near the collisional zone in the eastern shield and along other older structures where tectonic thickening was concentrated during the culminant orogeny, for example, along the Hulayfah-Ad Dafinah-Nabitah-Hamdah serpentinite belt and also perhaps in the Egyptian crust where late granitic intrusives are particularly abundant.

The large volume of posttectonic granite was intruded mostly in circular or commonly in eliptical plutons oriented northward parallel to the old structural grain. A major mode for Rb-Sr ages from shield rocks suggests maximum emplacement of posttectonic granites about 600 Ma ago (fig. 35). The potassic magma of about 600 Ma old was intruded commonly as ring-structured plutons near the paleosurface and was voluminously erupted at the surface as rhyolitic rocks of the Shammar group. Much of this granitic rock is alkalic and has a peralkalic or paraluminous composition. It was most abundantly intruded in the northernmost part of the shield as at Jabal Aja and Jabal Salma and in a zone about 100 km wide to the west of the Hulayfah-Ad Dafinah-Nabitah-Hamdah serpentinite belt (Stoeser and Elliott, 1980), where prior tectonic thickening of the crust during the culminant orogeny may have been particularly significant. In comparison, only small volumes of alkalic granite are found dispersed across the shield.

The posttectonic granitic magma was bimodal with associated gabbroic magma deep in the crust. Gabbro, commonly fractionated and leucocratic, was intruded in circular, layered plutons that are conspicuons but not abundant in the eastern half of the shield. Some circular, ring-structured (the deep roots of calderas), granite plutons contain partial layers and pods of gabbro and diabase (Schmidt, 1980a; 1980b), well indicative of bimodal magmatism.

The posttectonic granites seem to be partial melts of primitive lower crustal rocks (Dodge, 1979; Stoeser and Elliott, 1980) that fractionated in time with increased K_2O content. The bimodal gabbroic magmas, originating in the mantle, likewise fractionated within the crust and was a major contributor of heat to the crust during the late crustal history of the shield. The two magmas did not mix, except subordinately where they mutually produced a few intrusive breccias of mixed rhyolite-diabase and a few intrusive hybrid rocks of metasometized rhyolite or diabase (Schmidt, 1980a).

The major mountain building of the culminant orogeny resulted in extensive erosion and deposition of molassic deposits of the Murdama group. The basal Murdama at any given locality contains granitic boulders and cobbles, indicating that everywhere Murdama deposition followed some early granite plutonism. Some granite plutons also invariably intrude the Murdama. The Murdama sedimentary deposits in many places contain a few silicic volcanic units, many of which may have been ignimbrites that had flowed considerable distances.

The Murdama molassic deposits filled basins between orogenic mountains and as the mountains were eroded the Murdama sediments transgressed across them.

The thickest and most extensive deposits are found in the eastern part of the shield; extensive, but generally thinner deposits, are found in the western shield; and only remnants of youngest basal Murdama are found along the wide zone along the Hulayfah-Ad Dafinah-Nabitah-Hamdah serpentinite belt. This emphasizes that the highest orogenic mountains, along zones of most intensive orogeny, were along this serpentinite belt and along the Al Amar-Idsas fault zone. Gneiss domes, which are the roots of the orogenic mountains, are particularly abundant on either side of the serpentinite belt. Along the margins of the domes, only small, thin, remnant, conglomeratic deposits of Murdama are found; these are commonly younger than the youngest granite plutons in the area--Murdama deposits within the orogenic mountains were scant and late. Thick marble deposits associated with a middle formation of the Murdama group, are indicative of an already stabilized continental crust.

The quartz-feldspar-biotite and quartz sericite-chlorite schists of the Abt formation (and Ar Ridayniyah formation) are most probably of Murdama age and are a thick, fine-grained, easterly facies of the Murdama group. The Abt sedimentary rocks were subjected to especially intense, late tectonism in the vicinity of the Al Amar-Idsas fault. Alternatively, the Abt schist may be a continental-marginal, sedimentary rock that was associated with the crustal block east of the Al Amar-Idsas fault (region E, fig. 17), and was tectonically emplaced during the collision between this east block and the Halaban crust (fig. 36).

The large batholithic complex in the Ad Dawadimi area is composed largely of granodioritic and subordinate granitic rocks that intruded the Abt deposits (Al-Shanti, 1976). It has been suggested that the highly tectonized and metamorphosed Abt schist (and Ar Ridayniyah formation, as well) is older than Murdama and the culminant orogeny. However, 100 km northeast, similar syntectonic granodioritic batholithic rocks intrude Murdama deposits, and it seems likely that either the Murdama and Abt metasedimentary rocks of this area are of early culminant-orogeny age or that the broad area west of the Al Amar-Idsas fault was orogenically active later, possibly as late as 600 Ma ago or even to just prior to the Najd faulting. If the tectonism of the culminant orogeny did persist in some areas to 600 Ma ago or slightly later, then the large volumes of granodiorite in the Ad Dawādimī area were unusually late in comparison to the rest of the shield where posttectonic, high-K_2O granites were being intruded at this time. We cannot determine the time variability of the culminant orogeny because Murdama deposition was at different times in different places within a time span of about 50 Ma.

Tectonic remnants of ultramafic rocks and serpentinite gabbro, sheeted dike complexes, tholeiitic metavolcanic rocks, and oceanic-floor metasedimentary rocks occur in varying combinations in many places in the shield. Many of these have been described as tectonized and deeply eroded ophiolites of either oceanic or back-arc crustal origin (Frisch and Al-Shanti, 1977; Delfour, 1979b; Bakor and others, 1976; Al-Rehaili and Warden, 1980).

Remnants of ophiolites are to be expected considering that most of or all the shield is a composite of many primary constructional blocks originally separated by oceanic crust. Further, it is likely that the different dismembered ophiolites in different parts of the shield are of different ages



Figure 36. Oblique aerial photograph viewed to the southeast from lat. 23°05' north, long. 45°05' east near the east edge of the shield. The Al Lamar-Idsas fault bounds the east side of the Sirdah plain which is underlain by the Abt schist. The lobate overthrust fault front is apparent along the southeastern extension. An ophiolite melange marks the fault zone including a southern bifurcation south of Jabal Minassa. The outcrops east of the fault zone comprise the Ar Rayn granitoid province (Shanti and Gass, 1983) with volcanic facies in Umm Duffar west of calc-alkaline to alkalic plutonic rocks.

because different constructional blocks were combined at different times and involved different oceanic crusts and (or) back-arc basinal crusts.

Most of the exposed ophiolites of the shield are small remnants because erosion has been deep and only those remnants that had been structurally placed deep in the crust by tectonism have been preserved. All ophiolites should be associated with specific sutures between different constructional blocks, but the relation is obscured in most places.

The Hulayfah-Ad Dafinah-Nabitah-Hamdah serpentinite belt is a highly tectonized zone that was especially orogenically active during the culminant orogeny. This deeply eroded belt is most likely a suture zone in which in most places a mobilized serpentintite is the only remaining component of the former oceanic crust (Frisch and Al-Shanti, 1977; Schmidt and others, 1979). The much better preserved dismembered ophiolite at Bi'r Umq west of the serpentinite belt in the central shield, may be an ophiolite that was obducted (Al-Rahaili and Warden, 1980) before the suture closed during the collisional, culminant orogeny. The broad zone of major faults containing much tectonized serpentintite in the vicinity of--and within--the Al Amar-Idsas fault zone is also very likely a major tectonized suture zone (Al-Shanti and Mitchell, 1976; Schmidt and others, 1979).

Najd faulting event

The Najd faulting event or Najd orogeny of Brown (1972) was the final tectonism and final cratonization event of the Arabian Shield. East-west compressional forces acted one last time and the by then noncompressible, thick, cratonized shield was fractured along a few great shears (fig. 37) rather than by more penetrative internal compression as before. A northwest-trending, left-lateral, transcurrent fault system (Brown and Jackson, 1960; Moore, 1979) prevailed over the conjugate northeast-trending, right-lateral, transcurrent fracturing.

The shield was displaced left laterally more than 250 km (Brown, 1972) mostly along three major northwest-trending fault zones, each 5 to 10 km wide. This major, large fault movement on the Najd fault system is in a region 300 km wide by 1100 km long, but the effects of the Najd stresses can be found throughout the shield. At least some and possibly most of the northeast-trending structures between Jiddah and Yambu al Bahr (regions B, WS, and WC, fig. 17) may be as young as Najd age.

Each of the three major, northwest-trending fault zones is in part sinuous, braided, en echelon, and branching, and the whole movement system is convergent to the northwestern part of the shield and into the area of the ancestral Gulf of Suez. The sinuous and branching geometry of the fault zones resulted in a few extensional segments consisting of grabens filled with taphrogeosynclinal sedimentary and volcanic rocks of the Jubaylah group and a few ultra-compressional segments in which elongated gneiss antiforms (domes) rose (fig. 38).

The andesitic basalt volcanism of the Jubaylah group in the taphro-graben structures (Delfour, 1970; Hadley, 1974) trends from calc-alkalic to strongly alkalic in composition (fig. 24 and 28B), similar to some of the volcanism



Figure 37. Aerial view to the northwest of the Najd fault zone southwest of Afif. The infolded beds in near right are considered of Jibaylah and Shammar age with the Murdama group clastics on the near left infolded within metaclastics of Halaban age, according to J. Letalenet, B.R.G.M. Afif quadrangle.



Figure 38. Jabal Adhqan al Hajun at 22°41'N. lat., 44°06'E. long. Granite intruded into the Halaban group, at the southwestern base of the mountain, later sheared in the Najd fault zone near the end of shield cratonization. Aerial view northwest.

associated with large continental rifts. For the Najd system, however, these are small, localized continental pseudorifts. The Najd "grabens" formed in a crust that was fully continental and along newly formed, deep-crustal shear structures that tapped magma generated in the mantle.

The gneiss antiforms in the few ultra-compressional segments of the Najd fault system are exemplified in the Jabal Yafikh quadrangle (Schmidt, 1981b) where trondhjemitic orthogneiss, 3 km wide by more than 60 km long, rose within the fault zone at almandine-amphibolite-facies temperatures. The initial plutonic trondhjemite was part of the primary crust of Halaban (Hulayfah) age (dated, 766 $\pm$ 26 Ma old, initial $^{87}Sr/^{86}Sr$ = 0.7030; Kroner and others, 1979; area 6, fig. 17). The trondhjemite of the Halaban (Hulayfah) crust within the fault zone was heated by an increment of frictional heat within the highly sheared fault zone and additionally heated in part by mantle-derived magma. The magmatic heat is implied by small synkinematic plutons of alkalic granite that intruded along the margins of the gneiss antiform well within the fault zone. Mantle magmatism is implied by the very abundant (hence, voluminous) diabasic dikes of Najd age that intruded large areas between the major faults, by the mafic volcanism in the Jubaylah group, and by strong magnetic anomalies over most Najd fault zones, that may imply the presence of gabbroic intrusions at depth. The Najd-age magmatism was bimodal.

A few dated diabase plugs and granite plutons within the Najd fault zones and a few dated andesitic basalt flows in the Jubaylah group average about 530 $\pm$ 20 Ma by K-Ar, whole-rock method, but such a date for the Najd faulting event is too young. A high quality, whole rock Rb-Sr isochron of 577 $\pm$ 15 Ma (Baubron and others, 1976, p. 58) on a granite is probably only slightly older than the Jubaylah group, in that the granite intrudes the Murdama group and disconformably underlies the basal Jubaylah conglomerate. The granite date agrees with the suggestion that algal fossils in limestone of the Jubaylah group are about the age of the Precambrian-Cambrian boundary (about 570 Ma; Cloud and others, 1979; Binda and Ramsay, 1980). The Jubaylah was folded into asymmetric synclines during the final Najd fault movement, and K-Ar biotite dates averaging about 550 Ma (table 8) may represent this last spasmodic movement of the cratonization, whereas the 530 Ma average may represent crustal cooling after uplift and erosion. At least the northwestern part of the Najd fault system was covered by stable continental quartz sandstones by Late Cambrian time. Nearby in Jordan trilobites in limestone within the stable sandstones are dated as early Middle Cambrian (Bender, 1975, p. 16).

Age and strontium evolution

An overview of the evolution of the Arabian Shield in terms of Rb-Sr whole-rock geochronology is succinctly shown on figure 39 (adapted from Fleck and others, 1980). On figure 39, the primary crusts of the several volcanic-magmatic arcs of Baish-Bahah, Jiddah, and Halaban ages are well represented by low initial strontium ratios for the volcanic and plutonic rocks between 900 and 680 Ma old. The partial cratonization of Ablah age (early restricted collisional orogeny) is represented by granodioritic rocks between about 775 and 740 Ma old; these rocks have initial strontium ratios greater than those of the primary crusts. The final cratonization of the entire Shield is represented by granodioritic and granitic rocks between about 660 and 580 Ma old; these abundant rocks again have initial strontium ratios greater than those of the primary crust.

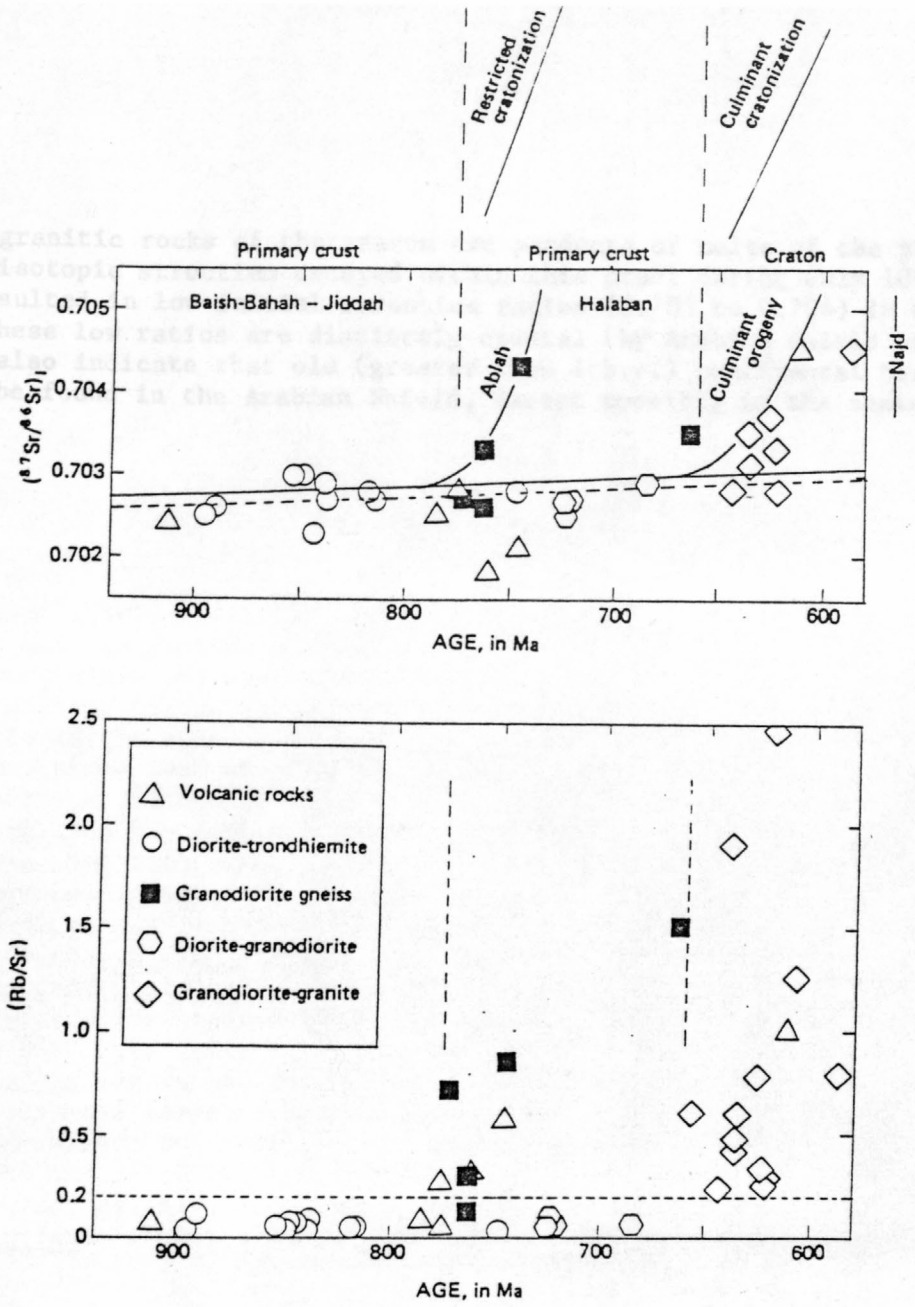

Figure 39. Diagrams showing variations in initial $^{87}Sr/^{86}Sr$ (upper diagram) and Rb/Sr (lower diagram) ratios with age (adapted from Fleck and others, 1980, fig. 26; event and rocks on upper diagram added for this report). Vertical dashed lines show major changes in strontium-isotope composition and Rb/Sr ratio of magmas corresponding to an earlier, regionally restricted orogenic event of partial cratonization of Ablah age and to a later, shieldwide culminant orogeny and cratonization. Strontium-evolution line (solid line; Faure and Powell, 1972) representing single-stage evolution from meteorite to average modern island arc is compared with least-squares fit (dashed lines) for Arabian Shield data having Rb/Sr ratios less than 0.2.

The granitic rocks of the craton are products of melts of the primary crust in which isotopic strontium decayed within this crust during only 100 to 300 Ma and resulted in low initial strontium ratios (0.703 to 0.704) in the granitic melts. These low ratios are distinctly crustal (by Arabian Shield standards), but they also indicate that old (greater than 1 b.y.) continental basement may not be found in the Arabian Shield, except possibly in the easternmost part.

PALEOZOIC SEDIMENTARY COVER ROCKS AT EDGE OF SHIELD

Cambro-Ordovician sandstones

Siq Sandstone

Except for a gap of 130 km along the eastern end of the northern flank which is occupied by the Great Nefud and 420 km along the eastern rim where the Khuff Limestone Formation of Permian age overlaps, the landward edge of the Arabian Shield is covered by sandstone beds of Cambro-Ordovician age. Of these, the Siq Sandstone is probably the oldest in northwest Arabia. It is a reddish-brown massive and arkosic arenite exposed immediately above the crystalline rocks at Sha'ib as Siq, lat. 35°56' E., long. 28°04' N., where Leopold Kober first saw it in 1910 (Kober, 1919). There the Siq Sandstone is exposed in a 65-m vertical cliff below a thinner section of reddish-brown, somewhat more stratified, flaggy sandstone on the plain above (fig. 40. From here the Siq extends eastward beneath the upland surface of the Hisma plateau to the isolated stacks and pinnacled mesas of the stratigraphically higher white and buff exposures of the Ram-Umm Sahm Sandstone.

The basal few meters are gritty arkosic sandstone and conglomerate containing pebbles from the underlying crystalline rocks, but the more massive vertical walls of the Siq are composed of fine- to medium-, occasionally coarse-grained quartz sandstone, channel crossbedded with most foresets to northwest and northeast. The beds extend northward into Jordan where Bender (1974b) considered them to be nonmarine and Lower Cambrian, the Quweira Sandstone of Quennell (1951). The flaggy upper member, which forms distinctive plains and benches, contains lenses and layers of silt, clay, and some manganiferous and hydrated iron-oxide concretions which on weathering leave a cavernous surface (fig. 40). Irregular calcareous cement also causes a cavernous weathering similar to that of the oxides. The reddish-brown-weathering Siq Sandstone thickens to 115 m above Wadi Hujayil 50 km to the southeast, and to 223 m, 10 km farther at Wadi Amdan, where it overlies the Jubaylah group across a basement graben. There the top of a middle massive section forms a bench 135 m above the shield rocks, and a second flagstone unit of the upper section extends above to the base of the younger cliff forming and massively crossbedded Ram-Umm Sahm Sandstone (fig. 40b). The sandstone thins southeastward and becomes more thin bedded; 275 km distant (38°42' E., 26°24' N.) in the Qalat as Sawrah quadrangle, the Siq is about 90 m thick at a 50-m cliff 7 km north of the northern rim of the shield. The lower section there is massive, red and tan, tabular, and trough-crossbedded sandstone under a 5-m thick slab of finer-grained silty sandstone whereon are trace fossils.

The Siq Sandstone questionably extends eastward along the northern edge of the shield from the Qalat as Sawrah area as far as long. 40°25' E., where outliers of flat-surfaced sandstone cap mesas in the easternmost of three basement grabens extending southeastward into the shield along the structural direction of the Najd fault system. West of long. 40°25' E., other outliers extend southward intermittently to the latitude of Al Madinah (lat. 24°30' N.). Most are small except in the vicinity of Bi'r Suwaydirah, east of Al Madinah, where about 250 km^2 of sandstone underlies the plain along a major Najd fault zone. The sandstone doubtless extends northwest under the Harrat Khaybar (Delfour, 1977, Bigot and Chapelain, 1973). The lithology is that

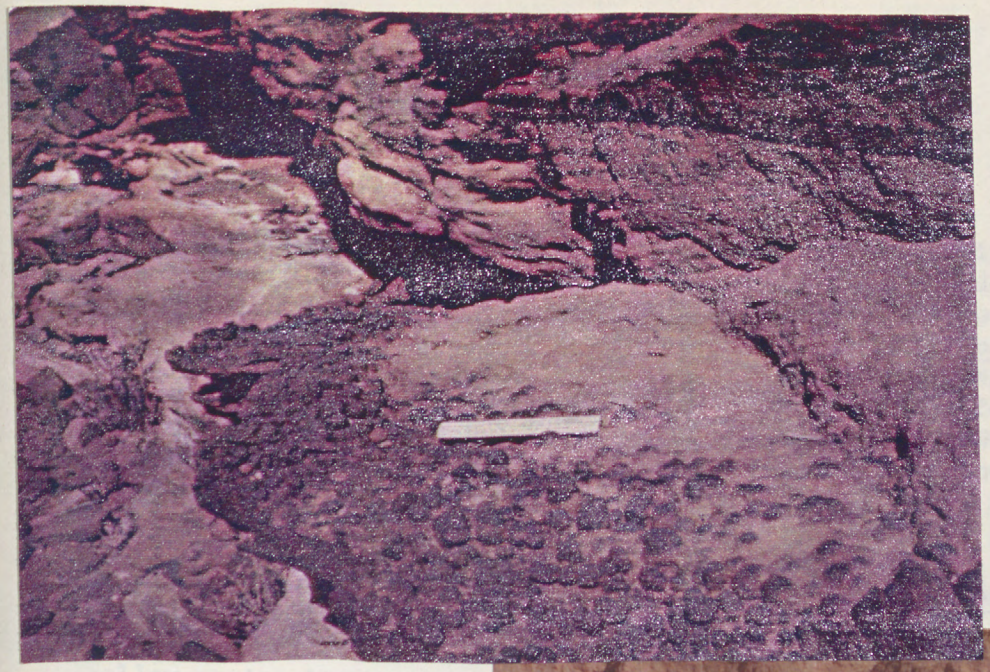

Figure 40a.

Ferric and manganiferous concretious in lenses and seams within the Siq Sandstone at the upper rim of the basal sandstone at the type locality.

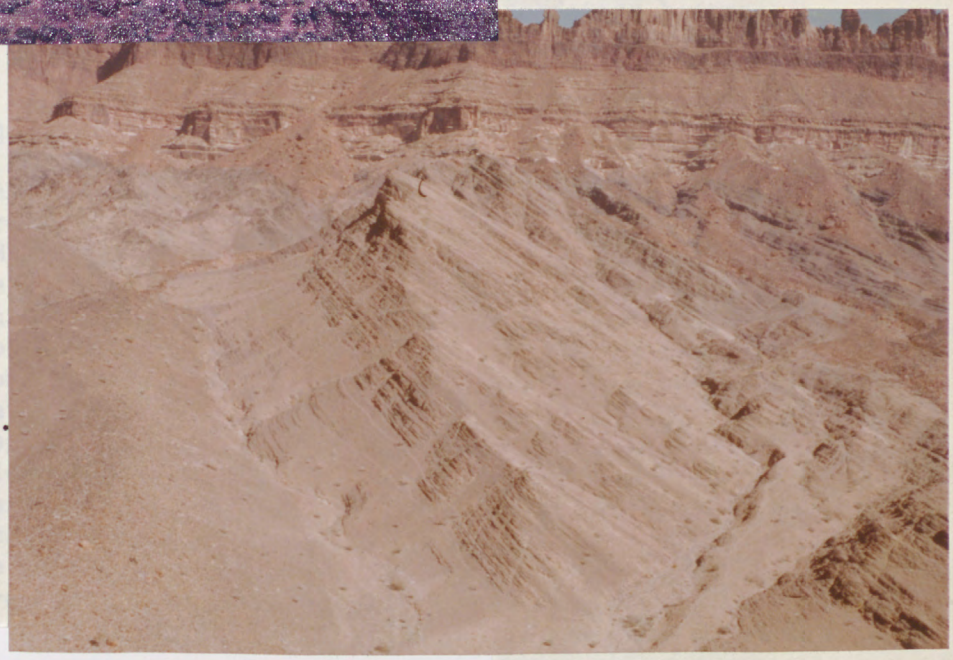

Figure 40b.

Siq Sandstone resting horizontally on Precambrian Hadiyah sediments and beneath pinnacled Ram Umm Sahmand Saq Sandstone. Headwaters of Wadi Shawaq.



Figure 40c.

Cruziana sp. track in Siq Sandstone. Markings to the right of the knife appear to be grazing marks of a gastropod, probably Climactichnites (?) sp. of Late Cambrian age. Near Jabal Abadiyah.

of the Siq Sandstone farther northwest, and we have shown it as such although no fossils were found except at Qalat as Sawrah (identified by A. Seilacher, written communication, 1978) and considered by Seilacher to be of Late Cambrian age. They are Cruziana sp. (not Cruziana aff. C. furcifera d'Ordigny nor Cruziana huberi (Meunier)), and what appear to be radula marks of a large grazing gastropod, possibly Climactichnites sp., which is found elsewhere in the Potsdam Sandstone of Late Cambrian age (fig. 40). At Wadi Siq the flaggy sandstone a few meters above the basement crystalline rocks contains limonite and psilomelane as well as calcareous concretions (fig. 40) reminiscent of the manganiferous and cupiferous sediments in the upper part of the Middle Cambrian Burj Limestone Group in southwest Jordan (Bender, 1965, 1974b). If this correlation is valid and if the Cruziana sp. and Climactichnites (?) beds 275 km southeast are Upper Cambrian (Potsdamian), the sandstone becomes progressively younger toward the southeast and represents an on-lapping shallow marine tongue.

Saq and Ram-Umm Sahm Sandstones

The Saq Sandstone of Arenigian age occupies the northeast flank of the shield where it is stratigraphically below the Hanadir Shale of Llanvirhian age (Bender, 1963) (lowermost Middle Ordovician) and above the crystalline rocks. Farther south the sandstone crops out between the crystalline rocks and the Permian Khuff Limestone, which overlaps the younger Hanadir Shale as well. The large-scale, planar-crossbedded, white, tan, and gray Saq Sandstone resembles and is stratigraphically equivalent to the Ram-Umm Sahm Sandstone of northwest Arabia and southwest Jordan in that it is a mature arenite, in many places often lacking arkosic beds. In places it rests on basement rocks without a basal conglomerate, although commonly there are lenses of grit and the basal few meters are reddish with iron cement. Cement may also be gypsiferous as well as calcareous, but the cement generally is present above the basal beds. Rare well-rounded pebbles, mostly quartz, some citrine, form local lenses in large-scale planar crossbedding of finer sand (N. Layne, written commun.; Powers, and others, 1966).

The only evidence for age reported heretofore are trace fossils collected from near the southern end of the outcrop near the top of the sandstone at Jabal Haqil, 37 km northeast of ad Dawadami. These were identified by P. E. Cloud, Jr., as Cruziana af. C. furcifera d'Orbigny and C. huberi (Meunier) which belong to the Cruziana rugosa group of Seilacher (1970). The C. rugosa traces are found in shale lenses in northwest Arabia and in Jordan in the upper part of the Ram-Umm Sahm Sandstone where they are considered to be of Arenigian age (uppermost lower Ordovician) (Bender, 1975).

Wajid Sandstone

The southeast edge of the shield is covered by the Wajid Sandstone, which crops out beneath the Permian Khuff Formation at Wadi ad Dawasir, 420 km south of the southernmost exposure of the Saq Sandstone. Flat-lying or gently arched, unmetamorphosed, and broken only by late Tertiary and Quaternary high-angle tension faults, and earlier considered devoid of fossils, it could be assigned only a pre-Permian and post-shield age.

The type locality is Jabal Wajid at lat. 19°06 N., long. 44°27 E., where a thickness of 950 m was calculated (Powers and others, 1966). More recently the sandstone has been drilled down-dip, east of the northern end of the outcrop where a thickness of 500 m was measured beneath a disconformity, a thickness comparable to an estimate of 600 m by Alabouvette and Villemur (1973). Shaly beds above the disconformity contain three chitinozoan species of Silurian age (D. Hemer, oral commun. ~) In addition, a recent study of the outcrop belt has yielded Tigillites, arthropod trails (Cruziana sp. ?), and conical or circular structures at the base of the Wajid (Alabouvette and Villemur, 1973), forms that are similar to those in the upper Saq Sandstone and, farther north, the Ram-Umm Sahm. Thus the Wajid in Jabal Wajid appears to be uppermost Lower Ordovician or possibly somewhat younger, as the Tigillites trace fossils are most abundant in the Tabuk Formation farther north.

The lithology also tends to make such an age reasonable. The bulk of the sandstone is composed of mature quartz grains and displays large-scale planar crossbedding. Indeed, the disconformity reported by Alabouvette and Villemur may be equivalent to the top of the Saq Sandstone and the bottom of the Tabuk on the northern flanks of the shield, although the basal Tabuk Hanadir shale with the Didymograptus index graptolite is missing. Intermittent exposures and subcrop in the Al 'Arid region east of Jabal Wajid including sandstone, boulder beds and fossiliferous shale ranging in age up to Middle or Lower Permian have recently been included in the Wajid Sandstone (McClure, 1980). The boulder beds appear to be glacigene and of Permian-Carboniferous age, similar to deposits in Yemen (Roland, 1978), in northern Ethiopia (Dow and others, 1971), and Oman (Frakes and others), so the uppermost outcrop farthest from the shield may be as young as Permo-Carboniferous.

Gabbro plugs are intruded into the Najd fault zone; one of possible 502-512 Ma age that was shown to G. F. Brown by Jaques Delfour is intruded into the Jubaylah. A similar rock at Wadi ar Rika (lat. 28°28' N., long. 44°34' E.), that was intruded after cessation of movement on the Najd faults, gave a whole-rock K-Ar age of 513 ± 17 Ma B.P. for the chilled edge of the plug (sample 149x; and 458 ± 15 Ma for the deuterically altered core sample 149y, table 8). These may be cooling ages but more recently a gabbro plug has been discovered, supposedly intruded into a lower disturbed part of the Wajid Sandstone but eroded and buried by the upper planar crossbedded sandstone. Thus if the plug in the Wajid terrane is of similar age to those intruded into the Jabaylah and all are intrusive, the lower part of the Wajid Sandstone in the southern exposures could be Upper Cambrian so that the structure may actually be a kopje (Stoesser, oral commun.). The descriptions of Alabouvette and Villemur show no organic forms in the south such as occur farther north near Wadi Dawasir (Jackson and others, 1963); furthermore, the calcareous cement and trough crossbedding resemble features described in the Siq Sandstone (Hadley, 1973), but by no means prove correlation.

A few widely scattered outliers deep within the shield are sandstone. A small sandstone crest at Jabal Tin, lat. 22°N, 600 km south of the northern rim of the shield and 260 km northwest of the nearest outcrops of the Wajid, resembles the Wajid. It is composed of 16 m of white, fine-grained massive sandstone, flat lying above basement gneiss.

Similarly a prominent outlier capping Jabal Tamiyah, 425 m above the desert floor at lat 25°36°N, long. 42° E., and 80 km west of the Saq Sandstone, at the eastern edge of the shield, is 82 m thick, flat lying, and crossbedded. There is no basal conglomerate as at the base of the Saq Sandstone near Ha'il. A Saq age at Jabal Tamiyah and a Wajid age at Jabal Tin (near Khurma) fits the concept of the younging of the lower Paleozoic fringe sandstones toward the southeast.

Khuff Formation

The eastern edge of the shield between outcrops of the Saq Sandstone and the Wajid Sandstone is nonconformably overlain by the Permian Khuff formation. Outcrops directly overlying the basement and overlapping the Saq sandstone are mostly in the area east of the Alamar-Idas fault, extending from 22° to 40°N to lat 24°28 N. Farther south the Khuff may rest on the basement, but the exposures are poor and may be those of an older Paleozoic paleosol.

The Khuff ranges in thickness to as much as 320 meters, but only 171.4 m was measured at the reference section between Wadi ar Rayn and Jabal ath Thwayr (Powers, 1968). The base is a lateritic duricrust resulting from Paleozoic weathering basal conglomerate and sandstone, only a few meters thick at most; the bulk of the formation above the paleosol is neritic dolomite, shale, or claystone, and limestone, all dipping gently eastward and resulting from a widespread marine transgression at the end of the Paleozoic. It has been divided into five informal members based on lithofacies changes both vertically and along the strike (Delfour and others, 1982).

MESOZOIC SEDIMENTARY ROCKS

Khums Formation

Definition.--The Khums Formation takes its name from Wadi Khums where it was first mapped in the foothills east of the Tihamat al Yemen (coastal plain) near the Yemen border (lat. 16°50' N., long. 43°01' E.) (Brown and Jackson, 1959.) At the type locality, crossbedded and graded grit of the Khums nonconformably overlies Precambrian crystalline rocks where the contact is not a fault. Elsewhere it overlies the Wajid Sandstone of Cambro-Ordovician age. The uppermost quartzitic sandstone of the formation underlies Upper Jurassic limestone, apparently comformably (fig. 41).

Occurrence and thickness.--The Khums Formation crops out in a belt 3 km wide or less and extends parallel to the Red Sea rift zone for 35 km north and south of Wadi Khums. A similar belt lies 10 km southeast and extends into the Yemen; both belts are partly bound by faults. Outliers occur on the crest of the scarp mountains to the east. The formation is of variable thickness, and because it is highly block faulted in places along the flank of the Red Sea rift, the thickness is somewhat difficult to estimate. Gillman (1968) measured a maximum of 880 m in the faulted section of the Wadi Khums belt where the sandstone is underlain by the Wajid Sandstone and overlain by the Jurassic Amran Formation. The Khums narrows to 10 m at the north end of the belt on the banks of Wadi Jizan, but its top is a fault. Thirty kilometers north of Wadi Jizan,

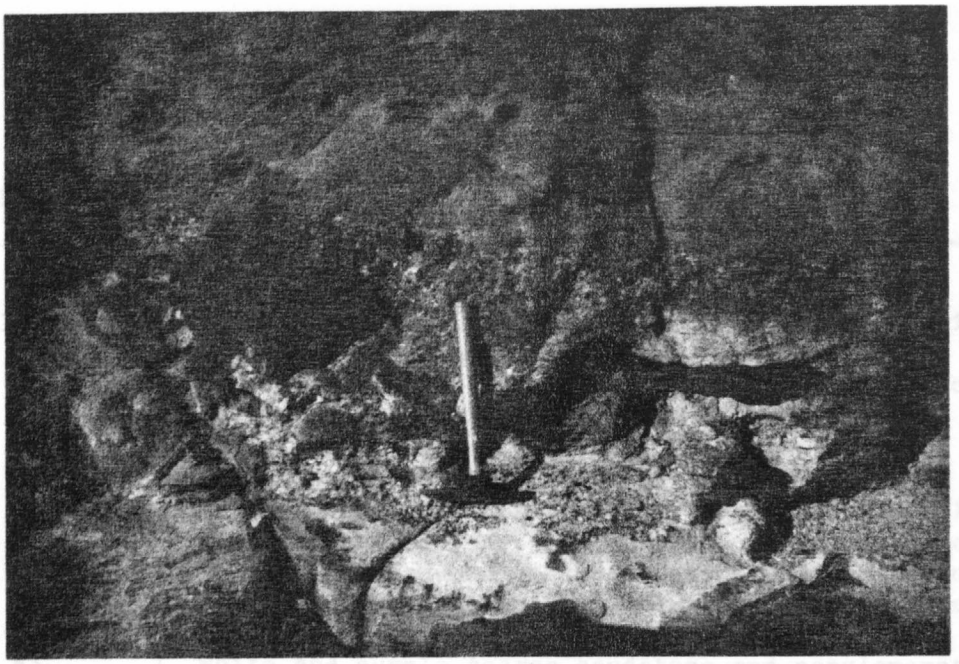

Figure 41a. Contact at base of Khums Sandstone marked by grit. Hammer rests on top of Wajid Sandstone.

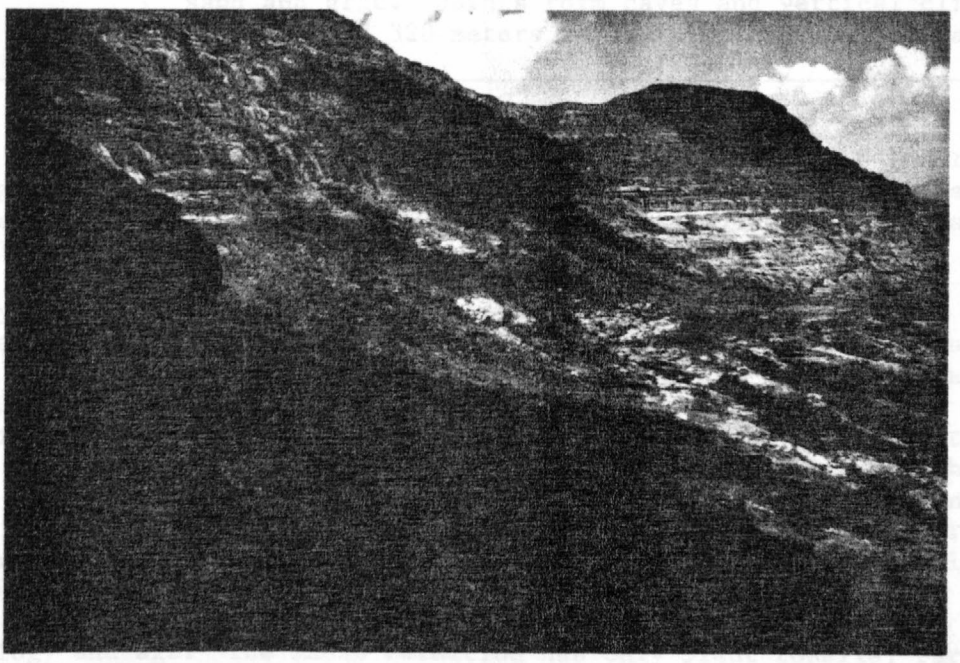

Figure 41b. View of the south slope of Jabal Hassan with the contact between the Cambro-Ordvican white Wajid Sandstone below and the tan Triassic Khums Sandstone above.

an isolated outcrop measures 100 m in thickness, and about 145 km northwest of the Wadi Khums locality and 15 km northwest by Ad Darb, a similar tectonized and quartzitic sandstone is associated with calcareous and kaolinitic beds that contain rare molluscan steinkerns of the Jurassic marine beds of Yemen, the Amran Series. However, the bulk of the small outcrop northwest of Ad Darb could be the lower Paleozoic Wajid Sandstone which caps the mountains to the east; a sliver of upper Khums with Amran-type fossils may overlie the Wajid. On the crest of the scarp mountains east of the Tihamat, the Khums clastic deposits overlie the Wajid Sandstone on the mesa crest of Jabal al Qahar and Abu Hasan 75 km north of Wadi Khums (fig. 41). At Jabal Abu Hasan, between altitudes of 1541 to 1861 m, we measured 320 m where the beds are relatively undisturbed. Subsequently, D. G. Hadley, and D. L. Schmidt measured a thickness of 160 m at nearby Jabal al Qahar (written commun., 1974). R. E. Anderson (1979, p. 20) measured another outlier near Alb Pass 40 km east of Abu Hasan on the high plateau of Al Yemen in Saudi Arabia near the Yemen border where he found a thickness of 125 m, the same thickness as that measured by Geukens (1966, p. 8) 90 km southeast near Sa'dah in Yemen for clastic rocks (Khohlan Series) above the basement and below the Upper Jurassic Amran Series.

Lithologic character.--The Khums Formation in the rift zone is mostly a hard quartzitic sandstone containing minor beds of siltstone and occasional pebbles and boulders of quartzite. Granitoid and metamorphosed basement rocks are well rounded in the basal grits. The siltstone is gray green or gray and reddish brown, and contains pebbles. The beds are highly disturbed and intruded by Tertiary basalt dike swarms that have contact-metamorphosed the sediments. Michel Gillman (1968) examined the Khums outcrops in more detail along the foothills and divided the formation into three members: A lower crossbedded and coarse sandstone (480 m); a middle member of fine-grained phosphatic sandstone, conglomerate, ferruginous shale (violet colored) with some tuffaceous beds (110 m); and an upper member of fine-grained siliceous sandstone (290 m). We, however, suggest that the lower sandstone probably in Wajid Sandstone. Our section on Jabal Abu Hasan, where the bedding is approximately horizontal, was measured in 1965 and is as follows:

Khums Formation on Jabal Abu Hasan

Altitude (meters)	Thickness	Amran Formation
1861		Upper member.
	189	Alternate massive and bedded tan sandstone, considerable large-scale cross bedding
	48	Tan massive sandstone; lower 10 meters has a reddish cast.
		Basal and middle member
1623		Top of bench is composed of dark red, sandy clay shale and silty sandstone; some concretionary sandstone, locally calcareous; algal markings and questionable echinoid fragments; upper silty beds cavernous. Boundary between clastic and calcareous sediments transitional, increasingly calcareous upward.
	83	White and purple coarse sandstone and conglomerate; minor shale lenses, poorly sorted pebbles and grains, mostly well rounded, white quartz although some are fragments of phyllite, andesite and quartzite. Calcareous cement but no recognizable organic remains were found in the samples collected.
	TOTAL 320	
1541	160+	Wajid Sandstone. Massive white and tan medium to coarse grained sand and grit. Joints form caves and vertical cliffs. This thickness of 320 meters maybe in excess due to imar block faults.

Anderson (1979) divided the Khums formation near Alb Pass into a lower 35 m of alternating sandstone and pebbly ferruginous shale, a middle 80 m of massive buff and crossbedded buff sandstone and gritstone, and an upper 10 m of grayish-red, red-purple and pale-yellow sandstone with ferruginous beds.

Lithology considerably dissimilar to the Khums Formation but cropping out in Yemen between basement rocks or the Wajid Sandstone and the Amran Series was described by P. Lamare (1930b) as 215 m thick near Amran, 280 m thick at Jabal Ashmur 20 km to the west (quoting C. Rathjens), and 700 m thick near At Tur, 40 km still farther west, and near the western edge of the scarp mountains; this gives an increase in thickness toward the Red Sea graben similar to that in Saudi Arabia. The beds change from alternating sandy marl and sandstone and lignitic beds in the upper part near Amran to increasingly arenaceous outcrops westward toward the Red Sea. These rocks in the Yemen are called the Khohlan Series (Geukens, 1960).1/

Paleontology and age.--The Khums Formation has only plant fossils, rare in outcrop, and the trace fossil Arthrophycus (Anderson, 1979, p. 20), a trail made by arthropods or worms and generally considered Ordovician-Silurian, although similar furrows are reported from Cretaceous and upper Tertiary beds (Hantzschel, 1975, p. W38-39). The beds containing questionable algal impressions and echinoid

1/ Since this was written a carbonaceous section of glaciogene sediments has been mapped above the basement or Wajid Sandstone and below the Khohlan Sandstone (Kruck and Thiele, 1983).

spines at Jabal Abu Hasan may belong in the overlying marine Amran Series. In Yemen, Geukens (1960) found worm borings, possibly Arthrophycus, in the uppermost beds at the same stratigraphic position as that described by Anderson near Alb Pass. P. Lamare and C. A. Carpentier (1932) reported a flora in lignitic lenses which he considered Lower Jurassic (Lias) or possibly uppermost Triassic (Rhaetian) which could be coeval with the Khums Formation. However, carbonaceous beds occur in marl and sandstone near Amran, 115 kms southeast of the Khums locality, where the lithology is considerably different.

The Khums Formation can be any age from Cambro-Ordovician to Early Jurassic, on the basis of adjacent formations, but the bulk of the evidence suggests that the Khums is paraconformable on the Cambro-Ordovician sandstone (Anderson, 1979) and possibly equivalent to part or all of the nonmarine Late Triassic Minjur Sandstone of central Arabia. The lithology at the Amran locality is similar in that the Minjur contains lignite beds in the subsurface at Riyadh. Three new species of the conifer Brachyphyllum, found in samples from below 1,110 m in a test water well at Riyadh were considered possibly to be Middle Liassic, entirely on the basis that the overlying Marrat Formation is Toarcian (upper Liassic) (Boureau, 1956), but because of the fragmentary nature and absence of stomata in the descriptions of the only conifer identified from the Yemen, Pagiophyllum peregrinum Sch., Boureau could not compare it with the Minjur fossils. However, in central Arabia the Minjur is truncated by a regional unconformity (Dubay, 1969) and Cameron (1974) in more recent study of palynomorphs from it has proven it to be of Late Triassic age.

Amran Formation

Definition.--A blue-gray lithographic limestone (fig. 42, 43), silicified and brecciated, crops out above the Khums Formation in the foothills at the east edge of the Tihamat of Yemen south of Wadi Khums. It was mapped in 1951 (Brown and Jackson, 1959) and named for the Hanifa Formation of Late Jurassic age in central Arabian on the basis of the similarity of its fossils to those of the Hanifa (Powers and others, 1966). Subsequent work has established that the fauna includes a greater time span than that of the Hanifa, as the Hanifa has later been more precisely defined, and that the rocks are homologous to the Amran Series of Yemen (Lamare, 1930b).

Occurrence and thickness.--The Amran Formation shown as the Hanifa Formation on the geologic maps of the Asir quadrangle (Brown and Jackson, 1959) and of the Arabian Peninsula (USGS-ARAMCO, 1963), crops out at Wadi Fija, 3 km north of Wadi Khums, and in faulted blocks about 10 km southeast of Wadi Khums near Umm Araj (lat. 16°46' N., long. 43°6' E.). Ten kilometers farther southeast, a more extensive outcrop extends 20 kms along the Yemen boundary and into Yemen. Smaller outliers occur on Jabal al Qahar-Abu Hasan and near Alb Pass where calcareous beds apparently disconformably overlie the Khums Formation. The Amran Formation is extensively exposed in northern Yemen; the name is taken from outcrops near the town of Amran, 45 km northwest of San'a' (Lamare, 1930b, Geukins, 1960, 1966, Grolier and Overstreet, 1978). Near Umm Araj, Gillman (1968) divided the formation, there 720 meters thick, into two major divisions, a lower unit (500 m) composed of three members and an upper unit (220 m) of phosphatic limestone.



Figure 42a. The Amran (Hanifa) limestone above Khums Sandstone on the top of Jabal Hassan.



Figure 42b. Toe of Asir mountains east of Gizan with the Jurassic Amran (Hanifa) Limestone dipping west beneath the coastal plain and overlying the Khums Sandstone which crops out in the left foothills. The sediments have been downfaulted to the west. At Wadi Khums, east of Jizam.

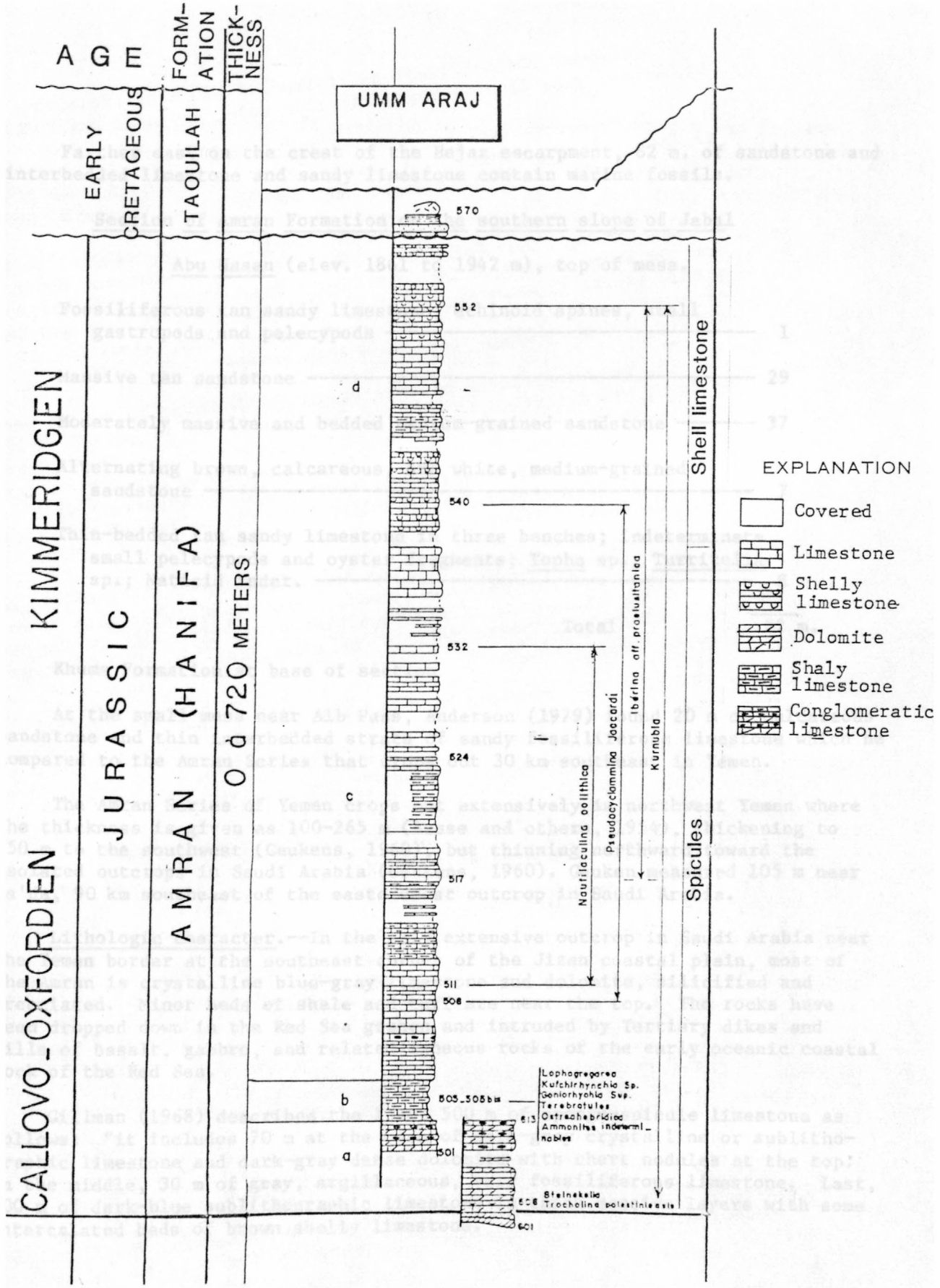

Figure 43. Type section of the Amran (Hanifa) formation at Umm Araj. From Michel Gillman, AUXIRAP.

Farther east on the crest of the Hejaz escarpment, 82 m. of sandstone and interbedded limestone and sandy limestone contain marine fossils.

Section of Amran Formation on the southern slope of Jabal Abu Hasan (elev. 1861 to 1942 m), top of mesa.

Fossiliferous tan sandy limestone, echinoid spines, small gastropods and pelecypods	1
Massive tan sandstone	29
Moderately massive and bedded medium-grained sandstone	37
Alternating brown, calcareous, and white, medium-grained sandstone	7
Thin-bedded tan sandy limestone in three benches; indeterminate small pelecypods and oyster fragments; Topha sp., Turritella sp.; Naticid indet.	8
Total	82 m.

Khums Formation at base of section

At the small mesa near Alb Pass, Anderson (1979) found 20 m of calcareous sandstone and thin interbedded strata of sandy fossiliferous limestone which he compared to the Amran Series that crops out 30 km southeast in Yemen.

The Amran Series of Yemen crops out extensively in northwest Yemen where the thickness is given as 100-265 m (Basse and others, 1954), thickening to 550 m to the southwest (Geukens, 1960), but thinning northward toward the isolated outcrops in Saudi Arabia (Geukens, 1960). Geuken measured 105 m near Sa'da, 90 km southeast of the easternmost outcrop in Saudi Arabia.

Lithologic character.--In the only extensive outcrop in Saudi Arabia near the Yemen border at the southeast corner of the Jizan coastal plain, most of the Amran is crystalline blue-gray limestone and dolomite, silicified and brecciated. Minor beds of shale and tuff are near the top. The rocks have been dropped down in the Red Sea graben and intruded by Tertiary dikes and sills of basalt, gabbro, and related igneous rocks of the early oceanic coastal rock of the Red Sea.

Gillman (1968) described the lower 500 m of sponge-spicule limestone as follows: "it includes 70 m at the base of dark-gray crystalline or sublithographic limestone and dark-gray dense dolomite with chert nodules at the top. In the middle, 30 m of gray, argillaceous, very fossiliferous limestone. Last, 400 m of dark-blue sublithographic limestone in thick massive layers with some intercalated beds of brown shelly limestone."

The upper shelly limestone "formed of 220 m of violaceous fragmental limestone, gray blue lithographic limestone, and marl and shale (with chi

In Yemen the limestone grades into a sandy facies, which farther east to interbedded gypsum and, in the eastern extension of Wadi Jauf, to salt that crop out in diapiric structures at the throat of Wadi Hadramaut (Brow

Nature of contact.--The Amran Formation rests parallel to the bedding the underlying Khums Formation, but as the Amran contains Upper Jurassic fo and the Khums Formation is most likely Upper Triassic (Rhaetian) or lower middle Liasic (lowermost Jurassic), there appears to be a substantial hiatu or a period of extremely slow deposition prior to deposition of the marine Amran. Geukens (1960) considered this an epirogenic period.

The only occurrence of overlying beds of Mesozoic age is reported by Gillman, who described 10 m of "coarse sandstone, breccia with limestone fra ments, and brown shale" which could be compared to the Lower Cretaceous Tawi sandstone in Yemen. However, the Early Cretaceous age may be open to questi as the Tawilah Group of sandstone beds cannot be separated with certainty fr the overlying, lithologically similar Medj-zir Series, which contain Paleoce or Eocene fossils (Geukens, 1960; Grolier and Overstreet, 1978).

Paleontology and age.--On the Asir 1:500,000-scale geologic map (Brown and Jackson, 1959), the Amran Formation was named the Hanifa Formation on the basis of the similarity of the megafossils and lithology to the Hanifa Formati in central Arabia. These fossils, as identified by R. A. Bramkamp (written commun., 1951) are:

Basal fauna north and south of Wadi Khums, east of the Red Sea coastal plain:

Somalirhynchia, 2 species

Gryphaea balli Stefanini

Lopha aff. solitaria Sowerby

Parallelodon sp.

Lower part of limestone, north bank of Wadi Khums:

Terebratula sp.

Rhynchonella sp.

Middle portion of the limestone section:

Cidaroid sp.

Ostrea sp.

Bramkamp at that time considered this fauna to be Hanifa, which was then questionably correlated with the Oxfordian stage of the European Jurassic, but he

had some reservation that it might be in part somewhat younger and of Jubaila Limestone equivalency (Lower Kimmeridgian) (Steineke and others, 1958). The limestone was studied more intensively following our early reconnaissance by Michel Gillman of AUXERAP (1968), who identified the following Foraminifera and pelecypods from the lower 70 m of limestone and dolomite.

Steinekella (Redmond)

Trocholina palestiniensis (Henson)

Kurniebia aff. jurassica-wellengsi

Pseydocyclammina sp.

From the next 30 m of argillaceous limestone:

Lopha gregarea Sowerby

Kutchirhynchia sp.

Goniorhynchia sp.

Terebratulas

Ostrea hibridica Sowerby

From the third unit of 400 meters of limestone:

Pseudocyclammina jaccardi

Iberina spirocyclina sp. Henson

Nauticulina oolithica

From the upper 220 m of limestone, marl, and shale:

Iberina aff. praelusitanica (Maync)

These fossils range in age from Bathonian (upper Middle Jurassic) to Kimmeridgian (Upper Jurassic), according to Gillman. The Amran Series in Yemen has been identified from at least four collections as Malm, the epoch which includes the Upper Jurassic stages, Oxfordian, Kimmeridgian, and Portlandian, whereas the Amran Formation at Umm Araj in Saudi Arabia seemingly does not include the younger Portlandian fossils, but extends downward into the Middle Jurassic. As the Hanifa Formation has more recently been restricted to the Lower Kimmeridgian (Powers, 1968), it seems desirable to apply the Yemen name to the outcrops along the Yemen border in Saudi Arabia.

Khurma Formation

A quartzitic sandstone locally including conglomerate and red shale is exposed on the Rakbah plain 150 km northeast of At Ta'if and northwest of Al Khurmah where it rests on Precambrian shield rocks and underlies early Tertiary lake beds and early Miocene basalt (Brown and others, 1963a); it contains numerous Tigillites borings associated with small pelecypod casts. Although the outcrops are poorly exposed and mostly bound by faults, the sandstone is at least 50 m thick. Likewise similar sandstone, tentatively correlated with the Khurma Formation, crops out beneath the Paleocene Umm Himar Formation 100 km east of At Ta'if and 75 km southeast of the widespread outcrops northwest of Al Khurmah (Madden and others, 1979). There the clastics include a basal quartz-pebble conglomerate resting on the crystalline basement. The sandstone is crossbedded with foresets indicating a northerly transport direction at the time of deposition. It is generally friable, locally cemented by secondary silica and iron oxides (Baghanem, 1972). Similar small outcrops of sandstone containing vertical borings are exposed at the edge of the crystalline shield on the coastal plain 70 km south of Jiddah. However, nearby sediments of Oligocene age suggest that these beds are younger than those exposed at Umm Himar. Likewise sandstone beneath the Paleocene(?) Usfan Formation northeast of Jiddah should probably be identified with the Khurmah Formation.

A precise age for the mature Khurma formation is not possible to determine with the information available to us. The age could range from early Paleozoic to Tertiary, as the Sabellarifex dufrenoyi (Tigillites dufrenoyi Rouault) in Ordovician sandstone in Jordan (which should be named Tigillites because it differs from Sabellarifex by its distinct annulation (Hantzschel, 1975, p. W 102)), extends into Arabia, and Tigillites (?) borings occur in all the lower Paleozoic sandstones fringing the shield, but many are not annulated as are the borings in the Khurma Formation. The lower Paleozoic sandstone extends south onto the shield in numerous small isolated outliers as far south as the latitude of Al Medinah (lat. 24°30' N.), 270 km northwest of the Khurma Formation as well as in a single outcrop at Jabel at Tin east of At Ta'if. However, these sandstones are massive, evenly bedded, and devoid of Tigillites vertical boreholes. Certainly the Khurma clastics are pre- or Early Paleocene, as they are disconformable below the Paleocene Umm Himar Formation (Madden and others, 1979). General evidence, including lithology and stratigraphic position suggest a Cretaceous age similar to the fluviatile (Nubian-type) clastics widespread in East Africa, Yemen, and Jordan.

These beds were first observed by Richter-Bernburg and Schott (1954, p. 44-45) who described silicified limestone with red sandy shale, greenish-gray marly somewhat silicified shale, coarse-grained sandstone, and purple and green varigated shale over a distance of about 21 km beginning 13 km west of Khurma, to which they gave the name "Khurma Series." As these beds strike N. 100°-150° E., and dip vertically and are underlain by greenschist and granitic gneiss striking N. 30°-60° E., they considered them younger than the basement. In a western belt, gastropod molds, undoubtedly from the lake beds, are associated with the Umm Himar deposits. Because of the vertical dips, it is problematic that they saw the quartzitic sandstone underlying the Paleocene which we have tentatively identified with the Lower Cretaceous Nubian sandstone of Egypt and the Sudan. An alternative explanation would require tectonism in the Khurma area during late Mesozoic

or early Tertiary, for which we have seen no evidence elsewhere on the upland plateau of the shield, although there is normal faulting of the sandstone.

MESOZOIC-CENOZOIC SEDIMENTARY ROCKS

Usfan Formation

Definition.--Tertiary fossiliferous sediments in western Saudi Arabia were first shown on a map prepared as part of a search for a water supply for Jiddah (Steineke and others, 1944). Cropping out in the low hills east and north of Jiddah, the continental and marine clastics contain bivalve and gastropod fossils that were identified as of Eocene age (R. A. Bramkamp, oral commun., 1944).

Subsequently Karpoff (1956) published a description of the sediments; he divided them into two units: the Usfan Series, a red continental series of clastics including a light-colored lacustrine limestone and rare leaf imprints as exposed at the Usfan Pass (lat 24°54.8' N. Long 39°21.2' E.) 50 km northeast of Jiddah, and the "Shumaysi Sandstone," a light-colored quartz-pebble sandstone, locally iron-stained and calcareous with a silicious limestone at the top, seen at km 45 east of Jiddah on the Makkah road. A year later he (Karpoff, 1957a) published a more comprehensive account following the identification of a marine fauna considered to be of Maestrichtian (Late Cretaceous) age from Usfan Pass which led him to assign that series to a Maestrichtian-Eocene(?) span. The overlying red clastics of continental origin, the "Shumazi (Shumadi) Series," he considered might be Oligocene-Miocene, based on resemblance to the Tertiary of North Africa (Karpoff, 1956).

On the 1963 geologic map of the Southern Hijaz quadrangle (Brown and others, 1963a), the Usfan Formation is shown in grabens trending more-or-less en echelon, parallel to the Red Sea rift, the Tertiary sediments flanked by Precambrian rock and overlain by Pliocene basalt. The nonmarine upper beds were split off and assigned to the Shumaysi Formation, following Karpoff.

Occurrence and thickness.--The Usfan Formation crops out in steeply dipping beds for an exposed thickness of 75 to 100 m across the Medinah-Makkah road at the Usfan Pass. Additional exposures, rim the basalt northwest of the pass for 20 km, and marine or littoral sediments 170 m thick, which may be an extension, crop out in a secondary graben at Haddat ash Sham, 45 km southeast of 'Usfan and 60 km northeast of Jiddah. Intermittent exposures extend north and south of Haddat ash Sham for 32 km and locally contain some marine fossils, but the sediments are almost entirely sandstone and were shown on the 1963 geologic map as part of the overlying Shumaysi. They were mapped by AUXERAP as an extension of the Usfan Formation, perhaps on the basis of marine Foraminifera, but if the lower part of the Shumaysi is Eocene, these outcrops should best not be assigned to the Usfan.

Lithologic character.--The Usfan at the type locality (fig. 44) at Usfan Pass 4 km northwest of the village of Usfan is mostly fine-grained sandstone, cemented by iron in some layers, and has a fossiliferous and nodular gray limestone near the base, and some glauconitic fine sandstone near the top. The uppermost bed

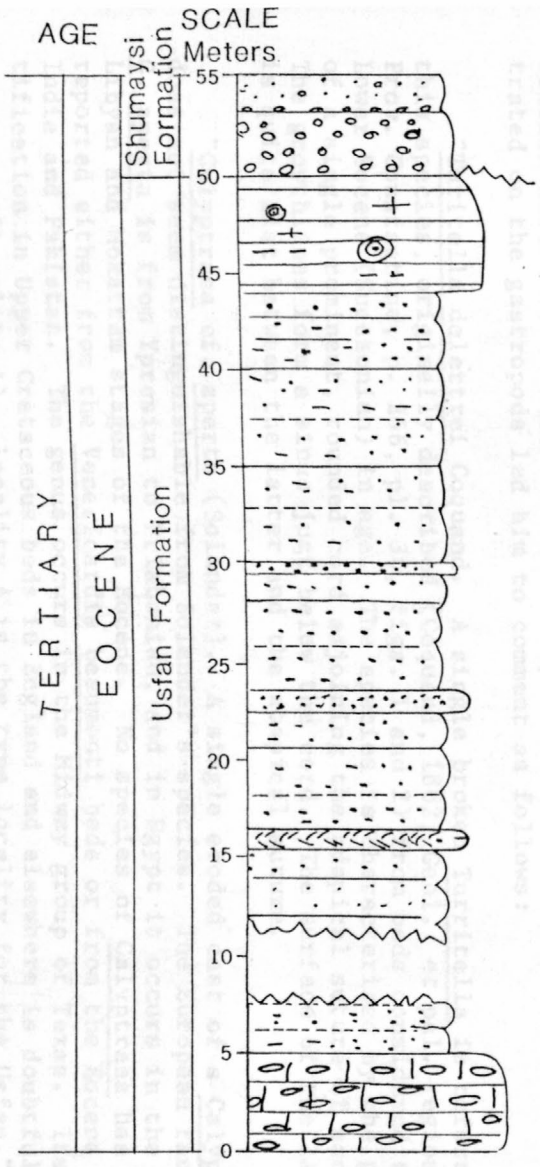

Basal 0.3 meter contains clean chert cobs 5-10 cm in diameter; rounded, mostly quartzite with pebbles, quartz predominate. Dark rusty red, iron-stained cemented chert fragment conglomerate; 60 percent cemented with iron oxide.

Arbitrary contact

Yellow brown ultra fine grained chert after limestone with fossil fragments; indistinct bedding, 10-30 cm; (shale and anhydrite). Dip 65°SE, N. 40°E.

3-4 meters of iron-stained, cemented green glauconitic fine-grained sandstone (43.7 ± 1 m.y. K-Ar).

Fine-grained, quartz sandstone; some fossils

Iron-cemented silty sandstone

Fine-grained buff quartz sandstone

Iron-cemented silty sandstone

Fine-grained buff quartz sandstone

Fine-grained buff sandstone; 1 mm laminae in beds 10cm thick; fine crossbedding; rootlets.

Bedded, fine-grained buff quartz sandstone

Approximately 25 m

Fossiliferous nodular, 5-10 cm beds, reefal gray limestone. Venericardia, not Burmanti (Baluchicardia)(Claibornicardia).

Fossiliferous nodular limestone, gray, dip 75-80° NW, N. 40°E. assumed to be overturned.

Figure 44. Type section of the Usfan Formation at Usfan Pass

127a

is 6 m of bedded phosphatic chert that is weathered, and elsewhere is lateritic (fig. 44). Poorly exposed sandstone beneath the lower fossiliferous limestone may be lowermost Usfan, but the beds have tubular borings across the bedding and contain plant fossils and ferruginous layers which may be either younger or older than the marine beds that are designated Usfan. The structure is obscure.

Nature of contact.--The Usfan Formation rests nonconformably on Precambrian crystalline rocks where the nonfaulted basal surface can be observed. It has been dropped down in a narrow graben so that sandstone or conglomerate adjacent to the crystalline rocks may be part of the overlying Shumaysi or, more likely, equivalent to the older Khurma Formation. The nonmarine Shumaysi disconformably rests on the Usfan; the basal sediment is a ferrous iron-cemented fragmental conglomerate composed of clasts of Usfan chert, limestone, shale, and pebbles and boulders of basement rocks.

Paleontology and age.--The bivalves determined by D. Mongin on which Karpoff (1957a) based his Maestrichtian age are as follows:

Cardita (Venericardia) ameliae Peron

Cardita (V.) ameliae var. orfellensis Rossi-Ronchetti

Corbula striatuloides Forbes

Lucina cf. L. desioli Ch-Rispoli

This fauna came from about 10 m above the base of a dark-gray limestone 3 km north of the village of Usfan (Karpoff, 1957a). Because the Maestrichtian age did not agree with the earlier determination by Bramkamp, we visited the outcrops and collected both bivalves and gastropods which were studied by F. S. MacNeil, USGS, who reported as follows:

From two localities: the type outcrop, 3 km north of Usfan and another exposure 9 km to the northwest:

Venericardia sp large and small, possibly two species

Phacoides (Miltha?)

Mesalia sp.

Turritella sp.

"If these fossils were from North America, I would say that a Paleocene or lower Eocene age is indicated. The large Venericardia recalls V. wilcoxensis Dall, V. smithi Aldrich, and V. bulla Dall, species from the Paleocene of the Gulf coast. The later is related to "Cardita" beaumonti from the Paleocene of India. The Arabian species looks to me more like these Paleocene species than it does the middle and upper Eocene species, V. alticostata (Courad). Even these likenesses might not be significant, however, considering that Arabia is nearly half way around the world."

"Large Mesalia of the type found in the Arabian material are also characteristic of the Paleocene and lower Eocene of the Gulf Coast. The Arabian Mesalia is very similar to M. mavericki Gardner from the Paleocene of Texas and to M. Wilcoxiana (Aldrich) from the Paleocene of Alabama. A smaller species with more spirals, M. alabamiensis (Whitfield) occurs in the lower Eocene (Wilcox) of Alabama.

"The Turritella also appears to be close to an Alabama Midway species, T. alabamensis Whitfield.

"The Phacoides is also similar to one described from the Paleocene of Texas by Gardner as Phacoides (Miltha?) albaripa.

"In spite of these similarities with the Gulf Coast Paleocene, I would not trust it entirely until comparison with faunas from Egypt, India, and East Africa had been made. It is certainly true that both, some species groups and some generic assemblages which characterize the lower Tertiary of North America, are found in much younger beds, and even Recent, in the Indo-Pacific region."

Subsequently MacNeil commented further:

"Finlay and Marwick (New Zealand Geol. Sur. Pal. Bull. 15) figures a gastropod as Kaitangata hendersoni which may be close to the Mesalia in the Arabian material. The New Zealand fossil is from the Wangaloan beds, dated as Danian (supposed to be between our Paleocene and our Upper Cretaceous).

"Cox (Annals and Mag., ser. 11, v. 1, 1938) described a species as Venericardia daviesi. This, as he says, is related to "Cardita" beaumonti. It comes from the Hangu shale of northwestern India which he assigns to the "Lower Eocene, Montian?. The Montian is the lower part of the Paleocene of Belgium."

Dr. Ralph Stewart examined the same collection and agreed with MacNeil's evaluation of Paleocene or early Eocene age. However, because of the long distances from North American fossils, he suggested that L. R. Cox of the British Museum could offer a valuable opinion. Cox's study in which he concentrated on the gastropods led him to comment as follows:

"Turitella delettrei Coquand. A single broken Turritella is referred to this species, originally described (Coquand, 1862, Geol. et pal. region sud Prov. Constantine, p. 266, pl. 30, figs. 1 and 2) from beds considered to be Lower Eocene (Suessonian) in age. The species is characterized by the presence of a single prominent, rounded cord adjoining the adapical suture of each whorl. The growthlines form a sinus just below the cord. The surface of the last whorl is quite flat between the latter and the abapical suture.

"Calyptraea cf. aperta (Solander). A single eroded cast of a Calyptraea does not seem distinguishable from Solander's species. The European range of C. aperta is from Ypresian to Priabonian, and in Egypt it occurs in the Upper Libyan and Mokattam stages of the Eocene. No species of Calyptraea has been reported either from the Venericardia beaumonti beds or from the Eocene of India and Pakistan. The genus occurs in the Midway group of Texas. Its identification in Upper Cretaceous beds in England and elsewhere is doubtfully correct. (Locality A). Locality A is the type locality for the Usfan."

"Phacoides sp. indet. A crushed, orbicular Phacoides of medium size is not clearly identifiable with any species described from the Eocene of the Middle East or Mediterranean area (Locality A)."

Commenting on the age of the fauna, Cox (written commun., 1957) states: "There is insufficient evidence for arriving at a definite conclusion as to the stage of the Eocene represented. Of the species definitely identified, Mesalia fasciata is long ranging, and the evidence of Turritella delettrei rests upon the Suessonian (Lower Eocene) age assigned (on unknown grounds) to the formation in which it was originally found. The smaller Venericardia has been referred, with qualification, to Venericardia sindensis Cox, authentic modern records of which are from the Middle Eocene (Lutetian), although it may possibly also occur in the Lower Eocene (Ypresian), the stage to which the Laki beds belong. It is probable that the Calyptraea is not earlier than Ypresian. As the large Venericardia is a new species it throws no light on geological age.

"I am inclined to dismiss the suggestion that the formation is as old as Paleocene. The presence of Turritella delettrei, if this species is correctly stated to have been found in the Lower Eocene in northern Africa, rather suggests that the age of the formation is lower Eocene (Ypresian)."

More recently Dr. Druid Wilson (written commun., 1979) examined specimens from the 5 m bed of gray limestone near the base of the exposure at Usfan and identified the larger bivalve as Venericardia (claibornicardia) sp. which is known with certainty only from the middle Eocene of eastern North America and the Paris basin, but he feels that this occurrence in Saudi Arabia should not be used as a basis for a firm age determination.

In connection with the paleontological age of the Usfan, an ostracod fauna has been described at a depth of 1637-1638.7 m from an exploration well drilled on Maghersum Island off the coast of Sudan 220 km southwest of Usfan (Masoli, 1969). The ostracods include uppermost Cretaceous and Paleocene species according to Masoli, who also identified three Foraminifera, of which one, Cibicides sp., was found in the Haddat ash Sham graben southeast of Usfan, and identified by Ruth Todd. She stated that no age determination could be made as the form occurs in both Cretaceous and Tertiary beds. Furthermore, the tests seem to have been replaced, suggesting redeposition (R. Todd, USGS, written commun., 1959).

Thus it appears that the Usfan formation can be either middle or lower Eocene or Paleocene but most likely is not Maestrichtian, from the available fossil evidence. This view is further strengthened from two K-Ar ages, 43.7 $\pm$ 1.0 and 56.4 $\pm$ 1.2 Ma, obtained from glauconite near the top of the exposure at Usfan Pass (34a, b table 8). These ages are middle Eocene and latest Paleocene and as argon can be lost from the mica by sufficient burial, the Paleocene age seems more reasonable, but the 56.4 $\pm$ 1.2 Ma age may represent a Paleocene detrital component in a middle Eocene deposit (Dalrymple and Lanphere, 1969, p. 172-173). The percentage of potassium is between 3.02 and 3.60, values that are lower than ideal for K-Ar ages (Hunziker, 1979, p. 60-62).

Umm Himar Formation-Paleocene

Lake beds questionably assigned to the Miocene on the 1963 geologic map (Brown and others, 1963a), on the basis of fresh-water gastropods have since been studied and more extensively mapped (Baghanum, 1972; Baghanum and Mickelson, 1972; Gonzales, 1973). The lowermost beds now constitute the Umm Himar Formation as exposed on the eastern flank of Jabal Umm Himar, 100 km east of At Ta'if (Madden and others, 1979). Madden and others divided the Umm Himar into three members: a basal ferruginous mudstone; a middle greenish-gray and yellow siltstone and shale containing fossil vertebrate bones; and an upper dolomitic limestone (fig. 45). The middle member contains numerous vertebrate fossils including sharks, rays, fish, turtles, primitive crocodiles, and a primitive lung fish, a fauna considered mid-Paleocene and indicative of coastal marine or estuarine environment (Madden and others, 1979).

Occurrence and thickness.--The lacustrine (and estuarine) beds are exposed intermittently within an elliptical ring enclosing an area 145 km north-south by 60 km east-west within a wide shallow basin on the Rakbah plain east of At Ta'if and surrounding the Harrat Hadan lava fields. The basalt beds rest on the older estuarine beds and are interbedded with younger beds. Most of the older (Umm Himar) beds are exposed in an area of about 200 km^2 along the southern and southeastern edge of the lava fields west and north of Turabah, but sporadic small outcrops lie within the lava fields or along wadi banks within the Harrat Hadan and on the plains in low hills throughout the outer ring. Its average thickness is 22 m.

Lithologic character.-The lowermost 3 m of ferruginous mudstone contains abundant root casts and oolitic and bog-iron ore. The middle 9 m includes vertebrate fossils in the lower 2 to 3 m of mudstone, and grades upward into bedded gray and yellow siltstone and fissile shale. The upper 10 m is dolomitic limestone, and includes some interbedded shale and siltstone in the lower part; it grades into cherty limestone at the top.

Nature of contacts.--The Umm Himar unconformably overlies either deeply weathered quartz monzonite, andesitic greenstone, or the Khurma Formation, all beveled by the Hejaz pediplain to topography conducive to low coastal marshes and lacustrine sedimentation. The beds overlying the Umm Himar are likewise iron-rich soils corresponding to the widespread pre-Miocene saprolite and laterite found in the Sudan, Ethiopia, and the southwestern uplands of the Arabian Peninsula. Latest Oligocene or earliest Miocene latite and phonolite (22.2 $\pm$ 3.5 Ma, table 8) intrude the Umm Himar Formation, and early Miocene basalt flows (16.4 $\pm$ 1.6 m.y. B.P., table 8) overlie both the Umm Himar and younger, probably earliest Miocene or latest Oligocene lake beds, which are interbedded with the lavas.

Laterite and saprolite

A deeply weathered saprolitic and laterized profile representing a post-Mesozoic erosion interval underlies the As Sirat basalt on the crest of the Hejaz range in southwest Arabia (fig. 46) (Overstreet and others, 1973, 1977).

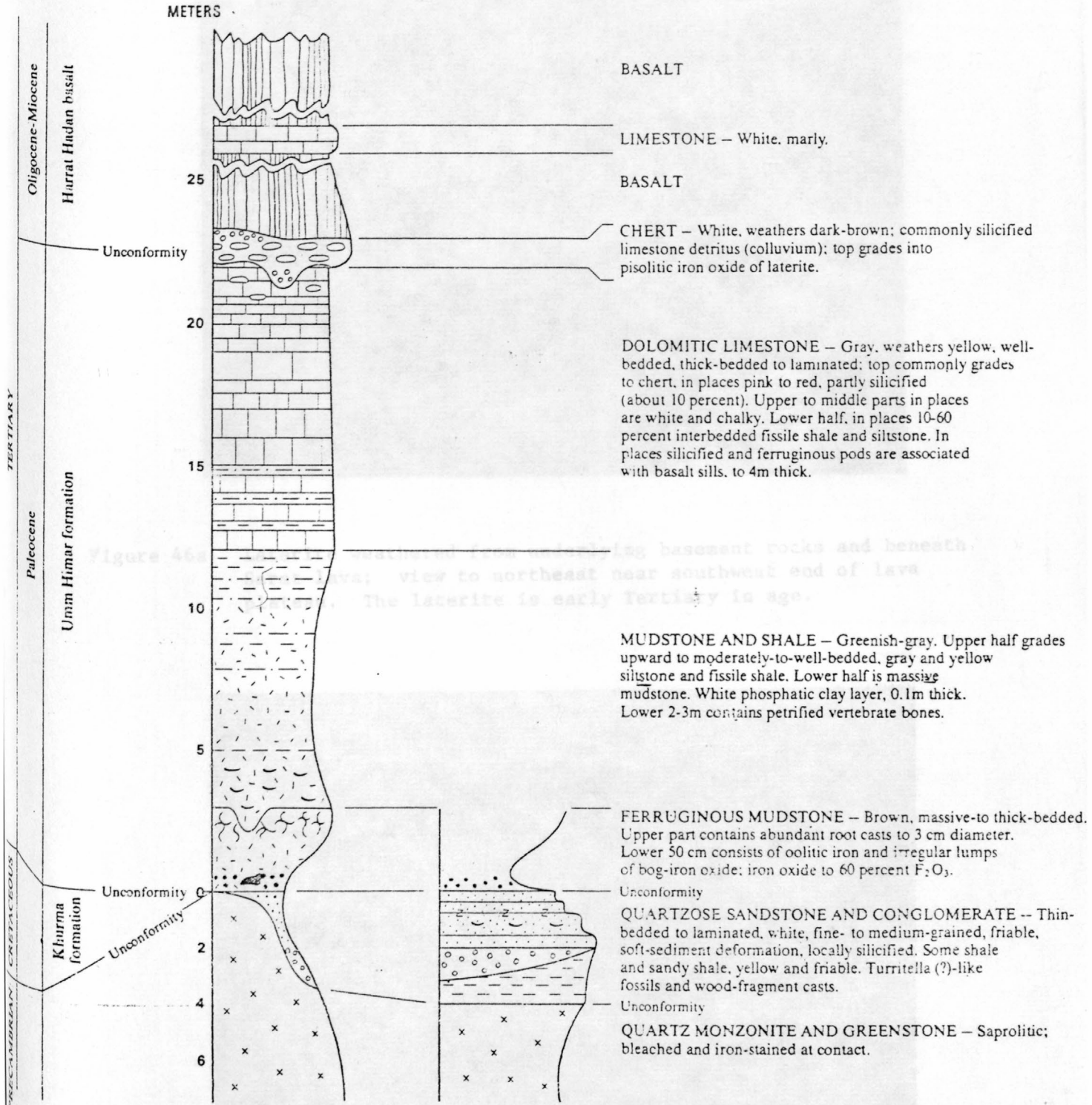

Figure 45. Composite columnar section of the Umm Himar formation and overlying and underlying rocks in the Jabal Umm Himar area. After C. T. Madden, I. M. Naqvi, W. C. Whitmore, Jr., Dwight L. Schmidt, Warren Langston, Jr., and Roger C. Wood, 1979.



Figure 46a. Laterite weathered from underlying basement rocks and beneath Sarat lava; view to northeast near southwest end of lava plateau. The laterite is early Tertiary in age.

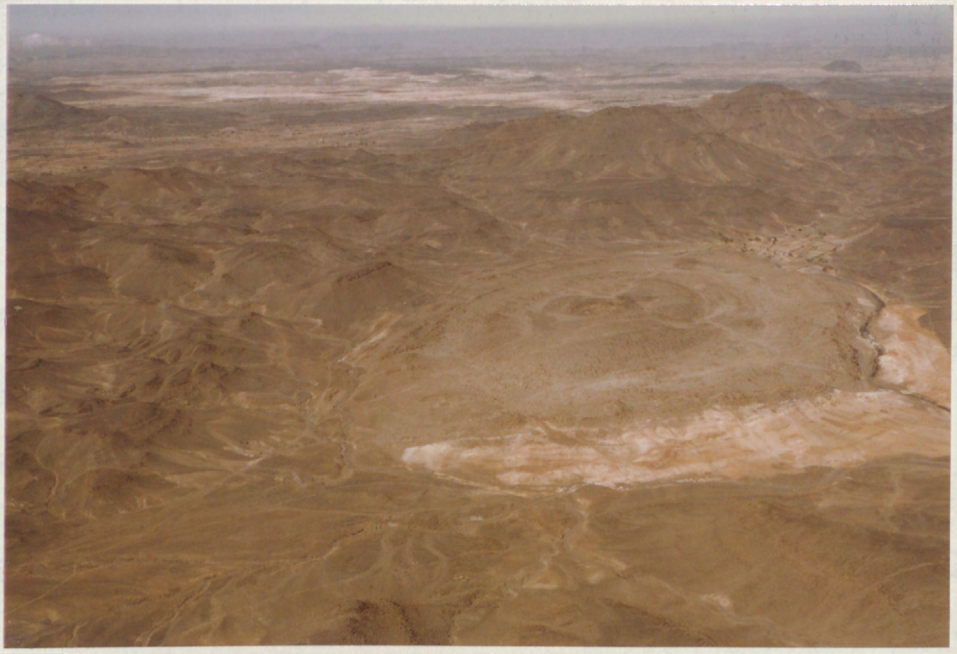

Figure 46b. Calcareous feldspathoidal syenite plug in the midst of the As Sarat lava plateau at Al Warah. The syenite transects the laterite and the lower beds of the Sarat basalt with an early Miocene age of 22 m.a. (table 15)

Of varying thicknesses ranging from a few centimeters to more than 50 m, but mostly 20 to 30 m, it is missing in places where the plateau basalt rests on the Wajid Sandstone and is thickest over Precambrian crystalline rocks rich in feldspar. The profiles are typical of those developed under tropical conditions, and have a surface zone of pisolitic material, here geothite or kaolinite, grading downward to bleached clays, above a zone of enrichment in silica (silcrete); the lower section customarily is a saprolite (Overstreet and others, 1977, p. 5). The most important clay minerals belong to the kaolinite group, with montmorillonite minor. Goethite has concentrated in the upper lateritic zones where the underlying rocks contain ferro-magnesian minerals or has been transported.

The age of the weathered zone is somewhat problematic. A minimum age is that for the base of the basalt, on the plateau of As Sirat, 30.1 Ma (table 9), using K-Ar decay rates established in 1976 by the International Union of Geological Sciences. A similar situation exists on the northern Ethiopian plateau where an age of 37.1 Ma (table 9) was obtained on a dike at Asmara, Ethiopia, which appeared to be intrusive into the lateritic red soils there underlying the plateau basalts. A recent date for a basal flow at Adigrat 130 km south of Asmara, utilizing the new decay constants, gave 30.0 $\pm$ 0.7 Ma (Jones and Rex, 1974). In that area the laterite has been described as the upper part of the Amba Aradam Formation of Cretaceous age (Arkin and others, 1971, quoting M. M. Shumburo, 1968). Likewise, the Trap Series in Yemen (plateau basalts) have recently yielded ages of 29 to 20 Ma, and volcanic rock overlying the Medj-zir (Eocene) northwest of Sa'na and in south central Yemen have been dated at about 25 Ma (Civetta and others, 1978). However, the lateritic profile is not shown in those areas, as it is limited to the basalt outliers northwest of the Jawf graben in extreme northwestern Yemen. Thus it would appear that the Sirat laterite could range in age from Eocene to mid-Oligocene (to about 30 Ma).

Shumaysi Formation

Definition.--The Shumaysi Formation was named by Karpoff (1956, 1957b) for clastic sediments, mostly sandstone of continental and lacustrine origin, as exposed along the western flank of Wadi Shumaysi, a southern distributary of Wadi Fatima 50 km east of Jiddah. On the Southern Hijaz geologic map (Brown and others, 1963a), it is shown extending intermittently beneath the Tertiary basalt flows in the Usfan graben from Wadi Khulays south to lat. 21° N. mostly as outliers on the crystalline basement. It is exposed farther east in the Haddat ash Sham graben and questionably includes sediments beneath basalt in the Tihamat foothills as far north as lat. 22° N. The type section at Shumaysi was divided by Al-Shanti (1966) into three members, a lower, mostly sandstone and conglomerate unit, a middle member including two oolitic iron ore beds, and an upper member dominantly composed of shale and siltstone. A reference section has been designated on the west flank of Wadi al Fajj 20 km northwest of Shumaysi and north of Wadi Fatimah where the lithology is similar, where underlying crystalline basement and overlying basalt flows are likewise exposed, and where the identified fossils have been found.

Occurrence and thickness.--The widely scattered and separated outcrops of the Shumaysi beds range in thickness from 77 to 191 m and are 148 m thick at the type locality (fig. 47) as measured by Al-Shanti (1966). They are faulted,

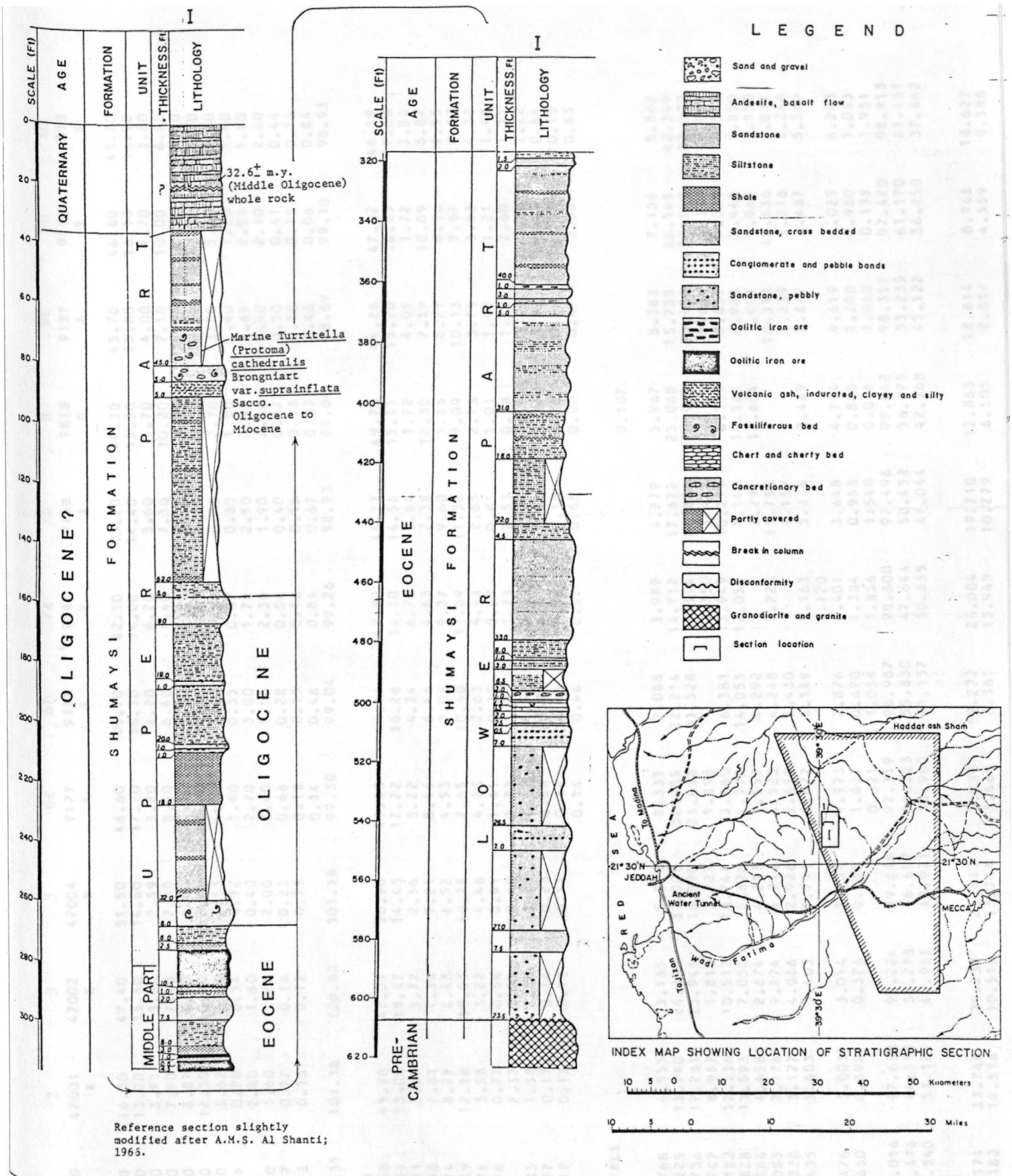

Reference section slightly modified after A.M.S. Al Shanti; 1965.

Figure 47. Type locality of the measured Shumaysi Formation.

Table 9. Chemical analyses of Tertiary igneous rocks

Map #:	1	2	3	5	6t	6b	7t	7b	8	9t	9b	10
Field #:	47000	47001	47002	47004	917T	917B	916T	916B	1818	915T	915B	913
SYMBOL	X	X	X	X	X	X	X	X	O	X	X	X
SIO2	46.30	46.30	47.40	51.50	46.60	45.70	42.50	43.70	49.30	43.70	46.60	45.70
AL2O3	14.60	13.20	15.60	14.60	17.10	16.10	14.00	14.40	15.30	15.00	16.10	16.90
FE2O3	6.40	3.91	3.80	2.59	3.20	4.20	6.70	3.60	1.70	4.00	1.70	3.80
FEO	4.90	7.90	7.40	7.30	8.40	6.40	4.40	7.30	10.20	7.10	10.00	6.80
MGO	8.10	8.87	8.50	6.60	4.50	8.00	9.20	9.50	5.80	8.60	6.90	4.50
CAO	11.20	12.30	10.60	10.40	7.60	10.30	11.80	11.20	9.00	10.00	7.50	10.80
NA2O	3.70	3.62	3.30	4.53	4.20	2.60	4.40	2.80	2.70	3.70	3.80	4.30
K2O	0.96	0.78	0.54	0.92	1.40	0.35	0.67	0.80	1.00	1.40	1.20	1.40
H2O		2.40	1.80	0.40	2.70	3.00	1.72	2.50	0.97	1.65	2.58	1.10
TIO2	1.80	1.60	1.60	2.00	2.60	1.50	2.30	1.90	2.50	2.40	2.10	2.20
P2O5	0.27	0.17	0.16	0.23	0.68	0.28	0.58	0.40	0.37	0.50	0.41	0.44
MNO	0.12	0.13	0.12	0.11	0.18	0.15	0.18	0.16	0.18	0.18	0.15	0.15
CO2					0.14	0.46	0.81	0.67	0.02	0.46	0.06	0.84
TOTAL(-O)	98.35	101.18	100.82	101.18	99.30	99.04	99.26	98.93	99.04	98.69	99.10	98.93
ADJUSTED OXIDES												
SIO2	47.08	45.76	47.01	50.90	46.93	46.14	42.82	44.17	49.78	44.28	47.02	46.19
AL2O3	14.84	13.05	15.47	14.43	17.22	16.26	14.10	14.56	15.45	15.20	16.25	17.08
FE2O3	6.51	3.86	3.77	2.56	3.22	4.24	6.75	3.64	1.72	4.05	1.72	3.84
FEO	4.98	7.81	7.34	7.21	8.46	6.46	4.43	7.38	10.30	7.19	10.09	6.87
MGO	8.24	8.77	8.43	6.52	4.53	8.08	9.27	9.60	5.86	8.71	6.96	4.55
CAO	11.39	12.16	10.51	10.28	7.65	10.40	11.89	11.32	9.09	10.13	7.57	10.92
NA2O	3.76	3.58	3.27	4.48	4.23	2.63	4.43	2.83	2.73	3.75	3.83	4.35
K2O	0.98	0.77	0.54	0.91	1.41	0.35	0.67	0.81	1.01	1.42	1.21	1.42
H2O		2.37	1.79	0.40	2.72	3.03	1.73	2.53	0.98	1.67	2.60	1.11
TIO2	1.83	1.58	1.59	1.98	2.62	1.51	2.32	1.92	2.52	2.43	2.12	2.22
P2O5	0.27	0.17	0.16	0.23	0.68	0.28	0.58	0.40	0.37	0.51	0.41	0.44
MNO	0.12	0.13	0.12	0.11	0.18	0.15	0.18	0.16	0.18	0.18	0.15	0.15
CO2					0.14	0.46	0.82	0.68	0.02	0.47	0.06	0.85
NORMATIVE MINERALS												
Q									0.107			
C												
OR	5.768	4.555	3.165	5.373	8.331	2.088	3.989	4.779	5.967	8.383	7.156	8.362
AB	21.225	13.740	24.350	31.008	32.285	22.214	14.712	17.622	23.068	15.739	28.141	22.349
AN	20.736	17.261	25.945	16.590	23.838	31.528	16.594	24.624	26.933	20.454	23.541	22.922
NE	5.747	8.957	1.813	3.725	1.898		12.350	3.428		8.660	2.333	7.817
WO	14.182	17.516	10.512	13.744	3.660	6.381	13.949	10.279	6.505	9.837	4.559	9.588
EN	11.828	11.593	7.050	8.620	1.978	14.055	12.055	7.140	14.585	6.986	2.448	5.890
FS	0.564	4.658	2.674	4.283	1.557	4.292		2.291	13.664	1.991	1.961	3.150
FO	6.085	7.176	9.774	5.344	6.523	4.248	7.728	11.756		10.313	10.436	3.811
FA	0.320	3.177	4.086	2.926	5.659	1.430		4.157		3.239	9.216	2.246
MT	9.435	5.603	5.465	3.711	4.672	6.149	8.163	5.276	2.489	5.877	2.487	5.569
HM							1.120					
IL	3.476	3.003	3.014	3.754	4.973	2.876	4.401	3.648	4.794	4.619	4.025	4.223
AP	0.650	0.398	0.376	0.538	1.622	0.670	1.384	0.958	0.885	1.200	0.980	1.053
CC					0.321	1.056	1.856	1.540	0.046	1.060	0.138	1.931
TOTAL	100.016	97.638	98.224	99.618	97.319	96.987	98.300	97.496	99.042	98.357	97.420	98.913
SALIC	53.476	44.513	55.273	56.697	66.353	55.830	47.644	50.452	56.075	53.235	61.170	61.451
FEMIC	46.540	53.125	42.951	42.921	30.965	41.157	50.655	47.044	42.968	45.122	36.250	37.462
DI	26.574	33.768	20.237	26.647	7.196	12.222	26.004	19.710	12.863	18.814	8.968	18.627
DIWO	14.182	17.516	10.512	13.744	3.660	6.381	13.949	10.279	6.505	9.837	4.559	9.588

Map #:	1	2	3	5	6t	6b	7t	7b	8	9t	9b	10
Field #:	47000	47001	47002	47004	917t	917b	916t	916b	1818	915t	915b	913
DIEN	11.828	11.593	7.050	8.620	1.978	4.475	12.055	7.140	3.282	6.986	2.448	5.890
DIFS	0.564	4.658	2.674	4.283	1.557	1.367		2.291	3.075	1.991	1.961	3.150
HY						12.506			21.891			
HYEN						9.580			11.303			
HYFS						2.926			10.589			
OL	6.405	10.353	13.859	8.271	12.182	5.678	7.728	15.912		13.552	19.653	6.058
OLFO	6.085	7.176	9.774	5.344	6.523	4.248	7.728	11.756		10.313	10.436	3.811
OLFA	0.320	3.177	4.086	2.926	5.659	1.430		4.157		3.239	9.216	12.246
WOL												
BARTH'S CATIONS												
SI	43.44	43.16	44.14	47.04	44.88	44.05	39.74	41.65	47.26	41.29	44.56	43.17
AL	16.15	14.50	17.12	15.72	19.41	18.29	15.43	16.18	17.29	16.71	18.15	18.81
FE+3	4.52	2.74	2.66	1.78	2.32	3.05	4.71	2.58	1.23	2.84	1.22	2.70
FE+2	3.84	6.16	5.76	5.58	6.77	5.16	3.44	5.82	8.18	5.61	8.00	5.37
MG	11.33	12.32	11.80	8.98	6.46	11.49	12.82	13.50	8.29	12.11	9.83	6.34
CA	11.26	12.28	10.58	10.18	7.84	10.64	11.82	11.44	9.24	10.12	7.68	10.93
NA	6.73	6.54	5.96	8.02	7.84	4.86	7.98	5.17	5.02	6.78	7.05	7.88
K	1.15	0.93	0.64	1.07	1.72	0.43	0.80	0.97	1.22	1.69	1.46	1.69
H		14.92	11.18	2.44	17.34	19.29	10.73	15.90	6.20	10.40	16.46	6.93
TI	1.27	1.12	1.12	1.37	1.88	1.09	1.62	1.36	1.80	1.71	1.51	1.56
P	0.21	0.13	0.13	0.18	0.55	0.23	0.46	0.32	0.30	0.40	0.33	0.35
MN	0.10	0.10	0.09	0.09	0.15	0.12	0.14	0.13	0.15	0.14	0.12	0.12
C					0.18	0.61	1.03	0.87	0.03	0.59	0.08	1.08
NIGGLI VALUES												
AL*	18.75	16.26	20.02	20.14	25.53	21.65	17.13	18.12	22.25	19.24	22.58	23.73
FM*	45.95	47.82	47.52	42.11	41.27	46.92	46.89	49.36	45.92	47.70	47.72	36.64
C*	26.15	27.54	24.74	26.09	20.63	25.18	26.24	25.63	23.80	23.32	19.12	27.57
ALK*	9.15	8.37	7.72	11.66	12.58	6.26	9.74	6.89	8.03	9.75	10.59	12.06
SI	100.89	96.77	103.24	120.58	118.04	104.26	88.22	93.34	121.66	95.10	110.88	108.88
RI	2.95	2.51	2.62	3.52	4.95	2.57	3.59	3.05	4.64	3.93	3.76	3.94
P	0.25	0.15	0.15	0.23	0.73	0.27	0.51	0.36	0.39	0.46	0.41	0.44
H		16.73	13.08	3.12	22.81	22.83	11.91	17.81	7.98	11.98	20.47	8.74
K	0.15	0.12	0.10	0.12	0.18	0.08	0.09	0.16	0.20	0.20	0.17	0.18
MG	0.57	0.58	0.58	0.55	0.41	0.58	0.61	0.61	0.46	0.58	0.51	0.44
SI'	136.60	133.50	130.87	146.63	150.30	125.04	138.97	127.55	132.13	139.00	142.35	148.24
QZ	-35.71	-36.73	-27.63	-26.04	-32.26	-20.78	-50.74	-34.21	-10.47	-43.90	-31.46	-39.36
AL203/SI02	0.315	0.285	0.329	0.283	0.367	0.352	0.329	0.330	0.310	0.343	0.345	0.370
FEO/FE203	0.766	2.020	1.947	2.819	2.625	1.524	0.657	2.028	6.000	1.775	5.882	1.789
D.I.	32.740	27.252	29.328	40.106	42.515	24.302	31.051	25.828	29.142	32.781	37.629	38.529

TERTIARY LAVAS

Map#:	12	13	14	15	16	17	18	19	19a	22	23	22
Field #:	912	1843	919	920	921	911	910	922	1309	907	909	908
SYMBOL	X	0	X	X	X	X	X	X	P	X	X	X
SIO2	43.40	46.50	46.60	46.20	44.10	47.40	44.80	45.30	39.80	46.70	43.20	45.00
AL203	15.20	14.90	16.70	16.90	15.20	16.50	16.70	15.80	13.40	16.50	14.60	14.90
FE203	3.00	5.00	3.60	2.10	4.10	2.40	3.90	2.30	4.60	1.20	5.30	2.20
FEO	8.40	9.80	8.90	10.30	7.40	9.20	9.70	8.20	8.20	9.10	5.60	9.20
MGO	9.80	4.90	7.20	6.50	9.50	8.00	6.00	9.00	9.90	9.20	9.80	10.50
CAO	9.90	7.60	8.60	8.60	9.50	7.50	7.50	9.90	11.80	10.80	11.70	9.80
NA2O	2.70	2.90	3.80	3.70	2.70	4.20	3.50	2.50	3.80	2.70	2.80	2.40
K2O	1.10	1.10	0.89	0.86	0.86	0.74	0.67	0.74	0.90	0.25	0.64	0.67
H2O	2.58	2.86	0.87	0.46	2.39	1.23	2.86	2.34	2.19	0.75	1.10	1.41
TIO2	2.40	3.90	2.10	2.40	2.40	2.20	2.60	1.70	2.80	1.50	1.70	1.80
P2O5	0.41	0.69	0.57	0.40	0.51	0.38	0.32	0.42	0.94	0.14	0.36	0.17
MNO	0.18	0.17	0.18	0.18	0.15	0.18	0.18	0.15	0.20	0.15	0.15	0.19
CO2	0.04	0.04	0.08	0.04	0.08	0.04	0.08	0.35	0.06	0.21	2.30	0.26
TOTAL(-O)	99.11	100.36	100.09	98.64	98.89	99.97	98.81	98.70	98.59	99.20	99.25	98.50
ADJUSTED OXIDES												
SIO2	43.79	46.33	46.56	46.84	44.60	47.41	45.34	45.90	40.37	47.08	43.53	45.69
AL203	15.34	14.85	16.68	17.13	15.37	16.50	16.90	16.01	13.59	16.63	14.71	15.13
FE203	3.03	4.98	3.60	2.13	4.15	2.40	3.95	2.33	4.67	1.21	5.34	2.23
FEO	8.48	9.76	8.89	10.44	7.48	9.20	9.82	8.31	8.32	9.17	5.64	9.34
MGO	9.89	4.88	7.19	6.59	9.61	8.00	6.07	9.12	10.04	9.27	9.87	10.66
CAO	9.99	7.57	8.59	8.72	9.61	7.50	7.59	10.03	11.97	10.89	11.79	9.95
NA2O	2.72	2.89	3.80	3.75	2.73	4.20	3.54	2.53	3.85	2.72	2.82	2.44
K2O	1.11	1.10	0.89	0.87	0.87	0.74	0.68	0.75	0.91	0.25	0.64	0.68
H2O	2.60	2.85	0.87	0.47	2.42	1.23	2.89	2.37	2.22	0.76	1.11	1.43
TIO2	2.42	3.89	2.10	2.43	2.43	2.20	2.63	1.72	2.84	1.51	1.71	1.83
P2O5	0.41	0.69	0.57	0.41	0.52	0.38	0.32	0.43	0.95	0.14	0.36	0.17
MNO	0.18	0.17	0.18	0.18	0.15	0.18	0.18	0.15	0.20	0.15	0.15	0.19
CO2	0.04	0.04	0.08	0.04	0.08	0.04	0.08	0.35	0.06	0.21	2.32	0.26
NORMATIVE MINERALS												
Q		2.203										
C												
OR	6.559	6.477	5.255	5.152	5.139	4.374	4.007	4.430	5.394	1.489	3.811	4.020
AB	14.862	24.451	28.088	26.548	22.264	30.692	29.973	21.433	2.974	23.029	23.872	20.492
AN	26.341	24.302	25.858	27.337	27.116	23.991	28.214	30.096	17.089	32.423	25.570	28.329
NE	4.437		2.187	2.813	0.455	2.632			16.057	0.001		0.068
WO	8.458	3.558	5.237	5.432	6.957	4.381	2.845	6.114	14.896	8.070	6.636	7.613
EN	5.664	12.160	3.155	2.868	4.971	2.623	3.268	7.083	10.585	4.813	6.163	4.829
FS	2.163	7.714	1.801	2.401	1.369	1.529	2.325	3.359	3.008	2.840	0.853	2.300
FO	13.288		10.343	9.491	13.283	12.128	8.307	10.951	10.108	12.813	12.914	15.220
FA	5.591		6.507	8.755	4.032	7.791	6.514	5.723	3.165	8.333	1.969	7.991
MT	4.389	7.224	5.215	3.087	6.011	3.481	5.723	3.379	6.765	1.754	7.743	3.238
HM												
IL	4.599	7.380	3.985	4.621	4.609	4.180	4.997	3.271	5.394	2.872	3.253	3.471
AP	0.980	1.628	1.349	0.960	1.222	0.900	0.767	1.008	2.258	0.334	0.859	0.409
CC	0.092	0.091	0.182	0.092	0.184	0.091	0.184	0.806	0.138	0.481	5.270	0.600
TOTAL	97.421	97.188	99.162	99.557	97.612	98.792	97.125	97.653	97.831	99.253	98.912	98.580
SALIC	52.198	57.433	61.388	61.849	54.974	61.689	62.193	55.959	41.514	56.942	53.253	52.908
FEMIC	45.223	39.755	37.774	37.708	42.638	37.103	34.931	41.694	56.316	42.311	45.659	45.672
DI	16.285	6.948	10.193	10.701	13.297	8.532	5.576	11.839	28.488	15.724	12.543	14.742
DIWO	8.458	3.558	5.237	5.432	6.957	4.381	2.845	6.114	14.896	8.070	6.636	7.613

Map #:	12	13	14	15	16	17	18	19	19a	22	23	22
Field #:	912	1843	919	920	921	911	910	922	1309	907	909	908
DIEN	5.664	2.074	3.155	2.868	4.971	2.623	1.595	3.883	10.585	4.813	5.189	4.829
DIFS	2.163	1.316	1.801	2.401	1.369	1.529	1.135	1.841	3.008	2.840	0.718	2.300
HY		16.483					2.863	4.717			1.109	
HYEN		10.086					1.673	3.200			0.974	
HYFS		6.398					1.190	1.517			0.135	
OL	18.879		16.850	18.246	17.315	19.919	14.821	16.674	13.273	21.146	14.883	23.211
OLFO	13.288		10.343	9.491	13.283	12.128	8.307	10.951	10.108	12.813	12.914	15.220
OLFA	5.591		6.507	8.755	4.032	7.791	6.514	5.723	3.165	8.333	1.969	7.991
WOL												
BARTH'S CATIONS												
SI	41.41	45.50	43.47	43.65	42.23	44.06	43.65	43.32	37.91	43.58	40.25	42.62
AL	17.09	17.18	18.36	18.82	17.15	18.08	19.18	17.81	15.04	18.15	16.03	16.63
FE+3	2.15	3.68	2.53	1.49	2.95	1.68	2.86	1.66	3.30	0.84	3.72	1.57
FE+2	6.70	8.02	6.94	8.14	5.93	7.15	7.90	6.56	6.53	7.10	4.36	7.29
MG	13.94	7.15	10.01	9.15	13.56	11.08	8.71	12.83	14.06	12.80	13.61	14.82
CA	10.12	7.97	8.59	8.71	9.75	7.47	7.83	10.14	12.04	10.80	11.68	9.94
NA	4.99	5.50	6.87	6.78	5.01	7.57	6.61	4.64	7.02	4.89	5.06	4.41
K	1.34	1.37	1.06	1.04	1.05	0.88	0.83	0.90	1.09	0.30	0.76	0.81
H	16.42	18.67	5.41	2.90	15.27	7.63	18.59	14.93	13.92	4.67	6.84	8.91
TI	1.72	2.87	1.47	1.71	1.73	1.54	1.91	1.22	2.01	1.05	1.19	1.28
P	0.33	0.57	0.45	0.32	0.41	0.30	0.26	0.34	0.76	0.11	0.28	0.14
MN	0.15	0.14	0.14	0.14	0.12	0.14	0.15	0.12	0.16	0.12	0.12	0.15
C	0.05	0.05	0.10	0.05	0.10	0.05	0.11	0.46	0.08	0.27	2.93	0.34
NIGGLI VALUES												
AL*	19.09	22.04	22.19	22.98	19.53	22.16	23.52	20.72	15.78	20.94	18.05	18.60
FM*	51.23	48.71	47.44	46.22	51.37	49.17	48.14	49.24	50.45	48.15	49.10	53.31
C*	22.60	20.44	20.78	21.26	22.19	18.31	19.21	23.60	25.26	24.93	26.30	22.25
ALK*	7.07	8.82	9.59	9.54	6.90	10.35	9.13	6.44	8.51	5.98	6.55	5.84
SI	92.49	116.71	105.09	106.59	96.16	108.02	107.08	100.79	79.53	100.59	90.63	95.35
RI	3.85	7.36	3.56	4.16	3.94	3.77	4.67	2.84	4.21	2.43	2.68	2.87
P	0.37	0.73	0.54	0.39	0.47	0.37	0.32	0.40	0.80	0.13	0.32	0.15
H	18.34	23.94	6.54	3.54	17.38	9.35	22.80	17.36	14.60	5.39	7.70	9.96
K	0.21	0.20	0.13	0.13	0.17	0.10	0.11	0.16	0.13	0.06	0.13	0.16
MG	0.61	0.38	0.51	0.48	0.60	0.55	0.44	0.61	0.58	0.61	0.62	0.62
SI'	128.29	135.27	138.35	138.16	127.61	141.42	136.52	125.77	134.03	123.93	126.20	123.34
QZ	-35.81	-18.56	-33.26	-31.57	-31.46	-33.40	-29.45	-24.98	-54.50	-23.33	-35.58	-27.99
AL203/SI02	0.350	0.320	0.358	0.366	0.345	0.348	0.373	0.349	0.337	0.353	0.338	0.331
FEO/FE203	2.800	1.960	2.472	4.905	1.805	3.833	2.487	3.565	1.783	7.583	1.057	4.182
D.I.	25.857	33.131	35.530	34.513	27.858	37.698	33.980	25.863	24.425	24.519	27.682	24.579

TERTIARY LAVAS

Map #:	25	26	27	28	30	33	36	37	38	40	41
Field #:	1314	923	905	904	GFB1	GFB2	902	47027	47026	47024	47023
SYMBOL	X	X	X	X	X	X	X	X	X	X	X
SIO2	44.30	46.60	47.40	47.00	48.50	45.50	44.40	47.30	46.50	61.40	43.70
AL203	17.38	15.20	16.20	16.60	14.20	14.20	16.40	16.50	13.60	15.30	14.50
FE203	4.54	4.00	3.60	1.70	3.03	6.01	5.60	3.40	7.29	6.50	6.20
FEO	6.70	7.40	7.40	9.50	7.90	5.90	5.30	7.60	4.60	0.28	5.60
MGO	7.29	9.50	8.60	8.10	9.12	8.22	6.50	8.10	8.60	0.12	8.50
CAO	11.61	9.80	10.30	10.80	10.10	10.60	12.00	10.60	7.84	1.90	10.50
NA2O	3.56	2.90	3.10	2.70	4.31	4.18	2.70	3.00	5.05	5.80	3.60
K2O	0.80	0.60	0.48	0.22	1.13	0.94	0.35	0.65	1.78	4.80	1.20
H2O	0.63	0.85	0.79	0.56	0.60	2.40	2.13	1.40	0.60	2.14	1.48
TIO2	1.50	1.60	1.40	1.40	1.50	2.00	1.70	1.60	2.40	0.38	2.40
P2O5	0.18	0.32	0.13	0.12	0.18	0.38	0.21	0.31	0.53	0.11	0.63
MNO	0.12	0.18	0.15	0.15	0.14	0.15	0.15	0.14	0.13	0.18	0.20
CO2		0.30	0.12	0.08			0.16			0.86	0.95
TOTAL(-O)	98.61	99.25	99.67	98.93	100.71	100.48	97.60	100.60	98.92	99.77	99.46
ADJUSTED OXIDES											
SIO2	44.92	46.95	47.56	47.51	48.16	45.28	45.49	47.02	47.01	61.54	43.94
AL203	17.62	15.31	16.25	16.78	14.10	14.13	16.80	16.40	13.75	15.34	14.58
FE203	4.60	4.03	3.61	1.72	3.01	5.98	5.74	3.38	7.37	6.51	6.23
FEO	6.79	7.46	7.42	9.60	7.84	5.87	5.43	7.55	4.65	0.28	5.63
MGO	7.39	9.57	8.63	8.19	9.06	8.18	6.66	8.05	8.69	0.12	8.55
CAO	11.77	9.87	10.33	10.92	10.03	10.55	12.30	10.54	7.93	1.90	10.56
NA2O	3.61	2.92	3.11	2.73	4.28	4.16	2.77	2.98	5.11	5.81	3.62
K2O	0.81	0.60	0.48	0.22	1.12	0.94	0.36	0.65	1.80	4.81	1.21
H2O	0.64	0.86	0.79	0.57	0.60	2.39	2.18	1.39	0.61	2.14	1.49
TIO2	1.52	1.61	1.40	1.42	1.49	1.99	1.74	1.59	2.43	0.38	2.41
P2O5	0.18	0.32	0.13	0.12	0.18	0.38	0.22	0.31	0.54	0.11	0.63
MNO	0.12	0.18	0.15	0.15	0.14	0.15	0.15	0.14	0.13	0.18	0.20
CO2		0.30	0.12	0.08			0.16			0.86	0.96
NORMATIVE MINERALS											
Q										8.096	
C											
OR	4.794	3.572	2.846	1.314	6.630	5.528	2.119	3.818	10.633	28.430	7.130
AB	13.390	24.724	26.318	23.094	19.951	19.404	23.407	24.692	24.304	49.191	21.270
AN	29.490	26.887	28.966	32.877	15.949	17.125	32.372	29.459	9.284	1.540	19.969
NE	9.295				8.809	8.558	0.001	0.293	10.235		5.069
WO	11.577	7.550	8.638	8.342	13.627	13.670	10.932	8.685	11.079	0.726	9.281
EN	7.916	8.407	5.768	6.431	8.869	10.685	8.427	5.641	9.575	0.300	7.593
FS	2.746	2.834	2.311	4.465	3.822	1.485	1.342	2.451			0.563
FO	7.355	10.814	11.017	9.783	9.589	6.790	5.718	10.099	8.463		9.594
FA	2.812	4.018	4.865	7.486	4.554	1.040	1.003	4.836			0.784
MT	6.675	5.843	5.237	2.491	4.362	8.672	8.319	4.900	8.384	0.390	9.038
HM									1.587	6.246	
IL	2.889	3.062	2.668	2.688	2.829	3.780	3.308	3.021	4.608	0.723	4.583
AP	0.432	0.764	0.309	0.287	0.423	0.896	0.510	0.730	1.269	0.261	1.500
CC		0.687	0.274	0.184			0.373			1.960	2.172
TOTAL	99.372	99.163	99.216	99.442	99.415	97.633	97.831	98.626	99.423	97.863	98.547
SALIC	56.969	55.184	58.130	57.285	51.340	50.614	57.899	58.263	54.457	87.257	53.438
FEMIC	42.403	43.979	41.086	42.157	48.075	47.019	39.932	40.363	44.966	10.606	45.110
DI	22.239	14.493	16.652	16.334	26.318	25.840	20.701	16.777	20.655	0.646	17.437
DIWO	11.577	7.550	8.638	8.342	13.627	13.670	10.932	8.685	11.079	0.347	9.281

Map #:	25	26	27	28	30	33	36	37	38	40	41
Field #:	1314	923	905	904	GFB1	GFB2	902	47027	47026	47024	47023
DIEN	7.916	5.193	5.721	4.717	8.869	10.685	8.427	5.641	9.575	0.300	7.593
DIFS	2.746	1.751	2.292	3.275	3.822	1.485	1.342	2.451			0.563
HY		4.297	0.065	2.904							
HYEN		3.214	0.046	1.714							
HYFS		1.084	0.019	1.190							
OL	10.167	14.832	15.882	17.270	14.143	7.830	6.721	14.935	8.463		10.379
OLFO	7.355	10.814	11.017	9.783	9.589	6.790	5.718	10.099	8.463		9.594
OLFA	2.812	4.018	4.865	7.486	4.554	1.040	1.003	4.836			0.784
WOL										0.379	
BARTH'S CATIONS											
SI	41.63	43.63	44.17	44.20	44.20	42.70	43.36	44.07	43.25	58.01	41.08
AL	19.25	16.77	17.79	18.40	15.25	15.71	18.88	18.12	14.91	17.04	16.07
FE+3	3.21	2.82	2.52	1.20	2.08	4.24	4.12	2.38	5.10	4.62	4.39
FE+2	5.27	5.79	5.77	7.47	6.02	4.63	4.33	5.92	3.58	0.22	4.40
MG	10.21	13.26	11.94	11.35	12.39	11.50	9.46	11.25	11.92	0.17	11.91
CA	11.69	9.83	10.28	10.88	9.86	10.66	12.56	10.58	7.81	1.92	10.58
NA	6.49	5.26	5.60	4.92	7.62	7.61	5.11	5.42	9.11	10.62	6.56
K	0.96	0.72	0.57	0.26	1.31	1.13	0.44	0.77	2.11	5.78	1.44
H	3.95	5.31	4.91	3.51	3.65	15.02	13.87	8.70	3.72	13.49	9.28
TI	1.06	1.13	0.98	0.99	1.03	1.41	1.25	1.12	1.68	0.27	1.70
P	0.14	0.25	0.10	0.10	0.14	0.30	0.17	0.24	0.42	0.09	0.50
MN	0.10	0.14	0.12	0.12	0.11	0.12	0.12	0.11	0.10	0.14	0.16
C		0.38	0.15	0.10			0.21			1.11	1.22
NIGGLI VALUES											
AL*	21.96	19.40	20.87	21.48	17.92	18.11	22.05	21.37	17.93	35.79	18.48
FM*	42.86	50.93	47.76	47.05	48.40	47.25	42.13	46.38	49.79	21.66	47.99
C*	26.68	22.75	24.13	25.41	23.18	24.58	29.34	24.96	18.79	8.08	24.33
ALK*	8.50	6.92	7.24	6.06	10.49	10.07	6.48	7.30	13.49	34.47	9.20
SI	95.00	100.95	103.64	103.22	103.88	98.46	101.31	103.93	104.01	243.72	94.51
RI	2.42	2.61	2.30	2.31	2.42	3.25	2.92	2.64	4.04	1.13	3.90
P	0.16	0.29	0.12	0.11	0.16	0.35	0.20	0.29	0.50	0.18	0.58
H	4.51	6.14	5.76	4.10	4.29	17.32	16.21	10.26	4.48	28.33	10.68
K	0.13	0.12	0.09	0.05	0.15	0.13	0.08	0.12	0.19	0.35	0.18
MG	0.54	0.60	0.59	0.56	0.60	0.56	0.52	0.57	0.58	0.03	0.57
SI'	133.98	127.68	128.96	124.23	141.97	140.26	125.93	129.21	153.96	237.88	136.81
QZ	-38.98	-26.73	-25.32	-21.01	-38.09	-41.81	-24.61	-25.27	-49.95	5.83	-42.30
AL203/SI02	0.392	0.326	0.342	0.353	0.293	0.312	0.369	0.349	0.292	0.249	0.332
FEO/FE203	1.476	1.850	2.056	5.588	2.607	0.982	0.946	2.235	0.631	0.043	0.903
D.I.	27.479	28.297	29.164	24.408	35.391	33.490	25.527	28.804	45.173	85.717	33.469

TERTIARY LAVAS

Map #:	42	43	44	45	46	46	51	51	51	52	52	52
Field #:	47022	47021	47025	926	927A	927B	623A	623B	623C	928A	928B	928C
SYMBOL	X	X	X	O	P	P	X	X	O	O	O	O
SIO2	43.20	44.20	44.50	70.30	46.20	46.60	52.50	51.50	51.50	53.80	48.40	61.90
AL203	14.30	14.50	14.50	14.70	22.10	22.90	17.60	15.02	16.90	18.20	13.40	14.60
FE203	6.60	4.20	2.90	2.50	2.90	2.00	3.78	4.45	3.83	5.40	7.00	4.80
FEO	5.10	7.70	8.80	0.20	3.60	3.30	5.50	8.60	7.00	3.80	8.70	2.50
MGO	9.00	9.80	11.00	0.28	3.80	3.40	4.38	3.32	3.98	1.60	4.30	1.50
CAO	11.10	9.20	10.00	1.10	13.30	12.50	8.90	8.95	8.95	6.10	7.00	3.70
NA2O	3.20	2.90	2.80	4.70	2.60	2.90	3.53	3.57	4.96	4.00	3.10	3.80
K2O	1.20	1.00	0.81	4.20	0.32	0.38	0.92	0.92	1.41	1.30	1.30	2.30
H2O	1.55	1.97	0.90	1.84	2.80	3.94	1.50	0.90	1.30	2.61	2.84	3.12
TIO2	2.30	2.60	2.00	0.18	1.10	0.88	1.20	2.80	1.40	1.60	3.00	1.10
P2O5	0.58	0.51	0.33	0.05	0.17	0.19	0.30	0.40	0.34	0.56	0.30	0.31
MNO	0.20	0.20	0.20	0.03	0.11	0.07	0.12	0.16	0.14	0.15	0.22	0.11
CO2	1.00	0.30	0.98	0.02	0.02	0.02				0.02	0.02	0.02
TOTAL(-O)	99.33	99.08	99.72	100.10	99.02	99.08	100.23	100.59	101.71	99.14	99.58	99.76
ADJUSTED OXIDES												
SIO2	43.49	44.61	44.62	70.23	46.66	47.03	52.38	51.20	50.63	54.27	48.60	62.05
AL203	14.40	14.63	14.54	14.69	22.32	23.11	17.56	14.93	16.62	18.36	13.46	14.64
FE203	6.64	4.24	2.91	2.50	2.93	2.02	3.77	4.42	3.77	5.45	7.03	4.81
FEO	5.13	7.77	8.82	0.20	3.64	3.33	5.49	8.55	6.88	3.83	8.74	2.51
MGO	9.06	9.89	11.03	0.28	3.84	3.43	4.37	3.30	3.91	1.61	4.32	1.50
CAO	11.17	9.29	10.03	1.10	13.43	12.62	8.88	8.90	8.80	6.15	7.03	3.71
NA2O	3.22	2.93	2.81	4.70	2.63	2.93	3.52	3.55	4.88	4.03	3.11	3.81
K2O	1.21	1.01	0.81	4.20	0.32	0.38	0.92	0.91	1.39	1.31	1.31	2.31
H2O	1.56	1.99	0.90	1.84	2.83	3.98	1.50	0.89	1.28	2.63	2.85	3.13
TIO2	2.32	2.62	2.01	0.18	1.11	0.89	1.20	2.78	1.38	1.61	3.01	1.10
P2O5	0.58	0.51	0.33	0.05	0.17	0.19	0.30	0.40	0.33	0.56	0.30	0.31
MNO	0.20	0.20	0.20	0.03	0.11	0.07	0.12	0.16	0.14	0.15	0.22	0.11
CO2	1.01	0.30	0.98	0.02	0.02	0.02				0.02	0.02	0.02
NORMATIVE MINERALS												
Q				24.286			4.057	4.861		11.768	5.323	21.859
C				0.588						0.513		
OR	7.139	5.964	4.800	24.794	1.910	2.266	5.424	5.405	8.192	7.749	7.714	13.624
AB	19.204	22.619	20.315	39.730	22.218	24.767	29.801	30.031	34.309	34.140	26.342	32.232
AN	21.253	23.813	24.673	4.999	48.158	48.794	29.393	22.111	19.354	26.707	18.888	16.026
NE	4.364	1.163	1.866						3.768			
WO	10.024	7.088	6.974		7.193	5.183	5.304	8.113	9.235		5.800	0.091
EN	8.522	5.061	4.633	0.697	5.989	3.969	10.883	8.220	5.031	4.019	10.754	3.745
FS	0.185	1.399	1.832		1.647	1.446	5.206	7.744	3.877	0.155	5.672	
FO	9.841	13.716	16.005		2.501	3.208			3.304			
FA	0.235	4.179	6.975		0.758	1.288			2.806			
MT	9.634	6.146	4.217	0.221	4.246	2.927	5.468	6.414	5.460	7.897	10.192	5.241
HM				2.345								1.197
IL	4.398	4.984	3.809	0.342	2.110	1.687	2.274	5.287	2.614	3.065	5.722	2.094
AP	1.383	1.219	0.784	0.118	0.407	0.454	0.709	0.942	0.792	1.338	0.714	0.736
CC	2.290	0.689	2.235	0.045	0.046	0.046				0.046	0.046	0.046
TOTAL	98.472	98.041	99.117	98.165	97.183	96.034	98.520	99.128	98.741	97.398	97.166	96.890
SALIC	51.960	53.560	51.654	94.397	72.286	75.827	68.676	62.407	65.623	80.878	58.267	83.741
FEMIC	46.512	44.481	47.463	3.768	24.897	20.207	29.845	36.720	33.118	16.521	38.899	13.149
DI	18.731	13.548	13.439		13.748	9.969	10.272	16.045	18.143		11.263	0.169
DIWO	10.024	7.088	6.974		7.193	5.183	5.304	8.113	9.235		5.800	0.091

Map #:	42	43	44	45	46	46	51	51	51	52	52	52
Field #:	47022	47021	47025	926	927A	927B	623A	623B	623C	928A	928B	928C
DIEN	8.522	5.061	4.633		5.141	3.508	3.361	4.084	5.031		3.577	0.078
DIFS	0.185	1.399	1.832		1.414	1.278	1.608	3.848	3.877		1.887	
HY				0.697	1.081	0.629	11.122	8.032		4.174	10.963	3.666
HYEN				0.697	0.848	0.461	7.523	4.136		4.019	7.177	3.666
HYFS					0.233	0.168	3.599	3.896		0.155	3.785	
OL	10.077	17.895	22.980		3.259	4.496			6.110			
OLFO	9.841	13.716	16.005		2.501	3.208			3.304			
OLFA	0.235	4.179	6.975		0.758	1.288			12.806			
WOL												
EARTH'S CATIONS												
SI	40.72	42.01	41.21	66.34	44.47	45.10	49.52	49.07	47.44	52.41	47.90	60.38
AL	15.89	16.24	15.82	16.35	25.07	26.12	19.56	16.87	18.35	20.89	15.63	16.78
FE+3	4.68	3.00	2.02	1.78	2.10	1.46	2.68	3.19	2.66	3.96	5.21	3.52
FE+2	4.02	6.12	6.81	0.16	2.90	2.67	4.34	6.85	5.39	3.10	7.20	2.04
MG	12.65	13.88	15.18	0.39	5.45	4.90	6.16	4.71	5.46	2.32	6.34	2.18
CA	11.21	9.37	9.92	1.11	13.72	12.96	8.99	9.14	8.83	6.37	7.42	3.87
NA	5.85	5.34	5.03	8.60	4.85	5.44	6.46	6.59	8.86	7.55	5.95	7.19
K	1.44	1.21	0.96	5.06	0.39	0.47	1.11	1.12	1.66	1.62	1.64	2.86
H	9.75	12.49	5.56	11.58	17.98	25.43	9.44	5.72	7.99	16.96	18.75	20.30
TI	1.63	1.86	1.39	0.13	0.80	0.64	0.85	2.01	0.97	1.17	2.23	0.81
P	0.46	0.41	0.26	0.04	0.14	0.16	0.24	0.32	0.27	0.46	0.25	0.26
MN	0.16	0.16	0.16	0.02	0.09	0.06	0.10	0.13	0.11	0.12	0.18	0.09
C	1.29	0.39	1.24	0.03	0.03	0.03				0.03	0.03	0.03
NIGGLI VALUES												
AL*	17.93	18.48	17.58	44.27	31.80	34.31	27.30	23.22	24.87	33.81	20.58	33.41
FM*	48.54	52.73	53.72	12.73	26.74	23.88	37.05	41.00	36.93	30.75	49.88	31.19
C*	25.30	21.32	22.05	6.02	34.80	34.05	25.10	25.16	23.95	20.60	19.55	15.39
ALK*	8.23	7.46	6.65	36.98	6.65	7.76	10.55	10.62	14.25	14.84	9.99	20.00
SI	91.91	95.61	91.57	359.27	112.83	118.48	138.19	135.12	128.61	169.60	126.14	240.38
RI	3.68	4.23	3.09	0.69	2.02	1.68	2.38	5.52	2.63	3.79	5.88	3.21
P	0.52	0.47	0.29	0.11	0.18	0.20	0.33	0.44	0.36	0.75	0.33	0.51
H	11.00	14.21	6.18	31.36	22.81	33.41	13.17	7.88	10.83	27.44	24.69	40.41
K	0.20	0.18	0.16	0.37	0.07	0.08	0.15	0.14	0.16	0.18	0.22	0.28
MG	0.59	0.60	0.63	0.17	0.52	0.54	0.46	0.32	0.40	0.24	0.33	0.28
SI'	132.91	129.85	126.59	247.90	126.62	131.06	142.21	142.48	157.02	159.35	139.97	180.01
QZ	-41.00	-34.23	-35.03	111.37	-13.79	-12.58	-4.02	-7.36	-28.40	10.25	-13.83	60.37
AL203/SIO2	0.331	0.328	0.326	0.209	0.478	0.491	0.335	0.292	0.328	0.338	0.277	0.236
FEO/FE203	0.773	1.833	3.034	0.080	1.241	1.650	1.455	1.933	1.828	0.704	1.243	0.521
D.I.	30.707	29.747	26.981	88.810	24.128	27.033	39.283	40.296	46.269	53.658	39.379	67.715

198a

TERTIARY LAVAS

Map #:	52	55	56	56	58	58	58	58	60	61	62	63
Field #:	928D	930	933A	933B	933C	BRK4A	BRK4B	BRK4C	935	938A	937	936
SYMBOL	0	0	0	0	0	0	0	0	0	X	X	0
SIO2	63.40	55.00	46.80	47.00	56.50	48.30	51.60	50.20	59.90	45.40	47.90	51.00
AL203	14.60	17.50	14.90	15.80	18.20	17.40	16.80	16.80	14.60	16.20	16.40	17.40
FE203	2.70	2.70	1.40	3.10	2.10	3.00	3.90	3.30	4.20	5.40	3.80	3.80
FEO	4.20	5.60	10.40	9.60	5.20	7.30	6.80	6.80	5.60	6.00	6.80	6.70
MGO	1.50	1.50	5.40	5.00	1.80	3.40	2.30	3.50	1.50	7.40	7.60	3.00
CAO	3.70	6.50	8.50	8.20	6.20	9.20	6.40	7.80	2.60	10.40	8.90	7.00
NA20	4.00	4.00	3.50	3.40	4.30	3.10	4.00	3.80	4.40	3.40	3.50	3.60
K20	2.60	1.80	0.89	1.20	1.70	0.95	1.30	1.20	2.90	1.00	1.20	1.60
H20	2.30	2.81	5.25	2.55	2.59	2.30	4.00	2.37	2.60	1.03	0.85	2.52
TIO2	0.98	1.30	2.80	3.10	1.20	2.60	1.40	2.20	0.96	2.60	2.00	2.20
P205	0.29	0.46	0.58	0.58	0.42	0.83	0.77	0.82	0.15	0.50	0.36	0.58
MNO	0.11	0.15	0.18	0.23	0.15	0.21	0.26	0.20	0.15	0.19	0.15	0.19
CO2	0.02	0.04	0.06	0.06	0.02	0.08	0.08	0.25	0.04	0.36	0.06	0.08
TOTAL(-O)	100.40	99.36	100.66	99.82	100.38	98.67	99.61	99.24	99.60	99.88	99.52	99.67
ADJUSTED OXIDES												
SIO2	63.15	55.35	46.49	47.08	56.29	48.95	51.80	50.58	60.14	45.45	48.13	51.17
AL203	14.54	17.61	14.80	15.83	18.13	17.63	16.87	16.93	14.66	16.22	16.48	17.46
FE203	2.69	2.72	1.39	3.11	2.09	3.04	3.92	3.33	4.22	5.41	3.82	3.81
FEO	4.18	5.64	10.33	9.62	5.18	7.40	6.83	6.85	5.62	6.01	6.83	6.72
MGO	1.49	1.51	5.36	5.01	1.79	3.45	2.31	3.53	1.51	7.41	7.64	3.01
CAO	3.69	6.54	8.44	8.21	6.18	9.32	6.43	7.86	2.61	10.41	8.94	7.02
NA20	3.98	4.03	3.48	3.41	4.28	3.14	4.02	3.83	4.42	3.40	3.52	3.61
K20	2.59	1.81	0.88	1.20	1.69	0.96	1.31	1.21	2.91	1.00	1.21	1.61
H20	2.29	2.83	5.22	2.55	2.58	2.33	4.02	2.39	2.61	1.03	0.85	2.53
TIO2	0.98	1.31	2.78	3.11	1.20	2.64	1.41	2.22	0.96	2.60	2.01	2.21
P205	0.29	0.46	0.58	0.58	0.42	0.84	0.77	0.83	0.15	0.50	0.36	0.58
MNO	0.11	0.15	0.18	0.23	0.15	0.21	0.26	0.20	0.15	0.19	0.15	0.19
CO2	0.02	0.04	0.06	0.06	0.02	0.08	0.08	0.25	0.04	0.36	0.06	0.08
NORMATIVE MINERALS												
Q	19.422	8.298			7.991	3.189	5.711	3.041	13.511			4.485
C												
OR	15.303	10.705	5.225	7.104	10.008	5.689	7.712	7.145	17.206	5.916	7.125	9.486
AB	33.712	34.065	29.422	28.822	36.248	26.585	33.979	32.401	37.381	24.349	29.044	30.563
AN	14.147	24.637	22.170	24.350	25.242	31.171	24.140	25.432	11.568	26.019	25.617	26.681
NE										2.414	0.387	
WO	0.886	1.895	6.505	5.106	1.061	3.790	0.909	2.743	0.060	8.388	6.682	1.608
EN	3.721	3.760	5.387	6.981	4.466	8.582	5.751	8.784	3.751	6.542	4.605	7.496
FS	4.052	6.225	5.468	5.817	6.088	7.119	7.466	6.550	5.529	0.929	1.538	5.904
FO			5.588	3.850						8.346	10.101	
FA			6.251	3.536						1.306	3.719	
MT	3.899	3.940	2.017	4.503	3.033	4.408	5.677	4.821	6.114	7.839	5.536	5.528
HM												
IL	1.854	2.485	5.283	5.898	2.270	5.005	2.669	4.210	1.831	4.944	3.817	4.192
AP	0.684	1.097	1.365	1.376	0.991	1.992	1.831	1.957	0.357	1.186	0.857	1.378
CC	0.045	0.092	0.136	0.137	0.045	0.184	0.183	0.573	0.091	0.820	0.137	0.183
TOTAL	97.725	97.198	94.816	97.478	97.443	97.715	96.028	97.657	97.399	98.997	99.166	97.504
SALIC	82.584	77.705	56.817	60.275	79.488	66.635	71.543	68.020	79.666	58.698	62.174	71.215
FEMIC	15.141	19.493	37.999	37.203	17.955	31.080	24.485	29.638	17.733	40.299	36.993	26.289
DI	1.761	3.819	12.897	10.056	2.124	7.464	1.817	5.383	0.121	15.859	12.826	3.162
DIWO	0.886	1.895	6.505	5.106	1.061	3.790	0.909	2.743	0.060	8.388	6.682	1.608

Map #:	52	55	56	56	58	58	58	58	60	61	62	63
Field #:	928D	930	933A	933B	933C	BRK4A	BRK4B	BRK4C	935	938A	937	936
DIEN	0.419	0.725	3.172	2.700	0.450	2.008	0.395	1.512	0.025	6.542	4.605	0.869
DIFS	0.456	1.200	3.220	2.250	0.613	1.666	0.513	1.128	0.036	0.929	1.538	0.685
HY	6.898	8.060	4.463	7.847	9.491	12.027	12.308	12.693	9.219			11.846
HYEN	3.302	3.035	2.215	4.280	4.016	6.574	5.355	7.271	3.726			6.627
HYFS	3.596	5.025	2.248	3.567	5.475	5.453	6.953	5.422	5.493			5.219
OL			11.839	7.386						9.652	13.820	
OLFO			5.588	3.850						8.346	10.101	
OLFA			6.251	3.536						1.306	3.719	
WOL												
BARTH'S CATIONS												
SI	60.65	53.33	45.87	45.44	53.75	47.23	50.71	48.50	58.02	42.57	44.78	49.33
AL	16.46	20.00	17.21	18.00	20.40	20.05	19.46	19.13	16.67	17.90	18.07	19.84
FE+3	1.94	1.97	1.03	2.26	1.50	2.21	2.88	2.40	3.06	3.81	2.67	2.77
FE+2	3.36	4.54	8.53	7.76	4.14	5.97	5.59	5.49	4.54	4.71	5.32	5.42
MG	2.14	2.17	7.89	7.20	2.55	4.96	3.37	5.04	2.17	10.34	10.59	4.33
CA	3.79	6.75	8.93	8.49	6.32	9.64	6.74	8.07	2.70	10.45	8.91	7.25
NA	7.42	7.52	6.65	6.37	7.93	5.88	7.62	7.12	8.26	6.18	6.34	6.75
K	3.17	2.23	1.11	1.48	2.06	1.19	1.63	1.48	3.58	1.20	1.43	1.97
H	14.68	18.17	34.33	16.44	16.43	15.00	26.22	15.27	16.80	6.44	5.30	16.26
TI	0.71	0.95	2.06	2.25	0.86	1.91	1.03	1.60	0.70	1.83	1.41	1.60
P	0.23	0.38	0.48	0.47	0.34	0.69	0.64	0.67	0.12	0.40	0.28	0.47
MN	0.09	0.12	0.15	0.19	0.12	0.17	0.22	0.16	0.12	0.15	0.12	0.16
C	0.03	0.05	0.08	0.08	0.03	0.11	0.11	0.33	0.05	0.46	0.08	0.11
NIGGLI VALUES												
AL*	33.12	32.86	22.06	23.18	34.20	27.47	29.35	27.30	31.05	21.26	22.29	29.00
FM*	30.31	28.93	45.11	44.83	27.87	36.45	36.37	37.38	36.83	45.15	46.13	37.03
C*	15.26	22.19	22.88	21.87	21.18	26.41	20.33	23.05	10.05	24.82	21.99	21.21
ALK*	21.31	16.02	9.95	10.11	16.75	9.67	13.95	12.27	22.07	8.76	9.59	12.76
SI	244.06	175.27	117.59	117.01	180.17	129.39	152.96	138.43	216.16	101.12	110.47	144.23
RI	2.84	3.12	5.29	5.80	2.88	5.24	3.12	4.56	2.61	4.36	3.47	4.68
P	0.47	0.62	0.62	0.61	0.57	0.94	0.97	0.96	0.23	0.47	0.35	0.69
H	29.53	29.87	43.99	21.17	27.55	20.55	39.55	21.80	31.29	7.65	6.54	23.77
K	0.30	0.23	0.14	0.19	0.21	0.17	0.18	0.17	0.30	0.16	0.18	0.23
MG	0.28	0.25	0.45	0.41	0.31	0.37	0.28	0.38	0.22	0.54	0.57	0.34
SI'	185.25	164.06	139.81	140.45	167.00	138.69	155.81	149.08	188.27	135.05	138.36	151.02
QZ	58.82	11.20	-22.22	-23.43	13.17	-9.31	-2.85	-10.64	27.89	-33.93	-27.89	-6.79
AL203/SI02	0.230	0.318	0.318	0.336	0.322	0.360	0.326	0.335	0.244	0.357	0.342	0.341
FEO/FE203	1.556	2.074	7.429	3.097	2.476	2.433	1.744	2.061	1.333	1.111	1.789	1.763
D.I.	68.437	53.068	34.647	35.926	54.246	35.464	47.403	42.587	68.098	32.679	36.556	44.534

TERTIARY LAVAS

Map #:	64	65	66	67	73	29a
Field #:	939	941	940	520	B74	500
SYMBOL	O	X	X	X	T	X
SIO2	51.50	47.00	47.00	52.50	47.70	51.50
AL203	18.60	15.50	17.10	11.80	15.70	12.10
FE203	2.90	3.20	3.90	4.75	4.90	2.17
FEO	5.80	8.90	7.60	7.20	7.20	8.40
MGO	2.40	9.20	5.60	4.64	7.10	10.20
CAO	7.00	8.90	8.70	7.00	10.30	9.09
NA2O	4.40	3.30	4.00	6.00	2.90	3.45
K2O	1.40	0.96	1.10	0.10	0.37	0.65
H2O	2.82	0.69	0.89	0.80	2.06	0.10
TIO2	1.60	1.90	2.40	2.80	1.40	1.30
P2O5	0.76	0.32	0.41	0.62	0.21	0.19
MNO	0.15	0.18	0.18	0.13	0.21	0.13
CO2	0.08	0.04	0.06		0.05	
TOTAL(-O)	99.41	100.09	98.94	98.34	100.10	99.28
ADJUSTED OXIDES						
SIO2	51.81	46.96	47.50	53.39	47.65	51.87
AL203	18.71	15.49	17.28	12.00	15.68	12.19
FE203	2.92	3.20	3.94	4.83	4.90	2.19
FEO	5.83	8.89	7.68	7.32	7.19	8.46
MGO	2.41	9.19	5.66	4.72	7.09	10.27
CAO	7.04	8.89	8.79	7.12	10.29	9.16
NA2O	4.43	3.30	4.04	6.10	2.90	3.48
K2O	1.41	0.96	1.11	0.10	0.37	0.65
H2O	2.84	0.69	0.90	0.81	2.06	0.10
TIO2	1.61	1.90	2.43	2.85	1.40	1.31
P2O5	0.76	0.32	0.41	0.63	0.21	0.19
MNO	0.15	0.18	0.18	0.13	0.21	0.13
CO2	0.08	0.04	0.06		0.05	
NORMATIVE MINERALS						
Q	2.181			0.371		
C						
OR	8.322	5.668	6.570	0.601	2.184	3.869
AB	37.453	24.820	29.781	51.627	24.514	29.405
AN	27.026	24.623	25.728	5.053	28.700	15.723
NE		1.668	2.399			
WO	1.004	7.160	6.182	10.915	8.627	11.879
EN	6.013	4.544	3.850	11.751	14.242	14.524
FS	5.927	2.161	1.961	4.998	5.841	6.705
FO		12.858	7.180		2.399	7.753
FA		6.739	4.032		1.084	3.944
MT	4.230	4.636	5.715	7.003	7.097	3.169
HM						
IL	3.057	3.605	4.607	5.408	2.656	2.487
AP	1.811	0.757	0.982	1.493	0.497	0.453
CC	0.183	0.091	0.138		0.114	
TOTAL	97.205	99.329	99.124	99.221	97.956	99.911
SALIC	74.981	56.778	64.478	57.652	55.399	48.997
FEMIC	22.223	42.551	34.646	41.569	42.557	50.914
DI	1.988	13.865	11.993	21.073	16.640	22.983
DIWO	1.004	7.160	6.182	10.915	8.627	11.879

Map #:	64	65	66	67	73	29a
Field #:	939	941	940	520	B74	500
DIEN	0.496	4.544	3.850	7.127	5.682	7.597
DIFS	0.489	2.161	1.961	3.031	2.330	3.507
HY	10.955			6.592	12.070	10.124
HYEN	5.517			4.624	8.560	6.927
HYFS	5.438			1.967	3.511	3.198
OL		19.597	11.212		3.483	11.697
OLFO		12.858	7.180		2.399	7.753
OLFA		6.739	4.032		1.084	3.944
WOL						
BARTH'S CATIONS						
SI	49.55	43.56	44.48	50.04	45.38	47.63
AL	21.09	16.93	19.07	13.26	17.61	13.19
FE+3	2.10	2.23	2.78	3.41	3.51	1.51
FE+2	4.67	6.90	6.02	5.74	5.73	6.50
MG	3.44	12.71	7.90	6.59	10.07	14.06
CA	7.22	8.84	8.82	7.15	10.50	9.01
NA	8.21	5.93	7.34	11.09	5.35	6.19
K	1.72	1.13	1.33	0.12	0.45	0.77
H	18.10	4.27	5.62	5.09	13.07	0.62
TI	1.16	1.32	1.71	2.01	1.00	0.90
P	0.62	0.25	0.33	0.50	0.17	0.15
MN	0.12	0.14	0.14	0.10	0.17	0.10
C	0.11	0.05	0.08		0.06	
NIGGLI VALUES						
AL*	31.90	19.77	24.13	18.82	21.12	15.99
FM*	31.25	51.34	42.59	44.98	46.73	53.75
C*	21.83	20.64	22.32	20.29	25.19	21.84
ALK*	15.01	8.25	10.96	15.91	6.96	8.43
SI	149.90	101.74	112.53	142.06	108.89	115.47
RI	3.50	3.09	4.32	5.70	2.40	2.19
P	0.94	0.29	0.42	0.71	0.20	0.18
H	27.38	4.98	7.11	7.22	15.68	0.75
K	0.17	0.16	0.15	0.01	0.08	0.11
MG	0.33	0.58	0.47	0.42	0.52	0.63
SI'	160.06	133.00	143.86	163.65	127.83	133.71
QZ	-10.16	-31.26	-31.33	-21.59	-18.93	-18.24
AL2O3/SIO2	0.361	0.330	0.364	0.225	0.329	0.235
FEO/FE2O3	2.000	2.781	1.949	1.516	1.469	3.871
D.I.	47.955	32.156	38.750	52.599	26.699	33.274

X= lava flow
O= hypabyssal dike
P= plug

139e

ramped and skewed in a clockwise direction, the dips mostly to the northeast within the Usfan graben and to a lesser degree in the Haddat ash Sham graben where about 200 m of sandstone crops out above a thin sandy shale containing ferrous oolites, Tigillites borings, and marine fossils, possibly reworked. Below the fossiliferous beds, which are 170 m thick, a coarse crossbedded sandstone may be part of either the Usfan or the Khurma sandstone (AUXERAP, 1967).

Lithologic character.--The three members of the Shumaysi have been described and mapped in detail by A. Al-Shanti (1966) and M. A. Yamani (1968). The lower beds are clastics ranging in grain size from pebbly to conglomeratic and from siltstone to fine-grained sandstone. Considerable brown thinly laminated shale is also present especially in the outcrops north of Wadi Fatimah. The middle member includes two beds of oolitic iron ore interbedded in shale and siltstone. Yamani (1968) has shown that the iron ore beds, which range in thickness from a thin layer to 5 m, are best developed in the vicinity of the Precambrian Fatimah formation, which crops out in the hills along the north side of Wadi Fatimah. His measurements of forsets and ripple marks in the Shumaysi Sandstone indicate that current directions for the water-laid clastics radiate from the outcrops of the Fatimah Formation, which he considers to be the source of the iron. In addition to the clastic material, the upper beds include volcanic ash and calcareous sediments, and are especially fossiliferous in the beds above the volcanic ash which outcrops about 40 m below the top of the formation.

Nature of contacts.--In most outcrops where the basal sandstone can be seen, it rests unconformably on Precambrian crystalline rocks, except where the Usfan Formation can be identified below. Where both formations can be seen, a lateritic breccia containing numerous vertical borings above glauconitic and phosphatic beds of the Usfan may represent a time break--a diastem--or a longer disconformity. Similar lateritic and siliceous beds overlie the Umm Himar Formation of Paleocene age 200 km east of Shumaysi. The overlying beds above the Shumaysi are basaltic and andesitic lava flows of middle to late Oligocene age, on the basis of K-Ar age determinations.

Paleontology and age.-The Shumaysi contains terrestrial, lacustrine, and marine fossils. Most of the pelecypods and gastropods are steinkerns. However, L. R. Cox (written commun., 1957) was able to identify a marine gastropod, Turritella (Protoma) cathedralis Brongniart, var. suprainflata Sacco of Oligocene-Miocene age in sandstone, near the top of the Shumaysi a few meters below a basalt flow dated at 32.6 ± 2 (K-Ar whole rock, table 9). Samples submitted by Al-Shanti and identified by Cox as Lanistes, late Eocene-Holocene age in northeastern Africa, Cox considered "differing slightly from the upper Eocene L. Antiqus, but on the other hand not identical with any described form of later date." Cox also identified fresh-water gastropods Melanoides (Tarebia) aff. M. barjacensis (Fontannes) of Oligocene age and Ischurestoma sp. of Eocene to Oligocene age.

Fossils from the Haddat ash Sham graben, including Haplophragmoides sp. and Cibicides sp., could not be assigned an age by Ruth Todd who identified them (written comm., 1960). She further stated that "the Cibicides seemed to have been replaced, and the Haplophragmoides was laterally compressed and probably filled. The rarity of the specimens together with their replaced and filled conditions suggest they may be redeposited fossils." Likewise I. G.

Sohn (USGS, written comm., 1960) reported that no age assignment could be made from very poorly preserved ostracodes from the same outcrops in the Haddat ash Sham area. However, the Foraminifera Operculina alpina multseptata Silvestri reported in the sedimentary section at Ar Rawdah on the north bank of Wadi Fatimah in the Haddat ash Sham graben (AUXERAP, 1967) was originally assigned to the lower Eocene in Libya (Silvestri, 1937 in Jordi and others, 1963). In Arabia it may represent uppermost Usfan or has been redeposited in the Shumaysi Formation during late Eocene or Oligocene. More recent work includes identification of pollen grains considered of early Eocene age including the non-bearing strata (Moltzer and Binda, 1981). Fossiliferous and arenaceous beds 8 m above the upper oolitic iron stratum are possibly the base of the Oligocene beds which carry Oligocene gastropods higher in the section which, in turn is capped by basalt of middle Oligocene age (32.6-25.8 Ma K-Ar).

Baid Formation

Definition.--The continental Baid Formation was named after exposures seen along Wadi Bayd (lat. 17°37'N., long. 42°22'E.) while mapping the Tihamat Al Yemen in 1951 (Brown and Jackson, 1959). Later it was also found farther north on the Tihamat ash Sham (Brown and Jackson, 1958). Most of the exposures of the siliceous nonmarine and volcaniclastic sedimentary beds and associated eruptive rocks are along the banks of the lower courses of wadis flowing toward the Red Sea on the coastal plain, and at the eastern edge of the coastal lowlands in more-or-less continuous belts between wadis. Following our reconnaissance survey, the formation was studied in much more detail by AUXERAP (Auxiliar Enterprise de Recherches et L'activities). As the discovery exposure represents only a fraction (40 m) of the distinctive Baid lithology, a better stratotype was designated 15 km northwest of Wadi Bayd near Ad Darb along the south side of Wadi Itwad where dissection of the coastal alluvium has exposed 1200 m of the underlying Baid (fig. 48)(Gillman, 1968). The Baid Formation has since been studied in detail from 10 km south of Wadi Qanunah to north of Wadi ad Duqah, the northernmost 75 km of outcrop (Hadley, 1975b, 1979; Greenwood, 1975a).

Occurrence, thickness, and lithology.--Intermittent exposures of the Baid Formation extend from south of Wadi Jizan at lat. 16°50' N. northwestward to lat. 19° 48' N., a distance of 370 km along the strike parallel to the coast; the exposures are in belts as much as 10 km wide and dipping generally 30° toward the Red Sea underneath surficial alluvial and coralline deposits. The exposure on Wadi Jizan was first, and correctly in our opinion, interpreted as septa within hypabyssal dikes and interbedded flows of dacite, diabase, and obsidian (Gillman, 1968), but more recently the siliceous argillite (silicite) of the Baid Formation has been described as resting discomformably on a dike swarm of the Tihama Asir igneous complex, which is considered part of an ophiolite suite (Coleman and others, 1979). Certainly the siliceous and volcaniclastic rocks are discomformable above the Khums Sandstone, and are intruded by diabase dikes that are part of a Miocene igneous complex.

At Wadi Bayd 40 m of the Baid Formation is exposed, striking N. 60° W., and dipping 14° southwest, 2 km downstream from agglomerate and metamorphosed mafic igneous rocks, all intruded by diabase. The Baid Formation is here cut by normal faults which also shear the diabase dikes (fig. 49). At Wadi Itwad near Ad Darb, the most complete section of the Baid Formation is exposed 1200 m west of the dike swarm and the shield on the coastal plain. According

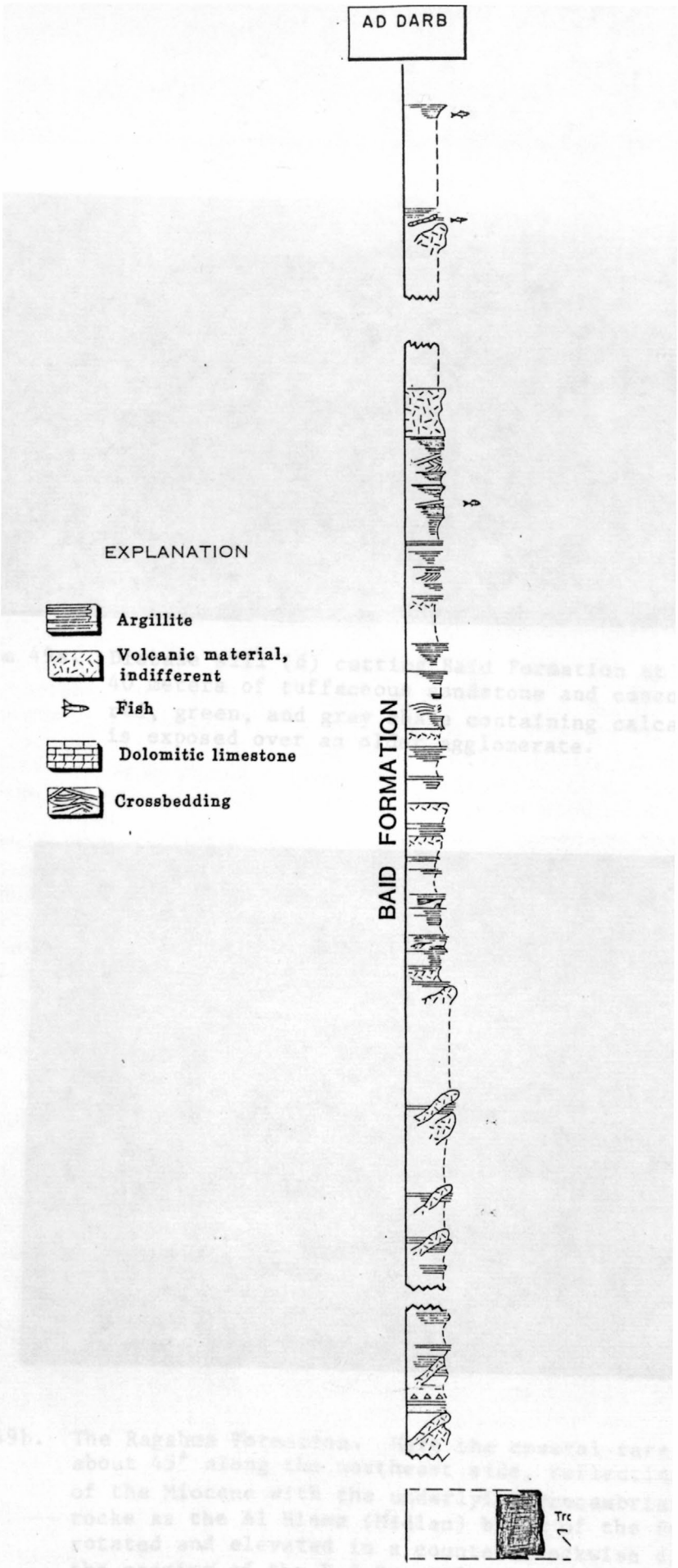

Figure 48. Stratotype section of Baid Formation, after Michel Gillman, AUXIRAP, 1968.



Figure 49a. Diabase sill (d) cutting Baid Formation at Wadi Baid. About 40 meters of tuffaceous sandstone and concoidal siliceous red, green, and gray shale containing calcareous concretions is exposed over an older agglomerate.



Figure 49b. The Ragahma Formation. Here the coastal terrace dips southwest about 45° along the northeast side, reflecting the ramping of the Miocene with the underlying Precambrian crystalline rocks as the Al Hisma (Midian) block of the Peninsula was rotated and elevated in a counter-clockwise direction during the opening of the Red Sea rift.

to Gillman (1968) it is "1200 m of chiefly gray, buff, red, or green silicite 1/ with fish fossils and intercalated green or violaceous shale (chlorite, illite and montmorillonite), volcanic tuffs, and diabase sills." (fig. 48).

Crystalline schists of the basement extend to the coast north of Ad Darb where they are nearly covered with Quaternary basalt and ash of the Al Birk lava fields. The Baid is faulted off, apparently as a result of sinistral movement on a Red Sea transform fault at Ad Darb (Coleman and others, 1979), but another coastal plain reentrant, the Tihamat ash Sham, extends north of the Al Birk harra, and the Baid Formation appears again along the eastern edge of the coastal plain. At Wadi Hali, about 60 m of argillite, silicite, conglomerate and related volcaniclastic rocks are exposed in low hills on the coastal plain north of the wadi and along the southern flank of Wadi Yiba 20 km farther north where the beds are more calcareous, especially in the upper part. Still farther north on the south flank of Wadi Qanunah, the lower 20 m is a polymict conglomerate with a thin bed of limestone near the top; it is in fault contact with Precambrian quartz diorite. The upper 17 m is argillite except 2 m of sandstone at the base (Hadley, 1975b). The volcaniclastic rocks continue northward across Wadis Limah, Ashiba, and ad Duqah. The lower part of the northernmost exposure 15 km north of Wadi ad Duqah is composed of tuff below tuffaceous siltstone and limestone (Hadley, 1979). Although a total thickness cannot be measured because of the alluvial cover and the faulting of the formation, the northern extension may be as much as 3000 m thick, of which 275 m in the mid-portion consist of basalt flows and diabase dikes and sills.

The rock, mostly volcaniclastic, ranges from coarse conglomerate, in places agglomeratic, through graywacke sandstone to silt and clay, the last in many places being indurated to shale and argillite which make up the majority of the exposures. Considerable tuff, both lithic and vitric, and chert are present and most sediments are siliceous, the silica probably derived ultimately from ash. The southernmost outcrops in the Jizan basin include flows and dikes of diabase, dacite, and obsidian (Gillman, 1968). An important difference from other ophiolitic suites is the nonmarine character of the younger assemblages, as evinced by the oxygen isotope ratios (Taylor and Coleman, 1977) and the continental or lacustrine origin of the Baid Formation.

The Baid Formation rests disconformably on the Jurassic Khums Formation at Wadi Jizan, according to Gillman (1968). Elsewhere it is intruded by the Tihama-Asir dike swarm, indicating that dikes represent a younger hypabyssal intrusive episode. The Baid is disconformably overlain by alluvial deposits, mostly outwash from the 'Asir scarp mountains.

Paleontology and age.--The Baid Formation contains few fossils, Gillman reporting only ostracods and fish impressions difficult to identify. Fish remains from the outcrops near Ad Darb were examined by Dr. A. H. Dunkle., U.S. National Museum (written commun., February 10, 1953) who commented as follows: "Included among this suite of specimens are representatives of two

---

1/ A petrologic term first used by T. S. Thomson in 1843 for labradorite, has since been considered obsolete. But the French name for this rock is most descriptive as it is highly siliceous, fine-grained, and resembles flint or novaculite.

families of freshwater fishes of widespread distribution in Asia and Africa today. One of these fishes is a cyprimid or minnow, which falls within the structural range of the recent genus Barbus. The other is of a cichlid, close, if not identical to the living Tilapia. The incompleteness of the present specimens makes specific comparisons unfeasible. The past history, although very incompletely known, suggests a middle Tertiary age for this occurrence--late Oligocene or Miocene" (Brown, 1970).

A K-Ar age of 19 ± 0.6 Ma (no. 54, table 9) for the diabase sill in the middle Baid of the Tihamat ash Sham basin agrees within instrumental error of three other ages of these sills reported by Coleman and others (1979), that is, an early Miocene age.

Bathan Formation - Miocene

Definition.--The Bathan Formation at its type locality is named for Wadi Bathan, a tributary of Wadi Lith, 15 km northeast of Al Lith (Hadley and Fleck, 1980a). The exposure adjacent to Wadi Bathan was first described, though not named, by Brown and others (1963a) as "dissected and not obviously related to present drainages" and that this boulder conglomerate may be much older than Quaternary. Brown mapped similar deposits east and northeast of Jiddah (Brown and others, 1963a) and Nebert and others (1972) described one of these deposits north of Wadi Fatima.

Lithology and thickness.--The Bathan is a terrigenous, polymictic clastic deposit consisting of boulder, cobble, and pebble conglomerate, sparse beds of coarse-grained sandstone, and rare, thin beds of red siltstone. Clasts consist of many types of Precambrian rocks, especially conspicuous Precambrian granite, as well as clasts of silicic tuffs and flows of the Baid Formation. The conglomerate is poorly sorted, commonly chaotically immature, and some thick massive beds contain boulders as much as 2 m across; many clasts are angular to sub-rounded. The thickness of the Bathan at its type locality probably well exceeds 700 m.

Occurrence and nature of contacts.--The Bathan, where mapped, underlies the Red Sea Coastal Plain or the adjacent low foothills. In most places it is poorly exposed, in fact, it is mostly identified by a flat surface of residual lag of coarse resistant boulders. Its upper surface everywhere is an erosional surface and its base where rarely exposed rests on a compound erosion surface cut across the Baid Formation, early Tertiary laterite, and Precambrian basement as at Wadi Bathan. At Harrat Tuffil (Shama), the Bathan rests on rhyolitic volcanic deposits associated with the Baid Formation (Pallister, 1982). Where bedding is visible, the beds dip gently as much as 15° either southwest or northeast in block-fault structures.

Paleontology and age.--To date no fossils have been found in the Bathan. It is younger than the stratigraphically underlying early Miocene Baid Formation and Tahamat Asir tholeiitic dikes. The Bathan Formation is probably about middle Miocene age as it is the erosional product of rapid uplift of the Red Sea Escarpment (Hadley and Fleck, 1980a) during the middle Miocene (Schmidt and others, 1982). During future mapping the Bathan probably will be identified between Jiddah and the Gulf of Aqaba and it will probably be found to lie beneath the Raghama Formation.

Raghama Formation - Miocene

Definition.--The Raghama Formation was mapped on three geologic maps: Geology of Wadi As Sirhan (I-200A, Bramkamp, Brown, and others, 1963), Geology of the Northwestern Hijaz (I-204A, Brown and others, 1963b), and Geology of the Arabian Peninsula (I-270A, USGS-ARAMCO, 1963). The type locality was chosen for the area where the most complete exposure of Miocene reef limestone, gypsum, and related clastics was found during the reconnaissance mapping.

Jabal al Raghamah forms the western flank of the lower alluvial plain of Wadi Afal in the Ash Shifa region east of the Gulf of Aqaba at lat. 28°20' N. The Raghama Formation is exposed from lat. 28°10' N. to 28°35' N., and extends westward from the alluvial plain of Wadi Afal to the Aqaba coast, the Maqna-Al Bad' area (Bramkamp, Brown and others, 1963).

The sediments there were first described in 1952 by Mustafa Sadek, who investigated the occurrence of native sulphur earlier reported by Burton (1878). The outcrops were revisited the following year by H. J. Philby and R. G. Bogue (Bogue, 1953) to further study the occurrence of the sulphur in the gypsiferous beds. Bogue described the area as basal coarse grit and conglomerate overlain by "sandstone, siltstone, and shale with interbeds of limestone and shale which often contains some volcanic tuff." Sulphur was identified with gypsiferous sandstone in the upper beds.

The following year W. Schott of the German Geological Survey described the following section (Richter-Bernburg and Schott, 1954, p. 32):

Sedimentary section near "Al Bade."

Sandy reef rocks

Sandstone, partly with boulders

Sandy claystone to clayey sandstone without microfossils about 25 m thick

Gypsum, light to whitish grey, partly compact, partly unclean, at least 300 m thick

Clayey marlstone, probably partly missing, about 15 m

Sandy reef rocks to coarse porous limestone 100-150 m

Coarse grained sandstone, crossbedded

_____Transgression

Nubian sandstone (? Paleozoic) sandy horizon, reddish grey with gravels and boulders

_____Transgression

Basement

He questionably assigned a Miocene age to the beds above the Nubian sandstone, including the gypsum.

In 1966, V. A. Trent and R. F. Johnson briefly investigated the economic possibilities of the area (Trent and Johnson, 1966), followed by a study of the sulphur possibilities by Bodenlos and Lari (1970), who divided the Raghama Formation into three major units: a basal coarse-grained clastic section; a middle unit of green marl, siltstone, and interbedded gypsum, with dolomite and sandstone in the upper part; and an upper unit of red sandstone containing a few thin beds of gypsum and siltstone.

A more detailed columnar section measured by Bigot and Alabouvette, French Bureau de Recherches Geologiques et Minieres, of the outcrops south of Magna and the Wadi Ifal plain could be considered the type section (Bigot and Alabouvette, 1976, fig. 6). However, they state that the Miocene in the Jabal Raghamah region (Magna-Al Bad area) cannot be correlated with the Jabal Dhaylan Series which is exposed on the coastal plain 350 km southeast of Jabal al Raghamah. There the Tertiary beds have been studied in connection with mineralization at the base of the middle Miocene. This latest study divides the Raghamah, as shown as a single unit on the USGS 1963 maps, into three series: a lower continental clastic section; a middle series of marine and littoral deposits, including reef limestones, gypsum, marl, and dolomite; and an upper series of clastics, oyster reefs, and gypsum.

Occurrence, thickness, and lithology.--The Ragahama Formation was shown on the USGS 1963 maps as outcropping intermittently from Yanbu at lat. 24° N. to the Magna-Al Badh area at lat. 28°35' N. The localities at Yanbu, Umm Lajj, Jabal Dhaylan, and north from Al Wajh were considered of Miocene age on the basis of meagre formal evidence. Thickness is variable, as might be expected from the marine transgressive reef and lagoonal evaporite. The basal conglomerate and sandstone are not present in all the outcrops, and the thickness where it has been measured ranges from less than a meter to more than 100 m (Bodenlos and Lari, 1970; Bigot and Alabouvette, 1973) with the maximum in the northern part of Jabal Raghamah near Al Bad; as much as 1500 m of sandstone, partly arkosic, has been reported from Tiran Island in the northern Red Sea, 30 km south of the Raghamah outcrop area east of the Gulf of Aqaba (Goldberg, 1963).

The middle unit is 400 m thick at the type locality at Raghamah, according to Bodenlos; it ranges from 25 m to several hundred meters at various places along the Tihamat, according to Bigot and Alabouvette, compared to 250-450 m on Tiran Island; and, according to Bodenlos, the upper unit of 100-200 m in the lowlands in the southwest corner of the peninsula south of Magna is comparable to 250 m at Tiran Island off the peninsular point.

The section on Tiran Island resembles the submarine Miocene of the Red Sea, as reported in various drilling records. The submarine section includes a mid-part of evaporite, mostly halite, but also anhydrite above and below the salt beds, which are more than 1200 m thick, and overlying 1000 m of middle Miocene marl characterized by Globigerina. The sediments above the evaporite series proper are mixed beds of conglomerate, calcareous sandstone, limestone, clay shale, anhydrite, and salt, as would be expected above a dynamic sea floor.

Nature of contacts.--The Raghama overlaps onto the crystalline basement in many places; more often it rests on sandstone and conglomerate of doubtful age, probably Oligocene, near Jiddah, but farther north it overlies the possibly Eocene or Cretaceous Nubian-type sandstone. At Ragahmah the sandstone beneath the marine beds was questionably considered to be Paleozoic by W. Schott, but sandstone of Early Cretaceous Senonian age is faulted down in a small graben 5 km east of Aqaba (Bender, 1968), and similar beds in a similar graben 5 km southeast of the first consists of 10 m of conglomerate and coarse arkosic sandstone below 5 m of fine-grained sandstone, varigated in color and cross-bedded, which is very likely the same clastic deposit described by Bender (Trent and Johnson, 1966). They may also be coeval with the basal sandstone at Raghamah, but without fossil evidence such a correlation is tenuous.

The Raghamah underlies Quaternary terrace deposits, including Pleistocene and Holocene coral reefs. Reefal coral of Miocene age overlies the volcaniclastic sediments of the Baid Formation east of Al Qunfidhah, and northwest of Yenbu, the Raghama is overlain by Quaternary basalt flows.

Paleontology and age.--The extensive exposures of Miocene reefs in the Yanbu' basin and northwestward toward Sharm al Khawr contains a coral Montastrea sp. cf. M. pedunculata (Duncan), previously known from the Miocene Gaj Formation of Pakistan, according to J.W. Wells, who identified it. Farther south and 10 km inland from Tuwwal, 80 km north of Jiddah, a dolomitic reef yielded the following Foraminifera and algae (collected by B. Steenstra and identified by H. A. McClure).

Foraminifera Borelis melo (common)

Heterorostegina sp.

Taberina ? malabarica

Peneroplis ? farsensis

? Cycloclypeus

Algae - Halimeda cf. H. monile or incrassata

McClure (written commun., 1975) considers that Borelis melo is a widespread guide fossil for the upper Burdigalian, thus marking the approximate lower boundary of the middle Miocene (about 15 Ma).

Still farther south and east of Al Qunfidhah, 320 km south of Jiddah and 15 km inland near Suq al Ahad, a coralline reef yielded the following corals identified by J.W. Wells:

Favites sp. cf. F. profunda (Michelotti)

Montastrea or Plesiastrea sp.

Montastrea sp. cf. M. reussiana (M.E. & H.) var. minor (Zuffardi)

The Favites sp. cf. F. profunda is known from the Miocene of Italy and Red Sea areas and the Montastrea sp. cf. M. reussiana var. minor is known from the Miocene of Cyrenaica (Libya) and Red Sea areas, according to Wells.

In addition, at Qunfidah F. S. MacNeill reported "several specimens of Cerithium belonging to the group of C. jonkeri Martin and C. poetjanganensis Altena. C. jonkeri has been reported from the upper Miocene to the Pleistocene in the East Indies and the Philippines; the latter, possibly only a subspecies of C. jonkeri from the Pleistocene of Nias and Java.

The oyster Ostrea crasissima Lamarck, which is synonymous with O. gryphoides, was found by us north of Umm Lajj; it was also found later near Al Wajd and south of Al Muwaylih by W. Schott who reported (Richter-Bernburg and Schott, 1954) the opinion of K. Staesche that the source beds were Miocene. Although a review of post-Miocene Ostreidae by L. R. Cox (1929) indicates that it extends up into the Pliocene, according to him it became extinct in the Mediteranean fauna at the end of the Miocene, but he proved on the basis of the mollusca that the beds above the thick Miocene evaporate section are of Indian Ocean affinity. The end of the Miocene coincides with the top of the evaporite sequence. This datum is marked by an accoustic reflector--now dated at 5 Ma near the beginning of the Pliocene when the Red Sea opened anew to allow ingress of Indian Ocean fauna.

As these limestone beds overlie the Baid Formation which contains a basalt lava flow (19.1 $\pm$ 0.6 Ma, K-Ar, table 15) most of the evidence points to a middle to younger Miocene age for the Raghamah with the possibility that some of the upper reefs may be Pliocene.

In this connection the basalt flow east of Tuwwal, which caps the ridge containing the approximate lower boundary of the middle Miocene, was dated by K-Ar methods at 4.4 $\pm$ 0.4 Ma (table 9), thus establishing a minimum age.

Cenozoic igneous rocks

Igneous activity in western Saudi Arabia appears to have been dormant from late Proterozoic or earliest Cambrian until mid-Tertiary when the opening of the Afro-Arabian rift system renewed magmatic upwelling which has continued until the present. Although some K-Ar radiometric ages greater than about 30 m.y. are reported from the Tertiary igneous rocks on the flanks of the rift system, they are suspect, especially where the magma has penetrated thick Precambrian terrane rich in argon (Megrue and others, 1976; table 9 this report).

Hypabyssal Tertiary igneous rocks

Intrusive igneous rocks associated with the Tertiary opening of the Red Sea include dikes, pipes or plugs, small stocks, and laccolithic cumulates (Brown, 1960; Brown and Hase, 1971; Coleman and others, 1977; Blank, 1977). Dikes predominate although they are areally insignificant when compared to the coeval harras (flood lava fields). The dikes consist of a swarm of hydrothermally altered diabase sheets associated with granophyre and cumulative gabbro pods which together comprise the Tihamat-Asir complex. It extends intermittently 150 km north from Yemen as far as lat 17°45' N. where it is terminated by the Ad Darb Red Sea transform fault.[1/] Northward beyond the Ad Darb fault, the

1/ Since this was written, J. S. Pallister has mapped a Tertiary dike swarm at Wadi Ad Damn 100 km SE of Jiddah with similar composition and age as the Tihamat-'Asir complex (Pallister, 1982).

individual dikes, which there transect continental rocks, are much larger and separated by Precambrian screens, and are designated continental dikes by Blank and Coleman (Blank, 1977, Coleman and others, 1979). They extend northward 1375 km to lat 28°30' N. in Ash Shifa, east of the Gulf of Aqaba, thence across Southern Sinai (fig. 50) (Bartov and others, 1980). Whereas the Tihamat-Asir dike swarm extend inland 50 km, the continental dikes are found as much as 100 km from the Red Sea Coast. They are characterized by remarkably linear and predominately negative magnetic anomalies (Blank, 1977), range in width from 50 to 300 m, and are mostly gabbro, anorthosite, or diorite, although a few are as alkaline as quartz syenite (fig. 51).

Within the southern complex segment, the sheeted dikes and associated rocks resemble the ophiolites of Cyprus, Oman, and Newfoundland, and are so considered in the Tihamat-Asir by Coleman and others (1979), who found that a plot of FeO* (total iron as FeO), SiO_2, and TiO_2 against FeO/MgO places the granophyre and continental dikes as well as the sheeted dikes and pillow lavas of the complex within the tholeiitic series rather than the calc-alkalic. The continental dikes between Jiddah and the Yemen border range in K-Ar age from 273 $\pm$ 20 to 18 $\pm$ 1.3 Ma, (table 9), but the older ages undoubtedly represent additional argon derived from the invaded Precambrian terrane, a situation similar to that in Liberia where tholeiitic dikes parallel to the Atlantic coastline gave anomalous old ages in the Precambrian but concordant and younger ages in Paleozoic sedimentary rocks (Dalrymple and others, 1975). One dike 175 km southeast of Jiddah (no. 51, table 9) gave ages of 177 $\pm$ 13 and 273 $\pm$ 20 Ma (K-Ar whole rock normalized to the Sydney decay rate) from the mid-zone, whereas a sample from the chilled edge gave 21.5 $\pm$ 2.3 Ma, most likely near the age of emplacement. Nine whole-rock samples from five other dikes range from 18 $\pm$ 1.3 to 25.3 $\pm$ 1.7 Ma with an arithmetic mean of 22.1 Ma (table 9). A gabbroic body (normative anorthosite) in a small outcrop 70 km. south of Jiddah at Jabal Sita' gave 26.8 $\pm$ 4.5 and 27.9 $\pm$ 5.5 Ma; it (table 9) is probably to be correlated with the continental dikes. If so this marks the northern end of the southern continental dike swarm (fig. 50). A linear magnetic low in the eastern Red Sea west of Jiddah strikes S. 63° E. and passes near the leucocratic gabbro (normative anorthosite) outcrop (Kabbahi, 1970). The magnetic anomalies associated with the southern continental dikes reappears north of Makkah 80 km to the northeast, suggesting either a transverse fault with horizontal movement, possibly a transform, or an en echelon fracture pattern allowing ingress for the dike magma as suggested by Blank (1977). The age of the Jabal Sita' rock is comparable to five wholerock samples from the layered gabbro at Jabal Ţirf which range from 20.5 $\pm$ 2.0 to 24.9 $\pm$ 1.0 Ma with a mean of 22.7 $\pm$ 2 Ma as part of the Tihamat-'Asir ophiolite, and an age of 21.8 $\pm$ 1.4 Ma for labradorite from a layered gabbro at Wadi Baysh 60 km northwest of Jabal Tirf.

The Tihamat-Asir complex intrudes the Precambrian basement, the overlying Paleozoic and Mesozoic sedimentary rocks, and the Miocene fresh-water Baid Formation. Diabase sills intruded into the Baid Formation at lat. 19°15' N. gave a K-Ar age of 19.1 $\pm$ 0.6 Ma. (no. 54, table 9), concordant with the ages measured by Fleck (Coleman and others, 1979) and suggesting that the ophiolite is younger than the Baid Formation.

In addition to the continental dikes, numerous isolated plugs and feeder pipes are exposed inland on the crystalline shield (Brown, 1972). Most of these can be identified with nearby plateau flood basalts, both chemically and

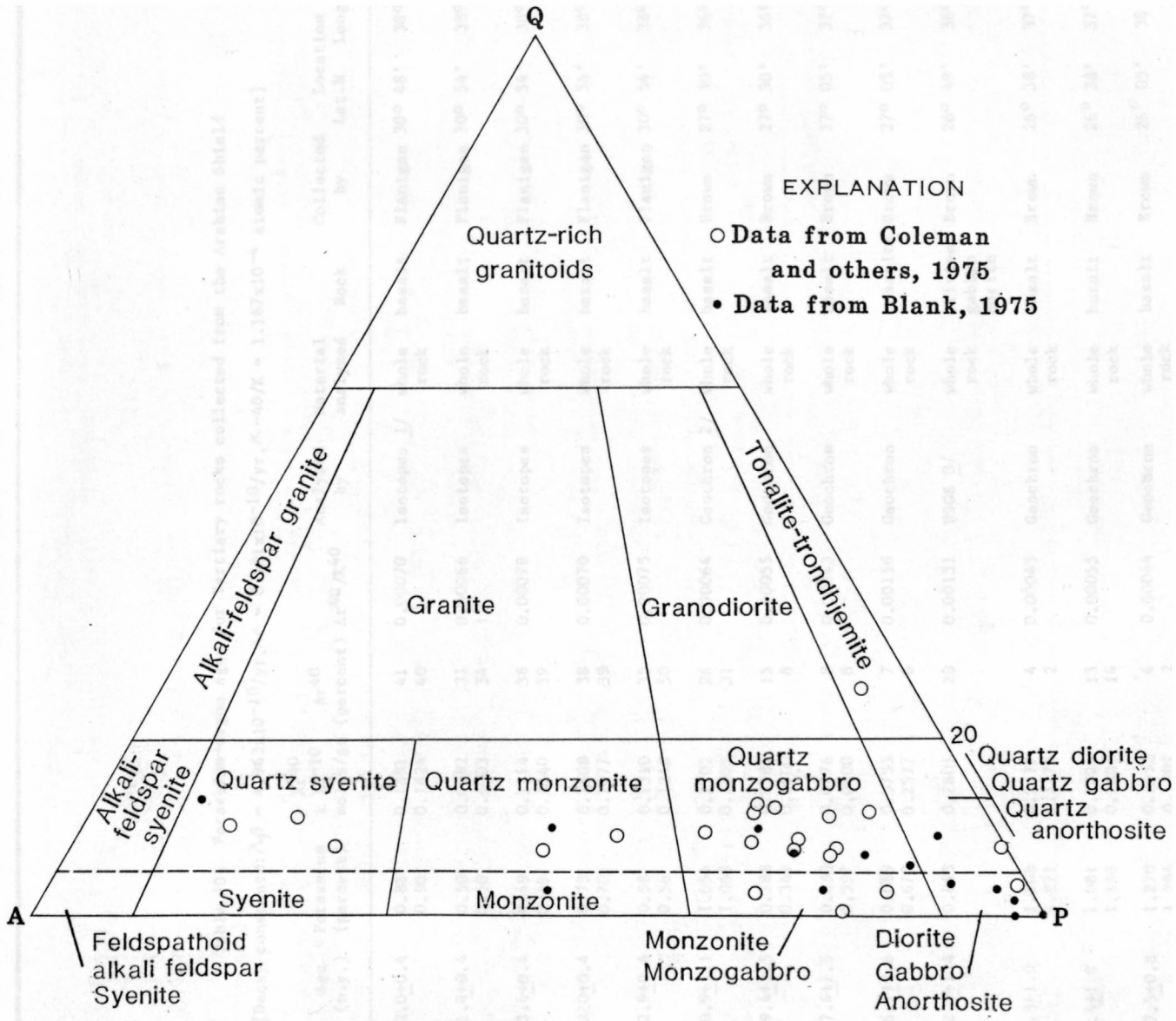

Figure 51. Modal analyses of Tertiary continental dikes plotted on quartz-alkali feldspar-plagioclase diagram (Streckeisen, 1976)

age-wise, especially in the As Sirat region where the Jabal As Sirat basalts have been eroded possibly from an area extending as far as 70 km northwest of the flows (Coleman and others, 1977). Similar pipes are exposed east of At Tai'f at lat. 21° N., either from erosion of the Harrat Hadan or from isolated intrusions; at lat. 26°15' to 26°35' N. possibly in connection with the growth of Harrat Ithnayn (Hutaym) and Harrat Khaybar; and at lat. 26°45' to 27°20' N. in a belt extending northeastward across the northeastern corner of the shield in the Jabal Shammar region. The last are not related to a widespread flood basalt but rather to a recent accumulation of local basalt and ash centers east of Jabal Salma at lat. 27° N., long. 42°25' E., the Harrat Hutaymah.

The Sirat feeder pipes are alkaline, either nepheline basalt or basanite (Coleman and others, 1977), as are pipes at or near other lava fields farther north. One isolated volcanic neck forming a spine in the Jabal Shammar belt, within the southern part of the granite batholith of Jabal Aja' at the north edge of the shield, is normative nepheline basanite (table 10). The basanite pipes near As Sirat are 24.7 $\pm$ 2 and 25.4 $\pm$ 2.7 Ma based on K-Ar ages (Coleman and others, 1977).

Coeval felsic intrusives form stocks 2 km in diameter. One stock in Jabal As Sirat near the Yemen border is analcite-bearing syenite surrounded by an analcite trachyte rim, whereas a contemporary plug at Jabal 'In 410 km northwest has a core of trachyte or hornblende latite with a rim of phonolite (Richter-Bernburg and Schott, 1954; Gonzales, 1973). The As Sirat stock is 85 percent orthoclase, 5 percent augite, 7 percent opaque minerals, 2 percent calcite and 5 percent analcite, as determined by Salman Bloch (USGS, written commun.) whereas the chilled edge is 71 percent albite and anorthoclase, 15.5 percent aegirine-augite, 7.5 percent opaque, and 6 percent analcite. The Jabal 'In stock, which is one of four in the neighborhood, is 45 percent potassium feldspar, 35 percent plagioclase, 15 percent hornblende and 5 percent magnetite (Gonzales, 1973), and is dated at 22.2 $\pm$ 3.5 Ma on K-Ar determinations from a whole-rock sample, compared to 22.5 $\pm$ 0.7 Ma for the Sirat stock (table 9). A coeval age of 22.7 $\pm$ 0.9 Ma (table 9) from the granite of Jabal Safir at 13°30' N. lat. is one of many Tertiary alkalic granite and diorite plugs, stocks and plutons continuing southward in the Yemen Arab Republic where many are concentrated along the rift scarp (Grolier and Overstreet, 1978).

Basaltic lava flows

Lava fields (harras) are scattered along the eastern seaboard of the Red Sea and upon the western Arabian highlands. They extend intermittently northward from the Yemen Volcanics ("Trap Series"), which cover as much as 35,000 km^2 of the southwestern Yemen Highlands to the Hauran of Jabal ed Drouz of comparable size in Syria. There the lavas extend across Eastern Jordan and into Saudi Arabia where they are known as Al Harrah or Harrat Ash Shamah. Within Saudi Arabia the extent of the larger harras are as follows (fig. 50):

Table 10. Potassium-argon ages for Tertiary rocks collected from the Arabian Shield

[Decay constants: $\lambda\beta = 4.963 \times 10^{-10}/yr$, $\lambda\epsilon = 0.581 \times 10^{-10}/yr$, $K\text{-}40/K = 1.167 \times 10^{-4}$ atomic percent]

Field No.	Map No.	Age (m.y.)	Potassium (percent)	Ar^{40} x 10^{-10} moles/gm	Ar^{40} (percent)	Ar^{40}/K^{40}	Analyzed by	Material analyzed	Rock	Collected by	Location Lat.N	Location Long.E
47000	1	12.0±0.4	0.88 0.90	0.1891 0.1824	41 40	0.00070	Isotopes 1/	whole rock	basalt	Flanigan	30° 48'	38° 06'
47001	2	11.4±0.4	0.50 0.50	0.0982 0.1003	31 34	0.00066	Isotopes	whole rock	basalt	Flanigan	30° 54'	38° 08'
47002	3	13.4±0.4	0.49 0.49	0.1144 0.1140	36 39	0.00078	Isotopes	whole rock	basalt	Flanigan	30° 54'	38° 10'
	4	12.0±0.4	0.73 0.70	0.1508 0.1477	38 39	0.00070	Isotopes	whole rock	basalt	Flanigan	30° 54'	38° 11'
47004	5	12.9±0.6	0.58 0.56	0.1310 0.1248	35 50	0.00075	Isotopes	whole rock	basalt	Flanigan	30° 54'	38° 12'
917 T	6	10.9±1.1	1.054 1.053	0.2102 0.1902	26 31	0.00064	Geochron 2/	whole rock	basalt	Brown	27° 30'	36° 46'
917 B	6	9.4±2.5	0.388 0.349	0.0701 0.0500	15 8	0.00055	Geochron	whole rock	basalt	Brown	27° 30'	36° 46'
916 T	7	7.4±1.5	0.630 0.597	0.0976 0.0600	8 8	0.00043	Geochron	whole rock	basalt	Brown	27° 05'	37° 18'
916 B	7	26.7±2.6	0.689 0.670	0.3753 0.2577	7 6	0.00156	Geochron	whole rock	basanite	Brown	27° 05'	37° 18'
B1818	8D	22.9±1.4	0.845	0.2801	20	0.00131	USGS 3/	whole rock	olivine gabbro norite	Brown	26° 49'	36° 05'
915 T	9_t	7.8±1.0	1.208 1.271	0.2177 0.1176	4 2	0.00045	Geochron	whole rock	basalt	Brown	26° 38'	37° 43'
915 B	9_b	9.4±1.0	1.081 1.138	0.1826 0.1801	13 14	0.00055	Geochron	whole rock	basalt	Brown	26° 38'	37° 43'
913	10	7.5±0.8	1.270 1.286	0.2052 0.1301	4 2	0.00044	Geochron	whole rock	basalt	Brown	26° 05'	38° 42'
912	12	11.5±2.3	1.015 1.006	0.2477 0.1576	11 8	0.00067	Geochron	whole rock	basalt	Brown	25° 28'	38° 54'

[Decay constants: λ_β = 4.963×10^{-10}/yr, λ_γ = 0.581×10^{-10}/yr, $^{40}K/K$ = 1.167×10^{-4} atomic percent]

Field No.	Map No.	Age (m.y.)	Potassium (percent)	Ar^{40} x 10^{-10} moles/gm	Ar^{40} (percent)	Ar^{40}/K^{40}	Analyzed by	Material analyzed	Rock	Collected by	Location Lat.N	Location Long.E
919	14	*	0.796	-	-	-	Geochron	whole rock	basalt	Brown	25° 09'	37° 26'
			0.767	-	-	-						
920	15	6.2±0.8	0.775	0.0901	20	0.00036	Geochron	whole rock	basalt	Brown	25° 09'	37° 28'
			0.764	0.0751	17							
921	16	*	0.823	-	-	-	Geochron	whole rock	basalt	Brown	24° 44'	37° 40'
			0.823	-	-	-						
911	17	21.2±2.1	0.713	0.2902	18	0.00124	Geochron	whole rock	basalt	Brown	24° 50'	38° 42'
			0.729	0.2427	18							
910	18	28.3±2.9	0.606	0.3628	13	0.00166	Geochron	whole rock	basalt	Brown	24° 48'	38° 48'
			0.593	0.2302	18							
922	19	*	0.611	-	-	-	Geochron	whole rock	basalt	Brown	24° 25'	37° 45'
			0.627	-	-	-						
3729Br	20	9.3±0.7	0.315	0.0525	10	0.00054	Geochron	whole rock	basalt	Brown	24° 40'	39° 16'
			0.301	0.0475	8							
907	22	1.1±1.0	0.269	0.008	1	0.00006	Geochron	whole rock	basalt	Brown	25° 02'	40° 14
			0.254	0.002	0.1							
909	23	62.6±4.3	0.554	0.6855	10	0.00370	Geochron	whole rock	basalt	Brown	24° 41'	39° 20'
			0.539	0.5179	7							
				0.6080	6							
908	24	20.0±2.0	0.665	0.2152	8	0.00117	Geochron	whole rock	basalt	Brown	24° 36'	40° 13'
			0.641	0.2277	10							
				0.2402	8							
923	26	*	0.592	-	-	-	Geochron	whole rock	basalt	Brown	23° 03'	39° 08'
			0.606	-	-	-						
905	27	12.6±2.5	0.416	0.0926	3	0.00074	Geochron	whole rock	basalt	Brown	23° 05'	39° 43'
			0.393	0.0851	3							
904	28	13.2±1.5	0.216	0.050	4	0.00077	Geochron	whole	basalt	Brown	22° 46'	39° 46'
			0.196	0.045	4							

[Decay constants: $= 4.963 \times 10^{-10}$/yr $= 0.581 \times 10^{-10}$/yr, K - 40/K = 1.167×10^{-4} atomic percent]

Field No.	Map No.	Age (m.y.)	Potassium (percent)	Ar^{40} x 10^{-10} moles/gm	Ar^{40} (percent)	Ar^{40}/K^{40}	Analyzed by	Material analyzed	Rock	Collected by	Location Lat.N	Location Long.E
GFB1	30	4.4±0.4	0.35 0.37	0.0270 0.0283	12 10	0.00026	Isotopes	whole rock	basalt	Brown	22° 14'	39° 27'
GFB3	32	4.2±0.8	0.45 0.44	0.0353 0.0295	16 14	0.00024	Isotopes	whole rock	basalt	Brown	21° 56'	39° 15'
GFB2	33	19.1±0.6	0.61 0.61	0.2019 0.2056	48 59	0.00112	Isotopes	whole rock	basalt	Brown	21° 58'	39° 18'
	34_a	43.7±1.0	3.60 3.56	2.758 2.738	53 44	0.00257	Isotopes	glau-conite	sandstone	Brown	21° 58'	39° 21'
	34_b	56.4±1.2	3.02 3.04	2.961 3.059	60 66	0.00333	Isotopes	glau-conite	sandstone	Brown	21° 58'	39° 21'
WELL 4 Area 1	35	32.6±2	0.594 0.589	0.3403 0.3353	47 46	0.00191	Geochron	whole rock	basalt	Brown	21° 34'	39° 32'
902	36	25.8±5.0	0.381 0.351	0.1776 0.1526	3 2	0.00151	Geochron	whole rock	basalt	Brown	21° 50'	39° 42'
47027B	37_a	8.7±2.0	0.493 0.494	0.0450 0.0851 0.0926	2 7 2	0.00050	Geochron	whole rock	basalt	Flanigan	21° 51'	40° 44'
47028	29	2.4±0.8	1.184 1.207	0.0375 0.0826 0.0275	2 5 1	0.00014	Geochron	whole rock	basalt	Flanigan	22° 40'	41° 24'
47026	38	8.0±0.5	1.121 1.150	0.1676 0.1501	9 8	0.00047	Geochron	whole rock	basalt	Flanigan	21° 40'	40° 58'
WELL 3 Area2A	39	25.9±3.0	0.395 0.385	0.1826 0.1701	21 22	0.00152	Geochron	whole rock	basalt	Brown	21° 24'	39° 39'
47024	40D	22.2±3.5	4.187 4.166	1.596 1.841 1.409	14 14 11	0.00130	Geochron	whole rock	homeblende latite phonolite	Flanigan	21 18'	41 10'

[Decay constants: = 4.963×10^{-10}/yr, = 0.581×10^{-10}/yr, -40/K = 1.167×10^{-4} atomic percent]

Field No.	Map No.	Age (m.y.)	Potassium (percent)	Ar^{40} x 10^{-10} moles/gm	Ar^{40} (percent)	Ar^{40}/K^{40}	Analyzed by	Material analyzed	Rock	Collected by	Location Lat.N	Long.E
47023	41	16.6±1.5	0.854	0.2477	18	0.00097	Geochron	whole rock	basalt	Flanigan	21° 21'	41° 20'
			0.861	0.2477	19							
47022	42	3.4±0.5	0.912	0.0550	1	0.00020	Geochron	whole rock	basalt	Flanigan	21° 20'	41° 20'
			0.876	0.0500	1							
47021	43	16.2±1.8	0.796	0.2702	24	0.00095	Geochron	whole rock	basalt	Flanigan	21° 20'	41° 25'
			0.774	0.1927	21							
				0.2027	31							
47025	44	*	0.599	-	-	-	Geochron	whole rock	basalt	Flanigan	21° 05'	41° 35'
			0.595	-	-							
926	45	19.3±0.9	3.785	1.284	28	0.00113	Geochron	whole rock	rhyolite	Brown	20° 56'	39° 31'
			3.843	1.286	33							
927A	46_a^P	26.8±4.5	0.272	0.1351	6	0.00157	Geochron	whole rock	gabbro	Brown	20° 58'	39° 35'
			0.263	0.1151	4							
927B	46_b^P	27.9±5.5	0.282	0.1576	6	0.00164	Geochron	whole rock	gabbro	Brown	20° 58'	39° 35'
			0.266	0.1101	4							
	47	7.0±4.3	0.17	0.0295	1	0.00041	Isotopes	whole rock	basalt	Brown	20° 56'	39° 36'
			0.19	0.01415	1							
66	48^P	21.3±2.1	3.40	1.101	7	0.00125	Geochron	whole rock	andesite	Gaskill	20° 53'	39° 38'
			3.37	1.376	9							
				1.301	8							
	49	2.9±0.2	1.00	0.0516	22	0.00017	Isotopes	whole rock	basalt	Brown	20° 44'	39° 40'
			0.96	0.0480	24							
	50	2.8±0.1	1.33	0.0652	32	0.00016	Isotopes	whole rock	basalt	Brown	20° 42'	39° 42'
			1.31	0.0623	35							
623A	51_a^P	177±13	0.50	1.632	53	0.0108	USGS	whole rock	gabbro	Brown	20° 26'	40° 13'
			0.51									

[Decay constants: $= 4.963 \times 10^{-10}$/yr, $= 0.581 \times 10^{-10}$/yr, $-40/K = 1.167 \times 10^{-4}$ atomic percent]

Field No.	Map No.	Age (m.y.)	Potassium (percent)	Ar^{40} x 10^{-10} moles/gm	Ar^{40} (percent)	Ar^{40}/K^{40}	Analyzed by	Material analyzed	Rock	Collected by	Location Lat.N	Location Long.E
623B	51_b[D]	21.5±2.3	0.91 0.90	0.3397	26	0.00126	USGS	whole rock	gabbro	Brown	20° 26'	40° 13'
623C	51_c[D]	273±20	0.54 0.53	2.731	41	0.0171	USGS	whole rock	gabbro	Brown	20° 26'	40° 13'
928A	52_a[D]	18.0±1.3	1.364 1.317	0.4153 0.4253	17 16	0.00105	Geochron	whole rock	monzonite	Brown	20° 22'	40° 21'
928B	52_b[D]	25.3±1.8	1.008 1.022	0.4504 0.4479	26 26	0.00148	Geochron	whole rock	monzonite	Brown	20° 22'	40° 21'
928C	52_c[D]	23.6±1.3	2.221 2.210	0.9107 0.9032	24 24	0.00137	Geochron	whole rock	monzonite	Brown	20° 22'	40° 21'
928D	52_d[D]	20.8±1.2	2.246 2.307	0.7981 0.8532	10 11	0.00121	Geochron	whole rock	monzonite	Brown	20° 22'	40° 21'
	53	1.8±1.2	0.68 0.66	0.0204	14	0.00010	USGS	whole rock	basalt	Brown	20° 51'	42° 17'
	54	19.1±0.6	0.49 0.48	0.1615 0.1617	39 28	0.00112	Isotopes	whole rock	basalt	Brown	19° 15'	41° 19'
930	55_a[D]	22.4±1.4	1.723 1.705	0.6855 0.6530	14 14	0.00131	Geochron	whole rock	diorite	Brown	18° 45'	41° 32'
	55_b	12.4±1.2	0.917 0.923	0.1977 0.1977	1 4	0.00072	Geochron	whole rock	basalt	Brown	18° 45'	41° 32'
933A	56_a[D]	43.1±3.0	0.880 0.855	0.6180 0.6931	31 33	0.00253	Geochron	whole rock	diorite	Brown	18° 32'	41° 38'
933B	56_b[D]	41.7±2.8	0.847 0.836	0.6105 0.6205	23	0.00245	Geochron	whole rock	diorite	Brown	18° 32'	41° 38'

154

[Decay constants: = 4.963×10^{-10}/yr, = 0.581×10^{-10}/yr, -40/K = 1.167×10^{-4} atomic percent]

Field No.	Map No.	Age (m.y.)	Potassium (percent)	Ar^{40} x 10^{-10} moles/gm	Ar^{40} (percent)	Ar^{40}/K^{40}	Analyzed by	Material analyzed	Rock	Collected by	Location Lat.N	Location Long.E
933C	56$_c$ D	34.7±2.1	1.245	0.7731	34	0.00203	Geochron	whole rock	grano-diorite	Brown	18° 32'	41° 38
			1.280	0.7606	33							
	57$_a$	2.1±1.0	0.691	0.025	3	0.000121	Geochron	whole rock	basalt	Brown	18° 28'	41° 31'
			0.694	0.025	4							
	57$_b$	2.8±1.5	0.669	0.0450	6	0.00016	Geochron	whole rock	basalt	Brown	18° 28'	41° 31'
			0.685	0.0200	3							
934	59	12.4±3	0.549	0.0926	3	0.00072	Geochron	whole rock	basalt	Brown	18° 08'	41° 34'
			0.509	0.135	4							
935	60 D	19.2±1.1	2.753	0.9458	42	0.00112	Geochron	whole rock	grano-diorite	Brown	18° 09'	41° 40'
			2.696	0.8807	42							
938A	61	12.1±1.5	0.798	0.160	9	0.00070	Geochron	whole rock	basalt	Brown	18° 07'	41° 44'
			0.799	0.175	9							
937	62	4.3±0.6	1.090	0.0901	8	0.00025	Geochron	whole rock	basalt	Brown	18° 04'	41° 45'
			1.084	0.0726	8							
936	63 D	23.0±1.5	1.375	0.5755	26	0.00135	Geochron	whole rock	diorite	Brown	18° 04'	41° 46'
			1.367	0.5254	25							
939	64 D	25.3±1.7	1.298	0.5680	35	0.00148	Geochron	whole rock	gabbro	Brown	18° 02'	41° 53'
			1.313	0.5855	28							
941	65	5.1±1.5	0.881	0.0776	7	0.00029	Geochron	whole rock	basalt	Brown	18° 30'	42° 02'
			0.885	0.0776	7							
940	66	5.1±1.5	1.049	0.0776	7	0.00030	Geochron	whole rock	basalt	Brown	18° 01'	42° 05'
			1.082	0.113	8							
520	67	25.3±0.5	1.34	0.5901	92	0.00148	Isotopes	whole rock	basalt	Brown	18° 10'	43° 10'
			1.32	0.5865	93							
518	69	30.1±1.0	0.52 0.54	0.2773 0.2799	36 32	0.00176	Isotopes	whole rock	basalt	Brown	17° 57'	43° 12'

[Decay constants: = 4.963×10^{-10}/yr = 0.581×10^{-10}/yr, K - 40/K = 1.167×10^{-4} atomic percent]

Field No.	Map No.	Age (m.y.)	Potassium (percent)	Ar^{40} x 10^{-10} moles/gm	Ar^{40} (percent)	Ar^{40}/K^{40}	Analyzed by	Material analyzed	Rock	Collected by	Location Lat.N	Location Long.E
103B	70	21.8±1.4	0.23 0.20	0.0830 0.0808	14 20	0.00128	Isotopes	labra-dorite	diorite	Brown	17° 26'	42° 36'
516C	72_a	20.5±2	0.093 0.080	0.0290 0.0327	13 18	0.00119	Isotopes	whole rock	gabbro	Brown	17° 03'	42° 55'
517C	72_b	24.9±1.0	3.12 3.15	1.351 1.371	26 27	0.00145	Isotopes	whole rock	hornfels	Brown	16° 57'	42° 57'
514-5	73_b	23.4±2	0.14 0.14	0.0051 0.0595	19 15	0.00137	Isotopes	whole rock	gabbro	Brown	16° 58'	42° 57'
515A	74_a	21.1±0.6	3.17 3.13	1.171 1.143	43 43	0.00123	Isotopes	whole rock	grano-phyre	Brown	16° 56'	42° 58'
515B	74_b	23.9±1.0	1.71 1.70	0.7209 0.7048	26 29	0.00140	Isotopes	whole rock	grano-phyre	Brown	16° 56'	42° 58'
					ETHIOPIA							
Asmara[D]		37.1±1.2	0.29	0.1884 0.1826	32 32	0.00218	Isotopes	whole rock	basalt	Brown	15° 17'	38° 56'

* Radiogenic argon could not be measured. This factor is thought to be due to the very young age of the basalt.
P = Plug
D = dike

	approximate area (km^2)
Khaybar-Ithnayn-Hataym-al Kurama'	21,400
Ḥarrat Rahaṭ	18,100
Al Harrah	15,200
Nawaṣif-al Buqūm	10,800
Ḥarrat ar Rahāh-al 'Uwayriḍ	7,150
Kishb	6,700
Ḥadan	3,700
Al Birk	1,800
Lunayyir	1,750
Kuramā'	1,100
Al Hutaymah	900
As Sirat	750
Jabal Jilab	320

Besides the above, there are numerous spatter or cinder cones and small flows or ash fields. K-Ar dates on the lavas range from 62.6 ± 4.3 Ma to historical times. Most dates fall between 18 and 28 Ma and 14 to <1 Ma (fig. 52, table 9; Gregory and others, 1982). The most widespread lower flows of the lava fields between Makkah and Madinah are 12-13 Ma (middle Miocene) the same age span as the lower flows in the Al Harrah of Wadi Sirhan and the basalt flows of the Hebron Formation in the Jordan Valley. All are interbedded with lacustrine marls. Where the lava has ascended via narrow vents through basement rocks enriched by argon, the apparent ages determined from K-Ar ratios tend to be older, because of argon enrichment, than physiographic evidence and degree of weathering would indicate. The larger flows seem to have escaped much of this contamination. The early eruptions followed fissures parallel to the Red Sea and are composed of picrite-ankaramite where interbedded with shallow water sediments (Gregory and others, 1982). Younger more widespread flows are alkali olivine basalts containing peridotitic inclusions, the most recent becoming bimodal with silicic flows and ash intermingling with the hawaiite devoid of mantle inclusions and reflecting sources from the sialic Arabian plate (53) (Coleman and others, 1983).

The harras

Al Harrah: The northernmost harra, Harrat Ash Shamah or Al Harrah, extends from Jordan along the northeastern flank of Wadi Sirhan. It covers about 15,200 km^2 of Saudi Arabia or one-third of the total area from Jabal ed Drouz in Syria where it is known as the Hauran. In Saudi Arabia the basalt flows extend southeastward 210 km in a belt averaging 75 km. wide with a maximum relief of 300 m. and reaching altitudes of as much as 1100 m. in Jabal al Amud (Donald Holm, written commun. 1960). There are numerous flows and many craters, calderas, and cones; in Jordan six major emissions culminated with outpourings of basaltic tuffs and fissure eruptions (dikes) parallel to the Red Sea rift (Bender, 1974). Of these, the lower three are known only in drill cores.

The surface rocks of Al Harrah in Jordan have been divided into four units, the lower three separated by lacustrine sediments, and are considered to range in age from Miocene to Pleistocene. In Arabia the lower flows, which are interbedded with calcareous lacustrine sediments, range in K-Ar age from 13.4 ±0.4 to 11.4 ± 0.4 Ma where sampled in outcrops along the

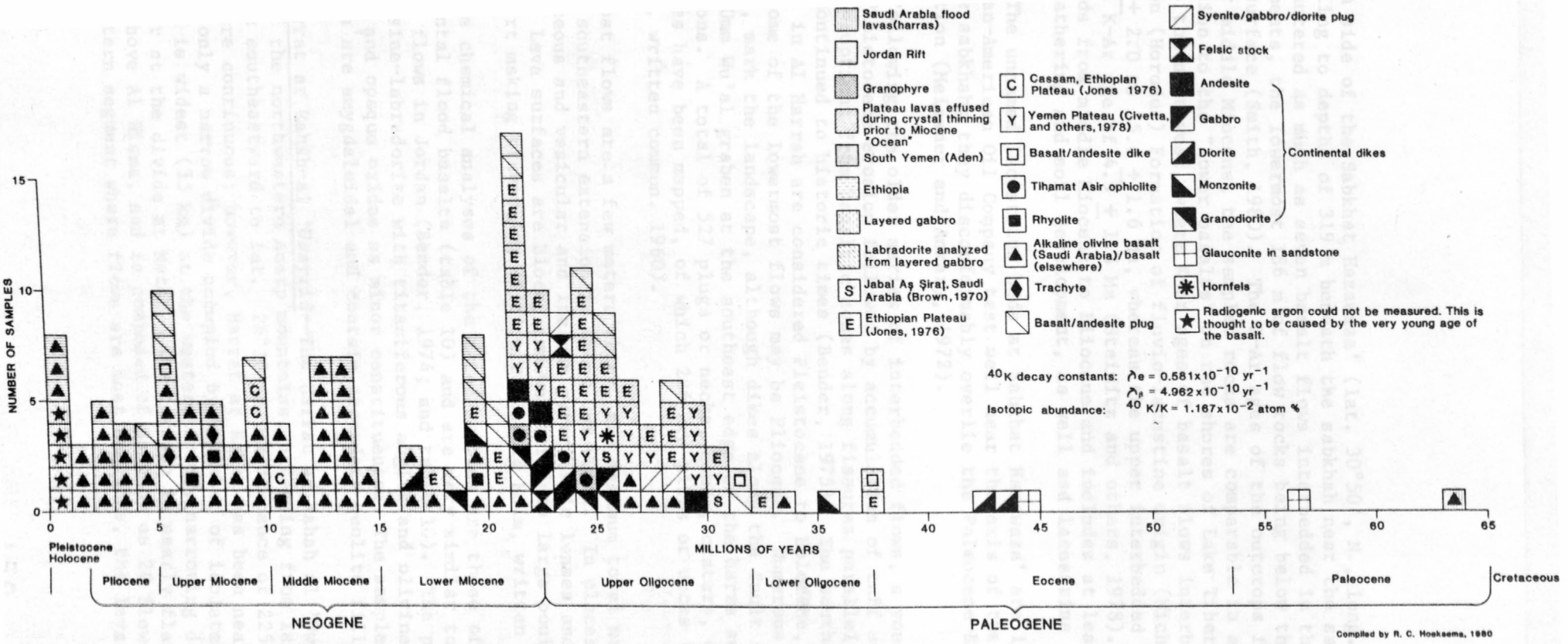

Figure 52. Histogram of selected Tertiary igneous rocks and glauconite from around the Red Sea.

north side of the Sabkhat Hazawaza' (lat. 30°50', N., long. 38°10' E.). Test drilling to depths of 319 m beneath the sabkhah near the sample localities encountered as much as seven basalt flows interbedded in the lacustrine sediments, the lowermost 186 m of flow rocks being below the dated flows on the surface (Smith, 1980). The K-Ar ages of the outcrops fall within the upper middle Miocene; the sampled rocks are comparable in age and stratigraphic position to the "lower basalts" on the shores of Lake Tiberias (Jordan) 360 km to the northwest, where K-Ar ages of basalt flows interbedded in the Hebron (Horodus) Formation of fluvio-lacustine origin (Michelson, 1978) are 10.3 $\pm$ 2.0 to 15.6 $\pm$ 1.6 Ma, whereas the upper interbedded flow of the Hebron has a K-Ar age of 4.9 $\pm$ 1.3 Ma (Steinitz and others, 1978). This time span extends from middle Miocene to Pliocene and includes at least four periods of weathering and soil development, as well asd lacustrine deposition.

The unnamed lacustrine beds at Sabkhat Hazawaza' are 150 m thick in an Arabian-American Oil Company test well near the axis of the trough occupied by the sabkhah; they disconformably overlie the Paleocene-Eocene Hibr formation (Meissner and Ankary, 1972).

Following the older series of interbedded flows, a younger flow exhibits late Pleistocene erosion followed by accumulation of tuff and cinder cones. Final eruptions from basaltic cones along fissures parallel to the Red Sea have continued to historic times (Bender, 1975). The southeasternmost lava fields in Al Harrah are considered Pleistocene to Holocene, with the reservation that some of the lowermost flows may be Pliocene. Numerous craters, some eroded, mark the landscape, although dikes along the fault flank of the Khawr Umm Wu'al graben at the southeast edge of the harra suggest fissure eruptions. A total of 527 plugs or necks, cones, craters, dikes, and tholoids or domes have been mapped, of which 286 are plugs or necks (Donald Holm, ARAMCO, written commun. 1960).

Most flows are a few meters thick, the maximum total measured is 100 m at the southeastern extension in Khwar Umm Wu'al. In places flows are scoriaceous and vesicular and include pyroclastic lenses and thin leucocratic dikes. Lava surfaces are blocky and weather into large boulders, for the most part making traversing difficult (Donald Holm, written commun. 1960).

The chemical analyses of the dated samples are those of typical subalkalic continental flood basalts (table 10) and are very similar to the average for similar flows in Jordan (Bender, 1974; and table 10). The predominate mineral is andesine-labradorite with titaniferous augite and olivine as major and calcite and opaque oxides as minor constituents. The samples from Sabkhat Hazawaza' are amygdaloidal and contain secondary zeolite fillings.

Harrat ar Rahāh-al 'Uwayrid--The Harrat ar Rahah al 'Uwayrid forms the crest of the northwestern scarp mountains, extending from lat. 28°05' N. in Al Hisma southeastward to lat. 26°30' N., a distance of 225 km. The two harras are continuous; however, Harrat ar Rahah has been nearly split by erosion, leaving only a narrow divide occupied by a number of isolated volcanic plugs. Ar Rahah is widest (35 km) at the western front, narrowing down to less than a kilometer at the divide at Matar. The terrain is nearly flat, standing 150-300 meters above Al Hisma, and is composed of as many as 20 flows. Within the southeastern segment where flows are most numerous, the lava shield rises 550

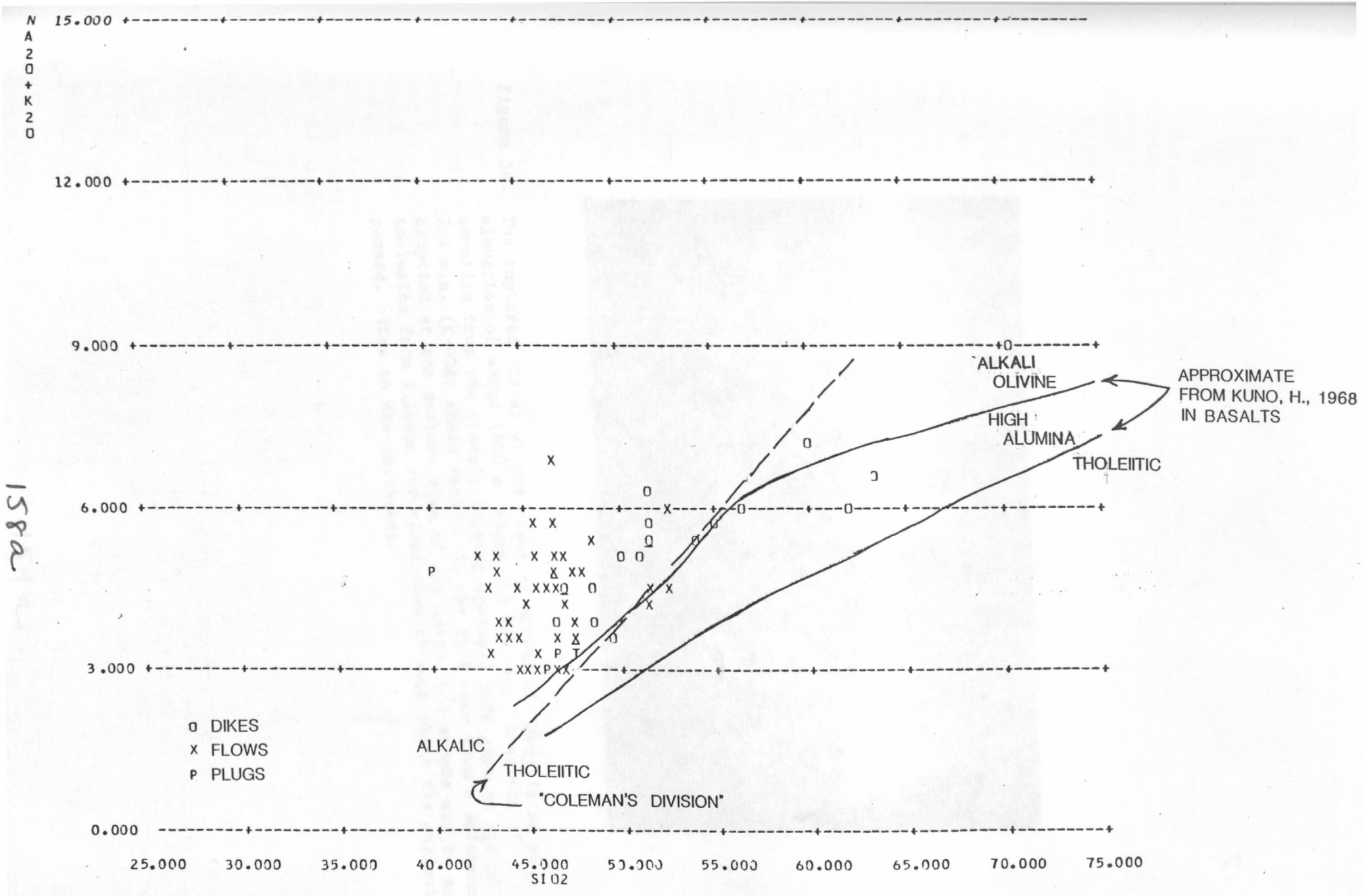

Figure 53. Alkalies plotted against silica for Tertiary igneous rocks.

meters above the plain. The flows were extruded from pipes (or perhaps from fissures that are no longer discernible). One such volcanic throat, Al Batra, stands on the sandstone plain west of the lava field. The flows are of three distinct ages, the lower, Miocene age (K-Ar determination) flows forming the cliffs facing the Red Sea and rising above the Cambrian Siq Sandstone, the upper flows being Pleistocene and Holocene. Both the sandstone and the harra are deeply dissected along the southern and southwestern fronts. Most of the lava flowed in a northeasterly direction, some along wadi channels no longer extant, suggesting eruption following ramping, the lava-filled channels now form interstream divides. More recent drainage dissects the older flows or is parallel to them. An explosion crater in the longest of these flows north of the harra attests to continuing volcanic activity in the recent past.

The southeastern segment of the Ḥarrat ar Rahāh is similar to the northwestern part except that the number of flows increases to as many as 25, for a total thickness of 515 m, including several weathered zones. The lava shield there rises to a maximum altitude of 1950 m compared to 1750 m for the northwestern block (fig. 54).

The southeastern extension, Ḥarrat al 'Uwayriḍ, is comparable in extent to the Ḥarrat ar Rahāh, rises to a reported height of 1920 m, and is somewhat more deeply eroded. However, the region of Al Jaww, a depression partly separating the harrah, was the site of the most recent eruption in the lava plateau. A dome in the Tabuk Formation at the northwestern corner of this belt appears to be a volcanic diapir of perhaps Tertiary age that failed to reach the surface (Brown and others, 1963). Even though wind scour from sand blasting through the gap has cut lineations trending N. 45° E., the flows and cinder cones are little eroded. Indeed an eruption at Hallat al Badr on Jabal Thadra in the Jaww was reported to have destroyed Bedouin and their flocks in historic time (Musil, 1926). Likewise, the name Harrat an Nar (the fire harrah) of ancient geographers was considered by Musil to be Ḥarrat ar Rahāh-al 'Uwayriḍ, although the ancient reference may have been to Jabal al Abyad in the Ḥarrat Khaybar or Jabal Ithnayn in the Harrat al Ithnayn, which likewise are surmounted by fresh cinder-ash cones of Holocene age.

Samples of basalt gave K-Ar whole-rock ages ranging from 26.7 Ma to 7.4 Ma, the oldest from 5 m above the base of Ḥarrat al 'Uwayriḍ and above the bed of Wadi Jizl (table 9, no. 7b, 7t). However, basal samples from northern Al 'Uwayriḍ and the southern tip gave 9.4 $\pm$ 2.5 and 9.4 $\pm$ 1.0 Ma, respectively, a more likely age for the inception of volcanism. Samples taken from the highest flows were 7.8 $\pm$ 1.0, 7.4 $\pm$ 1.5 and 10.9 $\pm$ 1.1 Ma. The last sample, however, came from lava out of a Holocene crater, and the age is obviously too great when a sample from the basal flow nearby analyzed 9.4 $\pm$ 2.5 Ma. The deeply eroded lower flows are possibly late Miocene, ranging in age from 9.4 to 7.5 Ma (table 9). The younger flows in Ar Rahāh came from eruptions after the present drainage system was established, altering the older incised meanders to form more recent flood channels, suggesting a middle to late Pleistocene age. Thus the latest eruptions are undoubtedly Holocene.



Figure 54. The ruptured crater at the crest of Harrat al 'Uwayrid at an elevation of about 1900 m. above the Red Sea. A sample of hawaiite from the steeply dipping westward tuff gave an age of 7.4 m.a. (K-40Ar whole rock). As the tuff came from a Holocene eruption at the eastern edge of the harra, the sample may be an inclusion from a lower and older flow through which the explosion passed. View to the northwest.

Estimation of age from the erosion rate of the basalt is difficult because of climatic change, and the erosive differences of sand-blasting by wind and erosion by water, especially where there is a wide range of rock fragment size in bed load. Doughty (1888 p. 419, vol. 1) describes conditions in the Ḥarrat al ʿUwayriḍ thus:

"Viewing the great thickness of lava floods, we can image the very old beginning of the Harra--those streams upon streams of basalt, which appear in the walls of some wady-breaches of the desolate Aueyrid. Seeing the hillian are no greater, we may suppose that many of them (as the Averine Monte Nuovo) are the slags and the powder cast up in one strong eruption. The earlier over-streaming lavas are older than the configuration which is now of the land: - We are in an amazement, in a rainless country, to see the lava-basalt pan of the Harra, cleft and opened to a depth of a hundred fathoms to some valley-grounds as Thirba. Every mass is worn in grooves in the infirmer parts by aught that moves upon it; but what is this great outwearing of 'stones of iron', indomitable and almost indestructible matter. We see in the cliff-inscriptions at Medain, that the thickness of your nail is not wasted from a face of soft sandstone, under this climate, in nearly 2000 years."

Doughty's observations are true where the inscriptions are a few meters above the land surface, but where the sandstone tomb facades with dated Nabatean inscriptions at Mada'in Salih are exposed to the wind near the land surface, sand blasting and spalling has undercut as much as a meter into the lower one or two meters of the face during the last 2000 years (fig. 55)(Brown, 1960). This amounts to 500 meters per million years. As sandstone underlies the lavas all along the western front of Ḥarrat ar Raḥāh-al ʿUwayrid, a time span of 9 Ma (the K-Ar age of the earliest volcanic eruption) would allow a scarp retreat of 4.5 km under present climatic conditions. If this process functioned alone, the lava cliffs should stand directly above the sandstone face, spalling off as the sandstone face retreated. Instead we see the lava removed ahead of the sandstone, all indented by a dendritic drainage pattern among isolated sandstone buttes, then sandstone buttes capped with basalt, and finally in the head waters the basalt front along the toe of the mountain face above a sandstone bench (fig. 56). Evidently insolation and the wide diurnal temperature range causes the lava to fracture so that most exposures are great piles of boulders often faceted into windkanter from sand blast. The boulders and cobbles are removed down the slopes by gravity, especially during the occasional desert rainstorms, to form the present terrain. Isolated lava-capped buttes suggest that the harra scarp have receded as much as 5 km during the desert erosion cycle. As this rate must be more rapid than that of the present day desert cycle, a late Miocene age for the oldest flows would be maximum.

The lava we sampled from the base and top of the volcanic pile of Harrat al 'Uwayrid are alkali olivine basalts with either phenocrysts of forsterite olivine, some zoned toward fayalite rims and clinopyroxene, or opaque oxides with some interstitial calcite and chlorite, according to Salman Bloch (USGS, written commun., 1976). Sample 7b, table 10, is unusually rich in olivine phenocrysts, as is also the youngest flow at the crater crest near the center of the harra where the olivine is glomeroporphyritic and zoned; some phenocrysts of fayalite are rimmed with iron oxides. Amydgules contain calcite and stilbite; and rare picotite is rimmed with opaque ore minerals.

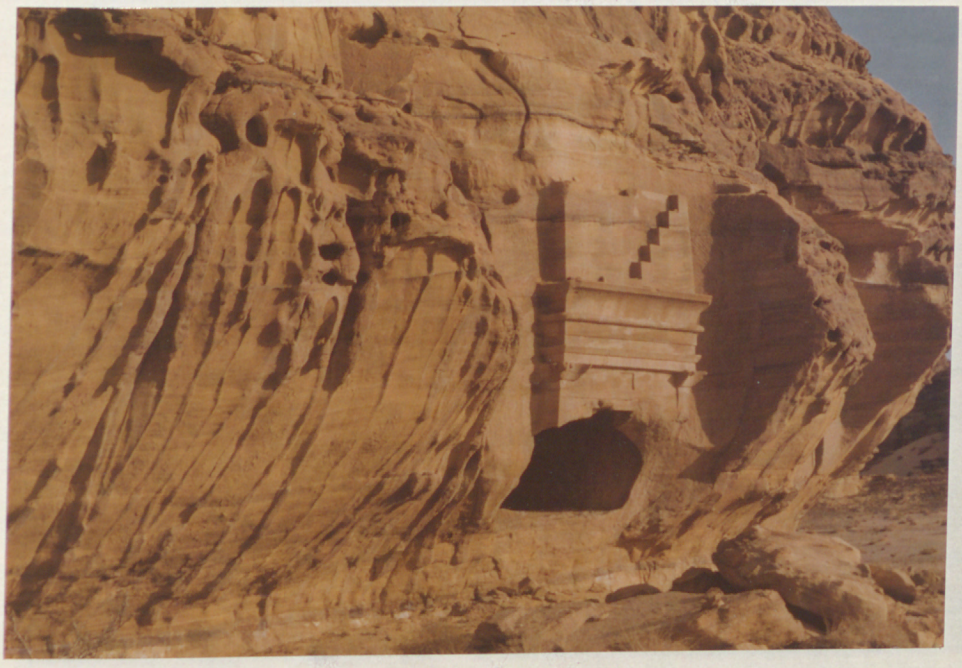

Figure 55. Nabatean tomb (65 A.D.) at Medain Salah showing one meter of wind scour and spalling for two millennia.



Figure 56. Harrat ar Rahah front on the right. The lower basalt flow of picrite-ankaramite was dated at a late Miocene age of 9.4± 2.5 m.a. (K-Ar whole rock). A Holocene eruption formed silicic domes and necks on the skyline (Coleman and others, 1983). Boulders in the foreground compose one of discontinous earlier Tertiary clastics outliers. The Ordovician Ram Umm Sahm Sandstone forms white pinnacles in the background, the darker reddish Siq Sandstone is probably Upper Cambrian. View to the northwest.

Harrat Khaybar--The Harrat Khaybar, the adjoining Harrat al Ithnayn on the northeast, and the southwestern extension, known locally as Harrat al Kura, together form the largest plateau-basalt field in Saudi Arabia, although it is only slightly larger than the Harrat Rahat between Al Madinah and Makkah. Harrat Khaybar extends from long. 38°30' E. to long. 40°46' E. and from near Madinah at lat. 24°39' N. to lat. 26°11' N. The Harrat al Ithnayn segment extends an additional 75 km north and as much as 85 km farther east. The basalt plateau rises from 475 m at the crystalline basement along Wadi Hamd to 2015 m in Jabal al Abyad in the center of the pile 115 km to the east. Boreholes have proven basalt thicknesses of more than 500 m (Delfour and Dhellemmes, 1980).

The older flows cover the western part, extending at least as far as the Madinah-Khaybar road; K-Ar ages normalized to the Sydney constants range from 11.5 $\pm$ 2.3 to 7.5 $\pm$ 0.8 Ma (table 9) for the part of the harra called Al Kura. The age of the base of a flow at the south edge of the Khaybar oasis is 9.3 $\pm$ 0.7 Ma. Thus the time span for the Harrat al Kura flows is similar to that for Harrat al 'Uwayrid. The degree of erosion appears similar, with some evidence that the lavas flowed westward prior to the ramping of the Red Sea flank. The basalt outlier west of the elbow of capture of Wadi Jizl at the junction with Wadi Hamd suggests, but does not prove, that the lava streamed down the ancestral Wadi Jizl valley to the northwest. All more recent flows which comprise the eastern half of Khaybar and Harrat al Ithnayn (Hutaym) flowed radially from volcanic centers, but the general trend during the Quaternary is eastward down wadis into the Wadi ar Rimah drainage (no. 22, table 9), most recent volcanic activity being within historical time.

The older lavas are alkalic olivine basalt, where sampled. Sample 12 (11.5 $\pm$ 2.3 Ma, K-Ar) at the western base may be considered a basanite from the normative analysis with exceptionally low silica content (table 9). Sample 10 from an outlier northwest of Harrat Khaybar in the Qal'at as Sawrah quadrangle falls within the basanite or hawaiite field on the A.F.M. diagram (fig.57). Similar lavas in the lower part of the Harrat Khaybar around and near Jabal al Abyad (fig. 58) are reported to be largely hawaiite, according to Baker and others (1973), who include nephelinite, trachybasalt, trachyandesite, phonolite, trachyte, and rhyolite as minor rock types. The more alkalic flows are generally the youngest, and at Jabal al Abyad (the white mountain) peralkaline rhyolite and rhyolitic crystal tuff is concurrent or slightly older than the youngest unweathered alkali basalts. The peralkaline rocks of Jabal al Abyad are unique among the great bulk of the Tertiary and Quaternary alkaline basaltic volcanism on and near the Arabian Shield in Saudi Arabia, although the latest eruptions in all the harras are ash cinder cones, generally indicating a more silicious termination. More recently the chemical variation from basanite to peralkaline rhyolite has been confirmed (Delfour and Dhellemmes, 1980)

Harrat Ithnayn, the northeast extension of Harrat Khaybar, is made up of rocks similar to the volcanic deposits around Jabal al Abyad. The largest volcanic cone, Jabal Ithnayn (fig. 59) on the meridian of the north-south line of cones through Jabal al Abyad, and 22 km north, is a gray dome-shaped cinder cone surmounting a black Holocene basalt flow at an altitude of 1416 m. Recent volcanic activity was suggested to Doughty in 1883 by Beduin who described a warm smoking vapor around the crest after winter rains. The numerous cones of cinder, ash, and agglomeratic and scoracious flows trend northwesterly parallel



Figure 57. Bathan boulder conglomerate in the foregound overlying the Miocene Jizan Group in the middle distance. The Jizan Group here is altered silicious and limonitic tuff of the Baid formation. View downstream toward the Red Sea and along Wadi ad Duqah in the Jabal Shada quadranglė.

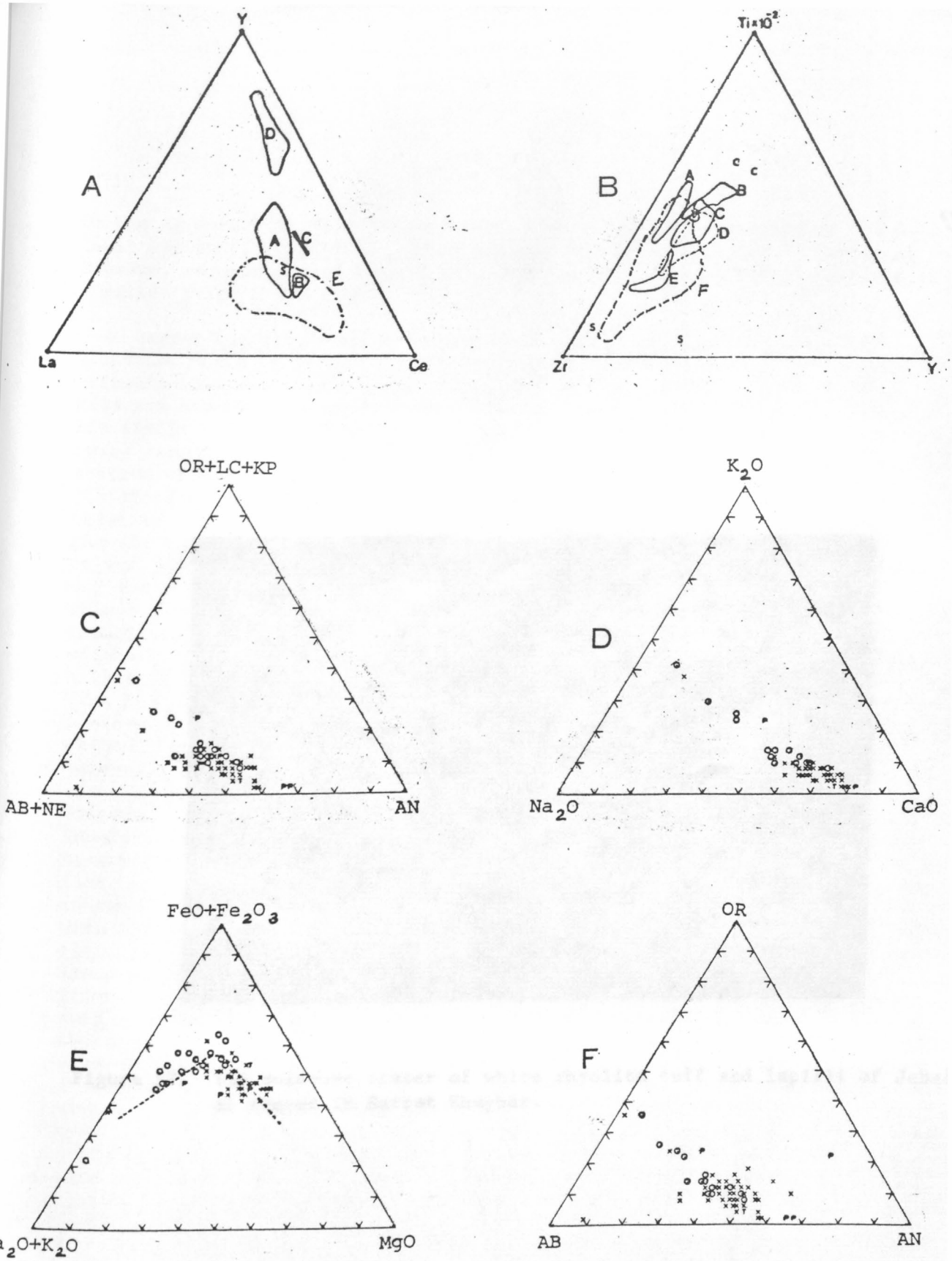

FIGURE 58. Ternary diagrams of Tertiary igneous rocks

x Flow
P Plug
o Dike
T Jabal at Tirf
s Pipes
c Precambrian intrusives



Figure 59. The Holocene crater of white rhyolite tuff and lapilli of Jebal al Abayad in Harrat Khaybar.

to the Al Harrah at Wadi Sirhan and to a northwesterly extension of the Najd fault system (Brown, 1972). Jabal Hibran, the largest crater in Harrat al Ithnayn, is composed of layered ash, scoria, and bombs of welded trachyte or rhyolite (fig. 60).

Harrat Lunayyir--Harrat Lunayyir, on the lower slopes of the scarp mountains north of Yanbu' (lat. 25° N.), was formed during two principal volcanic episodes during Pleistocene, possibly late Pliocene, and Holocene time and has been mapped by Kemp (1981) and Pellaton (1982). The lava fields lie mostly at 1000 m above the Red Sea, but flows spread down wadi channels in every direction, reaching the Red Sea at two places. Although parts are covered with alluvium on the coastal plain, the coastal lava overlies Pleistocene terraces and individual flows are both younger and older than coralline benches on the coast (Bigot, 1975). The some 50 vents whence came the flows lie some 60 kms inland where the harras overlies Precambrian crystalline rocks. The age determined for sample 15 (table 9), (K-Ar age of 6.2 $\pm$ 0.8 Ma, is undoubtedly too old, as the sample came from the most recent flow and samples 14 and 16, also from the most recent eruptions, contain insufficient radiogenic argon to measure, thus indicating an age in keeping with the physiographic evidence. Kemp (1981) has divided the younger episode with five eruptions; the last possibly occurring in the 10th century or earlier (Von Wissman and Neumann van Padang, 1963). Sample 16 comes from a small isolated eruption at Jabal al Qishr (fig. 61) which terminated with an only slightly eroded cinder ash cone 20 km south of Harrat Lunayyir. The same volcanism continued intermittently furthur south to near Yanbu al Bahr and is also too young to measure by K-Ar methods. The youngest sample comes from a Holocene unweathered small flow in Wadi al Ajal (sample 26, table 9) and contains insufficient argon to measure. Thus a series of small, very recent, perhaps historical flows and cinder cones are widely scattered from Harrat Lunayyir (lat. 25° N.) to the Harrat al Birk (lat. 18° N.) along the coastal plain and in the foothills and are apparently contemporaneous or penecontemporaneous with the scores of cinder and ash cones above the source fissures of the larger flood basalt harras. These flows are black, scoriaceous, often calcareous and mixed with ash, in contrast to the reddish brown and gray-weathered older flows. Chemically, the Holocene flows are all alkali olivine basalts where sampled (sample 14 approaches hawaiite from the normative andesine). Some of the scoriaceous and vesicular flows contain secondary calcite; ophitic to subophitic textures are formed by phenocrysts of olivine and labradorite in a groundmass of clinopyroxene, labradorite, olivine, and opaque iron-bearing minerals. Inclusions of the underlying crystalline shield rocks and ultramafic xenoliths are fairly common. They appear similar to those in the Al Birk coastal plain lavas in the Tihamat al Yemen farther south, composition ranging from alkali olivine basalt (basanite) to hawaiite with xenoliths of chrome spinel bearing wehrlite in the older flows (Kemp, 1981, p. 36).

Harrat Ishara-Khirsat- and Harrat Harairah.--Remnants of older flows cap hills near Madinah and northwestward along the southwestern flank of Wadi Hamd and Wadi al Jizl as far as 26°30' N. lat. (Pellaton, 1976, 1979). The mesa and butte cappings range in thickness from 5 m to more than 400 m and K-Ar ages range from 7.7 $\pm$ 0.7 - 11.1 $\pm$ 0.8 Ma (Baubron, 1976, reported in Pellaton, 1979) to 62.6 $\pm$ 4.3 Ma (table 9). The oldest sample came from the uppermost of three flows west of Jabal al Bayda, 35 km northwest of Al



Figure 60. The tholoid of Jabal Ithnayn, Harrat Hutaym.



Figure 61. The crater of Jabal Hibran, Harrat Hutaym.

Madinah where olivine basalt contains zoned xenocrysts of fosterite rimmed by fayalite in a ground mass of plagioclase (An_{60}), clinopyroxene, and accessory opaques. The content of calcite is high in amygdules and in the ground mass, according to Salman Bloch. The normative values are similar to those of the lower flows of Harrat Khaybar being especially low in silica (43.7 percent). As all other K-Ar ages of flows are less than 32.6 m.y., the age seems excessive, especially when the lavas forming brittle tops at Al Jarf 50 km northwest range from 21.2 $\pm$ 2.1 and 28.3 $\pm$ 2.9 Ma, ages comparable to those at Harrat Hadan and Jabal As Sirat farther south. The older age is from the basal flow of hydrothermally altered basalt containing olivine that is partially altered to bowlingite and the clinopyroxene is partially changed to chlorite and calcite. The labradorite is not altered, according to Salman Bloch. The younger age is from the topmost 15 m flow which is 12 or more flows above the lower sample. It is typical alkali olivine basalt. The deeply eroded basalt pile at Al Jarf is 820 m thick (some of which may be due to fault repetition) and rests locally on flat-lying varve-like silt and fine sand of lacustrine or deltaic origin. Farther northwest at Harrat Harairah a conglomerate bed above the basement and below the lowermost flow contains chert boulders with casts of Eocene fossils (Brown, 1970). But the fossiliferous boulders were not seen at the northernmost outcrop of the harra at the head of Wadi Ash Schizm. There a small mesa rises above 1500 meters at the crest of the peninsular divide. Twelve flows aggregate about 200 m of amydaloidal and olivine-rich basalt. Two beds of gravel are interbedded in the flows above the basal gravel which overlies Precambrian basement.

The variable measurements of argon suggesting a long time span, make the ages of volcanism questionable and are discordant with other evidence. The occurrence of post-Eocene gravel and conglomerate (fig. 62), the pre-ramping direction of flows, and the extensive erosion suggest that the harras are of similar age to Harrat al Uwayrid northward and to Harrat Hadan and As Sirat southward (Coleman and others, 1983). The general sequence of picrite-ankaramite below peridotite-nodule-bearing olivine basalt and overlain by diktytaxitic alkali olivine basalt is common to widespread outcrops (Coleman and others, 1983), suggesting a general correlation for the older vulcanism. Perhaps two general eruptive episodes are late Oligocene-early Miocene (29-20 Ma) and middle to late Miocene (10-7 Ma).

Harrat Kuramā'.--This relatively small harra which lies directly south of Harrat Khaybar and due east of the north end of Harrat Rahat at Al Madinah is also known as Harrat Hirmah (Pellaton, 1981). The area is drained by Wadi Shaqrah and its tributaries, terminating at the Qa Hazawza' which is a sabkha formed by the lava dam of Harrat Rahat. The wadi nearly bisects the harrah into two lobes, the westernmost part apparently the older and the only part sampled. An eroded and cratered cone rises 90 m above the harrah surface near the northwestern edge of the lobe and is the source of the surrounding flows. The scoriaceous and subophitic olivine basalt (no. 24, table 10) contains amygdules of calcite; the olivine is not zoned, in contrast to other samples, but some grains are altered to iddingsite according to Salman Bloch. The K-Ar analysis yielded an early Miocene age of 20.0 $\pm$ 2.0 Ma (no. 24, table 9) which may be excessive. However, the weathering of the basalt and the well developed drainage on a general southwesterly sloping surface suggests preramping flowage into the ancestral Wadi Hamd valley and an epoch older



Figure 62. Cinder-ash cone, Jabal al Qishr, an easternmost vent of Harrat al Birk, probably an historical eruption. Lat. 18°31' N., long. 41°48' E.

than that of adjoining, much larger olivine basalt floods. The lobe east of Wadi Shaqrah is marked by hummocks forming irregular lineaments similar to those in the southern portion of Al Harrah near the Jordan frontier; they were evidently formed by younger very fluid flows. The eruption came from a crest of 960 m in the central part of the harra, and surrounds the collapsed Hirma crater in the west-central part. The crater is 6 x 4 km in area and has vertical walls at least 25 m in height. Although the floor is a saline silt plain and the lower walls are sandstone, similar to the Siq Sandstone exposed southeast of the harrah, the entire thickness of the basalt flows is exposed.

Harra Rahat--Harrat Rahat extends from Madinah at lat 24°30' N. to Wadi Fatimah north of Makkah (lat 21°40' N.), a distance of 310 km; the harra has an average width of 60 km. The basalt has filled the upper valley of Wadi Hamd, whose ancestral thalweg probably extended from the headwaters of Wadi Fatimah northward to Al Madinah, thence beyond to Wadi Jizl where the present channel sought a more direct course to the Red Sea through a narrow gap in the foothills at lat 26° N. The harrah surface rises southward from 650 m above the Red Sea at Al Madinah to a maximum altitude of 1640 m at lat 23° N., decreasing somewhat in the southern part where the crest is 1570 m. The high points are linear clusters of cinder and ash cones (many breached) or Holocene domes and represent four centers of late volcanicity, so Harrat Rahat is actually four coalescing harras. They are Harrat Madinah which is essentially contiguous with Harrat Abu Rashid to the south; Harrat Beni Abdullah still farther south; Harrat Turrah which includes the crest; and Harrat ar Rukah the southernmost. The cone and dome eruptions occur as segments of the north-south volcanic central linear ridge that continues northward en eschelon across Harrat Khaybar and probably represent fissure (fault) control (Brown and others, 1963a). The youngest peaks are near Al Madinah where the latest flow errupted in A.D. 1256 (Doughty, 1888 p. 593). Numerous cones in the segment some 75 km south, the Harrat Abu Rashid, likewise have young black flows, mostly aa-type and similar to the Harrat Madinah flows with eruptive centers trending N. 20° W. but somewhat scattered compared to a trend of N. 10° W. for Harrat Bani Abdullah. Many of the black scoriaceous flows occurred after a period of more siliceous cinder and ash eruptions, a sequence similar to that at Jabal al Abyad in the Harrat Khaybar (Pellaton, 1981). Another segment of medial cones and craters, erupted on the older flows of the Harrat Turrah, the eruptive centers trending N. 08° W., very similar to the trend of Harrat Rukha'. The weathering and fracturing of the blocky basalt and ventifacts developed an extremely rough terrain. Lava has moved centrifugally from each center, abutted flows from adjoining centers, and then flowed either east or west onto the flanks of the ancestral Hamd valley. On the west numerous flows from the three southernmost harrat have flowed through passes in the scarp mountains and down the broad wadis draining the westward front of the Hejaz scarp. The fluid basalt streams then flowed out onto the coastal plain; most of the flows lie on a pediplain that was about 75 meters above the present surface (Brown and others, 1963a). The Harrat Rahat has been drilled at numerous places for water supply, notably south of Al Madinah and along the NE border. A thickness of 70 m was drilled at Dhumariyah, 85 km southeast of Al Madinah near the north edge of the Harrat abu Rashid, where three flows are separated by white marl (Durozoy, 1972). Most flows are only a few meters thick. The decrease of maximum altitude toward the southern edge of the harrah suggests that the younger flows total at least 170 m in thickness, assuming that the ancestral Hamd valley slopes uniformly northward.

The drilling at Dhumariyah (Durozoy, 1972) penetrated a carbonaceous marl overlying basement rocks; red marl, sand, and gravel overlies the basal marl and underlies the basal lava. The carbonaceous marl contains a microflora of probable Oligocene age which may, however, correlate with the uppermost nonmarine and carbonaceous sediments of the Shumaysi Formation west of Makkah where basalt flows or sills overlying the Shumaysi are dated as 25.8 ± 5.0 and 32.6 ±2 Ma from bore samples (nos. 35 and 36, table 9) and 20.1 ± 0.7 Ma from a basalt outcrop (Coleman and others, 1979). The Shumaysi Formation contains fresh-water fossils of Eocene and Oligocene age, the middle and lower carbonaceous beds containing Eocene spores below an upper and meager Oligocene fauna (Al Shanti, 1966; Moltzer and Binda, 1982). Another surface sample from Haddah ash Sham, west of the southern Ḥarrat Rahat, gave an age of 25.8 ± Ma. This basalt overlies sediments containing early Tertiary, apparently Eocene but possibly redeposited, marine Foraminifera. Thus it appears that the earliest Harrat Rahat lavas are Oligocene or younger. Indeed, two K-Ar whole rock ages from the lowermost of the upper lava streams overflowing the scarp divide, are 12.6 ± 9.5 and 13.2 ± 1.5 Ma (samples 27 and 28, table 9), or middle Miocene in age.

Younger flows at Khulays and the harrah north of Sharm Abhur 40 km north of Jiddah (nos. 30, 32, table 9) are dated as 4.4 ± 0.4 and 4.2 ± 0.8 Ma. All are normative alkali basalt, including sample locality 37 at Harrat Biss (Ashayrah) which is separated from but near the southeast corner of Harrat ar Rukha which yielded an age of 8.7 ± 2 Ma. However, flow rock from locality 38, a small lava field at Jabal al Barz, 35 km southeast of Ashayrah gave a coeval age of 8.0 ± 0.5 Ma and an analysis of 6.83 percent $K_2O + Na_2O$ and 10.24 percent normative nepheline, a composition approaching that of nearby and older Jabal' In which is hornblende latite-phonolite. Sample locality 33 from lava overlying the early Tertiary Usfan sediments in the Usfan graben north of Jiddah contains 5.15 percent $K_2O + Na_2O$ and 8.56 normative nepheline. The K-Ar age is 19.1 ± 0.6 Ma. Youngest flows in Harrat Rahat are alkali olivine basalt which erupted soon after a late episode of producing sodic lavas ranging from soda mugearite to phonolite (Smith, 1980, 1982; Kemp and others, 1982).

Ḥarrat Kishb.--Ḥarrat Kishb lies east of the southern part of Harrat Rahat, and is Pleistocene and Holocene as the radiogenic argon was insufficient to measure age except for sample 29, which gave an age of 2.4 to 0.8 Ma from a 3 meter basal flow at the south edge of the harra. A partial chemical analysis falls within the basanite field on the alkali-silica diagram, but many of the white eruptions are tholoids (domes) and doubtless are trachytic or dark rhyolitic. The earlier flows are dark gray and more recent flows are vitreous. More than 150 cinder and scoriae cones, many breached with small lava flows, and tholoids rise above the lava field. A remarkable explosion caldera or crater, Al Wahbah, is 2 km wide and 270 m deep midway along the western margin of the harra (fig. 63). The walls are Precambrian granitoid and the crater is rimmed with ash and other ejecta formed by a phreatic explosion. A more recent basalt flows around the ash rim. Ultramafic xenoliths are scattered through the ash. On the harrah the cones often lie along lines following sublava fissures; the most prominent in the northwestern quadrant of the harra trends N. 15° W., about parallel to similar lines of cones on Harrat Rahat.

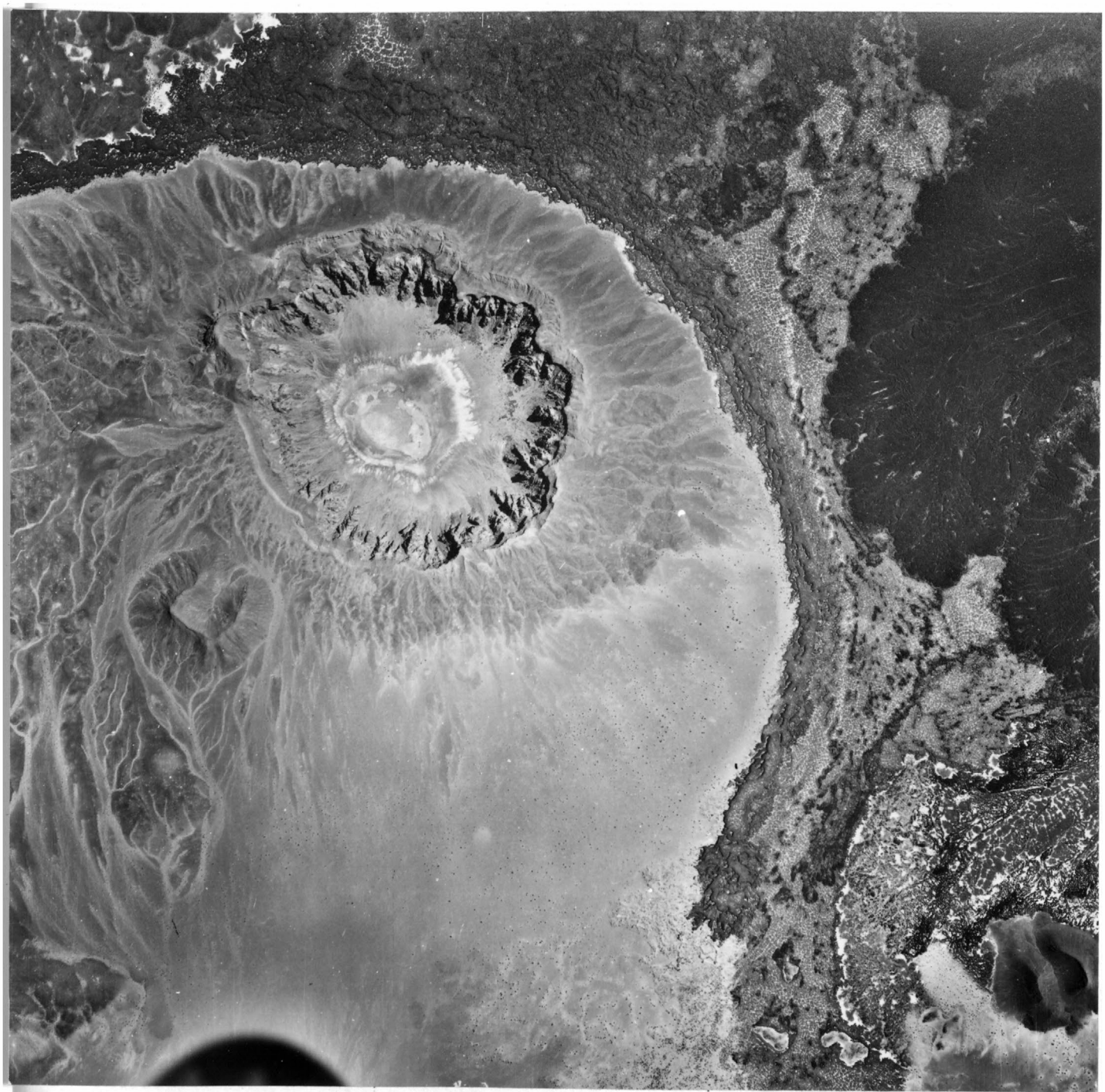

Figure 63. Wabar phreatic crater from a Holocene eruption at the northwestern corner of Harrat al Kishb. The crater is two km wide and 270 m deep and is blasted out of basement crystalline rocks.

Harrat al Hutaymah.--Craters similar to Al Wahbah are scattered on crystalline rocks east of Jabal Salma in the Harrat al Hutaymah at the extreme northeast corner of the shield and like Al Wahbah expose crystalline basement rocks in the shattered walls of the craters rimmed by ejecta and volcanic ash. One at Jabal Humayyan is 1.25 km wide and 110 m deep (Bramkamp, Ramirez, and others, 1963). Lava flows are of the pahoehoe type at Al Jubb (al Na'ai), a village in a collapsed cone, according to J. Mytton (written commun., 1964), that lies within the crags of Jabal Selma. The ash at many craters contains large basaltic hornblende crystals and inclusions from the underlying rocks. The chemical analysis of a 12-m-thick flow above 40 m of volcanic ash at Jabal Humayyan is that of an alkaline basalt approaching basanite (no. 25, table 10).

Harrat Hadan.--Harrat Hadan lies on the plain east of Ta''f and south of Harrat al Kishb. The alkali olivine basalt rests on a laterite above the Paleocene Umm Himar sedimentary rocks. The flows and subordinate interbedded lake beds of marl and tuff (Madden and others, 1979) are about 300 m thick; they dip gently eastward, are deeply weathered to saprolite, and are deeply eroded. The lower flows are 16.6 $\pm$ 1.5 and 16.2 $\pm$ 1.8 Ma old from two samples near the southern end (nos. 41 and 43, table 9). The youngest, uppermost flow gives an age of 3.4 $\pm$ 0.5 Ma (42, table 9) that is probably too young according to the geomorphology. The chemical analyses of three samples are similar and lie within the basanite field of the alkali-silica field (Cox and others, 1979). At least the older flows erupted from feeder pipes now exposed along the western edge of the harra as isolated hills on the plain; however, other isolated hills are lava-capped outliers.

Harrat Nawasif-al Buqum.--The large flood basalt of Harrat Nawasif-al Buqum extends in a northeasternly direction southeast of Harrat Hadan and is the fourth largest lava-covered region in western Saudi Arabia. The Quaternary harra series involves three episodes. The oldest eruptions are exposed only in the deep wadis that drain eastward, the middle eruptions cover most of the harra, and the youngest black flows at the northeastern corner are coeval with or slightly younger than the Holocene scoria cones and ash rings that extend N. 20° E. in a belt averaging 20 km wide along the center of the harra (fig. 50).

Deeply weathered basalt was sampled on the bank of Wadi Ranyah near Ranyah where a long tongue of lava flowed down Wadi Ranyah for 30 km east of the edge of the harra. The sample yielded a K-Ar age of 3.5 $\pm$ 0.3 Ma (Hotzl and others, 1979), and the flow may be part of the oldest eruptions but this age seems excessive. The widespread middle and less weathered basalt gave an age of 1.1 $\pm$ 0.3 Ma, according to Hotzl and others, from a sample 30 km west-northwest of Ranyah. A sample from the Wadi Ranyah canyon, 75 km southwest of Ranyah, is 1.8 $\pm$ 1.2 Ma old as determined by R. F. Marvin, H. H. Mehnert, and Violet Merritt in the USGS Denver Laboratory (no. 53, table 9). A sample from the uppermost flows on the west of Harrat Nawasif contained insufficient argon to measure (no. 44, table 9) but the chemical analysis is that of an alkali olivine basalt similar to the older flows (table 10). The youngest black flows at the northwest corner of the harra were not sampled.

Harrat ad Damm and Harrat Tuffil.--From 70 to 105 km south of Jiddah small lava flows overlie crystalline basement or Tertiary rhyolite on the coastal plain and the foothills of the scarp mountains. Harrat ad Damm, the oldest, occurs as elongate erosional remnants on the crystalline foothills where they extend seaward on the plain. A sample from the northwesternmost remnant analysed 7.0 ± 4.3 Ma by K.-Ar, whole rock (47, table 9), an age comparable to those from the upper lavas of Ḥarrat al' Uwayrid and the erosional remnant west of Ḥarrat Khaybar in the Qal'at Sawrah quadrangle. Harrat Tuffil flowed out on the younger coastal pediplain similar to the harrat at Yanbu' al Bahr and al Birk. However, the Tuffil lava came from a single vent rising 38 meters above the general altitude of the coastal plain which is there about 350 m above the Red Sea. Two samples (49-50, table 9) analysed 2.9 ± 0.2 and 2.8 ± 0.1 Ma by whole-rock K-Ar dates. This basalt overlies rhyolitic tuff of the Baid formation along the west edge and granite farther east. The sheared and brecciated tuff was considered Precambrian on geologic map I-210 (Brown and others, 1963a) but a sample at Jabal Abu Shidad at the north end of the area analysed 19.3 ± 0.9 Ma (whole rock K-Ar), an early Miocene age within the range of the continental dikes that extend from the Tihamat al Yemen to the Gulf of Aqaba, but somewhat younger than the leucocratic gabbro intrusive nearby (fig. 64). Subsequent work has extended the rhyolite south to beneath the western edge of Harrat Tuffil (Laurent, 1976).

Ḥarrat al Birk.--The Birk lavas, also known as Ḥarrat Hayil or Hubhub al Sheikh cover the coastal plain from lat 18° 45' to lat 17° 45' N., separating the Tihamat ash Sham from the Tihamat 'Asir. Volcanic activity appears to be limited to two episodes, an older, possibly, late Miocene and an extensive Quaternary out-pouring culminating with Holocene cinder cones. Near Al Birk the older bluish, olivine-rich basalt underlies a coquina terrace which is 3 m above the sea and is overlain by 15-20 m of reddish weathering basalt. Two samples from the lower flows on the southeast of the lava field analysed 12.1 ± 1.5 and 4.3 ± 0.6 Ma by K-Ar whole rock (table 9); these analyses are most likely too old, as more recent samples from the lower flows gave 1.19 Ma ± 0.24 Ma and 0.94 ± 0.39 Ma (Coleman and others, 1983). The younger flows were measured as 2.1 - 2.8 Ma (K-Ar ratio) but certainly some flows are as young as Holocene as shown by more recent analyses, ranging down to 0.25 Ma ± 1.04 Ma (Coleman and others). A study of ultramafic inclusions of the Birk lavas, especially in the ejecta of the Quaternary cinder cones, identified a mixture of harzburgite, websterite, and gabbro in contrast to inclusions farther south in the Tihamat Asir coastal plain where only harzburgite inclusions were found. The differences are attributed to magmatic penetration through of a thick sialic crust in the Birk area, whereas the southern lava fields came from pipes that penetrated a thinner oceanic crust (Ghent and others, 1980; Gettings, 1977). The older K-Ar ages of the Birk lavas could be attributed to excess argon derived from the underlying Precambrian crystalline rocks which are argon-rich.

The cinder cones are dispersed throughout the harra and represent feeder pipes rather than the fissure eruptions of much of the older lava. Farther east of the Birk lava fields at Jabal Ba'a (Hadley, 1975a), isolated patches of ash on the mountain slopes around a vent are freshly eroded and appear to represent an eruption during the last century (fig. 61).

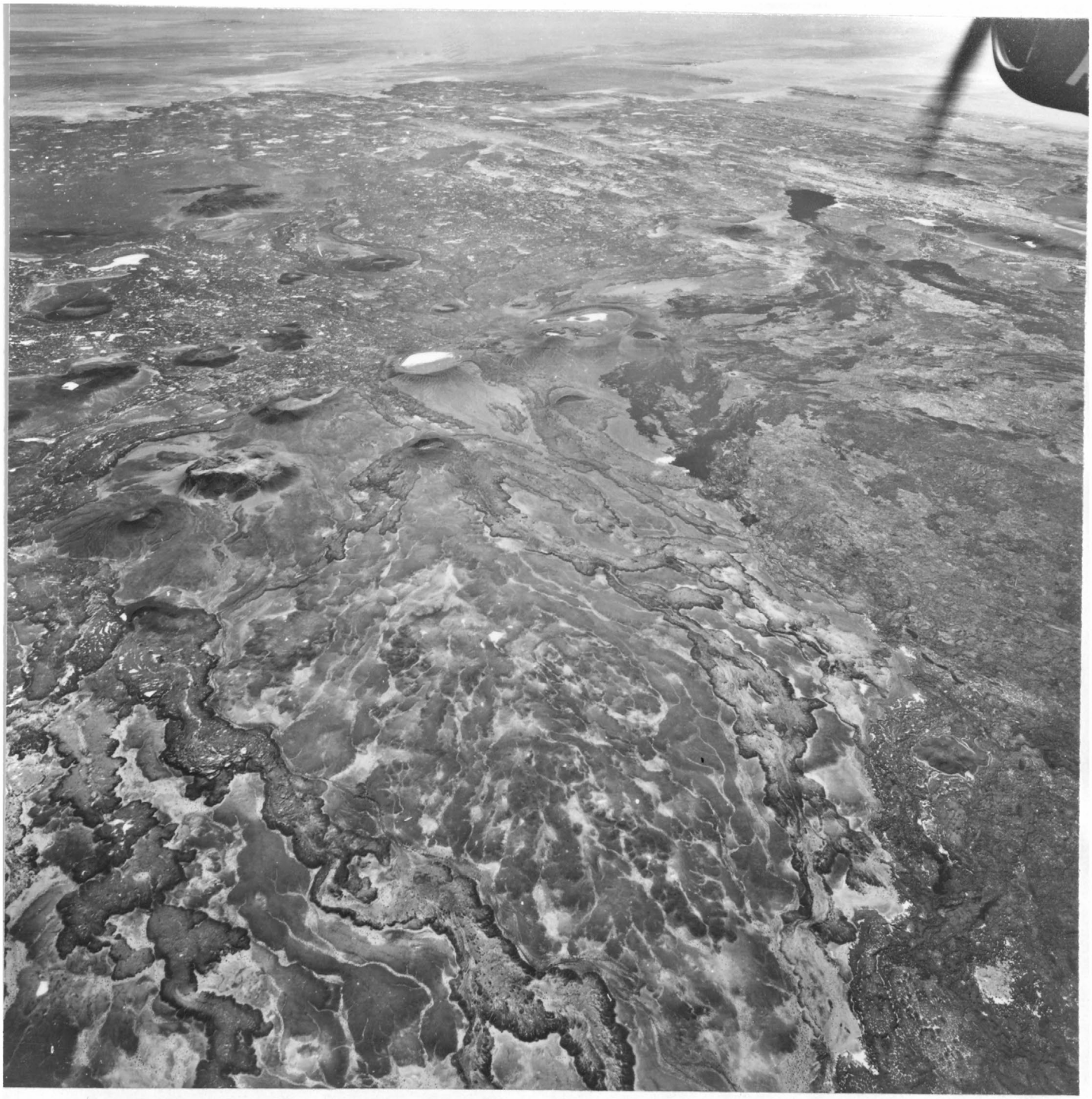

Figure 64. Oblique aerial view of Harrat al Kishb showing linearity of Holocene craters. Wabar crater can be seen in the distance on right skyline.

Elsewhere on the Tihamat 'Asir both east of the Birk harra and south on the Jizan plain, separate volcanoes ejected ash as well as alkali olivine basalt. These appear young, especially on the Tihamat 'Asir. Lava from the two volcanoes east of the Birk harra, Jabal Baqarah and Jabal al Haylah, contain alkali olivine basalt as well as hawaiite and the basanite variety of alkali olivine basalt (Coleman and others, 1970-1977). Samples from the basal flows analysed 5.1 ± 1.5 Ma (K-Ar whole rock, 65, 66 table 9) but a later analysis of a sample from Jabal al Haylah gave an age of 0.18 Ma ± .05 Ma (written commun., R. J. Fleck), a more reasonable age, especially for the cone, which sits on a surface containing rolled Achulean axes in the valley of Wadi Tayyah (Overstreet, 1973). However the basal flow that was originally sampled may be the former age and the volcanic cone the latter. Youthful volcanos on the Jizan plain, Jabal Akwah and Jabal Umm al Qumm, have been dated by K-Ar, whole-rock at 0.31 ± 0.32 and 0.53 ± 0.08 Ma and basalt flows in the foothills at Wadi Jizan give an age of 0.99 ± 0.23 Ma in addition to a sample too low in argon to yield a radiometric age (Coleman and others, 1977).

Jabal As Sirat.--The southernmost harra on the 'Asir highlands, Jabal As Sirat, extends to the Yemen border and appears to be a northern remnant of the lower portion of the Yemen volcanics (Trap Series) as it is of about the same age--30.1 ± 1.0 Ma to 25.3 ± 0.5 Ma (nos. 67, 69, table 9) compared to a range in the Yemen Trap Series of 29.7 ± 0.9 - 20.8 ± 1 Ma and of the northern Ethiopian Plateau volcanics at Adigrat (30.0 ± 0.7 to 19.4 ± 0.6 Ma), late Oligocene to earliest Miocene (Coleman and others, 1977, Civetta and others, 1978, Jones and Rex, 1974, Jones, 1976) (fig. 52). However the Yemen volcanics include besides alkali olivine basalt, hawaiite, mugearite, and ignimbrite (rhyolite) as well as andesite, trachyte porphyry and tuff, whereas As Sirat flows are picritic basalt at the base grading up to alkali olivine basalts (basanite) to hawaiite. The 17 to 20 flows total 580 m in thickness (Coleman and others, 1977), considerably less than half the maximum thickness of the Yemen volcanics.

Cycles of erosion 2/

To understand the terrain development in western Arabia, one should first visualize the morphology of land forms in a waterless desert, that is, in a true arid cycle (fig. 65). In general, subaerial physiographic features are produced by the degrading and weathering action of water, gravity, ice, winds, and organisms in opposition to the aggrading internal agencies of diastrophism and volcanicity. The action of weathering agents tends to decrease altitude and, although the end product may be a plain or may approach a plain, increase in relief is an early and normal result of the action of any of them. As the action of water and gravity are nearly universal, the so-called normal erosive process is the humid or fluvial cycle. In subfreezing temperatures ice action is dominant (glacial cycle), and where both ice and water play a subordinate role, the wind produces the characteristic features of the true arid cycle.

The arid cycle

In an area of diverse rocks exposed only to the action of the wind, gravity, and temperature changes, the regional terrain must of necessity be initially tectonic. The wind readily attacks the softer beds wherever they are exposed; gravity works on the steeper slopes, fragments becoming available through fracturing because of pressure release and by insolation (the breakage of rocks by surface changes of temperatures), because temperature fluctuations are great in such waterless areas. There is very little rock decomposition; rather, unstable minerals persist in the weathering products. Thus sandstone and shale are carved out at a rate depending on relative hardness and cementation, the grains less than 0.08 mm being carried away from the region until they reach a place having sufficient moisture to hold them; whereas grains of 0.08 to 1 mm are moved into sand masses, such as dunes, sand sheets, and ergs. The sand scours the bedrock (fig. 66) wherever it is carried over the exposed surfaces and impinges against the rock surfaces, abrading them and slowly releasing more material for transport. As the process continues, the harder beds form ridges of increasing vulnerability to attack by the elements, and they too eventually are reduced until an extensive plain, cutting across all rock types, is formed, without reference to the usual concept of base level. Such a process of bevelling must be many times slower than erosion by water or ice, in part because the sand forms a protective cover over an ever-increasing part of the terrain. Indeed, if the wind direction were constant, the sand probably would early form thin sheets or make sand shadows protecting the low areas on the lee side of the rock ridges, and eventually the sand would move out of the region until it reaches a place of anchorage by vegetation or blows into a distant sea. If there should be conflicting winds, and none dominant enough to carry the sand out of the region, the sand would probably form expanding ergs which would grow in depth and area, shifting from place to

---

2/ Adapted after Brown, G. F., 1948, Geology and ground water of Al Kharj District, Nejd, Saudi Arabia: unpublished PhD. thesis, Northwestern University, Evanston, Illinois.

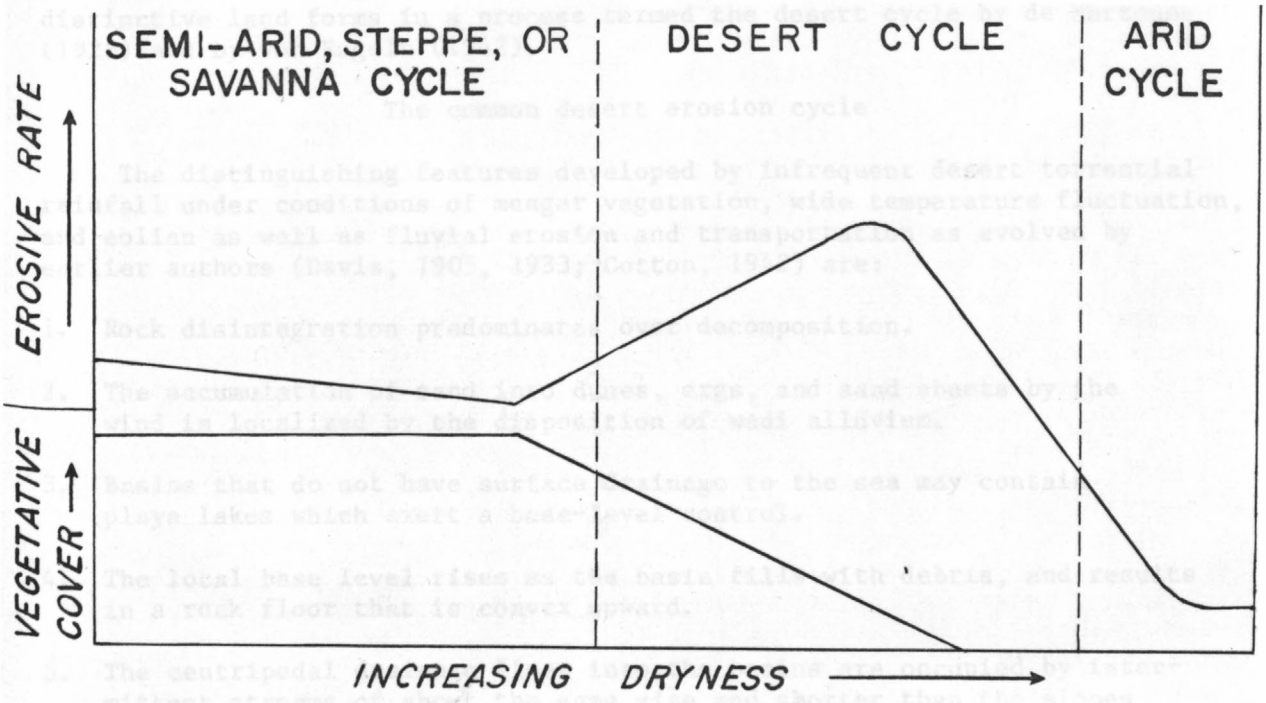

Figure 65. The arid cycle.

place, until the region would be covered with sand and the rock floor beneath the dunes would have an undulating pattern, hollows developing where wind erosion had been active longest. Under these conditions the process might be thought of as operating under inverse control by an ever-moving base level at the surface of the sand.

Apparently no area has been rainless sufficiently long to allow such an eolian-dominated process to develop a plain--at any rate, such a plain has not been recognized. In most desert areas sufficient rain falls, usually of the torrential type, to impose special terrain features that are ultimately more subdued than those described above. The combination of wind and water together with the other less important agents produces distinctive land forms in a process termed the desert cycle by de Martonne (1926) and by von Engeln (1942).

The common desert erosion cycle

The distinguishing features developed by infrequent desert torrential rainfall under conditions of meager vegetation, wide temperature fluctuation, and eolian as well as fluvial erosion and transportation as evolved by earlier authors (Davis, 1905, 1933; Cotton, 1942) are:

1. Rock disintegration predominates over decomposition.

2. The accumulation of sand into dunes, ergs, and sand sheets by the wind is localized by the disposition of wadi alluvium.

3. Basins that do not have surface drainage to the sea may contain playa lakes which exert a base-level control.

4. The local base level rises as the basin fills with debris, and results in a rock floor that is convex upward.

5. The centripedal drainage lines into the basins are occupied by intermittent streams of about the same size and shorter than the slopes of the basin flanks; the spottiness of desert rainfall prevents a development of master valleys.

6. Pediments or carved plains are formed that rise on slopes of 0.5 to 7 percent from the local or regional base level to the base of desert mountains;they are cut with uniform grade across different structures and rock types.

7. As the region becomes more mature, the spreading basins intersect, resulting in coalescence of base levels and integration of drainage.

8. In maturity, wind action becomes more effective as fluvial power decreases, but, if the deserts are in a rain shadow and the erosive processes lower the mountain fringe, rainfall may increase and the cycle shift into a more humid form.

The relative importance of wind and running water in desert regions has been debated at length. As a desert becomes drier, the vegetative cover decreases and the erosive action of the increasingly intermittent storms increases. When the periods between rains are sufficiently long and relative humidity becomes too low for effective dews, the vegetation, if any, is too sparse to materially retard the rate of erosion. This acceleration of erosion by water during increasing desiccation makes the effects of eolian erosion difficult to distinguish, except for the local and rather small-scale effects of corrasion such as polished and fluted rocks, pedestals, and yardang. It is more difficult to recognize the larger forms of eolian erosion such as those caused chiefly or wholly to deflation. The problem is illustrated qualitatively by figure 65, which shows that as vegetative cover decreases, the erosive rate by water increases, until there is no effective vegetative cover. Thereafter erosion is largely a function of rainfall concentration and effects of wind abrasion.

Most of the large features of deserts appear to result from water action, although wind-scoured hollows as much as 400 feet deep and 10 or 12 miles across have been described in Mongolia (Berkey and Morris, 1927). Their origin seems to require deflation on soft sands and silts (but some are on granites in Arabia), aided by gullying in the short walls on the flanks. According to Berkey and Morris, the basins progress downward, possibly to the water table, then grow laterally at a rate faster than debris is brought in by the centripedal gullies. This vertical removal of debris is at approximate right angles to the removal of bedrock in the arid cycle, and requires initiation by water.

Not all deserts have interior drainage; about one-third of the deserts have drainage to the sea (de Martonne, 1926), either by streams flowing across them that have headwaters in more humid regions, or from initial tectonic conditions. Furthermore, most if not all deserts, and in particular the Sahara and Arabian deserts, were more humid during episodes of the Pleistocene when the climate was at least as humid as semiarid or steppe-like. In Arabia during the Pleistocene, Wadi as Sahba' seems to have reached the Arabian Gulf, or nearly so, as did Wadi ar Rimah and possibly Wadi ad Dawasir, although the last may have debouched into lakes in the Rub al Khali basin.

Davis (1905) has pointed out that the evolution of the desert cycle is largely controlled by the initial relief, which may be a wide valley and range as in central Arabia, or a massive mountain as in the Hijaz. If the region is one of gently dipping sedimentary rock, as in the Najd, the cycle would begin in a manner similar to the ideal humid cycle operating on an uplifted peneplain formed either by former fluvial or marine planation or as a desert peneplain following a long period of cliff retreat. Once again the harder beds would form cuestas. There would be no substantial period of bahada accumulation, but the wind would keep pace with the gullying of promontories, and the pediment would extend to near the cliff base by "direct replacement of one already well-planed rock floor by another at a lower level" (Cotton, 1942). The desert cycle in such sedimentary rocks has been described in Australia, in the Libyan desert, the Kalahari, Mongolia, and in the mesa country of southwestern North America. The bevelled surfaces, that seem flattest in the drier areas are believed to have suffered greatest desiccation, in contrast to the formation of coalescing alluvial fans and

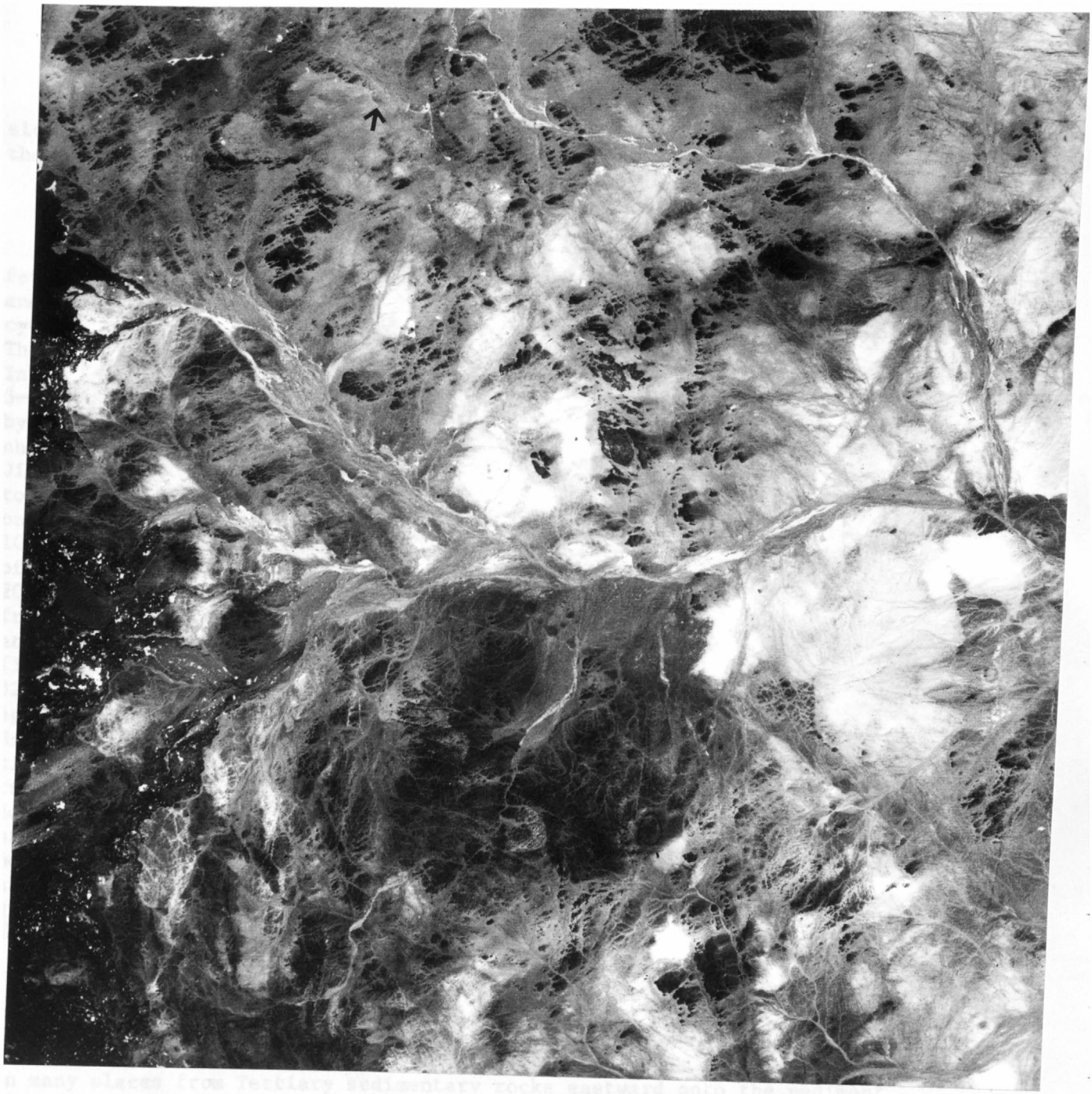

Figure 66. Landsat image showing effects of wind erosion. Regional wind direction about N. 70° E., north of Wadi ar Rimah and east of Harrat Khaybar and Ethnayn. Note preponderance of yardang troughs up wind from southeast-draining wadis, especially where there is a grus plain and paucity on the northeast flanks where the sand has been removed during floods, thus depriving the wind of a scouring tool. (see arrow).

sloping pediments in the areas where conditions have approached or entered the semi-arid cycle.

The Tihamat

The coastal plain (fig. 67) along the eastern shore of the Red Sea extends with few interruptions from the mouth of the Gulf of Aqaba to Yemen and beyond, and appears to have developed during alternations of desert and savannah cycles, with the Red Sea as a somewhat variable base level of erosion. The coastal plain ranges in width from narrow beaches to as much as 40 km. In the southern part, the Tihamat al Yemen or Tihamat al 'Asir, a 2- to 3-meter elevated beach, extends northward as far as Al Wajh. It is marked by low headlands and overhanging scarps ascribed by Guilcher (1952) to chemical weathering (solution) activated by surf and eolian action. Near Jiddah the surface rises eastward about 1.5 meters per km for about 5 km to altitudes of about 10 meters. Above 10 meters the slopes are steeper, on the order of 10 meters per kilometer, until a general altitude of about 100 meters is reached at the foot of the coastal mountain belt. Remnants of a 20-meter beach underlie a basalt flow north of Jiddah, and 6-, 10-, 20-, and 30-meter surfaces, mostly on coralline rocks, have been measured from Umm Lajj northward to near the Gulf of Aqaba. The surface culminates at an altitude of 525 meters on Tiran Island at the mouth of the Gulf (500m according to Goldberg, 1963), marine benches extend up to at least 320 m and face southwest (Schick, 1958). The elevation of the surfaces appears to be due primarily to vertical movement along the old transverse Najd fault system as part of the ramping of the northeast flank of the rift valley (Brown, 1972), although relative movement of blocks between transform faults that cross the Red Sea in a northeast direction may account for some if not all of the uplift. The generally accepted two-stage opening of the Red Sea as developed by Girdler and Styles (1974) and with two poles of rotation (Richardson and Harrison, 1976) would cause vertical uplift from compression during the second, Pliocene-Pleistocene-Holocene stage, as the sea widened in an easterly direction and the peninsula rotated about 7 degrees counterclockwise.

The seaward, lower part of the Tihamat is a depositional or coralline surface for the most part, that gradually merges eastward into an erosional pediment that extends across the rift fault zone of the eastern edge of the Red Sea rift. The coastal-plain surface can be followed continuously in many places from Tertiary sedimentary rocks eastward onto the pediment bevelled across the crystalline rocks of the Precambrian basement. Thus, most of the pediment developed after the last large-scale movement on the easternmost margin, a zone which is also the site, in the southern Tihamat, of gabbro and related sheet-dike swarms dating from the inception of the major period of the rift opening at about 22 Ma (see table 15; Coleman and others, 1979). The oldest part of the pediment, that is, the part nearest the sea, may be more than 2.8 $\pm$ 0.1 Ma at Harrat Tuffil, 100 km south of Jiddah where an isotopically dated (K-Ar) basalt overlies crystalline rocks midway between the coast and the eastern edge of the pediment on a 30-km-wide coastal plain.

At intervals along the present shore are small inlets called sharms; some are connected to present drainage debouchment from the coastal mountains (fig. 68), but more commonly they are not related to present drainage. Typically they are "T" or bottle-shaped, widening out landward from a narrow throat, about 30 meters deep, and maintaining a depth of as much as 10 meters behind the coralline ridges on the flanks of the throat entrances. As the coral was formed more than 40,000 years B.P., according to Meyer Rubin (USGS; in Brown, 1970), the sharms are obviously estuarine relics from an earlier epoch when the Red Sea stood at a lower level then at present (there is now no active, or only very minor, erosion) in the sharms. Also, as floods now rarely reach the Red Sea across the coastal plain except in a few of the largest wadis (the bifurcation and trifurcation noted by Gvirtzman and others, (1977) probably represent lagoons behind the beach ridge that existed before the reefs were breached), there must have been more rainfall then than there is at present. Goldberg and Yaron (1978) assign a Th^{230}/U^{234} age of 146,000 $\pm$ 16 years for younger terraces at 11 - 13 m altitude on the southeast coast of Sinai.

Recently described evidence from many sources (Deuser and others, 1976, Wendorf and others, 1976) indicates that periods of glacial maxima were coeval with aridity in the low latitudes, at least during late Pleistocene, even though the present interglacial epoch is arid (plate; Deuser and others, 1976; Wendorf and others, 1976; Bowler, 1976; Sarnthein, 1978). As the 40,000 years C^{14} age of the elevated coral at Jiddah can be considered a minimum, a possible age for the coral could be 54,000 $\pm$ 4,600 year from a Th^{230}/U^{234} ratio obtained from an uncrystallized mollusk Tridacna, in an elevated coralline reef in the Afar rift (Bonatti and others, 1971). The 30-meter depths at the throats of some of the sharms suggests a period of downcutting when the Red Sea was about 30 meters below present level or lower, a base level that existed at various times during the Quaternary as the sea level fluctuated. Flood erosion could have occurred at the same time as lake beds were deposited in the Rub al Khali, as determined by McClure (1977). His older lake beds dated by means of C^{14} are between 17,000 and 36,000 yr. B.P., with a cluster of ages between 21,000 and 30,000 years ago, about contemporary with the C^{14} ages of 20,400 to 24,630 $\pm$ 500 yr. B.P. for deep artesian water from widely scattered wells in central and eastern Arabia (Thatcher and others, 1961), as well as the iron oxide (deposition during fresh water influx) dates of 8,000 and 19,000 yr. B.P. from cores in the mid-Red Sea trench (Ku, 1969). McClure's younger lake beds range from 9,000 to 6,000 yr. B.P. The sharms could date from the period 20,000-25,000 yr. B.P. -- an interval of lower sea level and extensive Wurm glaciation. But more likely sufficient time under arid climate has since passed for eolian and flash-flood sediment to have filled the embayments.

Sarnthien (1978) gives wet periods for the Sahara at from 12,500 to 11,000 yr. B.P.; 10,000 to 7,500; and 6,500 to 5,500-5,000 yr. B.P. During the period 12,500-11,000 years, the Wurm ice cover was waning and the Red Sea level may have still been lower than at present. This oldest period coincides with an extensive pluvial period of the Nile (Fairbridge, 1977). Sarnthien states (1978) that, prior to the moist period, active sand dunes extended from lat. 10° to 37° N. in the Sahara about 18,000 yr. ago--synchronous with polar ice advance and aridity. This chronology is further strengthened by an analysis of oxygen isotope ratios from the

planktonic foraminiferal fauna of the Red Sea and the Gulf of Aden (Deuser and others, 1976), the cold periods for the Red Sea coinciding with periods of major deglaciation. The last of these recorded in the cores from the Deep Sea Drilling Project occur at about 17,000-8,000 yr. B.P., that is, between the the Wurm glacial maximum and the climatic optimum of the Paleolithic.

Thus much evidence relating to the origin of the sharms points to the period of climatic optimum at 9,000-6,000 years probably after complete glacial retreat from the Wurm glacial maximum toward present arid conditions as the sea level rose from the -120 meter depth and there was sufficient pluvial action for erosion into the sea. As a fossil coralline reef in the Gulf of Aqaba now at intertidal level has been dated at 4,770 $\pm$ 140 yr. B.P. (Friedman, 1965), the sharms must have been cut before this level. However, the present aridity during a time of glacial withdrawal contradicts the current concept of synchroneity of fluvial and interglacial epochs, and requires some further explanation, as do the C^{14} dates of older lake beds of McClure and of the deep artesian waters in central Arabia.

The pluvials of Arabia and Sahara seem to be of much shorter duration and more frequent than the glacial epoches hence maybe one should consider not the long-term events but the periods of change, i.e. periods of rapid ice advance and retreat as being the dynamic climatic control intervals. Nile floods come from a different climatic zone that may or may not be synchroneous with the the desert cycle.

The eastern and higher Tihamat is in places covered with eolian sand, generally accumulating transversely to the off-shore/on-shore winds, usually in barcan dunes. In several places where winds shift alternately from north-west to southwest and vis versa, long seif dune ridges accrete about perpendicular to the trend of the Coastal plain. In general, the sand grains are 3 and 4 mm in diameter, much coarser than the bulk of the sand accumulated in the great interior nafuds. They accumulate in para-ripples, the smaller grains generally deposited in dunes farthest from the shore line against the base of the scarp mountains (Guilcher, 1952).

The Scarp Mountains

The ramping of the eastern flank of the Red Sea rift and subsequent faulting has exposed a southwest-facing scarp (fig. 69) against which atmospheric weathering has been active, probably since the middle Miocene. This has formed a mountainous belt 40 to 140 km wide which rises eastward to the rim of the great interior plateau of Najd, the Hijaz-'Asir Highlands area in southern Arabia, and the Hismah Plateau in northern Arabia. The crest reaches a maximum of 3,000 meters in Jabal Sawdah in the 'Asir (fig. 69) near the Yemen border, and gradually declines northward to a minimum height of about 1,000 meters in the mountains northwest of Al Madinah where the mountainous belt is widest and where Wadi Hamd has been captured and now flows more directly to the Red Sea through a precipitous canyon.

Farther north another block is tilted upward along a series of faults that cut obliquely across the belt, forming the mountains of Ash Shifa' or Midian which lie in front of the Hisma plateau and extend into Jordan.



Figure 69a. Terrace benches at 6, 22, and 31 meters above the Red Sea here result from intermittent ramping of the Al Hisma (Midian) block of the peninsula during the Quaternary.



Figure 69b. Landsat image of the erosional scarp of Asir at lat 20° N. Red Sea on lower left, bordered by the Tihamat al Asir (coastal plains) and the Scarp Mountains cut back to the Najd pediplain. The pediplain has here been ramped up to altitudes of as much as 2,600 meters. The southern end of the plateau lavas of Harrat Buqum occupy the northeast corner of the scene. From Jet Propulsion Lab.

The highest point of Ash Shifa' is Jabal Al Lawz at 2,400 meters above the Gulf of Aqaba, although 5 peaks comprising the Ash Shifa' region extend 100 km south and are 2,000 meters or more in altitude above the Red Sea. A series of knife ridges and canyons mark the southwestern fronts of each block. These southwest-facing slopes are in places transected by north-trending valleys which permit egress from one canyon to the next. Some north-trending valleys are subsequent erosional valleys carved parallel to the structural grain in basement schist, but several narrow valleys are underlain by wide mafic dikes that weather more rapidly than the more stable calcic and calc-alkaline wall rocks. Many of these valleys are flanked with narrow walls representing the fine-grained chilled margins of the mafic dikes. Subsequent erosion has developed the north-south tributaries, although it is possible to cross watersheds at the heads of the subsequent streams without being aware of a change in slope, such was the extent of the pre-uplift pedimentation.

Many lower courses of the larger wadis draining the scarp mountains show stream capture (Brown, 1970). Wadi al Hamd is an outstanding example, with an elbow of capture at the junction of Wadi Jizl. Evidently the wadi prior to the uplift of Al Hijaz Mountains flowed out to the coast north of the present mouth at lat. 26° N, perhaps as far north as the emergence of the major Najd fault into the Red Sea at lat. 28° N. The schists of the shear zones formed valleys on the shield towards the end of the cratonization, a natural environment for the development of subsequent streams on the Early Tertiary lowland of the northern Red Sea coast (Madden and others, 1979). If so, the ancestral wadi was captured progressively southward as the peninsula rotated counterclockwise and ramped upward to the northwest in response to the compressional and sinistral stresses towards and along the Jordan rift. A subsequent outlet may have been via the Wadi Saluwah-Dama thalweg, followed by a later capture southward via Wadi Bayda and the lower Wadi as Sirr trough. As the tilting continued along the Najd fault system, Wadi Thalbah and Wadi Azlam captured the lower As Sirr valley and Wadi Hamd reached the sea via its present course. Regardless of the precise channel-ways, the northeast tilting (elevation) of the Al Hisma block undoubtedly caused the wadi to seek an outlet to the sea in a southerly or westerly direction as the earlier lower course was elevated.

In a similar manner, wadis farther south, notably Wadi al Far ah from the east side of Jabal Radwa, east of Yanbu'al Bahr, had a previous channel extending south and debouching through Wadi al Faqir onto the coastal plain 40 kms south of the present mouth, but seeking a western outlet as the country south of Wadi Al Faqir rose. Test drilling in Wadi al Faqir penetrated alluvium about 100 m thick whereas the current drainage in Al Far'ah has a shallow bed over granite. Similarly, Wadi Safra 30 km. farther southeast drains two merdional valleys - Musayjid (3 km wide) and Tashah (1 km wide)-through a 200 m wide gorge, creating a flood hazard on the Madinah-Jiddah road.

Wadi Fatima between Jiddah and Makkah likewise debouched southward through Wadi Shumaysi which has a deep alluvial valley in comparison to the nearly bare rock floor of the present lower Wadi Fatima whose debouchment is 30 km northwest of the ancestral valley. Farther south wadis Qununah, Yiba, and Hali in particular seem to have changed drainage directions. Thus the wadis draining the scarp mountains have been captured or have reversed flow

toward the northwest as the 'Asir block ramped, tilted and skewed in a counterclockwise direction under tensional conditions, whereas wadis on the southwest flank of the Hisma block north of the Najd faults moved southwest as the country rose to the northwest under compressional conditions.

Tertiary volcanic rocks, both hypabyssal and extrusive, have been emplaced along the original rift zone at or near the toe of the scarp mountains, often giving an initially deceptive rugged appearance to the lower foothills of the scarp mountain terrain as a whole when viewed from the Tihamat, but extensive pedimentation preceded volcanism and dissection from the lowered base level of the Red Sea.

The Hijaz and Hisma Plateaus

The Hijaz Plateau forms the uplifted and dissected southwestern corner of the Najd pediplain of western Arabia. Triangular in shape, it extends southward from At Ta'if to and beyond the Yemen border, an area of about 40,000 km^2 above 2,100 m in altitude. Broadening and increasing in altitude southward, it culminates in Jabal Sawdah at 3,000 m near Abha, the capital of the 'Asir province and the most salubrious region in Arabia. As the western lip next to the scarp mountains is approached, increased rainfall resulting from orographic convection over the scarp, especially during the late summer monsoon season, increases the amount of dissection, as do the fracturing and warping of the bedrock caused by the ramping in connection with the evolution of the Red Sea rift. Rainfall greater than 20 cm annually is limited to a crest zone 20-30 km wide; consequently eastward and northward wadi flow decreases rapidly downstream and deposition is greater than erosion near the eastern edge of the plateau. Berms and strath surfaces indicate intermittent uplift or climatic change, with at least one relatively static period.

The wadis widen in midcourse where runoff from tributaries coalesce, but many are constricted by narrow throats, particularly where reentering metamorphic terrain from a gruss plain underlain by granite rock. Such constrictions have ponded floods and deposited loessal silt (fig. 70) upstream (behind them) during periods of excessive flooding (Brown, 1960). The paucity of grit and gravel suggests low relief and gentle stream gradients at the time of silt deposition. Charcoal from fire hearths on the upper surface of the loessal silt have been dated by C-14 measurement at 6000 years B.P. (Schmidt and others, 1981) thus giving a minimum age of the Holocene pluvial epoch (9000 to 6000 years B.P.) as determined by C-14 dates of lacustrine deposits in the Rub al Khali (McClure, 1978). The accumulation upstream from constrictions was increased by the higher water table and longer moist periods so that vegetation accumulated as evidenced by abundant root casts in the silt deposit. The absence of fossil pulmanate gastropod shells seen in present-day loess may be attributed to dissolution of the carbonate by humid acid from the vegetation (Schmidt and others, 1981).

In northwestern Arabia east of the Gulf of Aqaba, the Hisma Plateau is an upland comparable to the Hijaz, lying between the scarp mountains of Ash Shifa' or Midian on the west and the great northern sandstone plains west of the Great Nafud. Likewise the high position of the Hisma Plateau results from concomitant ramping in connection with the rotation of Arabia away from Africa in a counterclockwise direction. The sandstone plateau rim extends



Figure 70. Loessal silt in Tathlith valley above Hamdh. Feb. 11, 1952.

southward from the Jordan border at an altitude of 1800 m descending to 1100 m at lat. 28° N., east of the mouth of the Gulf of Aqaba. The surface slopes eastward to the western edge of the Great Nafud basin to an altitude of about 800 m where the Hejaz railroad crosses the plain. The southern rim of the Hisma is higher south of lat. 28 N., where the multiple flows of plateau-type basalt have built up the surface to 2,000 m in the Harrat ar Rahah. Except for the plateau basalts in the southern Hisma, sandstone buttes and mesas dot the plain, increasing in height and numbers toward the rim east of and somewhat below the crests of the crystalline mountains of Ash Shifa'.

The Najd Pediplain

The crystalline Najd pediplain formed from coalescing pediments begins at the northeastern edge of the Hijaz Plateau where the ramping of the plateau flattens out toward the northeast. It is a vast reg or serir on which are scattered isolated inselbergs of more resistant igneous and metamorphic rocks; bornhardts and kopjes, generally granitic; and lava fields, mostly along the western edge (figs. 67, 71, 72).

Where granitoid rocks crop out, most of the terrain is nearly flat and featureless especially where the crystalline rocks have been tectonized and weathered to clay by periodic hydration of feldspars and where wind scour has removed the residual grains. The wide temperature range, especially when the cooling falls below the dew point and below freezing, hastens the disintegration. The differential rate of expansion and contracting of the multi-mineral rocks also hastens the process, even where there has been little or no post-crystalline tectonism. Thus the ridges and higher hills are composed mostly of lavas and meta sedimentary rocks, the isolated bornhardts being the exception.

From maximum altitudes of 2,100 m, the plains decline to a minimum of 670 m where Wadi Ar Rimah debouches onto the sedimentary Najd at Al Qasim. The desert floor is not a uniform slope but is broken hinge fashion along the northwest-trending Najd fault system into four segments or blocks--the southwest or 'Asir block, two central blocks between the 3 Najd Faults, and a northern or Shammar block. The surface of the 'Asir block slopes evenly from about 1,400 m to 1,000 m in a northeasterly direction to the southernmost Najd fault.

Two central blocks each lie between two flanking Najd faults and their surfaces are considerably flatter but are tilted somewhat, also to the northeast, falling from a general altitude of 1,050 m along the northern edge of the southern Najd fault to a low region of sabkhas (playas) at about 940 m, then rising to 1,100 m northeastward toward the middle of the three principal Najd fault zones (Map I-270A, USGS-ARAMCO, 1963). The elevation of the southern edge is dramatically shown at Wadi Subay', where ground water pumped up onto the elevated bank of the wadi flows by gravity northward (60 km) to Zalim, and a sabkha floor; yet the wadi entrenched in crystalline rocks flows east and south to be lost in the 'Uruq Subay' in and along the southern flank of the Najd fault. The central region, which falls between the flanking Najd faults and includes the lowest part of the Najd pediplain exclusive of the lower reaches of Wadi Ar Rimah, is nearly devoid of drainage lines and is characterized by numerous small irregular sabkhas in desert sinks seemingly scoured by the wind--they are nearly devoid of alluvial debris, the salt crust overlying decomposed bedrock.



Figure 71. Bornhardt at Jabal Kursh.

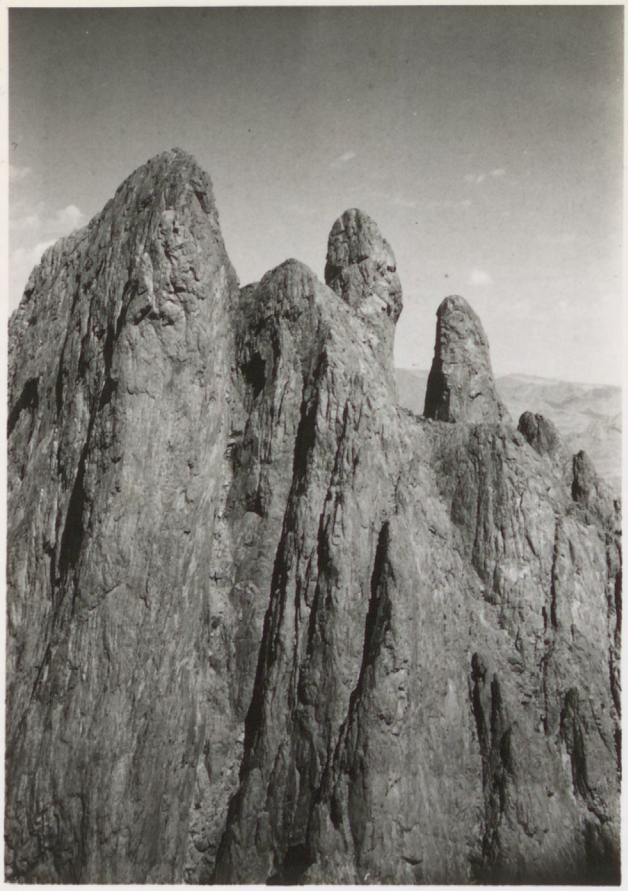

Figure 72a.

Spines of Jabal Shar rising to an altitude of 1990 meters east of Muwaylih on the Red Sea coast at 27°39' N. lat. The small batholith is composed almost entirely of post-tectonic graphic granite.



Figure 72b.

Conical inselberg of Jabal al Gharamul at lat. 21°51' N. long. 42°54' E. The jabal wall rises at an angle of 65° from the horizontal; the lower slope rising at 21° is underlain by contact-metamorphosed sediments of Murdamah age whereas the upper steeper slope is on posttectonic granite which is cut by a Najd fault. March 18, 1954.

The northern or Shammar block of the crystalline Najd pediplain falls from 1,100 m along the northernmost Najd fault to 950 m in the extreme northeast corner where Wadi Ha'il flows northeast onto the sedimentary rocks; and to 670 m at Ar Rass where Wadi Ar Rimah flows northeast off the crystalline rocks. Along the western part of this crystalline Najd surface, the larger wadis follow the northwest direction of the Najd fault system where large horizontal movements have created schistose shear zones that are readily deflated, or, where above grade, are scoured by floods to create thalwegs. Eastern portions drain northeastward into the well integrated, dendritic, and slightly entrenched drainage system of Wadi Ar Rimah.

The increased rainfall in the Shammar block is not easily explained from our limited knowledge of precipitation from vegetation and the short time span of measured rainfall (fig. 3). However, satellite images show a strong wind direction from S. 70° W., parallel to yardang troughlike grooves in the landscape, a direction confirmed from general sand movement eastward from sand sources on gruss plains and wadi floors (fig. 67). The western lava fields have increased in height from repeated eruptions and epeirogenic uplift to general altitudes of 1,300 m in Harrat Rabat between at Ta'if and Al Madinah and to a maximum elevation of 2,000 m at Jabal al Abyad in the Harrat Khaybar north of Al Madinah. This barrier together with the permanent low-pressure area generated from the rising thermal off the black lava fields and the southwest wind direction cause orographic convection and precipitation. Farther north away from the extensive lava fields, the rainfall declines to less than 50 mm until still farther north the westerlies of the Mediterranean climate begin to influence precipitation (fig. 3).

The Najd pediplain exhibits much evidence of the desert cycle of erosion. Besides accumulations of sand dunes and wind-scoured sinks (sabkhas), windblown sand, moving along the desert surface, cuts channels parallel to wind direction wherever there is an initial low area such as a schist belt, joint, fault, or other lineation. Once a channel starts, the accumulation of rain or even dew resulting from the wide diurnal temperatures range of the desert tends to chemically weather the thalweg of the groove or channel. Subsequent sand blast, concentrated in the lowest surfaces of the terrain removes the chemically or frost-loosened debris, which together with flash floods deepens the channel, further concentrating the sand blast, and creating streamlined valleys or "yardang troughs" (fig. 73). On the Najd pediplain these features form valleys and ridges that are often at large angles to structural lineations in the basement rocks, but where a transverse wadi carrying flash floods removes the sand, the trough ends because sand blast is missing downwind from the stream bed. These yardang troughs are most abundant from lat. 24° N., north to the north edge of the shield, particularly east of the wind gaps between Harrat Rahat and Harrat Khaybar, and at the north end of Harrat Khaybar where the yardang troughs are often 10 to 20 m deep especially in crystalline rocks (fig. 74).



Figure 73. Wadi Schism yardang valley.



Figure 74. Yardang troughs following one set of joints parallel to the wind direction, N. 70° E., southern end of Jabal Salma and rhyolite dike on the east side which has been dissected by sandblast downwind from the major yardang troughs. Jabal Salma is a complex late and post-tectonic pluton where two sets of joint systems are apparent. Jabal Shammar region, northeast corner of the Arabian shield. Vertical aerial photograph, scale 1:56,000.

REFERENCES CITED

Akaad, M. K., Noweir, A. M. 1969, Lithostratigraphy of the Hammamat-Um Seleimat District, Eastern Desert, Egypt: Nature v. 223, no. 5203, pp. 284-285.

Akaad, M. K., Noweir, A. M., 1978, Geology and lithostratigraphy of the Arabian desert orogenic belt of Egypt between latitudes 25° 35' and 26° 30' N. [abs.] Precambrian Research v. 6, p. A6.

Alabouvette, B., and Villemur, J. R., 1973, Reconnaissance of the Wajid sandstone: [France] Bureau des Recherches Geologiques et Minieres, Open-file report 73-JED-3, 22 p., 17 pl; map, appendix.

Alabouvette, B., and Pellaton, C., 1975, Geology and minerals exploration of the Wadi Kamal quadrangle, 24/37D: [France] Bureau des Recherches Geologiques et Minieres, Technical Record 75JED 18, 46 p., 1 fig., 3 maps.

Aldrich, L. T., 1956, Measurement of Radio Active Ages of Rocks: Science, 123, p. 871-875.

Aldrich, L. T., Davis, G. L., Tilton, G. R., and Wetherill, G. W., 1956, Radioactove ages of minerals from the Brown Derby mine and the Quartz Creek granite near Gunnison, Colorado: J. Geophys. Res. 61, p. 215-232.

Aldrich, L. T., Davis, G. L., and James, H. L. 1965, Ages of minerals from metamorphic and igneous rocks near Iron Mountain, Michigan: J. Petrology, 6, pp. 445-472.

Aldrich, L. T., Brown, G. F., Hedge, C. E., and Marvin, R. F., 1978, Geochronologic data for the Arabian Shield: U.S. Geological Survey, Saudi Arabian Project, Open-file Report SA(IR) 240, 20 p., 1 fig.

Al Rahaili, M. H., and Warden, A. J., 1980, Comparison of the Bir Umq and Hamdah ultrabasic complexes, Saudi Arabia; p. 143-156, in Cooray, P.G. and Tahoun, S.A., eds., Evolution and mineralization of the Arabian-Nubian Shield: Institute for Applied Geology Bulletin no. 3, Oxford, Pergamon Press, Ltd., vol. 4, 168 p.

Al-Shanti, M. S., 1966, Oolitic iron ore deposits in Wadi Fatima between Jeddah and Mecca, Saudi Arabia: Saudi Arabian Directorate General of Mineral Resources Bulletin 2, 51 p., 13 pl., 33 fig., 8 tables.

Al-Shanti, A. J., 1974, Al Ji'lani layered basin intrusion, Ad Dawadimi district, Kingdom of Saudi Arabia: Saudi Araban Directorate General of Mineral Resources, Bulletin 12, 45 p., 27 figs., 10 tables 1 pl.

Al-Shanti, A. M. S., 1976, Geology of Ad Dawadami district, Kingdom of Saudi Arabia: Saudi Arabian Directorate General of Mineral Resources Bulletin 13, 57 p., 33 fig., map 1:100,000 scale.

Al-Shanti, A. M., and Gass, I. G., 1983, The Upper Proterozoic Ophiolite melange zones of the easternmost Arabian shield: J. Geol. Soc. London, vol. 140, p. 867-876, 4 figs., 1 table.

Bakor, A. R., Gass, I. G., and Neary, C. R., 1976, Jabal al Wask, northwest Saudi Arabia: an Ecocambrian back-arc ophiolite: Earth and Planetary Science Letters, v. 30, no. 1, p. 1-9.

Bartov, Y., Steinitz, G., Eyal, M., and Eyal, Y., 1980, Sinistral movement along the Gulf of Aqaba - its age and the relation to the opening of the Red Sea: Nature, v. 285, p. 220-222. fig.

Baubron, J. C., Delfour, J., and Vialette, Y., 1976, Geochronological measurements (Rb/Sr; K/Ar) on rocks of the Arabian Shield, Kingdom of Saudi Arabia: [France] Bureau des Recherches Geologiques et Minieres Open-file Report 76-JED-22, 152 p.

Bayley, R. W., 1972, Geologic map and section of the Wadi Yiba quadrangle, Tihamat ash Sham area [Kingdom of Saudi Arabia]: Saudi Arabian Directorate General of Mineral Resources map GM-1, scale 1:100,000.

Bender, Fredrich, 1963, Stratigraphic der "Nubiochen Sandsteine" in Sud-Jordanien: Geol. Jb., vol. 81, p. 237-276. 11 fig., map.

Bender, Fredrich, 1965 Zur geologie der kupfererzvorkommen am ostrand des Wadi Araba, Jordan: Geol. Jb. series B, vol. 10, p. 16

Bender, Fredrich, 1968, Geologic map of Jordan-Aqaba Ma'in sheet, Federal Republic of Germany, Bundesanstalt fur Bodenforschung, Map, scale 1:250,000.

Bender, Frederich, 1974a, Geology of Jordan: Contributions to the regional geology of the Earth, Sebruder Borntraeger, Berlin, supp. ed., v. 7, p. 107.

Bender, Fredrich, 1975, Geology of the Arabian Peninsula; Jordan: U.S. Geological Survey Professional Paper 560-I, 36 p., map, scale 1:500,000.

Berkey, C. P., and Morris, F. K., 1927, Geology of Mongolia: American Museum of Natural History, v. 2, p. 56, 58, 146, 201.

Bigot, M., and le Chapelain, J. R., 1973, Geology and mineral exploration of the As Suwaydirah quadrangle (24/40A): [France] Bureau des Recherches Geologiques et Minieres, Open-file Report 73-JED-7, 26 p., 2 pl. scale 1:100,000.

Bigot, M., and Alabouvette, B., 1973, Geology and mineralization of the Tertiary Red Sea coast of northern Saudi Arabia: [France] Bureau des Recherches Geologiques et Minieres, Open-file Report 76-JED-5, 84 p. 7 pl., 11 figs.

Bigot, M., 1975, Geology and mineral exploration of the Umm Lajj quadrangle, (25/37C): [France] Bureau de Recherches Geologiques et Minieres, Open-file Report 75 JED 7, 47 p., 2 pl., scale 1:100,000.

Binda, P. L., and Bokhari, M. M., 1980, Chitinozoan-like microfossils in a late Precambrian dolostone from Saudi Arabia. Geology v. 8, p. 70-71.

Binda, P. L., and Ramsay, C. R., 1980, Earliest Phanerozoic or latest Proterzoic fossils from the Arabian Shield: Precambrian Research, vol. 13, p. 375-377.

Binda, P. L., 1981, The Precambrian boundary in the Arabian shield: A review: Jiddah, King Abdul Aziz University, Faculty of Earth Science Bulletin, no. 4, p. 107-120.

Blank, H. R., 1977, Aeromagnetic and geologic study of Tertiary dikes and related structures on the Arabian margin of the Red Sea, p. G1-G18; in Hilpert, L. S., ed., Red Sea Research 1970-1975: Saudi Arabian Directorate General for Mineral Resources Bulletin 22.

Blank, H. R., 1980, Total-intensity aeromagnetic map of the Precambrian Arabian Shield, Kingdom of Saudi Arabia: U.S. Geological Survey Saudi Arabian Mission Technical Report 6, SA (IR)-344, scale-1:2,000,000.

Blodget, H. W., and Brown, G. F., 1982, Geologic mapping in western Saudi Arabia by use of computer enhanced imagery: U.S. Geological Survey Professional Paper 153, 10 p., 2 pl.

Bodenlos, A. J., and Lari, Ahman, 1970, Possibilities of sulphur mineralization in Saudi Arabia: U.S. Geological Survey Saudi Arabian Mission report, SA(IR)-113, 29 p., 2 figs.

Bogue, R. G., 1953, Report on geologic reconnaissance in northwestern Saudi Arabia: Saudi Arabian Directorate General of Mineral Resources Open-file Report 27, 30 p.

Bogue, R. C., 1954, Reconnaissance of mineral deposits in a part of western Saudi Arabia: Saudi Arabian Directorate General of Mineral Resources Open-file Report 31, 66 p.

Bois, J., 1971, Geology and mineral exploration of the northwestern part of the Jabal Damkh quadrangle (sheet 23/44 A): [France] Bureau des Recherches Geologiques et Minieres Open-file Report 71-JED-2, 27 p., 3 appendices, scale 1:100,000.

Bonatti, Enrico, Emiliani, Cesare, Ostlund, Gote, and others, 1971, Final desiccation of the Afar rift, Ethiopia: Science (AAAS), v. 172, no. 3982, p. 468-469, sketch map.

Bounny, I., 1973, Geology and mineral exploration of the Wadi Dwayrah area, Kingdom of Saudi Arabia: [France] Bureau Recherches Geologiques et Minieres Open-file Report 75-JED-25, 72 p., 6 pl., 2 figs.

Boureau, Edourad, 1956, Contribution a l'etude de flores Jurassiques d'Asie, II, sur des coniferes noveaux d'Arabie Seoudite: Societe Geologique de France, Bulletin 6, p. 653-657, 2 figs.

Bowen, R. W., 1971, Graphic normative analysis program: U.S. Geological Survey Computer Contribution 13, 80 p., 2 tbls.

Bowler, J. M., 1976, Aridity in Australia: age, origins, and expressions in aeolian land forms and sediments: Earth-Science Review, v. 12, p. 279-310.

Bramkamp, R. A., Ramirez, L. F., Brown, G. F., and Pocock, A. E., 1963, Geologic map of the Wadi ar Rimah quadrangle, Kingdom of Saudi Arabia: U.S. Geological Survey Miscellaneous Geologic Investigations Map I-206A, scale 1:500,000.

Bramkamp, R. A., Brown, G. F., Holm, D. A., and Layne, N. M., Jr., 1963 Geologic map of the Wadi as Sirhan quadrangle, Kingdom of Saudi Arabia: U.S. Geological Survey Miscellaneous Geologic Investigating Map I-200-A, scale 1:500,000.

Bramkamp, R. A., Gierhart, R. D., Owens, L. D., and Ramirez, L. F., 1963, Geologic Map of the western Rub al Khali quadrangle, Kingdom of Saudi Arabia: U.S. Geological Survey Misc. Geol. Inv. Map I-218-A, scale 1:500,000.

Brown, G. F., 1948, Geology and groundwater of Al Kharj district, Nejd, Saudi Arabia: Ph.D. thesis, Northwestern University, Evanston, Ill., 128 p., 43 pl., 1 fig.

Brown, G. F. and Jackson, R. O., 1958, Geologic map of the Tihamat ash Sham quadrangle, Kingdom of Saudi Arabia: U.S. Geological Survey Miscellaneous Geologic Investigations Map I-216 A, scale 1:500,000.

Brown, G. F., and Jackson, R. O., 1959, Geology of the Asir quadrangle, Kingdom of Saudi Arabia: U.S. Geological Survey Miscellaneous Geologic Investigations Map I-217-A, scale 1:500,000.

Brown, G. F., 1960, Geomorphology of western and central Saudi Arabia: International Geological Congress, 21st, Copenhagen, 1960, pt. 21, p. 150-159.

Brown, G. F., and Jackson, R. O., 1960, The Arabian Shield: XXI International Geological Congress, 21st Copenhagen, 1960, part IX, p. 69-77.

Brown, G. F., Jackson, R. O., Bogue, R. G., and Maclean, W. H., 1962, Geologic map of the southern Hijaz quadrangle, Kingdom of Saudi Arabia: U.S. Geological Survey Miscellaneous Geologic Investigations map I-210A, scale 1:500,000.

Brown, G. F., Jackson, R. O., Bogue, R. G., and Elberg, E. L., Jr., 1963b, Geologic map of the northwestern Hejaz quadrangle, Kingdom of Saudi Arabia: U.S. Geological Survey Miscellaneous Geologic Investigations Map I-217-A, scale 1:500,000.

Brown, G. F., 1970, Eastern margin of the Red Sea and the coastal structures in Saudi Arabia: Royal Society of London Phil. Trans., A-267, p. 75-78.

Brown, G. F., and Hase, D. H., 1971, Explanatory note of the tectonics of the Pre-Cambrian Arabian segment of the African Shield: Tectonics of Africa, UNESCO sciences de la terre, v. 6, p. 429-430.

Brown, G. F., 1972, Tectonic map of the Arabian Peninsula: Saudi Arabian Directorate General of Mineral Resources, Arabian Peninsula Map, AP-2, scale 1:4,000,000

Brown, G. F., Delflour, J., and Coleman, R. G., 1972, Geologic formations in The Arabian Shield (summary): International Geological Congress, 24th, Montreal, 1972, sec. 1, p. 333.

Brown, G. F., and Jackson, R. O., 1979, An overview of the geology of western Arabia, p. 3-10, in Tahoun, S.A., ed., Evolution and mineralization of the Arabian-Nubian Shield: Oxford, Pergamon Press Ltd. vol. 1, 187 p.

Bureau des Recherches Geologiques et Minieres, 1966, Annual report February 1965 to January 1966: [France] Bureau des Recherches Geologiques et Minieres Open-file Report, SG-JED 66-A-7.

Bhutta, M. A., 1970, Geology and economic possibilities of the Wadi Hajir-Wadi al Fara area (23/39 D) Saudi Arabian Directorate General of Mineral Resources Report 363, 123 p. 5 fig. 5 pl.

Burton, R. F., 1878, The gold mines of Midian and the ruined Midianite cities: C. Kegal Paul & Co., London, 395 p.

Cameron, D. K., Jr., 1974, New Triassic palynomorphs from the Arabian Peninsula: Grana, v. 14, p. 4-10, 2 figs., 1 pl.

Church, B.N., 1975, Quantitative classification and chemical comparison of common volcanic rocks: Geological Society America Bulletin, vol. 86, no. 2, p. 257-263.

Civetta, Lucia, La Volpe, Luigi, and Liere, Lucio, 1978, K-Ar ages of the Yemen Plateau: Journal of Volcanology and Geothermal Research, v. 4, p. 307-314.

Cloud, Preston, Awramik, S. M. Morrison, Karen, and Hadley, D. G., 1979, Earliest Phanerozoic or latest Proterozoic fossils from the Arabian Shield: Precambrian Research, vol. 10, p.73-93.

Coleman, R. G., Fleck, R. J., Hedge, C. E., and Ghent, E. D., 1977, The volcanic rocks of southwest Saudi Arabia and the opening of the Red Sea, in Hilpert, L. S., ed., Red Sea Research, 1970-1975, Saudi Arabian, Directorate General of Mineral Resources Bulletin 22, p. D1-D30.

Coleman, R. G., Gregory, R. T., and Brown, G. F., 1983, Cenozoic volcanic rocks of Saudi Arabia: Saudi Arabian Deputy Ministry for Mineral Resources Open-file Report USGS-OF-03, 77 p., 23 figs., 6 tables.

Coleman, R. G., Ghent, E. D., Fleck, R. J., Griscom, Andrew, 1977, Jabal Sha'i gabbro in southwest Saudi Arabia: Saudi Arabian Directorate General for Mineral Resources, Bulletin 17.

Coleman, R. G., Hadley, D. G., Fleck, R. G., Hedge, C. T., and Donato, M. M., 1979, The Miocene Tihama Asir ophiolite and its bearing on the opening of the Red Sea, p. 173-186; in Tahoun, S.A., ed., Evolution and Mineralization of the Arabian-Nubian Shield: Institute for Applied Geology Bulletin no. 3, Oxford, Pergamon Press Ltd., vol. 1, 187 p.

Cooper, J. A., Stacey, J. S., Stoesser, D. C., and Fleck, R. J., 1979, An evaluation of the zircon method of isotopic dating in the southern Arabian craton: Contributions to Mineralogy and Petrology volume 68, p. 429-439.

Coquand, 1862, Geol et pal. region Sud Prov. Constantine, p. 266, pl. 30, figs. 1 and 2.

Cotton, C. A., 1942, Climatic accidents in landscape-making: John Wiley and Sons, Inc., New York, N.Y., p. 3-47.

Cox, L. R., 1929, Notes on the post-Miocene Ostride and Pectinidae of the Red Sea Region, with remarks on the geological significance of their distribution: Malacologia, Proc., v. 18, p. 165-185.

Cox, K. G., Bell, J. D., and Parkhurst, R. J., 1979, The interpretation of igneous rocks: George Allen Unwin, London, p. 14.

Dalrymple, G. B., and Lanphere, M. A., 1969, Potassium-argon dating: W. H. Freeman and Co., San Francisco, p. 172-173.

Dalrymple, G. B., Gromme, C. S., and White, R. W., 1975, Potassium-argon age and paleomagnetism of diabase dikes in Liberia: Initiation of central Atlantic rifting: Geological Society of America Bull., v. 86, no. 3, p. 399-411.

Daniel, E. J., 1963, International lexicon of stratigraphy for Jordan: Centre Nat. de la Rech. Sci. Int. Geol. Cong., Com de Stra., p. 360-369, and addendum, Bender, F., Litho-stratigraphic and time-stratigraphic subdivision of the Nubian sandstones in S. Jordan, p.403-419.

Davis, W. M., 1905, The geographical cycle in an arid climate: Journal of Geology, v. 13, p. 381-407.

Davis, W. M., 1933, Geomorphology of mountainous deserts: International Geological Congress, 16th, v. 2, p. 703-714.

Delfour, Jaques, 1982, Explanatory notes to the geologic map of the ad Dan a dimi quadrangle, sheet 24G, Kingdom of Saudi Arabia: Saudi Arabian Directorate of Mineral Resources, map GM60A, scale 1:250,000, 36 p. 21 fig.

Delfour, Jaques, and Dhellemmes, R., 1980, Geologic map of the Khaybar quadrangle, sheet 25D, Kingdom of Saudi Arabia: Saudi Arabian Directorate General of Mineral Resources Map GM-50-A, scale 1:250,000 with text, 24 p., 5 figs., 5 tables.

Delfour, Jaques, 1979a, Geologic map of the Halaban quadrangle, Kingdom of Saudi Arabia: Saudi Arabian Directorate of Mineral Resources, map GM-46-A, scale 1:250,000, with text, 32 p., 22 figs.

Delfour, Jaques, 1979b, Upper Proterozoic volcanic activity in the northern Arabian Shield, Kingdom of Saudi Arabia, p. 59-75; in Tahoun, S.A., ed. Evolution and Mineralization of the Arabian-Nubian Sheild: Institute for Applied Geology Bulletin no. 3, Oxford, Pergamon Press Ltd., vol. 2, p. 59-75.

Delfour, Jaques, 1977, Geology of the Nuqrah quadrangle, sheet 25E, Kingdom of Saudi Arabia: Saudi Arabian Directorate General of Mineral Resources, Map GM 28, scale 1:250,000 with text 32 p., 2 figs.

Delfour, Jaques, 1975, Vulcanism and mineral deposits of the Arabian-Nubian shield, [France] Bureau des Recherches Geologiques et Minieres Open-file Report 75-JED-24, 35 p. 6 ill, 2 tables.

Delfour, Jaques, 1970a, Le groupe de j'balah une nouvelle unite du bouclier Arabe: [France] Bureau des Recherches Geologiques et Minieres, Bulletin, ser. 2, sec. IV, no. 4, 5 figs., 2 tables, p. 19-32; See also, The J'Balah Group, a new unite of the Arabian Shield: [France] Bureau des Recherches Geologiques et Minieres Open-file Report 70-JED-4, 31 p., 5 figs.

Delfour, Jaques, 1967, Report on the mineral resources and geology of the Hulayfah-Musayna'ah region (sheet 78, zone 1 north): [France] Bureau des Recherches Geologiques et Minieres Open-file Report JED-66, 138 p., scale 1:100,000.

de Martonne, E., 1926, Geographie physique, v. 2, p. 965-967, Payot, Paris.

Deuser, W. G., Ross, E. H., and Waterman, L. S., 1976, Glacial and pluvial periods: their relationship revealed by Pleistocene sediments of the Red Sea and Gulf of Aden: Science, v. 191, p. 1168-1170.

Dodge, F. C. W., 1979, The Uyaijah ring structure, Kingdom of Saudi Arabia: U.S. Geological Survey Professional Paper 774-E, p. E 1 to E 17.

Dodge, F. C. W., Fleck, R. J., Hadley, D. G., and Millard, H.T., Jr., 1979, Geochemistry and 87 Sr/86Sr ratios of Halaban rocks of the Central Arabian Shield, p. 153-163; in Tahoun, S.A., ed., Evolution and Mineralization of the Arabian-Nubian Shield: Institute for Applied Geology Bulletin no. 3, Oxford, Pergamon Press Ltd, vol. 2, 205 p.

Doughty, C. M., 1888, Travels in Arabia Deserts: 2 volumes, Cambridge University Press, Cambridge, reprinted 1920, 1921. (Dover, 1980)

Dow, D. B., Beyth, Michael, and Hailu, Tsegaye, 1971, Paleozoic glacial rocks recently discovered in northern Ethiopia: Geologic Magazine v. 108, no. 1, p. 53-60.

Dubay, Lavesloo, 1969, Water development surveys, geological investigations; Italconsult. for Mineral Agriculture and Water, Kingdom of Saudi Arabia, unpublished report.

Durozoy, G., 1972, Hydrogeologie des basaltes du Harrat Rahat: Bull. [France] Bureau de Recherches Geologiques et Minieres, Sec. III, no. 2, p. 37-50, 6 figs., 2 tables.

Eijekelboom, Gerritt, 1966, The mineral resources and geology of the Jibal Damkh-Arwah region (sheet 115, zone II): [France] Bureau des Recherches Geologiques et Minieres Open-file Report, 66-A-13, 18 p., 1 fig., 9 appendices, scale 1:100,000.

Eijekelboom, Gerritt, 1969, BRGM mineral exploration and geological mapping in Mineral Resources. Research, 1967-68: Saudi Arabian Directorate General of Mineral Resources, p. 81-86.

von Engeln, O. D., 1942, Geomorphology: Macmillan Co., New York, p. 399-438.

Fairbridge, R. W., 1977, Global climate change during the 13,500 b.p. Gothenburg geomagnetic excursion: Nature, v. 265, Feb. 1977, p. 340-341, 1 fig.

Finlay, and Marwick, 1937, New Zealand Geol Sur [Pub] Paleontology Bull. 15 p. 41, figs. 4 and 5, plate V.

Fleck, R. J., Coleman, R. G., Cornwall, H. R., Greenwood, W. R., Hadley, D. G., Schmidt, D. L., Prinz, W. C., and Ratte, J. C., 1976, Geochronology of the Arabian Shield, western Saudi Arabia, K-Ar results: Geological Society of America Bull., v. 87, p. 9-21.

Fleck, R. J., Greenwood, W. R., Hadley, D. G., Anderson, R. E., and Schmidt, D. L., 1980, Rubidium-strontium geochronology and plate-tectonic evolution of the southern part of the Arabian Shield: U.S. Geological Survey Prof. Paper 1131 v 38 p. Also published as U.S. Geological Survey, 1979 Saudi Arabian Project report 245, 105 p.

Fleck, R. J., 1981, Age of diorite-granodiorite gneisses of the Jiddah-Makkah region Kingdom of Saudi Arabia: Saudi Arabian Deputy Ministry for Mineral Resources Open-file Report USGS OF-01-1, 18 p., 6 figs., 2 tables.

Fleck, R. J., and Hadley, D. G., 1982, Ages and strontium initial ratios of plutonic rock in a transect of the Arabian Shield: Saudi Arabia Deputy Ministry for Mineral Resources Open-file Report USGS OF-03-38, 43 p., 19 figs., 3 tables.

Frakes, L. A. Kepm, E. M., and Cowell, J.C., 1975, Late Paleozoic glaciation: Part VI, Asia: Geol. Soc, Am. Bull. vol. 86, p. 454-464.

Friedman, G. M., 1965, A fossil shoreline reef in the Gulf of Elat (Aqaba): Israel Journal of Earth Science, v. 14, p. 86-90.

Frisch, W., and Al-Shanti, A. M. S., 1977, Ophiolite belts and the collision of island arcs in the Arabian Shield: Tectonophysics, 43, p. 292-306.

von Gaertner, H. R. and Schurenburg, H., 1954, Final report Geological Research in western Arabia: Amt fur Bodenforschung, Hannover. 103 p.

Getting, M. E., 1977, Delineation of the continental margin in the southern Red Sea region from new gravity evidence; in Hilpert, L.S. ed., Red Sea Research 1970-1975: Saudi Arabian Directorate General of Mineral Resources Bulletin 22, p. K1-K11.

Ghent, E. D., Coleman, R. G., and Hadley, D. G., 1980, Ultramafic inclusions and host alkali olivine basalts of the southern coastal plain of the Red Sea, Saudi Arabia: American Journal of Science, vol. 280A, p. 499-527.

Geukens, F. P. M., 1960, Contribution a la geologie du Yemen: Inst. Geol. Univ. de Louvain, Mem., v. 21, p. 122-179, 8 pl., geol. map.

_____ 1966, Geology of the Arabian Peninsula, Yemen: U.S. Geological Survey Professional Paper 560 B., 23 p., 17 figs.

Gillman, Michkel, 1968, Primary results of a geological and geophysical reconnaissance of the Jizan coastal plain in Saudi Arabia: AIME Second Regional Technical Symposium, Dhahran, Saudi Arabia, Rept., p. 159-209.

Girdler, R. W., and Stlyes, P., 1974, Two stage Red Sea floor spreading: Nature, v. 247, p. 7-11.

Goldberg, M., 1963, The geology of Tiran Island: Proc. Israel Geological Society, v. 12, p. 83-84.

Goldberg, M. and Yaron, F., 1978, The Th^{230}/U^{234} ages of Raised Pleistocene marine terraces on the Island of Tiran and the southeastern coast of Sinai with some tectonic implications: 10th Int. Congress Sediment Jerusalem v. 1, p. 258-259.

Goldsmith, Richard, 1966, Section of the Fatimah Formation near Bahrah, Saudi Arabia: U.S. Geological Survey Saudi Arabian Project Report 65, 6 p., 1 pl.

Gonzales, Louis, 1973, Geologic map and sections of the Jabal 'In quadrangle: Saudi Arabian Directorate General of Mineral Resources map GM-2, scale 1:100,000, with text, 7 p.

Greenwood, W. R. and Brown, G.F., 1973, Petrology and chemical analyses of selected plutonic rocks from the Arabian Shield, Kingdom of Saudi Arabia: Saudi Arabian Directorate General or Mineral Resources Bulletin 9, 9 p.

Greenwood, W. R., 1975a, Reconnaissance geology of the Jabal Shada quadrangle, sheet 19/41A, Kingdom of Saudi Arabia: Saudi Arabian Directorate General of Mineral Resources, map GM-20, scale 1:100,000.

Greenwood, W. R., 1975b, Geology of the Jabal Ibrahim quadrangle, sheet 20/41C, Kingdom of Saudi Arabia, with a section on economic geology by R. G. Worl and W. R. Greenwood: Saudi Arabian Directorate General of Mineral Resources map GM-22 and text, 18 p., scale 1:100,000.

Greenwood, W. R., 1975c, Geology of the Biljurshi quadrangle, sheet 19/41B, with a section on geophysical investigations by G. E. Andreasen and a section on geochemical investigations and mineral resources by V. A. Trent and T. H. Kiilsgaard: Saudi Arabian Directorate General of Mineral Resources map GM-25, scale 1:100,000.

Greenwood, W. R., 1975d, Geology of the Al 'Aqiq quadrangle, sheet 20/41D: Saudi Arabian Directorate General of Mineral Resources map GM-23, scale 1:100,000.

Greenwood, W. R., Hadley, D. G., Anderson, R. E., Fleck, R. J. and Schmidt, D. L., 1976, Late Proterozoic cratonization in south-western Saudi Arabia: Royal Soc. London Philos. Trans, A. v. 280, p. 517-527.

Greenwood, W. R., 1979, Geology of the An Nimas quadrangle, sheet 19/42C, Kingdom of Saudi Arabia: Saudi Arabian Directorate General of Mineral Resources map GM-37, scale 1:100,000.

Greenwood, W. R., Anderson, R. E., Fleck, R. J., and Roberts, R. J., 1980, Precambrian geologic history and plate tectonic evolution of the Arabian Shield: Saudi Arabian Directorate General of Mineral Resources Bulletin 24, 35 p.

Gregory, R. T., Coleman, R. G., and Brown, G. F., 1982, Cenozoic volcanic rocks of Saudi Arabia: Evidence from the continent for a two-stage opening of the Red Sea: Geologocial Society of America Abstracts, v. 14, no. 7, p.502.

Grolier, M. J., and Overstreet, W. C., 1978, Geologic map of the Yemen Arab Republic (San'a'): U.S. Geological Survey Miscellaneous Geologic Investigations Inv. Map I-1143B, scale 1:500,000.

Guilcher, Andre, 1952, Formes et processus d'erosion sur les recifs coralliens du nord du bac Farasan (Mer Rouge). (Erosion forms and processes on coral reefs of the northern part of the Farasan bank): Revue de Geomorphologie Dynamique, An. 3, no. 6, p. 261-274, (French and English summaries).

Gvirtzman, Gdaliahu, Buchbinder, Binyamin, Sneh, Amihai, Nir, Yaacov, and Friedman, G. M., 1977, Morphology of the Red Sea fringing reefs: a result of the erosional pattern of the last-glacial low-stand sea level and the following Holocene recolonization: Mem. du Bur. des Recherches Geologique et Minieres, no. 89, 12 p.

Hadley, D. G., 1973, Geology of the Sahl al Matran quadrangle, Northwestern Hijaz, Kingdom of Saudi Arabia: Saudi Arabian Directorate General of Mineral Resources map GM-6, scale 1:100,000 with text, 11 p.

Hadley, D. G., 1974, The taphrogeosynclinal Jubaylah group in the Mashhad area, Northwestern Hijaz, Kingdom of Saudi Arabia: Saudi Arabian Directorate General of Mineral Resources Bulletin 10, 18 p., 19 figs., 2 tables.

Hadley, D. G., 1975a, Geology of the Wadi Hali quadrangle, sheet 18/41B, Kingdom of Saudi Arabia: Saudi Arabian Directorate General of Mineral Resources map GM-21, scale 1:100,000.

Hadley, D. G., 1975b, Geology of the Al Qunfudhah quadrangle, Tihamet ash Sham area, sheet 19/41C, Kingdom of Saudi Arabia: Saudi Arabian Directorate General of Mineral Resources map GM-19, scale 1:100,000, with text, 11 p.

Hadley, D. G., 1975c, Geology of the Qal'at as Sawrah quadrangle and petrographic data of selected layered and plutonic rocks from the Sahl al Matran quadrangle, Kingdom of Saudi Arabia (sheet 26/38 D): Saudi Arabian Directorate General of Mineral Resources map GM-24, scale 1:100,000.

Hadley, D. G., 1976, Geology of the Bi'r Juqjuq quadrangle, sheet 21/43D, Kingdom of Saudi Arabia: Saudi Arabian Directorate General of Mineral Resources Geologic Map GM-26, scale 1:100,000 with text, 30 p.

Hadley, D. G., 1979, Reconnaissance geology of the Musaylim quadrangle, sheet 19/40B, Kingdom of Saudi Arabia: Saudi Arabian Directorate General of Mineral Resources map GM-34, scale 1:100,000, with text, 7 p.

Hadley, D. G., and Fleck, R. J., 1980a, Reconnaissance geologic map of the Al Lith quadrangle, sheet 20/40C, Kingdom of Saudi Arabia: Saudi Arabian Directorate General of Mineral Resources Map GM-32, scale 1:100,000, with text, 10 p.

Hadley, D. G., and Fleck, R.J., 1980b, Reconnaissance geologic map of the Jabal Afaf quadrangle, sheet 20/40 D, Kingdom of Saudi Arabia: Saudi Arabian Directorate General of Mineral Resources map GM-33, scale 1:100,000, with text, 10 p.

Hantzschel, Walter, 1975, Trace fossils and problematics: Geological Society of America, Treatise on Invertebrate Paleontology pt. W., misc., suppl. 1, p. W38-39.

Hashad, A. H., 1980, Present status of geochronological data on the Egyptian basement complex, p. 31-46; in Cooray, P.G., and Tahoun, S.A., eds., Evolution and Mineralization of the Arabian-Nubian Shield: Institute for Applied Geology Bulletin no. 3, Oxford, Pergamon Press Ltd. Vol. 3, 164 p.

Hotzl, H., Lippolt, H. J., Maurin, V., Moser, H., and Rauert, W., 1979, Quaternary studies on the recharge area situated in crystalline rock regions: in Al-Sayari, S. S., and Zotl, J. G., eds., Quaternary Period in Saudi Arabia, p. 230-236, Vienna, New York, Springer-Verlag, 334 p.

Huber, Charles, 1891, Journe' 'un voyage en Arabie 1883-1884, 778 p., Illus. Atlas, Paris. Imp. Nationale, (with list and brief descriptions of Huber's rock collection).

Hunziker, J. C., 1979, Potassium-argon dating: Lectures in Isotope Geology; Springer-Verlag, New York, p. 58-63.

Irvine, T.N., and Baragar, W.R.A., 1971, A guide to the chemical classification of the common volcanic rocks: Canadian Journal Earth Sciences, Vol. 8, no. 5, p. 523-548.

Jackaman, Barry, 1972, Genetic and environmental factors controlling the formation of the massive sulphide deposits of Wadi Bidah and Wadi Wassat, Saudi Arabia: Saudi Arabian Directorate General of Mineral Resources Technical Record TR 1972-1, p. 243.

Jackson, R. O., Bogue, R. G., Brown, G. F., and Gierhart, R. D., 1963, Geologic map of the Southern Najd quadrangle, Kingdom of Saudi Arabia: U.S. Geological Survey Miscellaneous Geologic Investigations Geol. Inv. map I-211A, scale 1:500,000.

Japanese Geological Mission [Okuni, Shizuka; Komura, Kojiro; Hatanaka, Takefumi; Iso, Miyoji; and Kuwagata, Hisao], 1965, [revised 1967 by Hirayama, Ken], Gold deposits in Al Wajh district with data on limestone and water resources: Japanese Geological Survey Saudi Arabian Mission Open-file Report no.?, 216 p., 151 ill.

Japanese Geological Mission, 1967, Report on the iron ore deposits in the Wadi Sawawin district: Japanese Geological Survey Saudi Arabian Mission Report JGM-A-2. (Later revised and published as Technical Record TR-1978-11 Ministry of Petroleum and Mineral Resources, 62 p., 15 fig. 8 tables.)

Johnson, R. R., and Trent, V. A., 1966, Mineral reconnaissance of the Wadi al 'Ays quadrangle, Kingdom of Saudi Arabia: U.S. Geological Survey Saudi Arabian Project Report 45, 8 p., 1 fig.

Johnson, R. F., and Trent, V. A., 1967, Mineral reconnaissance of the Wadi as Surr quadrangle, Kingdom of Saudi Arabia: Saudi Arabian Directorate General of Mineral Resources Mineral Investigations map MI-5, scale 1:100,000.

Jones, P. W., and Rex, D. C., 1974, New dates from the Ethiopian plateau volcanics: Nature, v. 252, p. 218-219, 1 fig.

Jones, P. W., 1976, Age of the lower flood basalts of the Ethiopian Plateau: Nature, v. 261, p. 567-569.

Jordi, H. A., and Lonfat, F., 1963, Stratigraphic subdivision and problems in Upper Cretaceous-Lower Tertiary deposits in northwestern Libya: Revue l'Institut Francais du Petrole, Revue, v. 18, pt. 2, p. 1428-1436.

Kabbani, F. K., 1970, Geophysical and structural aspects of the central Red Sea rift valley: Phil Transactions Royal Society London v. A, 267, p. 89-97.

Kahr, V. P., 1961, Geology north of Yanbu al Bahr: Saudi Arabian Directorate General of Mineral Resources Open-file Report 126, 213 p., 289 figs., 3 pls.

Kannan, F.M., 1979, The geology, petrology, and geochemistry of the granitic rocks of Jabal al Hawshah and vicinity, Jabal al Hawshah quadrangle, Kingdom of Saudi Arabia: Saudi Arabian Directorate General of Mineral Resources, Bulletin 23, 114 p., 152., 18 table, 1 plate.

Karpoff, Roman, 1955, Observations preliminaries sur le socle Ancien de L'Arabie: Societe Geologique de France, Comp. Rend., p. 105-106.

Karpoff, Roman, 1956, Sur quelques series sedimentaires d'Arabie occidentale et centrale: Societe de Geologique de Frances, Compt. Rendu Sommaire des Seances, no. 2, Sea. Jan 23, p. 17-18.

Karpoff, Roman, 1957a, Sur l'existence du Maestrichtien au nord de Djeddah (Arabie Seoudite): Academie des Sciences, Paris, Compter Rendu t. 245, no. 16, p. 1322-1324.

Karpoff, Roman, 1957b, Esquisse geologique de l'Arabie Seoudite: Geologique Societe de France, 6 ser., v. VII, p. 672-676.

Karpoff, Roman, 1960, L'antecambrian de la peninsula Arabique: 21st International Geologic Congress, 21st, Copenhagen, Part IX, p. 80-93.

Kazmin, V., 1971, Precambrian of Ethiopia, Nature, Physical Science, v. 230 no. 16, p. 176-177, sketch map.

Kemp, John, Pelleton, C. and Calvez, J. Y., 1980, Geochronological investigations and geologic history in the Precambrian of northwestern Saudi Arabia: [France] Bureau des Richerches Geologiques et Minieres, Open-file report 01-1, p. 120, 41 figs.

Kemp, John, 1981, Geology of the Wadi Al 'Ays quadrangle, sheet 25C, Kingdom of Saudi Arabia, Saudi Arabian Deputy Ministry for Mineral Resources map GM 53-A, 1:250,000 scale with text, 39 p.

Kemp, John, Gros, Yves, and Prian, Jean-Pierre, 1982, Geologic Map of the Mahd adh Dhahab quadrangle, sheet 23 E, Kingdom of Saudi Arabia: Saudi Arabian Deputy Ministry for Mineral Resources Map GM-64A, scale 1:250,000 with text 39 p.

Kemp, John, 1981, Geology of the Wadi Al 'Ays quadrangle, sheet 25C, Kingdom of Saudi Arabia, Saudi Arabian Deputy Ministry for Mienral Resources Map GM 53-A, 1:250,000 scale with text, 39 p.

Kiilsgaard, T. H., Greenwood, W. R., Puffett, W. P., Naqvi, Mahammad, Roberts, R. J., Worl, R. G., Merghelani, Habib, Flanigan, V. J., and Gazzaz, A. R., 1978, Mineral exploration in the Wadi Bidah district, 1972-1976, Kingdom of Saudi Arabia: U.S. Geological Survey Open-file Report 78-771, (IR)SA-237, 83 p., 11 figs.

Kober, Leopold, 1911, Report on a trip through Hejaz: Akad. Wissen, Vienna, Anzeiger, v. 48, p. 285-286.

Kober, Leopold, 1919, The Northern Hejaz; Acad. Wiss. Vienna, Math. Natur. K. L. Denkschiften v. 96, p. 794-813.

Kroner, A., Roobol, M.J., Ramsay, C.R., and Jackson, N.J., 1979, Pan-African ages of some gneissic rocks in the Saudi Arabian Shield: Journal of the Geological Society, London, vol. 136, part 4, p. 455-461.

Kruck, Wolfgang, and Thiele, Joachim, 1983, Late Paleozoic glacial deposits in the Yemen Arab Republic: Geol. Jahr. Reiheb Haft. 46, 32 p., 3 figs., 7 plates.

Ku, T. L., 1969, Uranium series in sediments from the Red Sea hot brine area, p. 512-524: in Degens, E. T. and Ross, D. A., eds., Hot brines and recent heavy metal deposits in the Red Sea: New York, Springer-Verlag, 1969, 600 p.

Kuno, H., 1966, Lateral variation of basalt magma type across continental margins and island arcs: Volcanologique Bulletin, vol 29, p. 195-222.

Lamare, Pierre, 1923, Sur l'existence do granites alcaline dans le Shammar (Arabie), et sur la constitution geologique de cette region: Societe Geologique de France, Comp. Rend. Som. Seances, no. 16, p. 188-190, Nov.

Lamare, Pierre, 1930a, Etudes Geolog. en Ethiopie, Somalie, et Arabe Meridionale; Societe Geologique de France Mem. 14, n. s., t. VI, p. 32, 33.

Lamare, Pierre, 1930b, Nature et extension des depots secondaires dans l'Arabie, l'Ethiopie, et les pays Somalia: Societe Geologique France, Mem. 14 n. s. t. IV, p. 49-55.

Lamare, Pierre, and Carpentier, C. A., 1932, Vegetaux fossiles du Yemen: Societe Geologique de France Bull., series 5, v. 2, p. 83-92.

Laurent, D., 1976, A perlite deposit at Jabal Shama: [France] Bureau des Recherches Geologiques et Minieres Open-file Report 76JED24, 18 p. sketch map.

Le Maitre, R.W., 1976, The chemical variability of some common igneous rocks: Journal Petrology vol. 17, pt. 4, p. 589-633.

Letalenet, J., 1974, Geology and mineral exploration of the Jabal al Murdamah quadrangle, sheet 23/43 A. [France] Bureau des Recherches Geologiques et Minieres Open-File Report 74-JED-10, ___p., map, scale 1:100,000.

Letalenet, J., 1979, Geologic map of the Afif quadrangle, sheet 23F, [Saudi] Arabian Directorate General of Mineral Resources map GM-47-A scale 1:250,000 with text, 20 p.

Liddicoat, W. K., 1975, A review of Wadi Sawawin diamond drill core-logs and interpretation (interim report no. 1): Saudi Arabian Directorate General of Mineral Resources, Technical Record TR-1975-5.

Luce, R. W., Bagdady, A. Y., Roberts, R. J., 1975, Geology and ore deposits of the Mahd adh Dhabab district, Kingdom of Saudi Arabia: U.S. Geological Survey Saudi Arabian Project Report 195, 29 p., 1 pl., 13 figs.

Madden, C. T., Naqvi, I. M., Whitmore, F. C., Jr., Schmidt, D. L., Langston, Wann, Jr., and Wood, R. C., 1979, Paleocene vertebrates from coastal deposits in Harrat Hadan area, At Ta'if region, Kingdom of Saudi Arabia: U.S. Geological Survey Open-File Report 80-227, (IR)SA-269, 32 p., fig., 4 tables.

Mandaville, J. P., Jr., 1973, A contribution to the flora of Asir, Southwestern Arabia: Field Research Publications, Miami, 13 p.

Masoli, Mario, 1969, The Mukawwar Formation ostracofauna (Upper Cretaceous-Paleocene) of the Maghersum well 1 (Sudan): African Micropaleontological 3rd Colloquium, National Information and Documentation Center, Cairo, Proc., no. 5, p. 329-340.

McClure, H. A., 1977, Radiocarbon chronology of late Quaternary lakes in the Arabian desert: Nature, v. 263, no. 5580, p. 755-756.

McClure, H.A., 1978, Ar Rub'al Khali, p. 252-263; in Al-Sayari, S.S., and Zotl, J. G., eds. Quaternary Period in Saudi Arabia: Vienna, New York Springer-Verlag, 334 p.

McClure, H.A., 1980, Permian-Carboniferous glaciation in the Arabian Peninsula: Geol. Soc. Am. Bull. p. 1 vo. 91 p. 707-712; 3 figs.

Megrue, G. H., Norton, E., and Strangway, D. W., 1972, Tectonic history of the Ethiopian rift as deduced by K-Ar ages and paleomagnetic measurements of basaltic dikes: Journal Geophy. Res., v. 77, no. 29, p. 5744-5754.

Meissner, C. R., Jr., and Ankary, A. O., 1972, Phosphorite deposits in the Sirhan-Turayf basin, Kingdom of Saudi Arabia: Directorate General of Mineral Resources, Mineral Resources Report of Investigations 2, 27 p.

Meunier, S., 1888, Fossiles noveau provenant d'Arabie: Le Naturaliste 10, p. 204-205.

Michelson, H., 1978, Stratigraphy of the lake area in Lake Kinnert, p. 17-23, edited by C. Serruya, W. Junkby, Publishers, The Hague.

Ministry of Petroleum and Mineral Resources, 1977, Annotated bilbiography 1970-1975 A.D.: Saudi Arabian Directorate General of Mineral Resources Bulletin 20, 98 p.

Ministry of Petroleum and Mineral Resources, 1980, Annotated bibliography pre-1970 A.D.: Saudi Arabia Directorate General of Mineral Resources Bulletin 19, 126 p.

Ministry of Petroleum and Mineral Resources, 1981, Annotated bibliography 1396-1400 A.H. (1976-1980 A.D.): Saudi Arabian Deputy Ministry for Mineral Resources Bulletin 27, 102 p.

Miyashiro, Akiho, 1974, Volcanic rocks series in island arcs and active continental margins: American Journal Science Vol. 274, no 4, p. 321-355.

Moltzer, J. G., and Binda, P. L., 1981, Micropaleontology and palynology of the middle and upper members of the Shamaysi Formation, Saudi Arabia: Bull. Faculty of Earth Sciences, King Abdulaziz University, no. 4, p. 57-74, appendix.

Moore, J. M., 1979, Tectonics of the Najd Transcurrent Fault System, Saudi Arabia: Journal Geological Society London, vol. 136, p. 441-454.

Musil, Alois, 1926, The Northern Hegaz, v. 1, p. 215, American Geographical Society, Oriental explorations and studies, no. 1, New York.

Nasseef, A. D., and Gass, I.G., 1977, Granitic and metamorphic rocks of the Taif area, western Saudi Arabia: Geological Society America Bulletin, vol. 88, no. 12, p. 1721-1730.

Nebert, Karl, 1969, Geology of the Jabal Samran and Jabal Faiasan region: Saudi Arabian Deputy Ministry for Mineral Resources Bulletin 4.

Nebert, K., Alshaibi, A. A., Awlia, M., Bounny, I., Nawab, Z. A., Sharief, O. H., Sherbini, O. A., and Yeslam, A. H., 1974, Geology of the area north of Wadi Fatima, Kingdom of Saudi Arabia: Centre for Applied Geology, Jiddah; Bulletin 1, 31 p., 38 figs., 5 plates.

Overstreet, 1973, Contributions to the prehistory of Saudi Arabia, 1: Field Research Projects, 11 p. 99 fig. 3 Tbls. Miami, FL.

Overstreet, W. C., Overstreet, E. F., and Goudarzi, G. H., 1973, Mineralogical and chemical investigations of the laterite in the Sarat Mountains: U.S. Geological Survey Saudi Arabian Project Report 146, 66 p., 11 figs., Map, scale 1:100,000.

Overstreet, W. C., Stoeser, D. B., Overstreet, E. F., and Goudarzi, G. H., 1977, Tertiary laterite of the As Sarat Mountains, Asir Province: Saudi Arabian Directorate General of Mineral Resources Bulletin 21, 24 p., 11 figs., 1 pl. scale 1:100,000.

Pallister, J. S., 1982, Reconnaissance geologic map of the Harrat Tuffil quadrangle, sheet 20/39B, Kingdom of Saudi Arabia: U.S. Geological Survey Open-File Report USGS-OF 03-33, 3 pls., map, scale 1:100,000, 3 appendices.

Pellaton, Claude, 1976, Geology and mineral exploration of the Wadi Dahgalah quadrangle, sheet 26/37D, Kingdom of Saudi Arabia: [France] Bureau des Recherches Geologiques et Minieres report 76-JED-10, scale 1:100,000 with text, 24 p.

Pellaton, Claude, 1979, Geologic map of the Yanbu' al Bahr quadrangle, sheet 24c, Kingdom of Saudi Arabia: Saudi Arabian Directorate General of Mineral Resources map GM-48-A, scale 1:250,000 with text 24 p.

Pellaton, Claude, 1981, Geologic map of the Al Madinah quadrangle, sheet 24D, Kingdom of Saudi Arabia: Saudi Arabian Deputy Ministry for Mineral Resources map GM-52-A, scale 1:250,000 with text, 19 p.

Pellaton, Claude, 1982, Geologic Map of the Umm Lajj quadrangle, sheet 25B, Kingdom of Saudi Arabia: Saudi Arabian Deputy Ministry for Mineral Resources map GM-61-A, scale 1:250,000 with text, 14 p.

Powers, R. W., Ramirez, L. F., Redmond, C. D., and Elberg, E. L., Jr., 1966, Geology of the Arabian Peninsula, Sedimentary Geology of Saudi Arabia: U.S. Geological Survey Professional Paper 560-D, 147 p.

Powers, R. W., 1968, Lexique stratigraphique international, v. III, fas. 10bl, Arabie Saoudite: Centre national de la Recherche Scientifique, Paris, p. 76.

Prinz, W. C., 1981, Geology of the Wadi Hali quadrangle, sheet 18E, Kingdom of Saudi Arabia: U.S. Geological Survey misc. 24 p, 2 pls.

Quennell, A. M., 1951, Geology and mineral resources of (former) Trans-Jordan: Colonial Geology and Mineral Resources, 2, p. 85-115, London

Rathjens, Karl, 1942, Beobachtungen in Yemen: Geologische Rundschau, v. 33, p. 248-279.

Richardson, E. S., and Harrison, C. G. A., 1976, Opening of the Red Sea with two poles of rotation: Earth Planet Sci. Lett. 30, p. 135-142.

Richter-Bernburg, G., and Schott, W. (Amt fur Bodenforschung, Hannover, Germany), 1954, Geological researches in western Saudi Arabia: Saudi Arabian Directorate General of Mineral Resources Open-File Report 28, 69 p., 25 ill.

Reischmann, Thomas, 1981, Petrographie and geochemie spat Proterozoischer volkanite der Wadi Lith region, Saudi Arabia thesis, University Mainz, 172 p., 3 ap.

Roland, N. W., 1978, Jung palaozoisch Glazialspuren auf dem Arubischen Schild: Eiszeitalter u. Gegen, vol. 28, p.133-138, 4 fig.

Sahl, M., and Al Fatawi, B., 1981, Reconnaissance geology of the Tayyibal Ism Quad. sheet 28/34 B, Kindom of Saudi Arabia: Saudi Arabian Deputy Ministry for Mineral Resources Open-file report, 2 figs., 1 plate, 24 p.

Said, Rushdi, 1962, The geology of Egypt: Elsevier, New York, 377 p., 71 figs., 10 pls.

Sarnthein, M., 1978, Sand deserts during glacial maximum and climatic optimum: Nature, v. 272, p. 43-46.

Schick, A. P., 1958, Marine terraces on Tiran Island, Northern Red Sea: Geog. Ann XI, p. 63-66, 4 figs.

Schmidt, D. L., Hadley, D. G., Greenwood, W. R., Gonzalez, Louis, Coleman, R. G., and Brown, G. F., 1973, Stratigraphy and tectonism of the southern part of the Precambrian Shield of Saudi Arabia: Saudi Arabian Directorate General of Mineral Resources, Bulletin 8, 13 p.

Schmidt, D. L., Hadley, D. G., and Stoeser, D. B., 1979, Late Proterozoic crustal history of the Arabian Shield, southern Najd Province, Kingdom of Saudi Arabia: p. 41-48, in Tahoun, S.A., ed., Evolution and mineralization of the Arabian-Nubian Shield: Institute for Applied Geology Bulletin no. 3, Oxford, Pergamon Press, Ltd., v. 2, 224 p.

Schmidt, D. L., 1980a, Geology of the Al Junaynah quadrangle, sheet 20/42 D, Kingdom of Saudi Arabia; U.S. Geological Survey Saudi Arabian Mission Technical Record II (SA(IR)351.) scale 1:100,000, with text, 67 p.

Schmidt, D. L., 1980b, Geology of the Wadi al Miyah quadrangle, sheet 20/42B, Kingdom of Saudi Arabia: U.S. Geological Survey Saudi Arabian Mission Technical Record 12 (SA(IR)352) scale 1:100,000, with text 87 p.

Schmidt, D. L., 1981a, Geology of the Jabal al Qarah quadrangle, sheet 20/43C, Kingdom of Saudi Arabia: U.S. Geological Survey Saudi Arabian Mission Miscellaneous Document 31, Saudi Arabian SA(IR)-367, 52 p., scale 1:100,000.

Schmidt, D. L., 1981b, Geology of the Jabal Yafikh quadrangle, sheet 20/43B, Kingdom of Saudi Arabia: U.S. Geological Survey, Saudi Arabian Mission Miscellaneous Document 39, SA(IR)-397, 99 p., scale 1:100,000.

Schmidt, D. L., Puffett, W. P., Campbell, W. L., and Al-Koulak, Z.H., 1981, Gold placer and Quaternary stratigraphy of the Jabal Mokhyat area, southern Najd Province, Kingdom of Saudi Arabia: U.S. Geological Survey Saudi Arabian Mission Technical Record 19 (SA(IR)-375), 69 p.

Schmidt, D. L., and Brown, G.F., 1982, Major-element chemical evolution of the late Proterozoic shield of Saudi Arabia: Saudi Arabian Deputy Ministry for Mineral Resources, U.S. Geological Survey Open-File Report OF-02-88, 34 p.

Schmidt, D. L., Hadley, D. G., and Brown, G. F., 1982, Middle Tertiary continental rift and evolution of the Red Sea in southwestern Saudi USGS-OF-03-6, 56 p.

Schurmann, H. M. E., 1966, The Precambrian in North Africa: E. J. Brill, Leiden, 351 p., 88 pls.

Schott, W., 1953, Geologische Studienreise nach Yemen: Zeitschrift der Deutschen Geologischen Geselleschaft, Hannover, bd. 105, pt. 3, p. 548.

Scott, Hugh and Britton, E. B., 1941, British Museum (Natural History), Expedition to south west Arabia 1937-38: vol. 1, pt. h, repts. 1-8.

Seilacher, A., 1970, Cruziana stratigraphy of "non-fossiliferous" Paleozoic sandstone, p. 447-476; in Crimes, T.P., and Harper, J.C., Trace fossils: Liverpool, Seel House Press.

Shapiro, Leonard, 1967, Rapid analysis of rocks and minerals by a single-solution method: U.S. Geological Survey Professional Paper 575B, p. 187-191.

Shimron, A. E., and Horowitz, Akaron, 1972, Precambrian organic microfossils from Sinai: Pollen et Spores 14, no. 3 (Museum National d' Histoire Naturelle, Paris), p. 333-342, 15 figs.

Shimron, A. E., and Brookins, 1974, Rb-Sr radiometric age of late Precambrian fossil-bearing and associated rocks from Sinai: Earth and Planetary Science Letters, 24, p. 136-140.

Silvestri, Alfredo, 1937, Fossile eocenico singolare della Tripolitania: Societa Geologica Italiana, Bull. v. 56, p. 203-208.

Skiba, W. J., and Warden, A. J., 1969, Preliminary report on the geology of selected areas in the southern part of the Arabian Shield: Saudi Arabian Directorate General of Mineral Resources Open-File Report 325, 42 p., 2 maps.

Skiba, W. J., 1980, The form and evolution of late Precambrian plutonic masses in the Jiddah-Rabigh-Wadi Al-Quaha area, Saudi Arabia, p. 105-121, in Cooray, P. G., and Tahoun, S.A., eds., Evolution and Mineralization of the Arabian-Nubian Shield: Institute for Applied Geology Bulletin no. 3, Oxford, Pergamon Press, Ltd., vol. 3, 164 p.

Smith, J. W., 1980, Reconnaissance geology of the At Ta'if quadrangle, sheet 21/40 C. Kingdom of Saudi Arabia: Saudi Arabian Deputy Ministry for Mineral Resource Map GM 56, scale 1:100,000 with text, 33 p.

Smith, C. L., 1980, Brines of Wadi as Sirhan, Kingdom of Saudi Arabia: U.S. Geological Survey Saudi Arabian Mission Technical Report 1, SA(IR) 295, 26 p., 7 figs., 3 tables.

Smith, J. W., 1980, Reconnaissance geologic map of the Wadi Mahani quadrangle, sheet 22/40A, Kingdom of Saudi Arabia: Saudi Arabian Directorate General of Mineral Resources map GM-35, scale 1:100,000, with text 18 p.

Smith, J. W., 1982, Reconnaissance geologic map of the Wadi Hammah quadrangle, sheet 22/40C, Kingdom of Saudi Arabia: Saudi Arabian Deputy Ministry for Mineral Resources map GM-65, scale 1:100,000, with text 19 p.

Soliman, M. M., 1981, Petrology and geochemistry of some granitic rocks from the western Al-Quway'iyah region: Arab Journ. Sci. and Engr. F, no. 3, p. 289-297.

Stacey, J. S., Delevaux, M. H., Gramlich, J. W., Doe, B. R., and Roberts, R. J., 1980, A lead isotope study of mineralization in the Arabian Shield: U.S. Geological Survey Saudi Arabian Mission Technical Record 8 (Inter-agency Report 347), 30 p. 7 figs. 5 tables.

Stacey, J. S., and Hedge, C. E., in press, Direct evidence for early Proterozoic continental crust in the eastern Arabian-Nubian Shield: Geology.

Steiger, R. H., and Jager, E, 1977, Subcommission geochronology; convention on the use of decay constants in geo-and cosmochronology: Earth and Planetary Science Letters, vol. 36, p. 359-367.

Steineke, Max, Berg, E. L., and Wadsack, G., 1944, Preliminary map of the water resources and geology of the Jeddah-Usfan-Wadi Fatima area: U.S. Military Mission to Saudi Arabia in cooperation with the Arabian American Oil Co., unpublished, scale 1:100,000.

Steineke, Max, Bramkamp, R. A., and Sander, J. J., 1958, Stratigraphic relations of Arabian Jurassic oil, in Habitat of Oil: American Association of Petroleum Geologists, p. 1294-1329, 6 figs.

Steinitz, G., Bartov, Y., and Hunziker, J. C., 1978, K-Ar age determinations of some Miocene-Pliocene basalts in Israel; their significance to the tectonics of the Rift Valley: Geographic Magazine, v. 115, no. 5, p. 329-340.

Stoeser, D.B., and Elliott, J. E., 1980, Post-orogenic peralkaline and calc-alkaline granites and associated mineralization of the Arabian Shield, Kingdom of Saudi Arabia, p. 1-23 in Cooray, P. G., and Tahoun, S. A., eds., Evolution and Mineralization of the Arabian-Nubian Shield: Institute for Applied Geology Bulletin no. 3, Oxford, Pergamon Press, Ltd., vol. 4, 168 p.

Streckeisen, A. L., Chairman, 1973, Plutonic rocks, classification and nomenclature recommended by the IUGS subcommission on the systematics of igneous rocks; Geotimes p. 26-30.

Streckeisen, A. L., 1976, To each plutonic rock its proper name: Earth-Science Reviews vol. 12, no. 1, p. 1-33.

Streckeisen, 1979, Classification and nomenclature of volcanic rocks, lamprophyres, carbonatites, and melititic rocks; recommendations and suggestions on the systematics of igneous rocks: Geology (Boulder) vol. 7, p. 331-335, 1 table.

Stuckless, J. S. and VanTrump, G., Jr., 1979, A revised version of graphic normative analysis program (GNAP) with examples of petrologic problem solving: U.S. Geological Survey Open File Rept. 79-1237, 111 p.

Taylor, H. P., Jr., and Coleman, R. G., 1977, Oxygen isotopic evidence for meteoric-hydrothermal alteration of the Jabal al Tirf igneous complex, Saudi Arabia [abs.]: American Geophysical Union Trans. 58, p. 516.

Thatcher, Leland, Rubin, Meyer, and Brown, G. F., 1961, Dating desert ground water: Science, v. 134, p. 104-105.

Theobald, P. K., and Thompson, C. E., 1972, Geology and geochemistry of a part of the Ablah Formation at Jabal Rumur, Kingdom of Saudi Arabia: U.S. Geological Survey Saudi Arabian Project Report 88, 15 p., 8 figs.

Trent, V. A., and Johnson, R. F., 1966, Reconnaissance mineral and geologic investigation in the Maqna quadrangle, Aqaba area, Saudi Arabia: U.S. Geological Survey, Saudi Arabian Project Report 51, 5 p., 3 ill.

Tothill, J. D., ed., 1948, Agriculture in the Sudan: Oxford University Press 804 p.

Twitchell, K. S., 1958, Saudi Arabia, with an account of the development of its natural resources: Princeton University Press, 281 p.

Uchimizu, Mamoru, 1966, Geology and petrology of alkali rocks from Dogo, Oki Islands: Tokyo University Faculty of Science Journal, sec. 2, v. 16, part 1, p. 85-159, illus. (incl. geol. map, scale 1:80,000).

U.S. Geological Survey-Arabian American Oil Co., (USGS-ARAMCO) 1963, Geologic map of the Arabian Peninsula: U.S. Geological Survey Miscellaneous Geologic Investigations map p I-270-A, scale 1:2,000,000.

Vail, J. R., 1971, Geological reconnaissance in part of Berber District, northern province, Sudan: Sudan Geological Survey Department Bull. 18, Khartoum, 76 p., 6 figs., 2 tables, 2 pls., 1 map.

Vesey-FitzGerald, D. F., 1957, The vegetation of central and eastern Arabia: Journal Ecology, v. 45, p. 779-798, Blackwell Science Pub. Oxford, England.

_____ 1955, Vegetation of the Red Sea Coast south of Jeddah, Saudi Arabia: Journal Ecology, v. 43, p. 477-489, Blackwell Science Pub. Oxford, England.

Vidal, Gonzalo, 1979, Acritarchs from the upper Proterozoic and lower Cambrian of East Greenland, Gron. Geol. Under. Bull. 134, p. 8, 34-35.

Vincent, Gerard, 1968, Geology and mineral resources of the Halaban-Sabhah region (sheet 118, zone 2): [France] Bureau des Recherches Geologiques et Minieres Open-File Report 68-JED-1, 3 app., scale 1:100,000.

von Wissman & van Padang Newmann, 1963

Warden, A.J., 1982, Reconnaissance geology 7th Markas quadrangle, sheet 18/43B, Kingdom of Saudi Arabia: U.S. Geological Survey Open-File Report USGS-OF-02-41, 58 p., scale 1:100,000.

Wendorf, F., Schild, R., Said, R., Haynes, C. V., Gautier, A., and Kofusiewicz, M., 1976, The prehistory of the Egyptian Sahara: Science, v. 193, no. 4248, p. 103-114.

Wetzel, Rene, and Morton, D. M., 1959, Contribution a la geologie de la Transjordanie: Museum National d'Histoire Naturelle, Paris, France, notes et mem. sur le Moyen Orient, t. VII, p. 107-120.

Worl, R. G., 1978, Ore controls at the Mahd adh Dhahab gold mine, Kingdom of Saudi Arabia: U.S. Geological Survey Open-File Report 78-778, (IR)SA-232, 31 p., 1 pl., 4 figs.

Yamani, M. A., 1968, Geology of the oolitic hematite of Wadi Fatima, Saudi Arabia, and the economics of its exploitation: Ph.D. thesis, Cornell University, Ithaca, New York, 10 p., 9 figs., 2 pls.